# SOLID STATE NMR STUDIES OF TRANSITION METAL COMPOUNDS.

DEBORAH JANE SMITH

Thesis submitted to the University of Oxford in partial fulfilment of the requirements for the degree of Doctor of Philosophy.

Balliol College, Oxford

Michaelmas 1986

# Solid state nmr studies of transition metal compounds.

Deborah J. Smith
Balliol College
Oxford.

A thesis submitted to the University of Oxford in partial fulfilment of the requirements for the degree of Doctor of Philosophy.

Michaelmas 1986

## Abstract.

This thesis is concerned with a systematic study of phosphine-containing transition metal complexes and cluster compounds by high resolution solid state nmr spectroscopy, using the techniques of magic angle spinning and cross polarisation.

Previous work has indicated the potential of the solid state nmr technique to investigate a variety of materials: this is considered in the introduction to this thesis, and the reasons for choosing to study transition metal phosphine compounds are discussed.

The analysis of spinning sidebands to obtain the principle values of the shielding tensor is examined to determine how well the calculated values represent the true values. Simulations of slow MAS spectra are proposed as a means of testing and refining the calculated tensor components before attempting to correlate the shielding with structural parameters.

The results of a study of a series of crystalline phosphine-containing complexes and clusters are presented. The spectra are interpreted on the basis of the known crystal structures: in some cases separate resonances can be resolved in the solid state spectra from the distinct phosphine environments of a cluster framework, and from inequivalent sites in the unit cell. Information is obtained from the isotropic shifts, scalar couplings and the chemical shift anisotropy. Many of the compounds are fluxional in solution, some even at low temperature: whereas a number of these are found to be rigid in the solid state at room temperature, some of the crystalline compounds retain their fluxionality.

Investigations of the species formed when transition metal carbonyl clusters are anchored to oxide supports were carried out. These show the presence of several distinct phosphorus-containing species, some of which are not consistent with the simple attachment of the cluster to the surface. The unique importance of the solid state technique is demonstrated in the study of these supported species.

CONTENTS

## Acknowledgements

First and foremost I would like to express my thanks to my supervisor Chris Dobson, both for taking me on in the first place and for constant encouragement in matters spectroscopic and sporting ever since. I hope I haven't contributed too many grey hairs! Thanks also to Nigel Clayden for spectroscopic and mathematical assistance and teaching me to be tidy.

A large number of people have employed their synthetic skills to produce the compounds studied in this thesis, for which I am extremely grateful: in particular, I would like to express my thanks to Ian Salter for his enthusiastic approach to all matters chemical. Thanks are also due to Malcolm Green, for largely inspiring this project; Mike Mingos, for constructive and pertinent suggestions; and all of the Mingos group, especially Bob and Roy, for always being there to distract me.

Credit for three very happy years goes to the Dobson group, past and present, who made F12 a lively place to work at all hours of the day and night. This thesis would not have been the same without Gobi's witty repartee and cricket practices, Steve's cheerful smile, Mark's lively approach to almost everything, and endless heightist comments. Seriously, I would especially like to thank Lu-Yun, for her never-failing interest, help and encouragement, and Steve and Mark for practical help and (almost) keeping me sane through disc crashes.

Ian and Sara, who have been a constant source of support and cups of tea, and Alan, who set an example of determined thesis-writing, deserve much credit for the completion of this epic work; all nobly put up with my preoccupation with ~~rowing~~ nmr spectroscopy. Finally, my parents have supported and encouraged me throughout my studies, and none of this would have been possible without their help.

# Abbreviations

## Spectroscopic

| | |
|---|---|
| CP | cross polarisation |
| CSA | chemical shift anisotropy |
| EFG | electric field gradient |
| EXAFS | extended X-ray absorption fine structure |
| FID | free induction decay |
| HPPD | high power proton decoupling |
| INEPT | insensitive nuclei enhanced by polarisation transfer |
| i.r. | infra-red |
| MAS | magic angle spinning |
| nmr | nuclear magnetic resonance |
| ppm | parts per million |
| rf | radiofrequency |

## Formulae

| | |
|---|---|
| $Bu^t$ | tertiary butyl |
| COT | cyclooctatetraene |
| dppm | 1,2-bis(diphenylphosphino)methane |
| Et | ethyl |
| Me | methyl |
| Ph | phenyl |
| $Pr^i$ | isopropyl |
| CN-xylyl | 2,6-dimethylphenylisocyanate |

## Miscellaneous

| | |
|---|---|
| vbr | very broad |
| d | doublet |
| rms | root mean square |

# CHAPTER 1

## Introduction: solid state nmr spectroscopy and transition metal compounds.

In recent years there have been rapid advances in the field of high resolution solid state nmr spectroscopy [1]. These have come about with the development and widespread application of a group of experimental techniques to eliminate or greatly reduce the effects of the nuclear spin interactions, which are averaged by rapid isotropic motion in solution but which, in solids, would otherwise produce extremely broad, featureless lines. Using the techniques of high power heteronuclear spin decoupling [2] and magic angle sample spinning [3,4], and with the addition of cross polarisation [5] to increase the sensitivity of the dilute spin under observation, it is possible to obtain high resolution solid state nmr spectra from nuclei such as $^{13}C$, $^{29}Si$ and $^{31}P$.

One advantage of solid state nmr experiments is that they make possible nmr studies of relatively insoluble compounds, and of materials which are intrinsically solids. Moreover, nmr responds to short-range, rather than long-range, order, and so can be applied to investigations of glasses, cements and other non-crystalline materials [1,6] for which X-ray diffraction studies are of limited value. Meanwhile, when applied to compounds which are soluble, solid state nmr provides a bridge between X-ray crystallographic data and solution nmr studies. There are thus a large number of systems which can be investigated by this technique. Studies have already been carried out in areas ranging from biochemistry [7,8] to materials science [6,9,10], with samples as diverse as polymers [11], crystalline inorganic compounds [12,13] and small organic molecules

[14,15]. The technique is, however, still in its infancy, particularly in comparison with high resolution solution nmr, and there have been few systematic studies of relatively simple compounds. As a result, the factors affecting solid state nmr spectra are not well understood, which makes it difficult to interpret the spectra of complex systems. In general the interpretation of solid state nmr spectra is more complicated than the interpretation of their solution counterparts [16]. With this in mind, it is illuminating to look at the areas in which the successful interpretation of solid state nmr spectra has provided detailed information on the system studied.

Probably the most widely and successfully studied materials are zeolites, whose structures have become better understood as a result of $^{29}Si$ nmr spectroscopy. This work has recently been reviewed [17]. Why have these studies been so successful? One contributing factor is clearly the commercial importance of zeolites: with applications including ion exchange resins, molecular sieves, catalysts and catalyst supports [18], there is considerable practical importance and hence financial backing for research into these systems. Structural determination by means of X-ray diffraction is difficult, with a lack of single crystals, in some cases a distorted lattice and the difficulty of distinguishing between silicon and aluminium atoms. All of these factors, together with the presence of a suitable spin-1/2 nucleus ($^{29}Si$), indicate reasons why solid state studies of zeolites were initially carried out. ($^{27}Al$ nmr studies have also been made [18]). In addition, the zeolite samples themselves are amenable to MAS nmr experiments. But this does not explain the success of the nmr studies. The crucial point is that the $^{29}Si$ nmr spectra of the zeolites can be simply and accurately related to their structural properties [17-19]. Once such a correlation between structure and nmr

properties has been made, further structural investigations of similar samples and the interpretation of the spectra of unknown, related materials can follow.

In other areas investigated by solid state nmr, however, such correlations between structure and nmr properties have not always been made. The result is that, although solid state nmr spectra can be obtained from a particular sample, they may be difficult if not impossible to interpret. The aim of this work was therefore to carry out a systematic study on a group of related compounds and to try to understand the factors affecting the interpretation of their spectra. In choosing an area of investigation, what was required initially was a group of compounds well-characterised by both solution nmr and X-ray diffraction in order to facilitate interpretation of the solid state nmr spectra. Ideally a series of closely related compounds would be available, so that the effect on the spectrum of varying one particular structural parameter could be determined. Provided that the factors affecting the solid state spectra could be understood, it would then be possible to apply this knowledge to the study and characterisation of related but more complex systems. An appropriate choice of nucleus was important, necessitating a useful range of chemical shifts and a substantial body of solution nmr data.

After considering all of these factors, it was decided to carry out a systematic study of a number of transition metal phosphines. Solution nmr spectroscopy has been of fundamental importance in understanding the structures, dynamics and reactions of such compounds [20], and they are suitable for X-ray diffraction studies. Phosphines are widely used as co-ordinating ligands in transition metal chemistry [20], and the $^{31}P$ nucleus, with its wide range of chemical shifts and scalar couplings to other nuclei, is a

sensitive probe of structure [21]. The possibility of $^{13}C$ nmr studies of these compounds offered a further source of information. Examination of the literature revealed that, although no systematic study on this type of compound had been carried out, a number of investigations of organometallic and cluster compounds had been reported, indicating the potential of the high resolution solid state nmr technique in providing structural and dynamic information.

Wide line solid state nmr has been used to investigate the motion in fluxional organometallic compounds such as complexes of the ligands cyclooctatetraene and cyclopentadiene. Initial solid state $^{1}H$ nmr studies of these compounds [22,23] showed that motion was occurring in the solid at room temperature which could in some cases be halted on the nmr timescale by lowering the temperature. The lack of disorder in the crystal structure implied that this motion corresponded to the jumping of the arene ring between positions of minimum potential energy. Measurements of the relaxation times $T_1$ and $T_{1\rho}$ confirmed that this motion was occurring and gave values for the activation energies [24,25]. Measurements of the principal values of the chemical shielding tensor have also been used to provide dynamic information. In a $^{13}C$ nmr study of permethylferrocene [26], Wemmer *et al* were able to determine from the lineshapes characteristic of the shielding tensors that the arene ring reorientation occurs as jumps between symmetry-related orientations and not as random jumps, with preferred jumps of $2\pi/5$: they also derived the activation energy for this process. Comparison of the $^{13}C$ CSA's of a series of metallocenes [27] and of arene chromium tricarbonyl complexes [28] has suggested that the shielding anisotropy reflects the character of the bonding, and in a study of 6$\pi$-electron ring systems, Strub *et al* also observed a correlation between electron distribution and the $^{13}C$ shielding

tensor [29]. The chemical shift tensors of carbonyl ligands, too, have been used to aid in investigations of the structure and bonding in metal carbonyl compounds such as $Ni(CO)_4$ [30] and $Fe(CO)_5$ [30,31] and in various metal carbonyl clusters [32].

However despite the success of these experiments magic angle spinning $^{13}C$ nmr has so far been applied to a limited number of organometallic compounds. A study on a number of crystalline $\eta$-$(C_5H_5)$ and $\eta$-$(C_6H_6)$-containing compounds showed that in general the chemical shifts obtained correlated well with those measured in solution [33]. High resolution solid state nmr was used to investigate the fluxionality observed for $Ru_3(CO)_4(COT)_2$, in which all 16 ring protons are rendered equivalent in solution by a dynamic chemical exchange process so that a single $^1H$ resonance is observed. The room temperature $^{13}C$ solid state spectrum of the cluster [34] shows a single resonance for the ring carbon atoms, thought to be the result of a similar chemical exchange process to that occurring in solution; however at -180°C at least six lines in this region spread over a range of 50ppm can be resolved. In a study of the structure of the compound dicarbonyl(hexaethylbenzene)thiocarbonylchromium(0) [35], high resolution solid state $^{13}C$ nmr was used to show that the same stereoisomer was found in both the solid state and in solution. Preliminary experiments have demonstrated that, as the $^{13}C$ chemical shift of the thiocyanate ligand is characteristic of its mode of bonding, $^{13}C$ solid state nmr is a convenient means of determining the solid state structure of metal complexes of this ligand [36]. Other applications of $^{13}C$ CP/MAS nmr to transition metal compounds have concentrated upon the spectra of carbonyl ligands. Studies of $Fe_3(CO)_{12}$ [37] and $Co_2(CO)_8$ [38] have clarified the solid state structures of the two clusters, both of which show motion in the

crystal at room temperature. A series of carbonyl clusters were studied by Dorn et al [39], who observed a good correlation between solid state and solution $^{13}C$ chemical shifts. $^{17}O$ spectroscopy has also been applied to a series of solid transition metal carbonyls, showing that the CSA's are large and that magnetically nonequivalent $C^{17}O$ ligands may be distinguished [40]. A $^{15}N$ nmr study of two ruthenium nitrosyl complexes was able to distinguish between bent and linear nitrosyl ligands by means of their different chemical shift anisotropies [41].

The first report of high resolution solid state $^{31}P$ nmr spectroscopy of transition metal compounds was that of Diesveld et al [42], who studied various metal phosphine complexes. They obtained spectra from two copper phosphine complexes, both of which showed splittings of the $^{31}P$ resonances induced by the quadrupolar copper nucleus, and in the spectrum of Wilkinson's catalyst ($RhCl(PPh_3)_3$) observed scalar coupling between rhodium and phosphorus and between the inequivalent mutually trans phosphorus atoms. The solid state spectrum of a homonuclear gold phosphine cluster showed two resonances: whether the two lines resulted from two inequivalent phosphorus sites in one molecule, or from two inequivalent molecules in the unit cell, could not be determined as the crystal structure of the cluster was not known. This work and its interpretation in terms of the crystal structures of the compounds studied illustrates the quality of the spectra and degree of resolution possible and the type of information which may be obtained. However it also highlights some of the difficulties arising in spectral interpretation.

Further solid state $^{31}P$ nmr studies of transition metal compounds have been carried out by the research groups of Fyfe and of Maciel. In looking at a series of phosphine complexes of nickel,

platinum and palladium, the spectra of the platinum compounds were found to be particularly informative, with the magnitude of the Pt-P scalar coupling enabling the solid state geometries of the complexes to be determined in a manner analogous to that used in solution nmr [43,44]. A good correspondence between solution and solid state spectra was observed. However, when a number of diphosphine ligands and their rhodium (I) complexes were examined by solid state nmr [45], although the chemical shifts and coupling constants were generally similar to those measured in solution, in several cases there was a greater inequivalence of phosphorus sites in the solid state.

Solid state $^{31}P$ nmr has also been used to investigate the species formed when a number of the above-mentioned compounds are anchored to solid supports. The resonances of platinum complexes anchored to polymers [46,47], to silica and to glass beads [43,44] via a phosphine ligand were considerably broader than those of their precursors. The existence of a metal phosphine species on the surface could, however, be clearly established, and the magnitude of the Pt-P scalar coupling indicated the geometry of the immobilised complex. In a comparison of the relative merits of the two preparative methods used to anchor the complexes to silica and glass beads [43,44], both of which were believed to give the same product, the nmr studies showed that phosphination of the surface and then attaching the complex produced a considerable quantity (up to 60%) of a phosphorus (V) species, and that the alternative method, anchoring a phosphinated complex, was much more efficient. An oxidised phosphorus compound was also observed on the support in solid state nmr studies of phosphinated silica [48]. Methods of preparation of polymer-anchored metal complexes were also compared [46,47]. Both of the usual routes generated a substantial amount of an oxidised phosphorus species;

although this could be reduced, when the polymers were reacted with the metal compound a complex mixture of products were formed. A new route was investigated which proved to give a cleaner product.

A greater change in the solid state spectrum on anchoring to a support than had been found for the platinum complexes was observed when a diphosphine ligand and its rhodium (I) complex were bound to a polymer [45], implying that in this case there were major structural differences between the attached species and its precursor. When two ruthenium phosphines were anchored to silica prior to photochemical studies, the species formed were characterised by analysis and by spectroscopy, including solid state $^{13}C$, $^{31}P$ and $^{29}Si$ nmr [49]. For both compounds the results were consistent with the anchoring of intact molecular species to the surface. It has also been shown that $^{31}P$ nmr can be used to monitor the attachment of a metal complex to a surface when the phosphorus group is not the anchoring ligand [47].

These studies appear to be the only examples of the application of solid state $^{31}P$ nmr to supported transition metal phosphines. Solution nmr of solvent-swollen polymer-supported phosphines reacted with metal complexes has met with little success, the exception being when a linear polymer with a regularly-repeating phosphine unit was used, and even for this system only 5% of the phosphorus calculated to be present was observed by nmr [50].

Solid state $^{13}C$ nmr, too, has been used to study transition metal compounds anchored to surfaces. The work on ruthenium compounds has already been discussed [49]. Two studies have looked at $Mo(CO)_6$ supported on alumina [51,52], observing adsorbed molybdenum subcarbonyls in addition to physisorbed $Mo(CO)_6$. The surface reaction of the complex $(\eta\text{-}C_5H_5)Fe(CO)_2CH_3$ with alumina has been studied, with the predominant pathway identified as surface-induced migratory CO

insertion [53]. Supported organoactinides active in catalysis have also been investigated [54]. Furthermore, it should be noted that zeolites may be regarded as surfaces: a preliminary report using broadline $^{13}C$ nmr to investigate group VI carbonyls in Na-Y zeolite indicates rapid molecular motion within the zeolite, and shows the potential for further research in this area [55].

The potential of solid state nmr spectroscopy to characterise the structures, dynamics and reactions of surface-attached species is most clearly demonstrated in studies of more simple molecules on supports. The information provided is not confined to that contained in the chemical shift. For example, a study of $^{29}Si$ cross polarisation dynamics enabled the surface of silica gel to be characterised [56]. The structure and dynamics of pyridine adsorbed on silica-alumina have been investigated by $^{13}C$ and $^{15}N$ nmr [57], with the chemical shifts and linewidths and the results of variable CP time experiments providing a relatively detailed picture of the system. In an elegant study of 5'AMP adsorbed on zinc-exchanged clay, the principle values of the shielding tensor were used to suggest the mode of bonding of the phosphate to the surface [58].

The overall conclusion which may be drawn from these studies is that solid state nmr has great potential for the investigation and characterisation of transition metal complexes and clusters, both in the crystalline state and when anchored to a variety of supports. One particular interest in supported cluster compounds stems from their use in heterogeneous catalysis, of considerable importance in the chemical industry [59]. Solid state nmr has provided a considerable amount of information on the few supported systems which have already been studied, information which could not readily be obtained from the other techniques used as a means of characterisation of these systems.

It has in fact been suggested that studies of surface-immobilised species and their reactions have suffered because of the lack of a high resolution spectroscopic technique which is able to detect and characterise them [16]. There is clearly considerable scope for further solid state nmr investigations in this area, with an immense range of potential systems available to study and a number of spin-1/2 nuclei amenable to nmr experiments.

This thesis is concerned with the use of high resolution solid state $^{31}P$ and $^{13}C$ nmr spectroscopy to investigate transition metal phosphine complexes and clusters and the species they form on anchoring to oxide supports. In general well-resolved spectra were obtained from the many samples studied: these were interpreted in terms of the chemistry of the systems. Interactive work with other research groups utilised their synthetic expertise, enabling a wide range of compounds to be investigated. The systems studied and the methods employed are described in chapter 2. The following chapter examines the analysis of spinning sidebands to obtain the principle values of the shielding tensor, which should provide structural and bonding information. Having experienced difficulties in obtaining consistent tensor values from the usual methods of analysis, an investigation of these methods was carried out to determine how well the calculated values represented the true principle values of the tensor before attempts to correlate the shielding with structural parameters were made. Returning to the main theme of the thesis, the application of the solid state nmr technique to some simple transition metal compounds is discussed in chapter 4. This provided an understanding of many of the factors affecting the interpretation of the solid state nmr spectra of these compounds. The knowledge thus obtained was applied in the studies of more complex systems, namely

homonuclear gold phosphine clusters and heteronuclear metal clusters, presented in chapters 5 and 6. Finally in chapter 7 the results of solid state nmr investigations of surface-attached metal cluster compounds are discussed.

References.

[1] See for example Phil. Trans. R. Soc. A299 (1981) for a discussion of recent developments.

[2] M. Mehring, 'Principles of high resolution NMR in solids', 2nd ed., Springer-Verlag, Berlin (1983).

[3] E.R. Andrew, A. Bradbury and R.G. Eades, Nature 182 (1958) 1659.

[4] I.J. Lowe, Phys. Rev. Lett. 2 (1959) 285.

[5] A. Pines, M.G. Gibby and J.S. Waugh, J. Chem. Phys. 59 (1973) 569.

[6] S.A. Rodger, D.Phil thesis, Oxford (1986).

[7] G.R. Hays, R. Huis, B. Coleman, D. Clague, J.W. Verhoeven and F. Rob, J. Amer. Chem. Soc. 103 (1981) 5140.

[8] M.H. Frey and S.J. Opella, J. Chem. Soc., Chem. Commun. (1980) 474.

[9] E. Oldfield and R.J. Kirkpatrick, Science 227 (1985) 1537.

[10] E. Lippmaa, M. Magi, A. Samoson, G. Engelhardt and A.-R. Grimmer, J. Amer. Chem. Soc. 102 (1980) 4889.

[11] W.L. Earl and D.L. VanderHardt, Macromolecules 12 (1979) 762.

[12] J.R. Ascenso, R.K. Harris and P. Granger, J. Organomet. Chem. 301 (1986) C23.

[13] M.J. Collins, C.I. Ratcliffe and J.A. Ripmeester, J. Magn. Res. 68 (1986) 172.

[14] R.F. Childs, A. Varadarajan, C.J.L. Lock, R. Faggiani, C.A. Fyfe and R.E. Wasylishen, J. Amer. Chem. Soc. 104 (1982) 2452.

[15] E.T. Lippmaa, M.A. Alla, T.J. Pehk and G. Engelhardt, J. Amer. Chem. Soc. 100 (1978) 1929.

[16] C.A. Fyfe 'Solid state NMR for chemists', CFC Press, Guelph (1983).

[17] J. Klinowski, Prog. NMR Spectr. 16 (1984) 237.

[18] C.A. Fyfe, J.M. Thomas, J. Klinowski and G.C. Gobbi, Angew. Chem.

Int. Ed. Engl. 22 (1983) 259.

[19] X. Liu, J. Klinowski and J.M. Thomas, Chem. Phys. Lett. 127 (1986) 563.

[20] P.S. Pregosin and R.W. Kunz, NMR: Basic Princ. Prog. 16 (1979) 1.

[21] 'High resolution NMR spectroscopy' eds. J.W. Emsley, J. Feeney and L.H. Sutcliffe, Pergamon Press, N.Y. (1966) vol.2 881.

[22] A.J. Campbell, C.A. Fyfe and E. Maslowsky, J. Amer. Chem. Soc. 94 (1972) 2690.

[23] A.J. Campbell, C.A. Fyfe, R.G. Goel, E. Maslowsky and C.V. Senoff, ibid., 8387.

[24] A.J. Campbell, C.E. Cottrell, C.A. Fyfe and K.R. Jeffrey, Inorg. Chem. 15 (1976) 1321.

[25] Ibid., 1326.

[26] D.E. Wemmer, D.J. Ruben and A. Pines, J. Amer. Chem. Soc. 103 (1981) 28.

[27] D.E. Wemmer and A. Pines, ibid., 34.

[28] M.M. Maricq, J.S. Waugh, J.L. Fletcher and M.J. McGlinchey, J. Amer. Chem. Soc. 100 (1978) 6902.

[29] H. Strub, A.J. Beeler, D.M. Grant, J. Michl, P.W. Cutts and K.W. Zilm, J. Amer. Chem. Soc. 105 (1983) 3333.

[30] H. Mahnke, R.K. Sheline and H.W. Spiess, J. Chem. Phys. 61 (1974) 55.

[31] H.W. Spiess, R. Grosescu and U. Haeberlen, Chem. Phys. 6 (1974) 226.

[32] J.W. Gleeson and R.W. Vaughan, J. Chem. Phys. 78 (1983) 5384.

[33] S.J. Heyes, Part II thesis, Oxford (1985).

[34] J.R. Lyerla, C.A. Fyfe and C.S. Yannoni, J. Amer. Chem. Soc. 101 (1979) 1351.

[35] M.J. McGlinchey, P. Bougeard, B.G. Sayer, R. Hofer and C.J.L.

Lock, J. Chem. Soc., Chem. Commun. (1984) 789.

[36] N. Zumbulyadis and H.J. Gysling, J. Amer. Chem. Soc. 104 (1982) 3246.

[37] H. Dorn, B.E. Hanson and E. Motell, Inorg. Chim. Acta 54 (1981) L71.

[38] B.E. Hanson, M.J. Sullivan and R.J. Davis, J. Amer. Chem. Soc. 106 (1984) 251.

[39] H.C. Dorn, B.E. Hanson and E. Motell, J. Organomet. Chem. 224 (1982) 181.

[40] E. Oldfield, M.A. Keniry, S. Shinoda, S. Schramm, T.L. Brown and H.S. Gutowsky, J. Chem. Soc., Chem. Commun. (1985) 791.

[41] J. Mason, D.M.P. Mingos, J. Schaefer, D. Sherman and E.O.Stejskal, J. Chem. Soc., Chem. Commun (1985) 444.

[42] J.W. Diesveld, E.M. Menger, H.T. Edzes and W.S. Veeman, J. Amer. Chem. Soc. 102 (1980) 7935.

[43] L. Bemi, H.C. Clark, J.A. Davies, C.A. Fyfe and R.E. Wasylishen, J. Amer. Chem. Soc. 104 (1982) 438.

[44] L. Bemi, H.C. Clark, J.A. Davies, D. Drexler, C.A. Fyfe and R.E. Wasylishen, J. Organomet. Chem. 224 (1982) C5.

[45] G.E. Maciel, D.J. O'Donnell and R. Greaves, Adv. Chem. Ser. 196 (1982) 389.

[46] H.C. Clark, J.A. Davies, C.A. Fyfe, P.J. Hayes and R.E. Wasylishen, Organometallics 2 (1983) 177.

[47] C.A. Fyfe, H.C. Clark, J.A. Davies, P.J. Hayes and R.E. Wasylishen, J. Amer. Chem. Soc. 105 (1983) 6577.

[48] S. Shinoda, K. Nakamura and Y. Saito, Chem. Lett. (1983) 1449.

[49] D.K. Liu, M.S. Wrighton, D.R. McKay and G.E. Maciel, Inorg. Chem. 23 (1984) 212.

[50] A.J. Naaktgeboren, R.J.M. Nolte and W. Drenth, J. Amer. Chem.

Soc. 102 (1980) 3350.

[51] W.M. Shirley, B.R. McGarvey, B. Maiti, A. Brenner and A. Cichowlas, J. Mol. Catal. 29 (1985) 259.

[52] B.E. Hanson, G.W. Wagner, R.J. Davies and E. Motell, Inorg. Chem. 23 (1984) 1635.

[53] P.J. Toscano and T.J. Marks, Organometallics 5 (1986) 400.

[54] P.J. Toscano and T.J. Marks, J. Amer. Chem. Soc. 107 (1985) 653.

[55] 'Magnetic resonance in colloid and interface science' eds. J.P. Fraissard and H.A. Resing, Reidel, Holland (1980) 497.

[56] G.E. Maciel and D.W. Sindorf, J. Amer. Chem. Soc. 102 (1980) 7606.

[57] G.E. Maciel, J.F. Haw, I.-S. Chuang, B.L. Hawkins, T.A. Early, D.R. McKay and L. Petrakis, J. Amer. Chem. Soc. 105 (1983) 5529.

[58] N.J. Clayden and J.S. Waugh, J. Chem. Soc., Chem. Commun. (1983) 292.

[59] D.C. Bailey and S.H. Langer, Chem. Rev. 81 (1981) 109.

# CHAPTER 2

## Materials and methods.

### 2.1 Introduction.

In this chapter the samples used for the solid state nmr studies are briefly described. The experimental techniques and the computational methods used to analyse the nmr data are then discussed. The final two sections of the chapter compare solution and solid state nmr spectra in terms of linewidths and the number of resonance lines observed.

### 2.2 Materials.

The samples used for the solid state nmr experiments were obtained from many different sources. Details of the preparative methods are given in the appropriate chapters. Triphenylphosphine oxide and adamantane were obtained from Aldrich and were used as supplied. Potassium bromide (Fisons) and sodium dihydrogen orthophosphate (BDH) were finely ground in a pestle and mortar before use. $Rh(CN\text{-}xylyl)_2(PPh_3)_2$, $RhCl(PPh_3)_3$ and a series of homonuclear gold phosphine clusters were kindly lent by the research group of Dr. D.M.P. Mingos at Oxford. The samples were powders or microcrystalline and were used without further preparation. Sample quantities varied from 50-100mg for the gold clusters to ~250mg for the rhodium complexes.

In a project carried out with Dr. M.L.H. Green at Oxford, several arenetris(tertiary phosphine)molybdenum complexes were prepared by Dr. C. McAteer. The air-sensitive compounds were obtained as fine powders. Samples were packed into rotors in a glove-box in an inert atmosphere, the tops sealed with Teflon tape and the rotors kept under a nitrogen atmosphere until use. No appreciable sample

decomposition was observed during the accumulation period. A sample of $WH_6(PMe_3)_3$ was kindly lent by G. Parkin (from Dr. Green's research group); this sample was also handled under nitrogen.

A series of Group 1B heteronuclear metal cluster compounds were prepared by Dr. I.D. Salter at Exeter University. Recrystallisation of samples was initially carried out from $CH_2Cl_2$/light petroleum. However this was found to produce additional peaks in a number of the solid state spectra, possibly because solvent incorporation into the unit cell (observed for several of the metal clusters) reduced the symmetry of the molecular environment in the crystal. Later samples were recrystallised from diethyl ether/light petroleum. Generally 100-150mg of sample was obtained in a microcrystalline form. Samples were stored under nitrogen at -14°C until use.

Studies on rhodium, osmium and ruthenium carbonyl clusters and the species formed on anchoring them to solid inorganic supports were carried out in conjunction with the group of Dr. J. Evans at Southampton University. The metal clusters were prepared by Dr. S.L. Cook, Dr. R.J. Crowte and V. Alexiev, and were characterised by infra-red and solution nmr spectroscopy. Typically 5-20mg of cluster was used for solid state studies. $^{13}C$ enrichment of the carbonyl groups of $H_2Os_3(CO)_9PPh_3$ and $H_2Os_3(CO)_{10}PPh_3$ was carried out by V. Alexiev. The level of enrichment was typically 40%.

The inorganic supports used for anchoring the clusters were silica (Aerosil 380), titania and alumina. The metal clusters were first silylated by reaction with $(EtO)_3SiCl$. Anchoring was then achieved by stirring the silylated cluster with the support in dry $CH_2Cl_2$ under $N_2$ or CO. For the osmium clusters a second method of preparation, in which the support was phosphinated before the cluster

was anchored, was also employed. However this produced an additional broad resonance at ~40ppm in the solid state spectrum. Peaks in this region have previously been identified as phosphorus (V) species [1,2]. It appeared that during the anchoring reaction a significant amount of oxidation of the phosphine occurred, and it was therefore decided to abandon this route in favour of the alternative, which gave a cleaner reaction. All of the anchored samples consisted of fine powders, generally yellow or orange-brown in colour. The change in colour of the support from white during the anchoring process was used as an indication that a supported species had been formed. Typically loadings were of the order of 5-10% wt/wt metal on silica. Using a full rotor (~400mg) of sample, several thousand transients were necessary to obtain an acceptable signal-to-noise ratio.

In order to obtain maximum signal from small quantities of metal cluster compounds, the base of the rotor was first packed with finely ground KBr. A disc of paper was then inserted before addition of the sample to be studied by solid state nmr. This ensured that all of the available sample was inside the coil and able to produce a detectable signal. A further advantage of this method was that use of KBr enabled the magic angle to be adjusted on the $^{79}Br$ signal ([3]: section 2.3.4) immediately prior to accumulation of the spectrum.

## 2.3 Nmr methods.

### 2.3.1 Experimental details.

All solid state spectra were recorded on a Bruker CXP200 spectrometer operating at 80.96MHz for $^{31}P$, 50.32MHz for $^{13}C$ and 200.13MHz for $^{1}H$. The spectrometer was equipped with a multinuclear, proton-enhanced magic angle spinning probe with a single nitrogen bearing, and an Aspect 2000 data system. Variable temperature

operation was not possible with this probe. Magic angle sample spinning was carried out using Delrin or, for $^{13}C$, deuterated plexiglass Andrew-type rotors containing from 5-400mg of sample. Spinning speeds ranged from 1.2 to 3.7kHz. The magic angle was optimised on the $^{79}Br$ signal of KBr [3]. Sweep widths of 50kHz for $^{31}P$ and 20kHz for $^{13}C$ were used. Free induction decays (FID's) were generally defined by 8K data points and were Fourier transformed to a frequency domain of 8K data points. For spectra containing closely-spaced, narrow lines, such as the $^{13}C$ spectra of the metal carbonyl clusters and those showing metal-phosphorus scalar coupling, 16K data points were used for both the FID and the frequency domain in order to obtain better spectral definition. Exponential or Gaussian multiplication of the FID was used routinely to improve resolution. The number of transients varied from less than 200 for some standard samples to several thousand for the surface-attached species. A recycle delay of 2s was found to be sufficient for most experiments. A 5μs 90° pulse was used (see section 2.3.2).

$^{31}P$ chemical shifts were referenced to 85% phosphoric acid. Sodium dihydrogen orthophosphate was used as a secondary reference and to optimise experimental conditions. $^{13}C$ chemical shifts were referenced to TMS, using adamantane as a secondary reference and to set up the spectrometer. In both cases, downfield shifts were taken as positive.

The spectra of all proton-containing samples were accumulated using high power proton decoupling and cross polarisation. Magic angle sample spinning was used to obtain high resolution spectra. These techniques will be discussed in more detail below. In some of the solid state spectra, the overlap of isotropic peaks and spinning sidebands made even a qualitative analysis of the spectrum difficult,

and repeating the spectrum at a different spinning speed did not produce sufficient simplification to allow interpretation. In these cases the TOSS (TOtal Suppression of Sidebands) pulse sequence was used in an attempt to obtain sideband-free spectra [4]. Although the spectra obtained using this method were not totally without sidebands, probably as a result of slight variations in the spinning speed during the course of the experiment, the results enabled the isotropic peaks and spinning sidebands to be distinguished.

### 2.3.2 High power proton decoupling.

High power proton decoupling (HPPD) was used in the solid state nmr experiments discussed in this thesis to remove $^{1}H$-$^{31}P$ and $^{1}H$-$^{13}C$ heteronuclear dipolar interactions, which would otherwise have produced broadening of the resonances of the dilute spin under investigation [5]. It was achieved by applying a strong rf field to the abundant I spins ($^{1}H$) at their Larmor frequency, which produces a coherent averaging of the I-S dipolar interaction. The process is analogous to the removal of J coupling in liquids, but due to the greater strength of the dipolar interaction with respect to J coupling, the power requirements are greater. Consequently the decoupling power is left on for as short a time as possible to minimise heating effects, in the experiments in this thesis generally not longer than 40ms.

Insufficient proton decoupling power to completely remove the heteronuclear dipolar interactions will result in broad resonances in the solid state spectra. The experiments discussed here were carried out using a $90^{o}$ pulse of width 5μs, which corresponds to ~40kHz decoupling power. This was found to be sufficient to obtain maximum resolution of $^{31}P$ and $^{13}C$ resonances. The frequency at which maximum

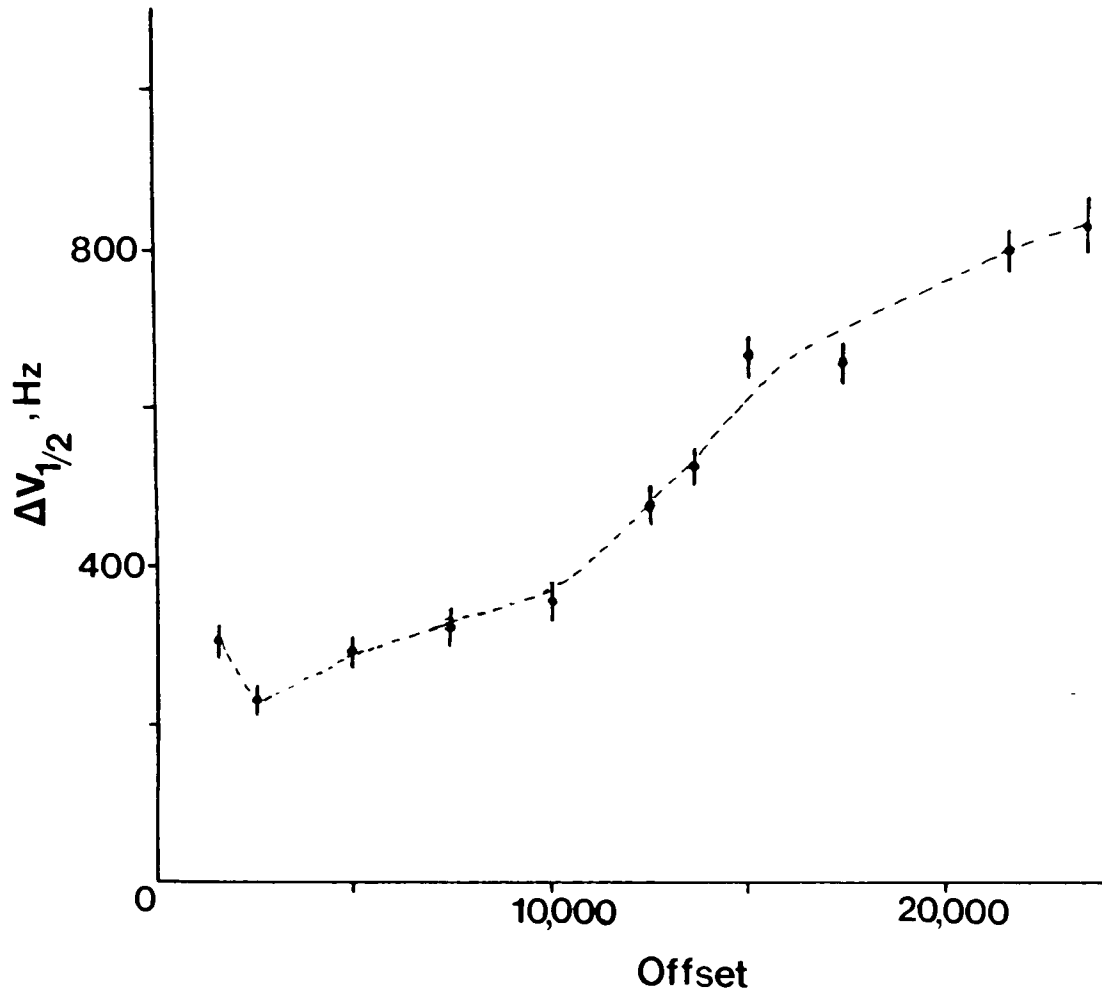


Figure 2.1

The effect of varying the frequency of decoupling on the linewidth in the solid state $^{31}P$ nmr spectrum of a tertiary phosphine.

decoupling was achieved in the $^{31}P$ spectra was determined by observing the effect of varying the decoupler field on the linewidth of a tertiary phosphine. This frequency, as shown in Figure 2.1, was well-defined. The optimum decoupling frequency for obtaining $^{13}C$ spectra of metal carbonyls was determined in a similar manner by Dr. L-Y. Lian.

### 2.3.3 Cross polarisation.

The cross polarisation (CP) technique was developed by Pines, Gibby and Waugh to enhance the nmr sensitivity of a dilute spin S in a solid [6]. The method aims to transfer magnetisation from an abundant species I, usually protons, to a dilute species S to which it is coupled. The species S may be either physically or chemically dilute in the sample, provided that the homonuclear dipolar interactions are small ( <1kHz).

In essence, the experiment consists of polarising the I spins and bringing them into contact with the S spins, which can be imagined as having no spin order. Polarisation is then transferred from the I to the S spins. The most widely used method of polarisation transfer is to allow both sets of spins to precess in their rotating frames at a common frequency. This may be visualised as the application of strong rf fields $B_{1I}$ and $B_{1S}$ at the respective I and S resonant frequencies. If the Hartmann-Hahn condition is satisfied, i.e.

$$\gamma_I B_{1I} = \gamma_S B_{1S}$$

the Zeeman levels in the rotating frame are matched and effective coupling between spins occurs via the dipolar interaction. After the transfer of polarisation, the decay of the S spin magnetisation is observed. Spin decoupling during the observation period is achieved by maintaining the high $B_{1I}$ field.

The sequence of events in the CP experiments described in

this thesis is shown in Figure 2.2. The procedure is as follows:-

(i) establish I spin polarisation in the static ($B_0$) field.

(ii) spin lock the I spin magnetisation along $B_{1I}$.

(iii) establish contact between the I and S spins by applying an rf field $B_{1S}$ to the S spins for a period of time D2 such that the Hartmann-Hahn condition is satisfied.

(iv) turn off the $B_{1S}$ field after allowing S magnetisation to build up, and observe the decay of the S spin magnetisation.

(v) turn off the $B_{1I}$ field and allow the spin systems to relax.

(vi) repeat the sequence.

In the experiments described here the Hartmann-Hahn condition was met using a $B_1$ field of 10G for $^1H$ and 24.7G for $^{31}P$ (39.8G for $^{13}C$).

A further gain in sensitivity may be achieved by repeating the contact between I and S spins ((iii) and (iv) above) before observation of the FID of the S spins. However as this requires the $B_{1I}$ field to be on for long periods of time it may lead to excessive heating of both electronics and sample. For the experiments in this thesis a single contact pulse sequence was used.

The efficiency of communication, and hence the rate of CP, between I and S spins is governed by the distance between the S atom and the nearest proton (the time constant for CP, $T_{SI}$, contains an $r_{SI}^6$ term) [7]. A non-protonated S atom will therefore generally cross polarise much more slowly than one which is protonated. Rapid internal motion such as the rotation of a methyl group will however reduce the effectiveness of the dipolar interactions between I and S spins. A study on the relative rates of CP of different carbon-containing groups [7] has shown them to follow the sequence:

$CH_3$ (static) > $CH_2$ > CH $\gtrsim$ $CH_3$ (rotating) > C (non-protonated)

Signal intensities in agreement with atomic ratios can be obtained

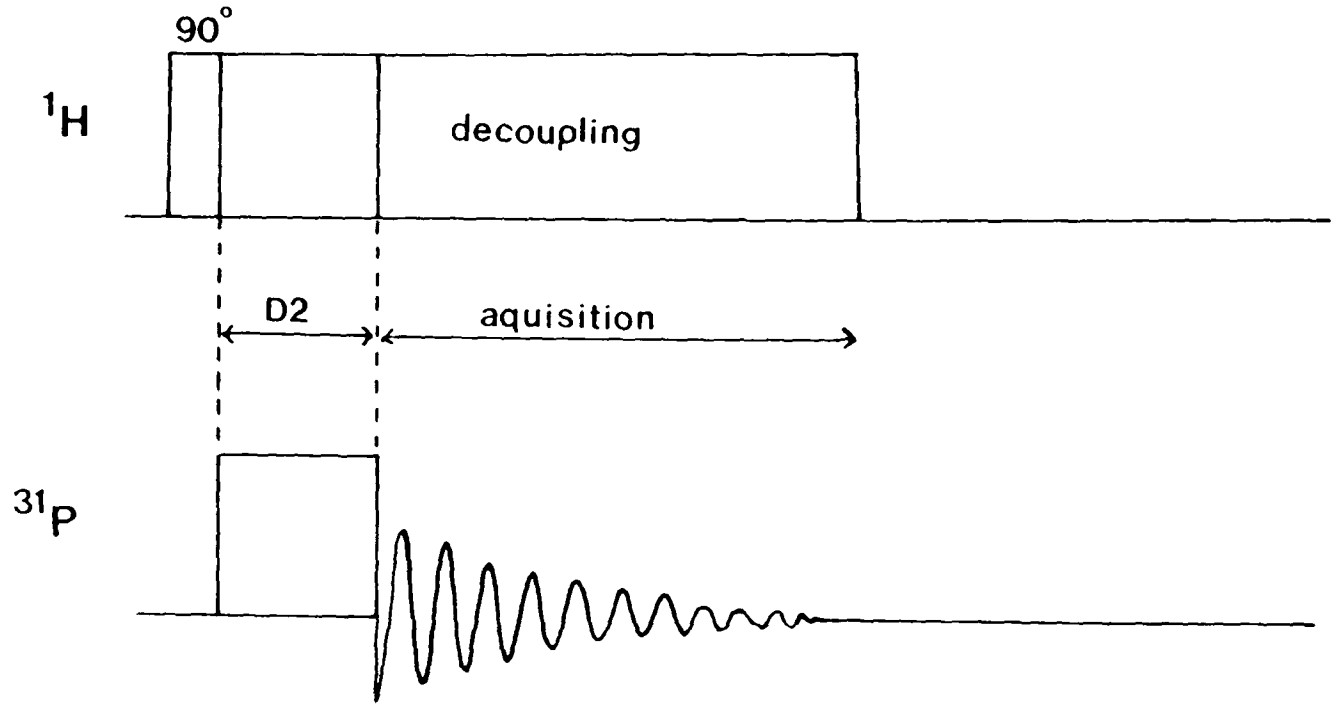


Figure 2.2

The pulse sequence used for the CP experiments.

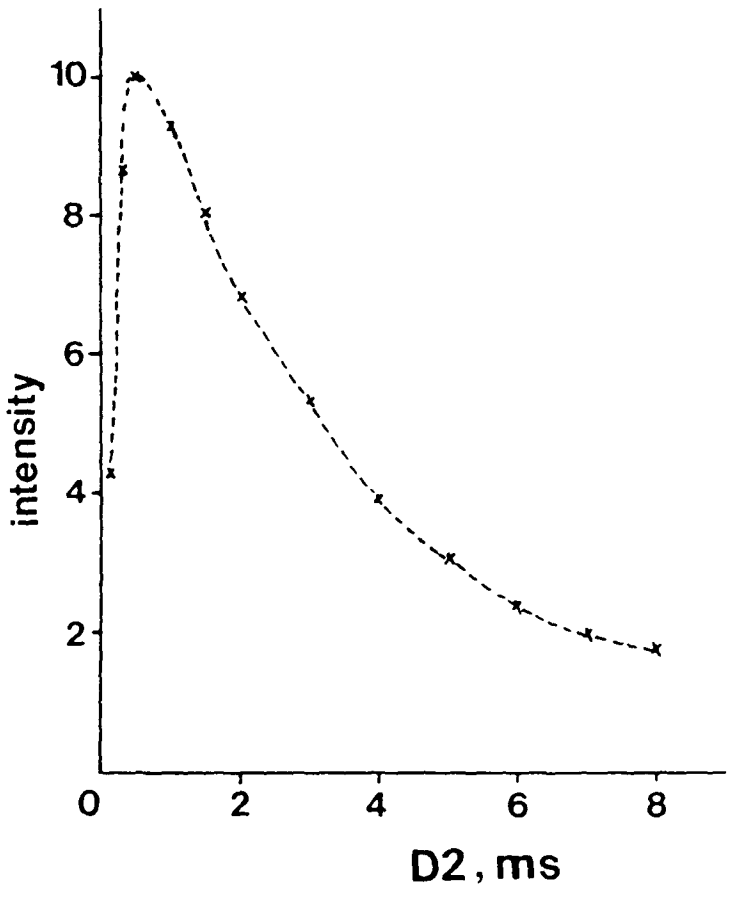


Figure 2.3

The effect of varying the contact time on the intensity of the phosphorus resonance for a tertiary phosphine.

from relatively proton-rich compounds using contact times often as short as 1ms provided that all of the S spins show similar CP behaviour. With compounds of low or remote protonation, accurate signal intensities cannot always be obtained [8]. On the basis of their different CP behaviour, specific structural units in the system under study can be selectively observed [9].

Variable CP time experiments were carried out on a number of the compounds studied in this work in order to determine the optimum CP time (D2). For a variety of transition metal phosphines efficient cross polarisation was observed using a contact time of 1.0ms (Figure 2.3). Before carrying out the phosphorus CP experiments the Hartmann-Hahn condition was optimised on sodium dihydrogen orthophosphate. In order to cross polarise the carbonyl groups from adjacent protons, a longer contact time of 2.0ms was used. Adamantane was used to set up CP conditions for the $^{13}C$ experiments.

The maximum enhancement of magnetisation which may be achieved by the use of CP is approximately equal to $\gamma_I/\gamma_S$. Thus for $^{13}C$ the signal is enhanced by a factor of 3.98, and for $^{31}P$ by 2.47. However a further improvement in signal-to-noise is obtained because the frequency of repetition of the pulse sequence is now dependent on $T_1^H$, the relaxation time of the protons, and not that of the dilute species $T_1^S$, which is generally much longer than $T_1^H$. This means that the recycle delay necessary is shorter, and in a given period of time more transients can be accumulated by using the CP method than with a simple one pulse experiment. For samples in which $T_1^H$ is also long, an nmr pulse sequence was used which included a pulse to flip any remaining $^1H$ magnetisation back to the z axis after accumulation of the S spin signal. This avoided the necessity to wait for the relaxation of the protons before the pulse sequence could be repeated.

2.3.4 Magic angle spinning.

The technique of magic angle sample spinning (MAS) was proposed independently by Andrew [10] and by Lowe [11] as a means of narrowing the nmr resonances obtained from solids, which are typically six orders of magnitude broader than those observed from liquid samples. This difference arises from the presence of anisotropic interactions, which are averaged out by rapid isotropic motion in liquids but remain in the solid state. In some solids, however, sufficient motion of the nuclei exists to reduce the linewidths such that a high resolution spectrum can be obtained. An example is the $^{31}P$ spectrum of polycrystalline $P_4S_3$ at 420K, for which a resolved $AB_3$ spectrum is observed [12]. The idea of imposing a physical motion upon the solid in an attempt to emulate nature was therefore formulated. An alternative and complementary approach, that of imposing a motion on the nuclei in spin space by means of a multiple pulse sequence, has also been developed successfully [13,14].

The major anisotropic interactions present in the solid state are homonuclear and heteronuclear dipolar coupling; the chemical shift anisotropy (CSA); the indirect electron coupled interaction; and the electric quadrupole interaction. An examination of the effect of rapid sample rotation on the Hamiltonians governing these interactions shows that, for rotation about an angle $\beta$ to the static field $B_0$, in all cases the spectrum retains an identical shape but is reduced in width by the factor

$$F(\beta) = 1/2(3\cos^2\beta - 1)$$

Thus rotation about an axis parallel to $B_0$ ($\beta = 0$) has no effect; rotation about an axis perpendicular to $B_0$ ($\beta = \pi/2$) should halve the spectral width; rotation about an axis at $54^{\circ}44'$ to $B_0$ should reduce the effect of all these interactions in the observed nmr spectrum to

zero. A high resolution spectrum comparable to that observed in solution should then be obtained, showing the isotropic chemical shift and any scalar (J) coupling present (except coupling to $^1H$, which will be removed if HPPD is applied). Experiments showed theory to be born out in practice, and the angle $54^o44'$ became known as the 'magic' angle in view of its singular properties [15].

The above discussion holds provided that the rate of sample rotation is large in comparison to the size of the interactions it aims to remove. In practice, speeds of up to 4kHz can be routinely obtained using a probe with a single nitrogen bearing. Inhomogeneous interactions such as the CSA are averaged by slower rates of rotation than homogeneous interactions. A line inhomogeneously broadened by the CSA breaks up almost immediately on sample rotation to give the isotropic peak and a train of rotational echoes spaced at the spinning frequency (Figure 2.4); these satellites disappear when the rate of rotation $\omega_r$ is greater than the CSA, and all the intensity is concentrated in the isotropic peak. Two methods of extracting the principle components of the shielding tensor from the intensities of the spinning sidebands have been developed [16,17], which should provide structural information additional to that contained in the chemical shift. These are discussed in detail in chapter 3. In some cases when the CSA is large, the isotropic resonance is not the most intense peak in the spectrum. The simplest way of identifying the isotropic peak from amongst the sidebands is to compare spectra obtained at different spinning speeds: the peak which does not alter its position upon change of speed is the isotropic resonance (Figure 2.4). In a spectrum showing two or more resonances it may also be necessary to vary the spinning speed in order to prevent a sideband from overlapping with an isotropic peak. Techniques for the total

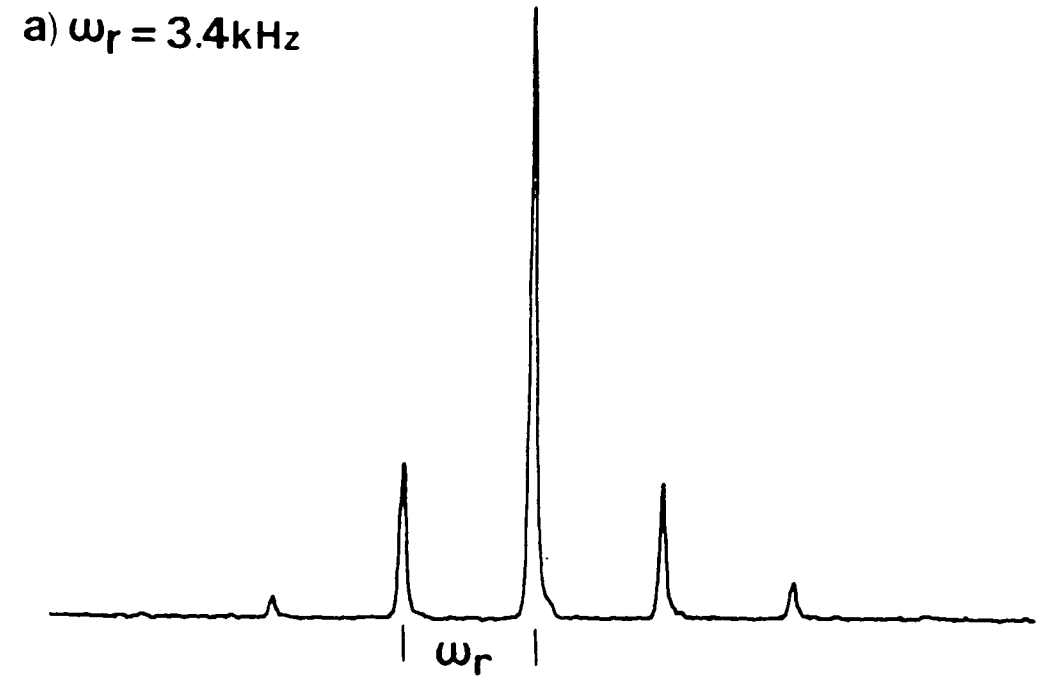


Figure 2.4

Solid state $^{31}P$ spectra of sodium dihydrogen orthophosphate spinning at the magic angle at two different speeds, showing the spinning sidebands resulting from the phosphorus chemical shift anisotropy.

suppression of spinning sidebands have been developed [4] to deal with situations of this type, and were used for some of the experiments in this thesis (section 2.3.1).

Figure 2.5 illustrates the effectiveness of MAS in suppressing the linebroadening from anisotropic interactions to produce a high resolution spectrum. The technique overlaps to some extent with HPPD (section 2.3.2), with both methods reducing the dipolar coupling between I and S spins (provided that the rate of MAS is large with respect to the magnitude of the coupling). However the additional benefits of MAS in removing other anisotropic interactions make the two techniques complementary. The different line narrowing effects of the methods discussed here in solid state nmr spectra are compared in Figure 2.5 in the case of adamantane [18]. Both HPPD and MAS will individually enable the two carbon sites to be resolved; a combination of the two results in further narrowing of the resonances, and the addition of CP provides a four-fold increase in signal-to-noise ratio.

In order to obtain maximum resolution in an MAS spectrum, the angle setting must be accurate. For every degree of deviation of the spinning axis from $54^{o}44'$ a line broadening of 2.5% of the static linewidth is introduced [19], distorting the lineshape towards that of the static (non-spinning) spectrum. It is possible to adjust the angle by observing the spectrum of a reference material such as hexamethylbenzene before inserting the sample of interest. However there are a number of problems inherent in this approach. The exact angle at which the spinner rotates is sensitive to such factors as gas pressure, spinner geometry, sample packing and sample density, and as a consequence is not exactly reproducible upon change of sample.

A simple technique for setting the magic angle suggested by

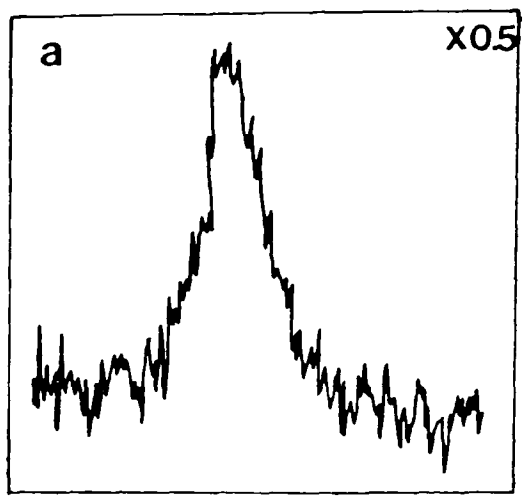


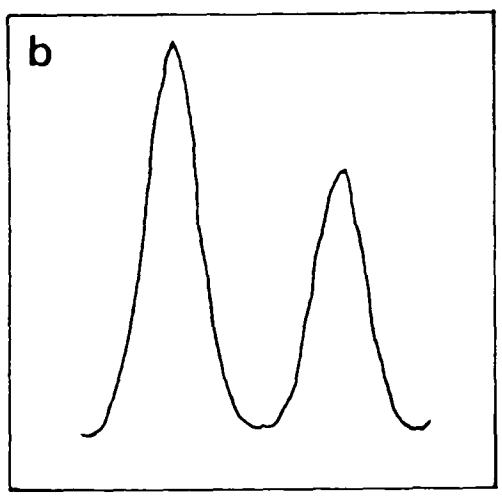


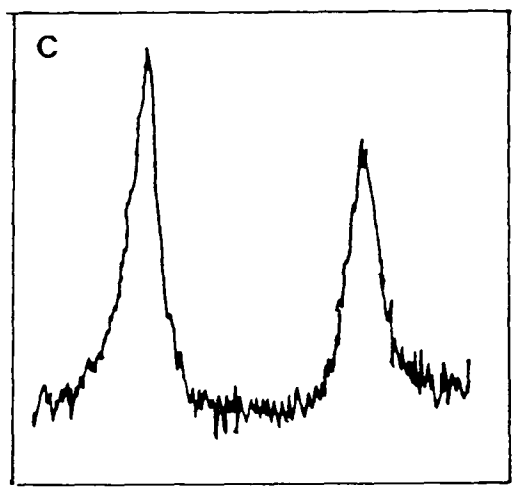


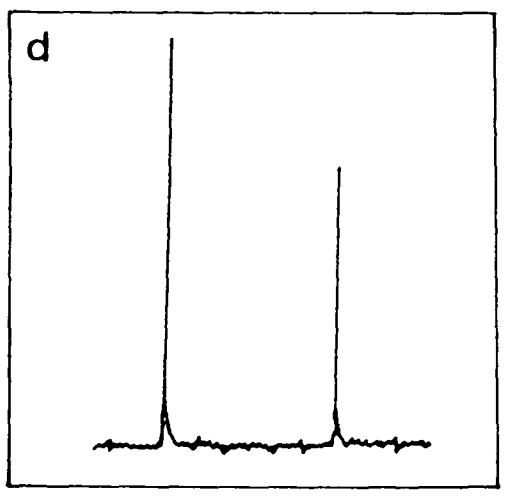


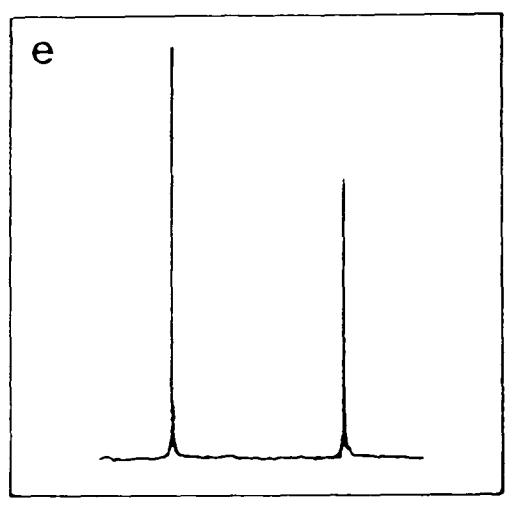


Figure 2.5

The effect of high power proton decoupling, magic angle spinning and cross polarisation on the solid state $^{13}C$ spectrum of adamantane.

(a) No decoupling or rotation (b) HPPD only (c) MAS only (d) MAS and HPPD (e) CP/MAS and HPPD: S/N increases 4x.

Frye and Maciel [3] has been shown to enable rapid and accurate angle adjustment to be made. This involves adding a small quantity of a compound containing a quadrupolar nucleus with half-integer spin to the sample of interest. If the nuclear environment is highly symmetric, the MAS spectrum of the quadrupolar nucleus shows a single sharp isotropic resonance (corresponding to the 1/2-1/2 transition) when the angle is improperly adjusted, but when the spinning axis is close to $54^{o}44'$ to the static field a large number of spinning sidebands are observed (Figure 2.6). By optimising the number and resolution of the sidebands adjustment of the spinning axis can be made to within $0.1^{o}(6')$ of the magic angle. The high sensitivity and short relaxation time of the $^{79}Br$ nucleus (I = 3/2) make it ideal for this purpose. In addition, the closeness of the $^{79}Br$ resonance to that of $^{13}C$ enables the bromine signal to be acquired without the need to retune the probe. Angle adjustment by this method is therefore generally carried out by adding potassium bromide to the sample of interest.

For the experiments described in this thesis the use of KBr to set the angle of sample rotation correctly was found to be highly successful. The compound was generally not mixed with the sample to be studied, but was separated from it in the rotor by a paper disc. Because the sidebands in the frequency spectrum correspond to modulations in the time domain, they may be recognised as spikes in the FID, and, as suggested by Frye and Maciel [3], the angle can be adjusted by observing the FID without the need to use the Fourier-transformed spectrum. This was the method adopted in this work (Figure 2.6c). Once adjusted for a particular sample, the angle was found to be stable for spinning speeds greater than 1.0kHz. The effect of varying the axis of sample rotation is illustrated in Figure 2.7.

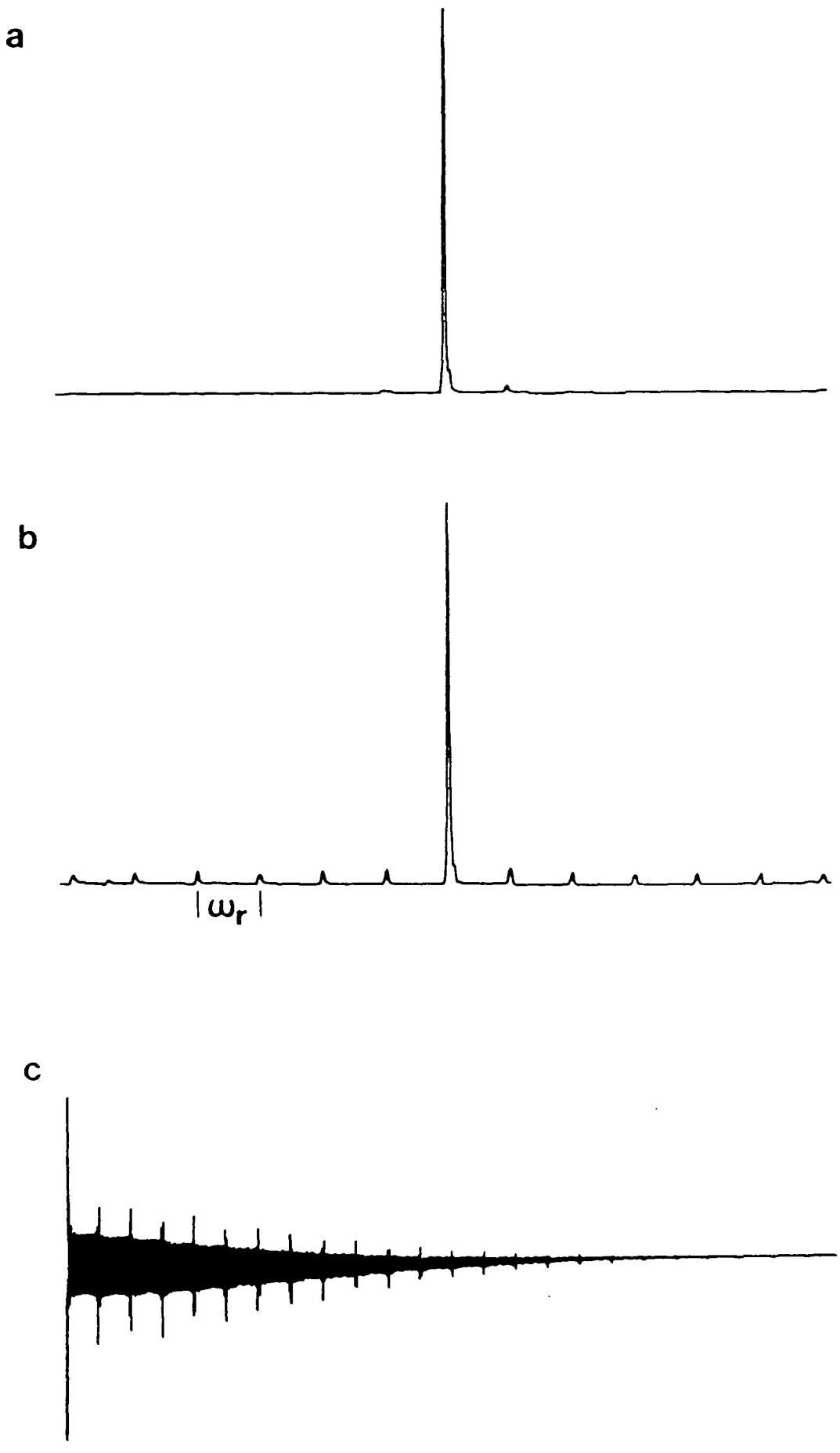


Figure 2.6

The $^{79}Br$ spectrum of KBr (a) spinning off angle (b) spinning at the magic angle. (c) The FID, showing the modulation corresponding to the spinning sidebands.

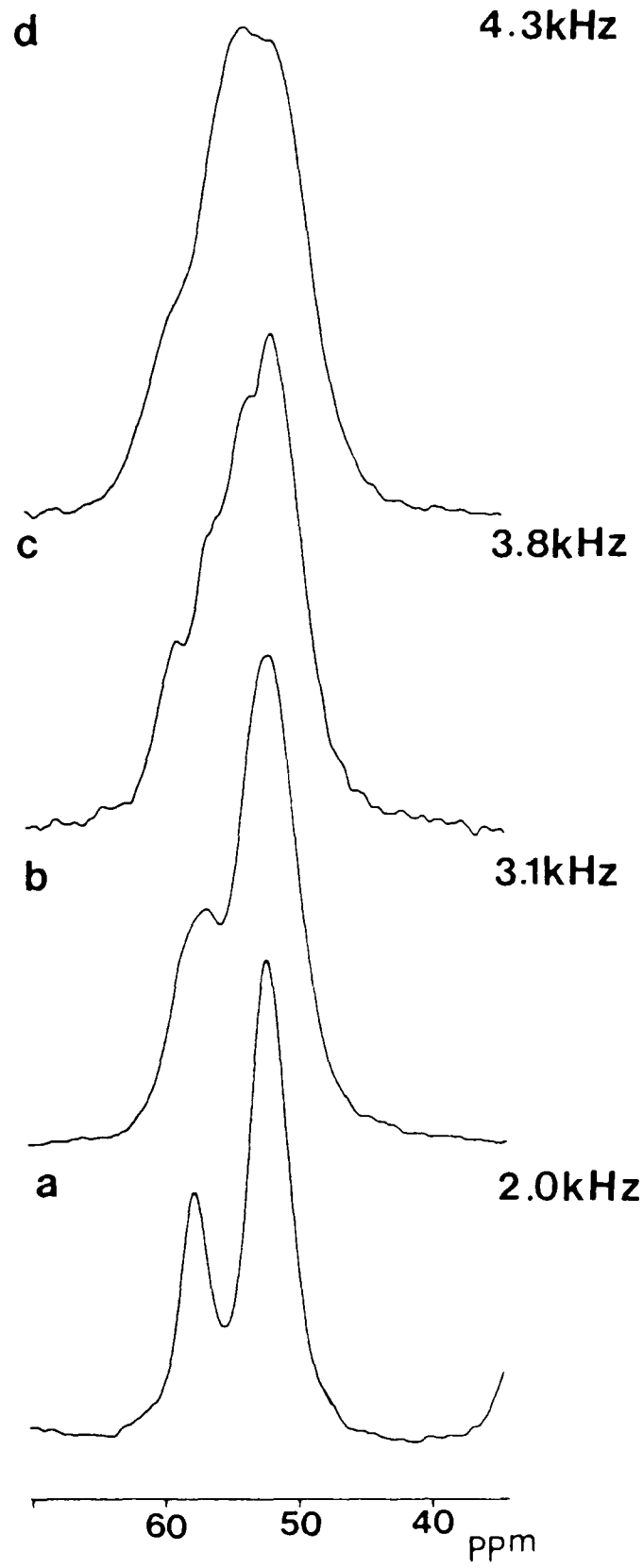


Figure 2.7

The effect of altering the magic angle on the two isotropic $^{31}P$ resonances of $[Au_9(P(p\text{-}C_6H_4OMe)_3)_8](BF_4)_3$. The angle was set at a spinning speed of 2.0kHz and the speed was then increased for successive spectra, altering the angle of sample rotation.

Improper adjustment of the magic angle may be detected by comparing the lineshape of an isotropic resonance with those of its manifold of spinning sidebands. If they are not closely similar, it is highly probable that the axis of rotation is not at $54^{o}44'$ to the static field.

## 2.4 Computational methods.

All of the computer programmes described here were run on the VAX 11/785 computer of the Oxford University Computing Service.

### (a) MOMCAL.

The moment analysis of the sideband intensities was performed using the program MOMCAL [16], which calculates the second and third moments from the input sideband intensities and the spinning speed. From these moments the chemical shift anisotropy $\delta$ and the asymmetry parameter $\eta$ can be derived where $\delta = \sigma_{33} - \sigma_{iso}$ and $\eta = \sigma_{11} - \sigma_{22}/\sigma_{33} - \sigma_{iso}$. Knowledge of $\delta$, $\eta$ and $\sigma_{iso}$ yields the principle components of the shielding tensor. The program was written by Dr. M.M. Maricq at MIT and modified for use in Oxford by Dr. N.J. Clayden.

### (b) POWSIM.

Powder pattern simulations were obtained using the POWSIM program in which the lineshape is computed directly from the analytical expression [5] for the shape of a powder pattern using the input values of the principle components of the shielding tensor. The lineshape is then convoluted by a Gaussian linebroadening. The program was written by Dr. N.J. Clayden.

(c) SIMNORM.

This program simulates the lineshape of the isotropic resonances obtained in a high resolution spectrum [5]. The isotropic chemical shifts are input and the data is convoluted with a Lorentzian linebroadening.

(d) SPIN.

Simulations of the MAS spectra were performed using the program SPIN based on the method outlined by Maricq and Waugh [16] which was written by Dr. N.J. Clayden. This involves calculating the free induction decay of the sample spinning at the magic angle. A rotational echo is calculated by evaluating this for a series of equally spaced intervals in the rotational period (0, $2\pi/\omega_r$) with the spacing chosen to ensure an adequate spectral width. Powder averaging was initially carried out over 0 to 180° in 2° steps. Increasing the powder average increment to 5° caused no significant changes in sideband intensities and given the time consuming nature of the 2° steps, taking over 30 min CPU time on the VAX computer, further powder averaging was carried out with 5° steps. After powder averaging the rotational echo was replicated to give either 512 or 1024 points in the time domain. An appropriate offset was added to the FID to give the correct isotropic resonant frequency and the FID was then apodised using a Gaussian function. Finally the FID was Fourier transformed to give the spinning sideband pattern.

(e) Herzfeld-Berger analysis.

Analysis of the ratios of the sideband intensities was carried out using the graphical method of Herzfeld and Berger [17]. The ratios of the sideband intensities were used to construct contour

plots, with the intersection of the contours giving values of the quantities $\mu$ and $\rho$. These are defined as $\mu = (\gamma B_0)(\sigma_{33} - \sigma_{11})/\omega_r$ and $\rho = (\sigma_{11} + \sigma_{33} - 2\sigma_{22})/(\sigma_{33} - \sigma_{11})$. From $\mu$, $\rho$, $\omega_r$ and the isotropic chemical shift the principle components of the shielding tensor may be obtained. In general, it is found that due to experimental errors the contours do not all intersect at one point: the degree of dispersion gives a measure of the uncertainty of $\mu$ and $\rho$.

## 2.5 Linewidths in solid state spectra.

Despite the use of the experimental techniques discussed earlier (HPPD and MAS) to produce high resolution solid state nmr spectra, the linewidths observed in the solid state are considerably greater than those measured in solution. The widths of the lines in the solid state spectra will be affected by factors associated with the experimental techniques, and an inhomogeneous magnetic field, inaccurate adjustment of the magic angle, rotor instability, off resonance decoupling or insufficient decoupling power will all lead to broadening of the resonances [19]. However these do not fully account for the observed differences in resolution between the spectra obtained in the two states.

One possible cause of broad resonances in solid state spectra are residual dipolar interactions resulting from the presence of quadrupolar nuclei in the molecule under investigation. If the quadrupolar interaction of the coupled nucleus is comparable in magnitude to the nuclear Zeeman interaction, the dipolar coupling will not be removed by MAS [20]. This is observed, for example, for the $^{13}C$ resonances of carbon atoms bonded to $^{14}N$ [20,21]. Counterions containing quadrupolar nuclei, such as $AlCl_4^-$, may also cause dipolar broadening, although this disappears if there is fast motion of the

counterion in the solid [22].

Excluding residual dipolar interactions, one of the most important factors determining linewidth is the degree of order in the solid sample under investigation. For highly crystalline materials, linewidths of the order of 0-3ppm are generally observed; these may reach 15ppm for amorphous solids such as glasses [23]. The broadening results from disorder in the molecular environment in the latter materials, which produces a distribution of crystalline environments for chemically equivalent nuclei. This disorder may be a variation in molecular conformations, in bond angles or in the next nearest neighbour distances, or may be the result of random molecular packing. For crystalline solids, anisotropy of the bulk magnetic susceptibility has been shown to produce significant line broadening, of the order of 0.7ppm [19]. This is analogous to the ring current shifts observed in solution spectra.

If the nmr spectrum is partially narrowed by molecular motion in a solid, in some cases MAS will not remove the remaining width [15]. In the case of fast restricted motion, for example about a defined molecular axis, the microscopic motion makes the task of macroscopic narrowing easier, needing only rotation at a rate comparable to the already reduced linewidth. However, if isotropic molecular rotation and diffusion is occurring in the solid sample, the frequency of MAS must be greater than that of the isotropic motion in order to produce further narrowing of the line. Motion of the order of the decoupler frequency will also lead to line broadening.

The conclusion of a study by VanderHart, Earl and Garroway [19] was that, with the exception of the spectra of rare solids such as adamantane, $^{13}C$ resonance lines in the solid state would never be as narrow as those observed for liquids. However this is not

necessarily such a gloomy picture. These linewidths may well be a souce of information on the interactions in the solid state which produce them, and so be of at least some value to the solid state nmr spectroscopist.

## 2.6 A comparison of solution and solid state nmr spectra.

The aim of this section is to discuss some of the factors which should be born in mind when comparing solution and solid state nmr spectra. The results obtained in the two states are not necessarily interconvertible, but in general a close similarity between solid state chemical shifts and their solution counterparts has been observed [24]. However a feature of some solid state spectra is the occurrence of additional lines not found in solution. There are a number of reasons as to why these 'extra' lines may occur.

A difference between the solution and solid state spectra of a molecule will, not surprisingly, be observed if it adopts a different structure in the two states. An extreme example is the compound $PCl_5$, which in the solid exists as $PCl_6^-PCl_4^+$ [25]. More frequently, the crystal lattice imposes a particular conformation upon a molecule, often by freezing out the free rotation of bulky substituents, and this renders atoms or groups which are equivalent in solution inequivalent in the solid state. Such intramolecular effects have been observed for aromatic ring carbons, which generally exist in asymmetric conformations in the solid state, making adjacent carbon atoms magnetically inequivalent; examples studied include peptides [26,27] and a series of substituted biphenyls [28]. Intramolecular hydrogen bond formation may also lead to the loss of molecular symmetry and thus to the splitting of spectral lines in solid state spectra [24].

More subtle, intermolecular, effects occur when the site of a molecule in the crystal lattice is of lower symmetry than that of the isolated molecule. Chemically equivalent nuclei then become inequivalent in the bulk crystalline solid, and additional resonance lines occur. This has been observed by Fyfe and co-workers [1] for the complex $PtCl_2(PPh_3)_2$, which shows a single $^{31}P$ resonance in solution but two lines in the solid state spectrum. The spectra have been interpreted as the result of the lattice fixing the conformation of the phosphine groups to make them inequivalent in the solid, whilst in solution rotation about the Pt-P bond makes the two equivalent, a conclusion in agreement with the X-ray crystal structure.

In principle, separate resonance signals could be observed from all of the nuclei in a molecule which are at inequivalent sites in the unit cell. Whether this is found in practice depends on the resolution of the experiment. For example, in a solid state $^{13}C$ nmr study of calcium, strontium and barium acetates the spectra unexpectedly showed evidence of four resonances in both carbonyl and methyl regions [29]. It was suggested that these resonances resulted from four inequivalent acetate sites in the unit cell. The crystal structures of two of the compounds were then determined; these confirmed the nmr results, showing in both cases the presence of four inequivalent acetate groups in the unit cell.

Polymorphism, too, is relatively common. X-ray diffraction studies are carried out on single crystals, whilst most nmr experiments use a bulk sample which may not be the identical conformer to the single crystal, and may even contain a mixture of polymorphs. The presence of more than one polymorph in the nmr sample will produce additional lines in the nmr spectrum.

Another possible cause of additional lines is the presence of

a quadrupolar nucleus adjacent to the nucleus under observation, as the dipolar interaction between the nuclei may not then be removed by MAS [20]. This may result in either a broadening of the nmr resonance (section 2.5) or a splitting of the line. For $^{13}C$ adjacent to $^{14}N$, such splitting produces an asymmetric doublet in the solid state $^{13}C$ nmr spectrum [20,21]; for phosphorus adjacent to copper, an asymmetric quartet is observed in the $^{31}P$ nmr spectrum [30].

Intermolecular interactions in the solid state may prevent motions necessary for chemical exchange to occur, and thus freeze out processes fast in solution; this will again lead to more resonances in the solid state spectrum than are observed in the solution spectrum. In semibullvalene, for example, the exchange process occurring in solution can only be frozen out at a temperature of -185°C, but there is no evidence for any such exchange in the solid state [31].

However, despite these possible differences between solution and solid state nmr spectra, in general there is a good correspondence between the two. When 'extra' lines do occur, their sources can usually be identified by a consideration of the structure of the compound under investigation, often providing information on the way either this structure or the motional properties of the molecule alter upon change of state. These differences between solution and solid state spectra reflect the sensitivity of magnetic nuclei to small changes in the structure and motion of the molecules containing them which make nmr a sensitive probe of relatively subtle effects on a molecular level.

## 2.7 References.

[1] L. Bemi, H.C. Clark, J.A. Davies, C.A. Fyfe and R.E. Wasylishen, J. Amer. Chem. Soc. 104 (1982) 438.

[2] S. Shinoda, K. Nakamura and Y. Saito, Chem. Lett. (1983) 1449.

[3] J.S. Frye and G.E. Maciel, J. Magn. Res. 48 (1982) 125.

[4] W.T. Dixon, J. Phys. Chem. 77 (1982) 1800.

[5] M. Mehring, 'Principles of high resolution NMR in solids', 2nd ed., Springer-Verlag, Berlin (1983).

[6] A. Pines, M.G. Gibby and J.S. Waugh, J. Chem. Phys. 59 (1973) 569.

[7] L.B. Alemany, D.M. Grant, R.J. Pugmire, T.D. Alger and K.W. Zilm, J. Amer. Chem. Soc. 105 (1983) 2133.

[8] Ibid., 2142.

[9] G.E. Maciel and D.W. Sindorf, J. Amer. Chem. Soc. 102 (1980) 7606.

[10] E.R. Andrew, A. Bradbury and R.G. Eades, Nature 182 (1958) 1659.

[11] I.J. Lowe, Phys. Rev. Lett. 2 (1959) 285.

[12] E.R. Andrew, W.S. Hinshaw and A. Jasinski, Chem. Phys. Lett. 24 (1974) 399.

[13] P. Mansfield and D. Ware, Phys. Rev. Lett. 22 (1966) 133.

[14] E.D. Ostroff and J.S. Waugh, Phys. Rev. Lett. 16 (1966) 1097.

[15] E.R. Andrew, Int. Rev. Phys. Chem. 1 (1981) 195.

[16] M.M. Maricq and J.S. Waugh, J. Chem. Phys. 70 (1979) 3300.

[17] J. Herzfeld and A.E. Berger, J. Chem. Phys. 73 (1980) 6021.

[18] Bruker catalogue of solid state spectra (1983).

[19] D.L. VanderHart, W.L. Earl and A.N. Garroway, J. Magn. Res. 44 (1981) 361.

[20] J.G. Hexem, M.H. Frey and S.J. Opella, J. Chem. Phys. 77 (1982) 3847.

[21] J.G. Hexem, M.H. Frey and S.J. Opella, J. Amer. Chem. Soc. 103 (1981) 224.

[22] C.A. Fyfe, J.R. Lyerla and C.S. Yannoni, Acc. Chem. Res. 15 (1982) 208.

[23] C.A. Fyfe, 'Solid state NMR for chemists', CFC Press, Guelph (1983).

[24] E.T. Lippmaa, M.A. Alla, T.J. Pehk and G. Engelhardt, J. Amer. Chem. Soc. 100 (1978) 1929.

[25] E.R. Andrew, A. Bradbury, R.G. Eades and G.J. Jenks, Nature 188 (1960) 1096.

[26] L.G. Pease, M.H. Frey and S.J. Opella, J. Amer. Chem. Soc. 103 (1981) 467.

[27] M.H. Frey and S.J. Opella, J. Chem. Soc., Chem. Commun. (1980) 474.

[28] A.M. Chippendale, R.S. Aujla, R.K. Harris, K.J. Packer and S. Purser, Magn. Res. Chem. 24 (1986) 81.

[29] C.J. Groombridge, R.K. Harris, K.J. Packer, M.B. Hursthouse and N.P.C. Walker, J. Solid State Chem. 59 (1985) 306.

[30] J.W. Diesveld, E.M. Menger, H.T. Edzes and W.S. Veeman, J. Amer. Chem. Soc. 102 (1980) 7935.

[31] R.D. Miller and C.S. Yannoni, J. Amer. Chem. Soc. 102 (1980) 7396.

# CHAPTER 3

## Chemical shift tensor analyses and simulations of slow MAS spectra.

### 3.1 Introduction.

The shift in resonant frequency between nuclei in different chemical environments (the chemical shift) is represented by a second rank tensor [1], which in solution is averaged by rapid isotropic motion to $\sigma_{iso}$, given by the trace of the tensor. In the solid state, however, the three principal components of the shielding tensor can be observed. One of the advantages of solid state nmr is that it allows the determination of the chemical shift tensor: this in principle provides more information about the local chemical environment of the nuclei than the isotropic chemical shift. However there have as yet been few empirical correlations reported between the chemical shift tensor and structural features ([2] and references therein), and in general the compounds studied have been too complex for ab initio calculations of the shielding tensor [3,4].

Assuming that the information provided by the principal components of the shielding tensor can be interpreted, how can the experimental values be obtained accurately? Nmr studies on single crystals involving rotation about defined axes are the most satisfactory means of obtaining the shielding tensor information [2], allowing the orientation of the principal axes of the shielding tensor in the molecular frame. For materials that cannot be obtained as single crystals, the principal components of the chemical shift tensor may be measured directly from the powder spectrum [5] or inferred from a computer fit to the lineshape. If more than one chemically distinct nucleus is present, and if the powder patterns overlap, this type of analysis can be extremely difficult. A number of methods have been

developed to overcome this problem. These include (i) one-dimensional experiments with off-angle fast spinning, giving powder patterns sufficiently scaled to avoid overlap [6]; (ii) slow spinning at the magic angle followed by interpretation of the resulting spinning sidebands [7,8]; (iii) 2-D methods in which the powder patterns are obtained in the second dimension [9,10]. Slow MAS is probably the most widely applicable of these methods. The chemical shift tensor is averaged to an isotropic resonance and a series of sidebands spaced at the spinning frequency, the intensities of which are related to the chemical shift anisotropy. Provided that the nuclei have different isotropic chemical shifts, the isotropic resonance of each nucleus and its series of sidebands may be resolved [11]. Two methods have been proposed to derive the principal components of the shielding tensor from the slow spinning MAS spectrum: a moment analysis of the sideband intensities [7] and a graphical method based on the ratio of the sideband intensities to the isotropic resonance intensity [8]. Having experienced difficulties with obtaining consistent results for near axial tensors with both of these methods, the use of simulations of slow-spinning MAS spectra as a method of analysing the spectra was explored before attempting to draw structural conclusions from the anisotropy data. Although simulations of MAS spectra have been suggested as a means to refine the tensor components obtained in a moment analysis [7] there have been few reported examples of their use [7,12,13]. In this chapter the results of MAS spectral simulations are discussed, and the tensor components derived from the simulations are compared with those obtained from powder patterns and from the initial sideband analysis.

## 3.2 Materials and methods.

Sodium dihydrogen orthophosphate (BDH) and triphenyl phosphine oxide (Aldrich) were used as supplied. $\alpha Zn_3(PO_4)_3$ and $Zn_{2.75}Mg_{0.25}(PO_4)_2$ were kindly lent by R. Jakeman. Magic angle spinning was carried out at speeds ranging from 1.2kHz to 3.7kHz. Spectra of proton-containing samples were accumulated with high power proton decoupling and cross-polarisation, using a contact time of 1.0ms.

Moment analysis of the sideband intensities was performed using the program MOMCAL [7], which computes the second and third moments from the input sideband intensities and the spinning speed (section 2.4(a)). Analysis of the ratios of the sideband intensities was carried out using the graphs of Herzfeld and Berger [8] (section 2.4(e)). Powder pattern simulations were obtained from the POWSIM program, in which the lineshape is computed directly from the analytical expression [1] (section 2.4(b)). Simulations of the MAS spectra were performed using the program SPIN based on the method outlined by Maricq and Waugh [7]. (section 2.4(c)).

## 3.3 Results.

### 3.3.1 Sodium dihydrogen orthophosphate.

The static powder nmr spectrum of sodium dihydrogen orthophosphate is typical of a non-axial pattern. In absorption mode it is difficult to distinguish $\sigma_{11}$ from $\sigma_{22}$ due to the natural line-broadening caused by $^{31}P$-$^{31}P$, $^{23}Na$ dipole-dipole interactions. In the derivative mode, however, this distinction is readily made, but the measurement of the principal components of the shielding tensor is not straightforward because the convolution of the lineshape by a broadening function causes the true values of the tensor components to

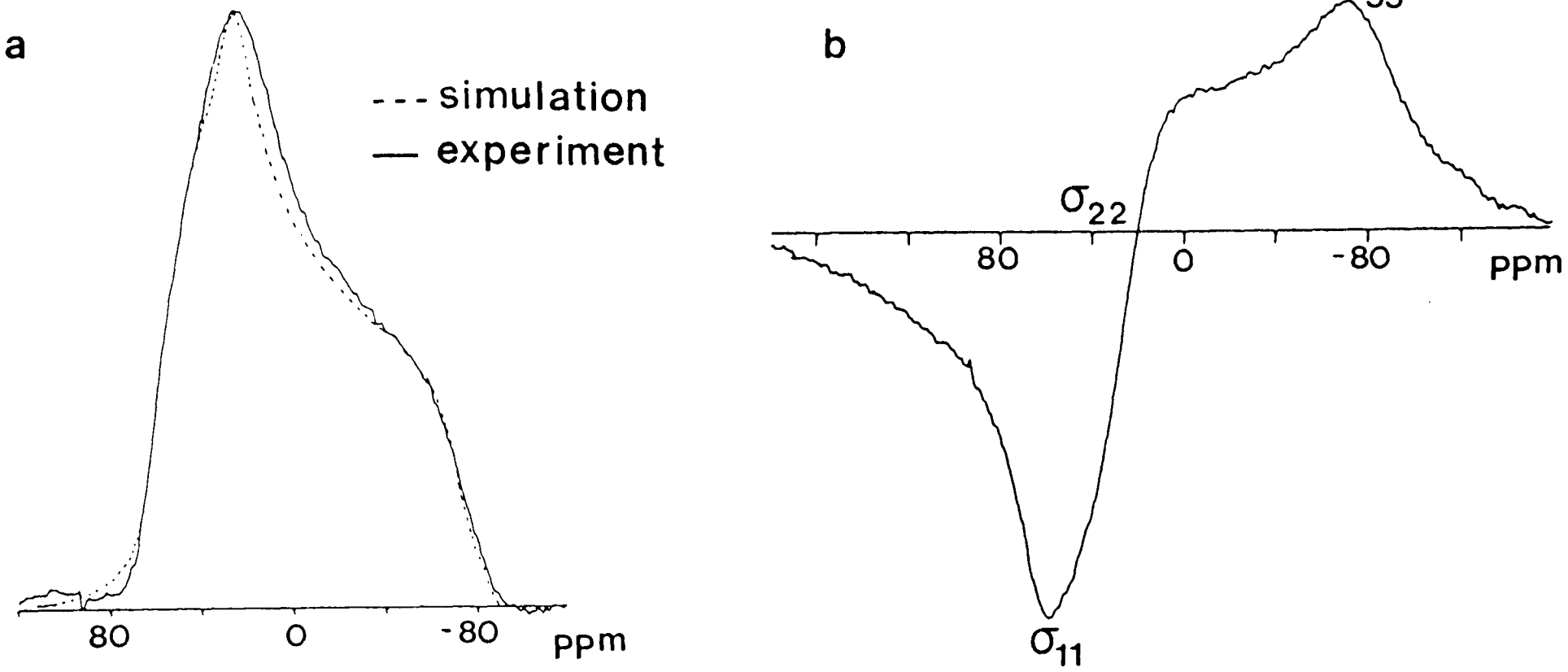




Figure 3.1

Non-spinning $^{31}P$ spectra of sodium dihydrogen orthophosphate.

(a) Comparison of experimental spectrum in absorption mode with a simulation obtained using tensor components of +60, +27, -70ppm.

(b) Experimental spectrum in derivative mode.

be displaced from the maxima in the derivative plot. This, together with the uncertainty in the phasing of a broad line spectrum, is estimated to lead to an experimental error of ±5ppm in the tensor components measured directly from the spectrum. A close agreement is seen between the observed and simulated static spectra using for the simulation the tensor components shown in Table 3.1 and with a linebroadening of 1000 Hz (Figure 3.1), demonstrating that the measured tensor components are truly representative of the shielding tensor.

Moment analysis of the sidebands in the slow spinning MAS spectrum was carried out for two different spinning speeds. A typical slow spinning spectrum is shown in Figure 3.2, and Table 3.1 shows the chemical shift tensor components derived from the MOMCAL calculations. The tensor components obtained for the two spinning speeds are equal within experimental error, revealing excellent internal consistency, and are in good agreement with the static pattern values.

In order to obtain accurate results from a moment analysis $M_2$ and $M_3$ must be accurately determined. Their values are strongly dependent on the higher order spinning sidebands. Experimentally, however, the highest order sidebands will be lowest in intensity; they may be obscured by noise and thus not included in the moment analysis. The effect of this was considered by repeating the analysis neglecting the highest order sidebands. A significant effect on the tensor components was found, although not all of the principal values were equally affected. Overall, as expected, neglecting higher order sidebands reduces the apparent chemical shift anisotropy: this reduction is in excess of the experimental error in the tensor components measured from the static spectrum, despite removing sidebands of only 1% of the intensity of the most intense sideband.

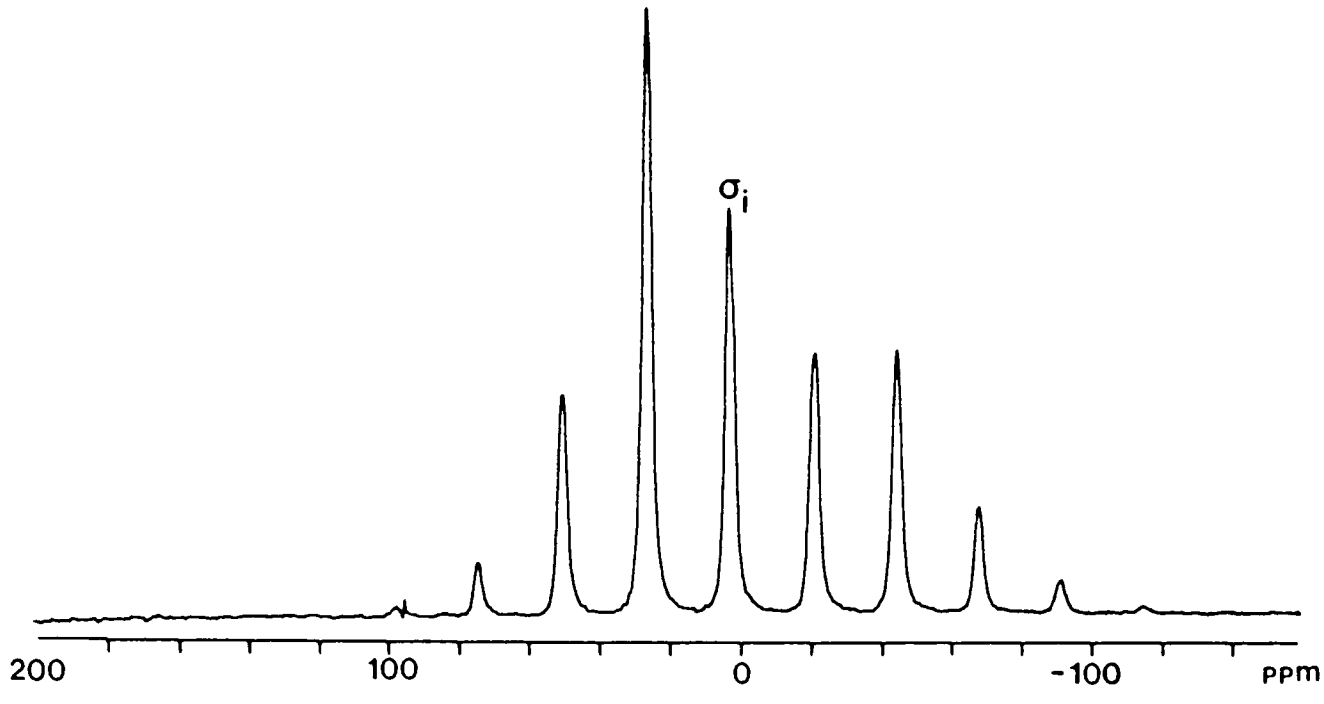


Figure 3.2

Slow MAS spectrum of sodium dihydrogen orthophosphate (20 scans, spinning speed 1.9kHz).

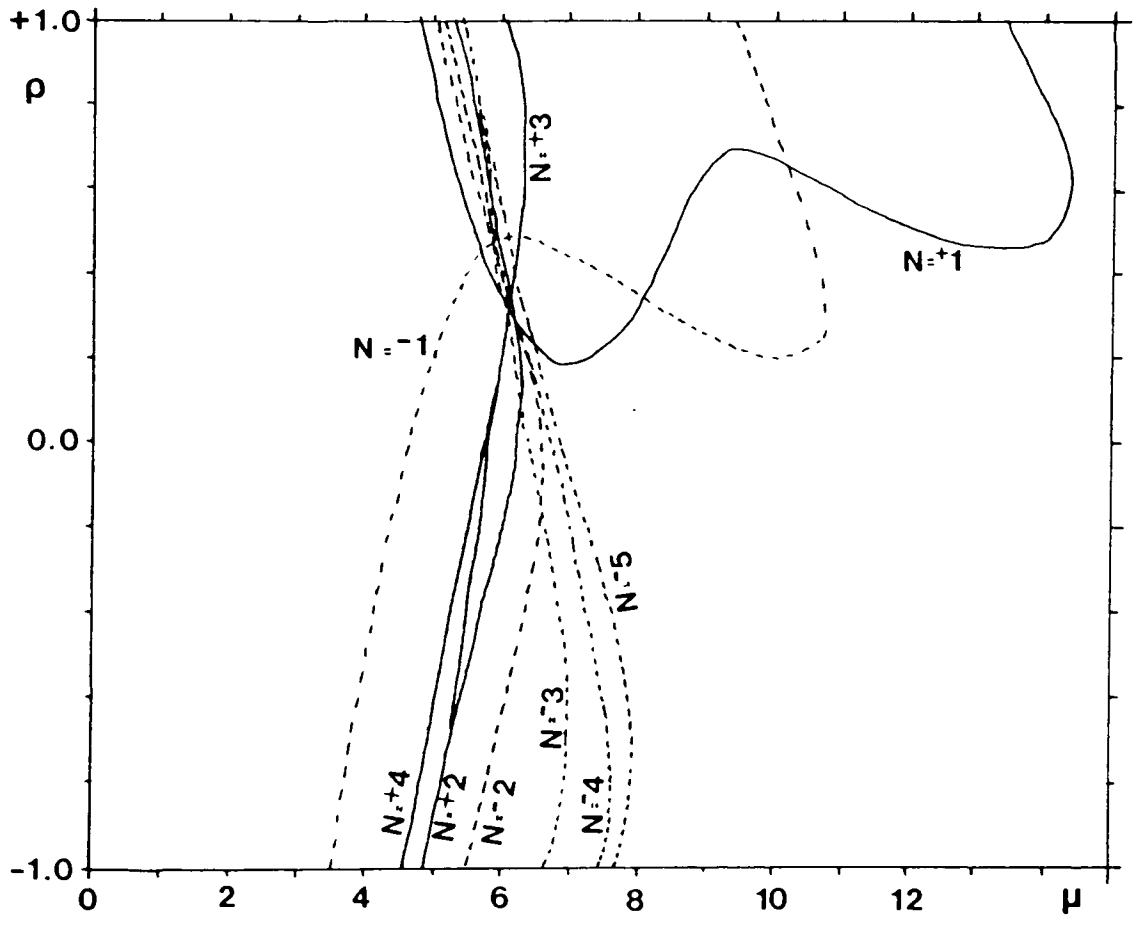


Figure 3.3

Contour plot for sodium dihydrogen orthophosphate spinning at 1.9kHz, using the method of Herzfeld and Berger [ 8 ]. Intersection of contours occurs at $\rho = 0.36$, $\mu = 6.0$.

TABLE 3.1

Results of sideband analysis for sodium dihydrogen orthophosphate.

| Method of analysis | $\sigma_{11}$ | $\sigma_{22}$ | $\sigma_{33}$ |
|---|---|---|---|
| Moment analysis (fast) | -62 | -20 | 76 |
| Moment analysis (slow) | | | |
| --complete data set | -64 | -24 | 80 |
| --omitting +5 | -67 | -17 | 76 |
| --omitting +5,-4 | -61 | -23 | 77 |
| --omitting +5,+4,-4 | -66 | -11 | 69 |
| Graphical (fast) | -60 | -22 | 76 |
| Graphical (slow) | -64 | -19 | 76 |
| Experimental | | | |
| --absorption mode | -54 | -27 | 76 |
| --derivative mode | -60 | -20 | 72 |

All tensor values are given in ppm.

Clearly accurate shielding tensor components can only be obtained from a moment analysis of spectra with excellent signal-to-noise ratios.

A typical plot showing the analysis of the sideband intensities using the graphs of Herzfeld and Berger is shown in Figure 3.3. The tensor components derived from this analysis at two spinning speeds are shown in Table 3.1. Again consistent results were obtained at the two spinning speeds which are in good agreement with the static pattern. The plot in Figure 3.3 shows that the cross-over is very good for all sidebands except the -1, so that the neglect of a higher order sideband does not significantly affect the overall shielding tensor components. Thus in this respect the graphical method is superior to moment analysis.

Both moment analysis and the graphical method will in general give a set of tensor components consistent with the measured sideband intensities. This does not, however, necessarily imply that the sideband intensities generated in a MAS simulation using these tensor components will be the same as those observed experimentally. To illustrate this statement the example of the schematic three line spectrum shown in Figure 3.4a was considered. Moment analysis gives tensor components $\sigma_{11}$ = 19.53, $\sigma_{22}$ = 0, $\sigma_{33}$ = -19.53ppm. A simulation of the MAS spectrum expected for such tensor components is shown in Figure 3.4b. The differences are striking; not only are there more sidebands in the simulated spectrum but the relative intensities of the -1,0 and 1 sidebands have changed greatly. A simulation using the tensor components obtained from a graphical analysis correctly reproduces the -1,0,+1 sidebands, but still gives many more sidebands than in the example.

At its simplest, then, a comparison of simulated and observed MAS spectra allows the extent to which the experimentally measured

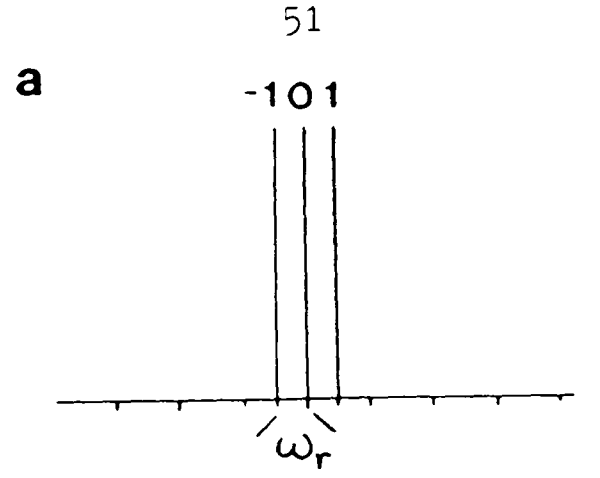


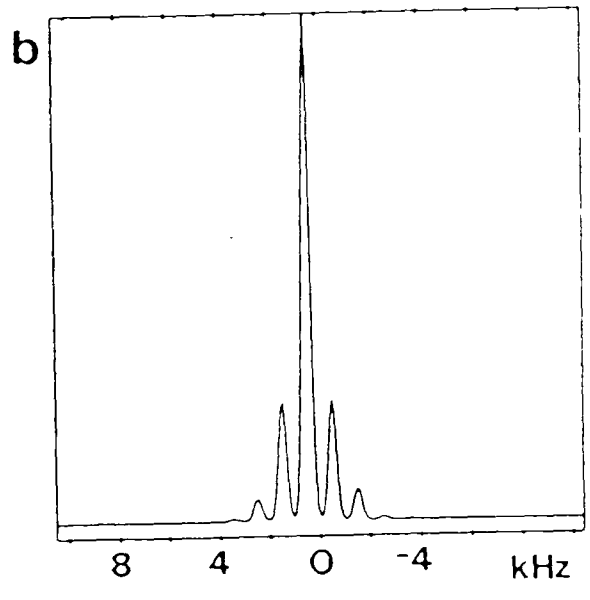


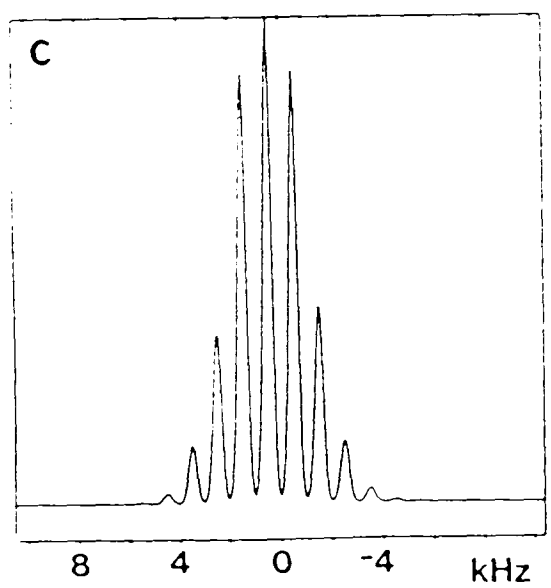


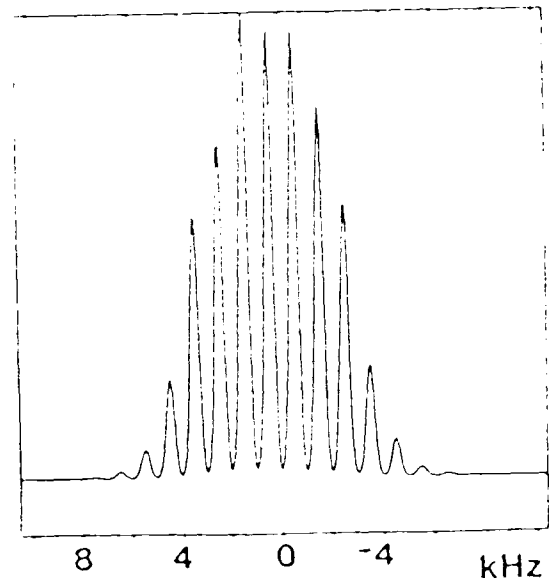


Figure 3.4

Comparison of schematic and simulated three-line spectrum.

(a) Schematic spectrum. All the lines have the same intensity; the spinning speed is 1.0kHz.

(b) Simulated spectrum using tensor components of +19.5, 0, -19.5ppm obtained from a moment calculation.

(c) Simulated spectrum using tensor components of +38, 0, -38ppm and +53, 0, -53ppm obtained from analysis using the graphical method. Two spectra are as shown.

sideband intensities are consistent with a single well defined chemical shift tensor to be established. To consider a different example, the observed MAS spectrum of sodium dihydrogen orthophosphate can be compared with one simulated using the tensor components from the (+5,+4,-4) truncated sideband moment analysis (Figure 3.5). This corresponds to a case where a poor signal-to-noise ratio prevents the observation of the highest order sidebands. Clear differences can be seen between the experimental and simulated sideband intensities. In particular, the intensity of a low order sideband, in this case the +1, is very badly reproduced despite the source of error being the neglect of the highest order sidebands.

A more sophisticated use of MAS simulations is to refine the tensor components. This requires that criteria are established for a 'goodness of fit' of the simulated spinning sideband intensities to the experimental intensities. Two criteria seem necessary, firstly, that the root mean square (rms) deviation of the calculated from the observed intensities is minimised, and secondly, that no one sideband intensity difference deviates by more than a defined margin, say twice the noise level. As an example the tensor components derived from the moment analysis of the truncated sideband set have been compared with those obtained from the powder pattern. The rms deviations for these cases are shown in Table 3.2. The smallest rms deviation was observed for the complete sideband data set, as would be anticipated, whilst the next best fit, with an rms deviation nearly twice that of the best fit, corresponds to changes of only 3ppm in $\sigma_{11}$ and $\sigma_{33}$. At the other extreme lies the +5,+4,-4 truncated set, and between the two the static powder pattern data. These results suggest that the tensor components can be refined to obtain a minimum standard deviation between simulated and experimental sideband intensities.

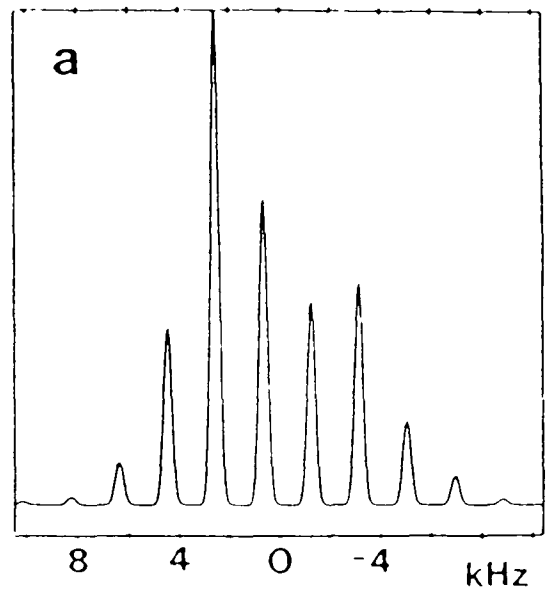


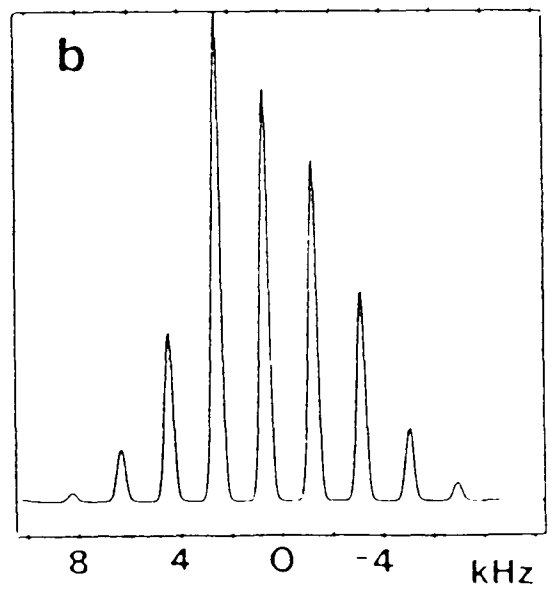


Figure 3.5

Slow MAS simulations using the tensor values obtained from a moments calculation for sodium dihydrogen orthophosphate (spinning at 1.9kHz).

(a) Using the full spinning sideband set.

(b) Using the (+5,+4,-4) truncated data set (Table 3.1).

TABLE 3.2

Comparison of the results of simulating the slow MAS spectrum of sodium dihydrogen orthophosphate using tensors derived from a moment analysis using various data sets.

| Method of analysis | Root mean square deviation |
|---|---|
| Moment analysis | |
| --complete data set | 0.16 |
| --omitting +5 | 0.44 |
| --omitting +5,-4 | 0.24 |
| --omitting +5,+4,-4 | 0.99 |
| Powder pattern simulation | 0.55 |

3.3.2 Phosphine oxide.

In contrast to sodium dihydrogen orthophosphate, phosphine oxide has a static powder spectrum typical of an axial or near axial pattern (Figure 3.6). Previous workers have suggested that the pattern is non-axial, with $\sigma_{11} - \sigma_{22}$ ($\Delta$) equal to 10ppm [14,15]; evidence for this is provided by the spectrum in the derivative mode. Due to the natural linebroadening a visual inspection of the simulated powder pattern for a truly axial or near axial pattern cannot distinguish between the two.

Sideband analysis in a slow spinning MAS spectrum was carried out for two spinning speeds. Figure 3.7 shows the spectrum at the slower spinning speed. The result of the moment analysis for a full sideband data set for both spinning speeds and for two truncated sets for the slower speed are shown in Table 3.3. A striking feature is that the spectrum obtained at the faster spinning speed has an apparent sideband intensity distribution which cannot be accounted for by a shift tensor with real values of the principal components. This is indicated by the imaginary value for the asymmetry $\eta$, which occurs because the value for $M_2$ is too large relative to $M_3$. Moreover, the slower spinning speed gives a significantly non-axial set of tensor components with $\Delta$ = 25ppm, $\eta$ = 0.2 (using the full sideband data set). An imaginary value for the asymmetry can also result from analysis of this spectrum, as shown by the -4 truncated sideband data. Ignoring the +5 sideband has a different effect, that is a more positive $\eta$; the anisotropy is less axial, with $\Delta$ = 48ppm, and $\eta$ = 0.4. The extreme sensitivity of the derived $\eta$ value to the number of sidebands used and their intensity is further illustrated by the increase in $\eta$, from 0.2 to 0.33, when the full sideband set is used but increasing the intensity of the -4 sideband from 0.1 to 0.2.

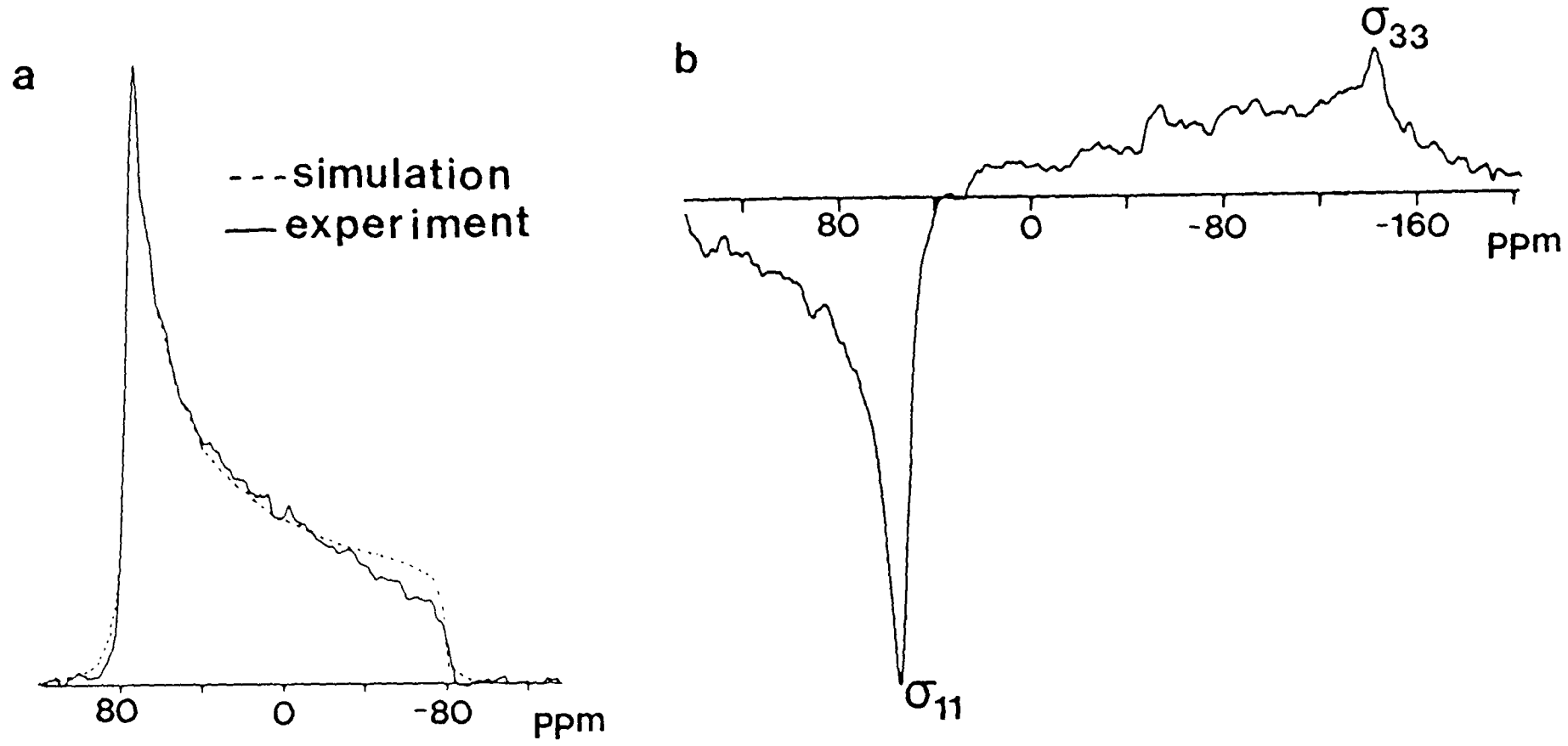


Figure 3.6

Static spectra of triphenylphosphine oxide.

(a) Comparison of experimental spectrum in absorption mode (2400 scans) with a simulation obtained using tensor components of +97, +97, -98 ppm.

(b) Experimental spectrum in derivative mode.

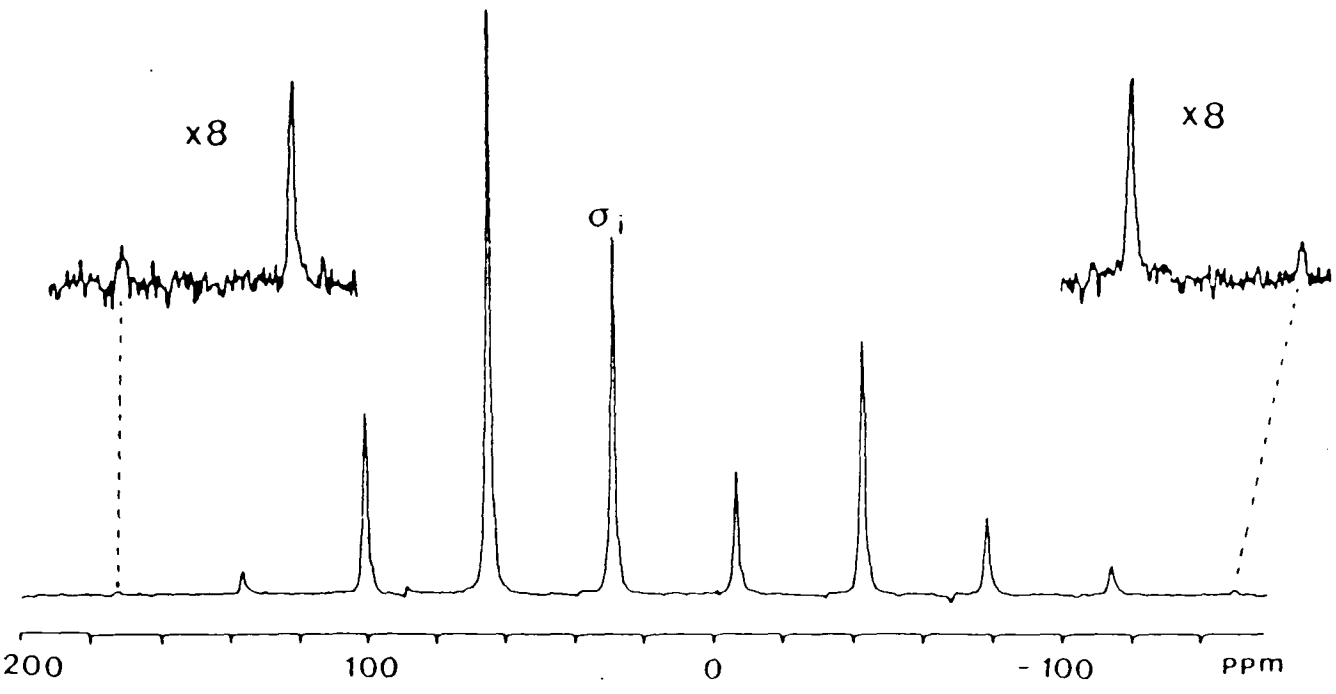


Figure 3.7

Slow MAS spectrum of triphenylphosphine oxide (1700 scans, spinning speed 2.9kHz).

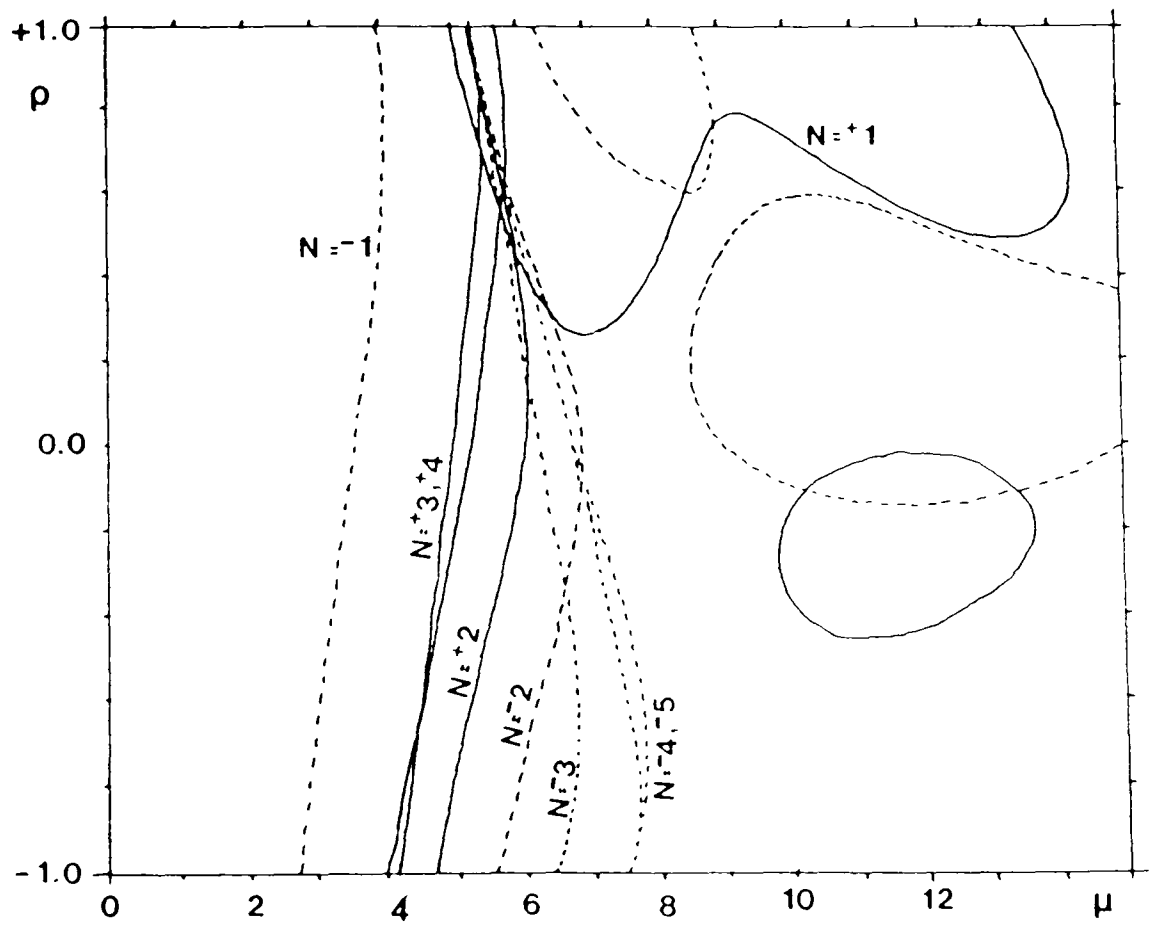


Figure 3.8

Contour plot for triphenylphosphine oxide spinning at 2.9kHz using the method of Herzfeld and Berger [ 8 ]. There is no clear point of intersection of the contours.

TABLE 3.3

Results of sideband analysis for phosphine oxide.

| Method of analysis | $\sigma_{11}$ | $\sigma_{22}$ | $\sigma_{33}$ | $\Delta$ | $\eta$ |
|---|---|---|---|---|---|
| Moment analysis (fast) | - | - | - | - | imaginary |
| Moment analysis (slow) | | | | | |
| -complete data set | -104 | -79 | 99 | 25 | 0.2 |
| -omitting +5 | -113 | -65 | 95 | 48 | 0.4 |
| -omitting -4 | - | - | - | - | imaginary |
| -doubling intensity of -4 | -111 | -70 | 97 | 41 | 0.33 |
| Graphical(fast) | -96 | -96 | 109 | 0 | 0 |
| Graphical (slow) | -91 | -91 | 99 | 0 | 0 |
| Experimental powder | -91 | -91 | 104 | 0 | 0 |

All tensor values are in ppm.

$\Delta = \sigma_{11} - \sigma_{22}$

Despite the range in asymmetry values (from 0.2 to 0.4) relatively small changes take place in $\delta$, which is more insensitive to small changes in sideband intensities. These results demonstrate that a moment analysis of spinning sidebands to give accurate values of the tensor components will only be possible in the most favourable cases when the symmetry of the shift tensor approaches axial.

Severe problems also arise in the use of the graphical procedure for a near axial anisotropy pattern. For axial symmetry $\rho = \pm 1$, and hence the contours should converge on one or other of the horizontal borders of the contour plots. A typical contour plot is shown in Figure 3.8. Four contours converge from $\rho = 0.8$ to 1.0, while two others cross around $\rho = 0.6$, close to the previous four,and then diverge. A closer examination of the published contour plots [8] indicates that all the contours have a similar curvature near $\rho = \pm 1$ and thus a unique convergence at these values would be hard to establish, even in the ideal case. Although a range of $\rho$ values is consistent with the cross-overs in the graph $\mu$ is much better defined. As in the case of moment analysis, the overall anisotropy is reasonably well defined, but the asymmetry is not.

Because of the uncertainty in the above analyses with respect to the asymmetry, the principal concern in the MAS simulations for phosphine oxide was to ascertain the sensitivity of the spinning sideband pattern to changes in the asymmetry. Simulations of the MAS spectra were therefore carried out with a constant $\delta$, maintaining the overall anisotropy, and increasing $\Delta$ and hence $\eta$. A plot of the normalised % change in intensity of the spinning sidebands as a function of the asymmetry is shown in Figure 3.9. It is apparent that the intensity of most sidebands is rather insensitive to changes in the asymmetry until $\eta > 0.2$. In addition, changes in the intensities

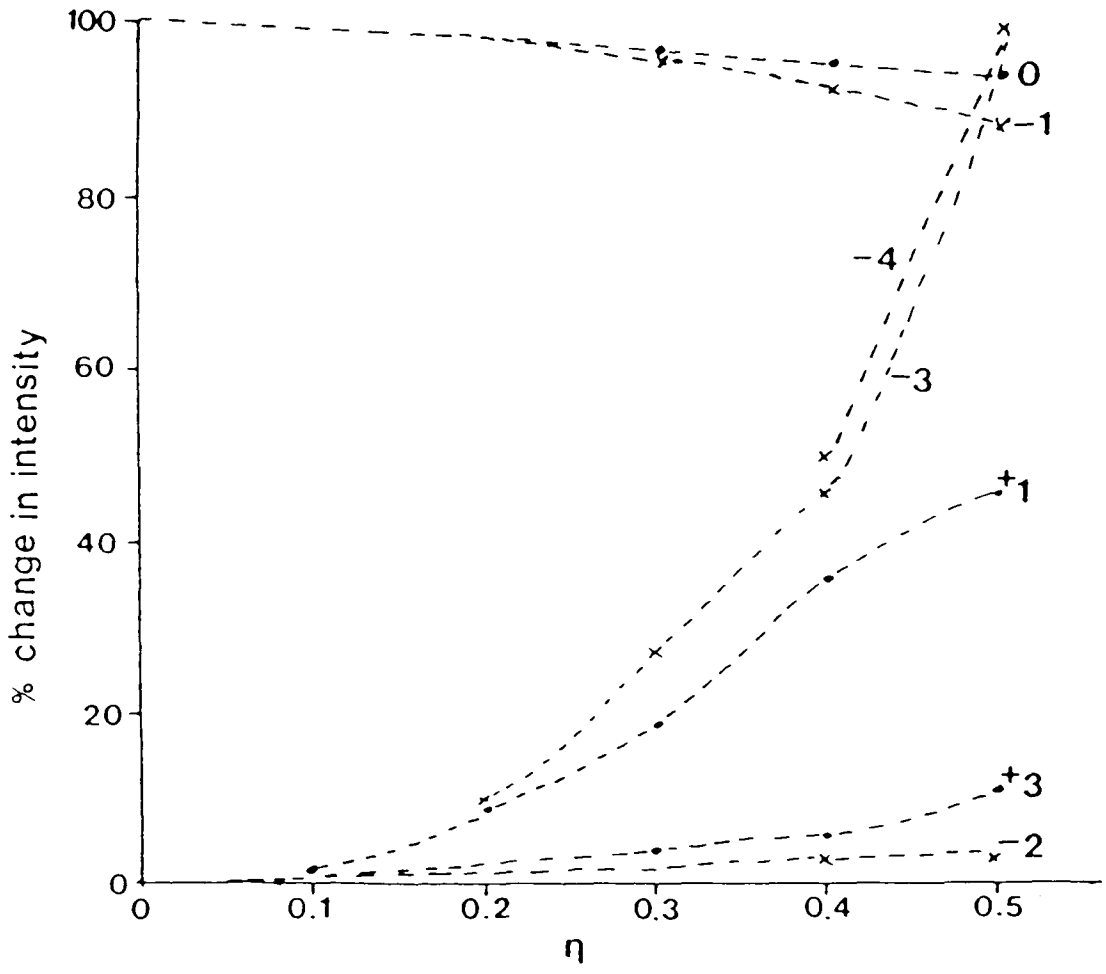


Figure 3.9

Plot showing the normalised % change of spinning sideband intensity against asymmetry. The intensity of most sidebands is insensitive to changes in asymmetry until $\eta > 0.2$. Due to the low intensity of the -4 sideband, changes in its intensity cannot be measured accurately until $\eta = 0.4$.

of the higher order sidebands, especially the -4, correspond to small absolute changes in intensity. In practical terms the most useful feature shown in the graph is the sensitivity of a lower order, specifically the +1, sideband to the changes in asymmetry. An 18.5% change is seen in the +1 sideband on going from an axially symmetric pattern ($\eta$= 0) to a non-axial ( $\eta$ = 0.3), corresponding to an absolute change in intensity of 0.55: this is the largest absolute change observed for any sideband. Two conclusions can be drawn from this. Firstly, the changes in sideband intensities necessary to assign a shielding tensor as axial from a MAS spectrum occur in a low order sideband which will in general be observed with a sufficiently good signal-to-noise ratio to measure its intensity accurately. Secondly, and less favourably, below $\eta$ = 0.1 the intensity differences between the axial and non-axial case are so small that there is almost no measurable difference in the spinning sideband patterns. Under these circumstances it is meaningless to distinguish between axial and near axial i.e. when $\sigma_{11} - \sigma_{22}$ = 10ppm.

## 3.4 The advantages of slow MAS simulations.

Comparison of the shielding tensor components derived from a static powder pattern with those obtained from either moment analysis or graphical analysis of the spinning sideband intensities has shown that severe problems are encountered with axial or near axial chemical shift anisotropy tensors. When the tensor is non-axial both moment analysis and graphical analysis are good, although the sensitivity of moment analysis to the loss of higher order sidebands makes the graphical method superior in practice. Simulations of the MAS spectra then provide a crucial link with the experimental spectra, allowing a direct comparison between the two to be made to establish the validity

of the derived tensor components. This will be particularly important in cases where unrealistic tensor components may be obtained. Simulations of the MAS spectrum also allow refinement of the tensor components.

When the shift tensor is axial or near axial ($\eta < 0.1$) simulations of the MAS spectra indicate insignificant changes in the sideband intensities between the two. Consequently it is unrealistic to expect sideband analysis of a MAS spectrum to enable a distinction to be made between axial and near axial symmetry. It is therefore not surprising to find that neither moment analysis nor the graphical method accurately determines the asymmetry of such tensors. However both methods are able to determine the overall anisotropy. Having obtained approximate tensor components from sideband analysis, the greater sensitivity of MAS simulation can be used to define the range in $\eta$ values more accurately.

### 3.5 A test for unrealistic tensor components.

The use of MAS simulations in determining whether unrealistic tensor components had been derived from the analysis of spinning sidebands has already been mentioned. Two possible cases where unrealistic tensor components might be obtained would be when motional averaging of the CSA occurs and when a dispersion of chemical shift anisotropies is present, both of which cannot readily be ruled out by direct observation of the spectrum. A test of whether the derived tensor components will reproduce the observed sideband intensities is therefore necessary. This is provided by a comparison of the computer simulated slow MAS spectrum with the observed spectrum. To obtain a measure of the difference between the two spectra, a statistical analysis must be carried out. Two examples, one

theoretical and one real, were examined in this way; both consisted of two phosphorus species with identical isotropic shifts but different chemical shift anisotropies, corresponding to the case in which a distribution of CSA's is present.

A comparison of the observed and simulated sideband intensities will give a set of differences in intensity, $\Delta_i = I_O - I_S$. To test the derived tensor components it is necessary to determine whether these errors are statistically significant, implying that the observed spectrum does not correspond to the tensor components used in the simulation, or whether the differences are within an acceptable spread. Assuming that the data has not been refined, the errors represented are (a) inaccuracies in measuring sideband intensities in the observed spectrum and (b) small errors in $\sigma_{ij}$ derived from moment or graphical analysis which result from errors in calculation. The series of $\Delta_i$ obtained in any one analysis can be considered to correspond to a sample of n, where n is the number of sidebands, from an infinite population of $\Delta_i$ values. The errors will have a normal distribution with a mean of zero. An appropriate choice of the standard deviation of the error is difficult to establish. It should ideally be obtained from the distribution of $\Delta_i$ found in a large series of simulations where the tensor components are known to be good, but the question arises as to how do we know that the tensor components obtained for any particular example are good. As a compromise, an initial analysis was performed using the standard deviation found for the errors in the case of sodium dihydrogen orthophosphate, which has a single well-defined shielding tensor. s was therefore taken to be 0.063.

Using the normal distribution of errors N(0, 0.063) the $\Delta_i$ for a given simulation can be tested to determine whether they

represent a sample of these errors [16]. Two tests are possible: first, whether the mean of the sample is statistically different from zero, and second, whether the standard deviation is statistically different from s. The test of the standard deviation was chosen as being more sensitive to both the magnitude and the sign of the error than the test of the mean. For a normal distribution, the inner and outer confidence limits are taken to be 2.5% and 0.1%. The method of calculating these limits is given in Appendix A. The standard deviations obtained for the two examples were tested to determine if they fell outside these limits for the distribution of errors being considered. If they lie outside the 0.1% limit, it can be stated with confidence that the error distribution in the example does not correspond to a sample of the normal error distribution, which effectively means that the tensor components used to simulate the MAS spectrum do not provide a realistic description of the experimental spectrum.

For the theoretical example the two species were chosen to have an isotropic shift of 0ppm and tensor values of 70.0, 0, -70.0 ppm and 25.0, 25.0, -50.0 ppm respectively; the overall anisotropy of both species was the same. These tensor values were used to simulate the individual slow MAS spectra, and the results are shown in Figure 3.10 together with the composite spectrum obtained by adding the two spectra. Moment analysis of the sidebands in the composite spectrum gave the tensor components 54.4, 7.2, -61.6 ppm; graphical analysis gave a contour plot with no clear point of intersection (Figure 3.11). A comparison of the slow MAS spectrum simulated using these tensor values with the composite spectrum showed a considerable difference between them: the standard deviation of the simulated spectrum from the composite was 0.63. The inner and outer control limits for this

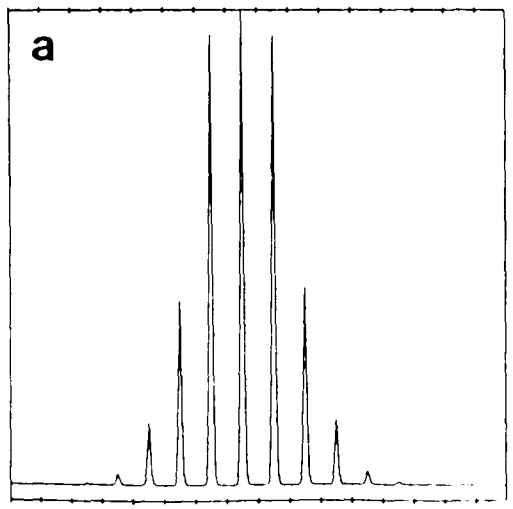


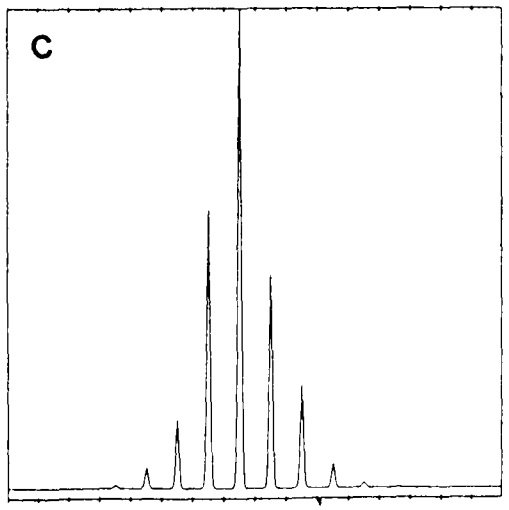


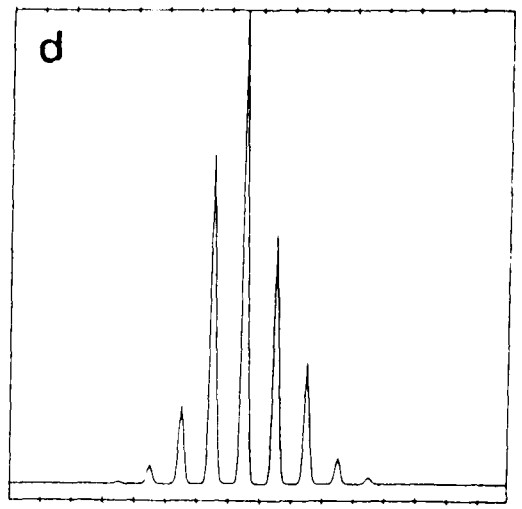


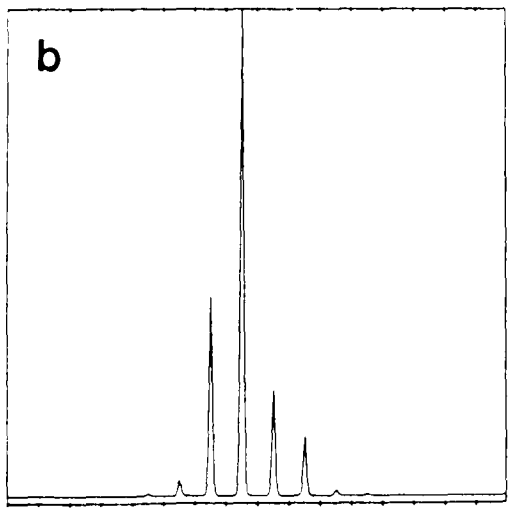


Figure 3.10

Slow MAS simulations for the theoretical example of two species with the same $\sigma_{iso}$ and different CSA's.

(a) Using tensor components 70, 0, -70ppm.

(b) Using tensor components 25, 25, -50ppm.

(c) Composite spectrum obtained by adding (a) and (b).

(d) Spectrum simulated using tensor components 54, 7, -61ppm obtained from a moment analysis of the composite spectrum.

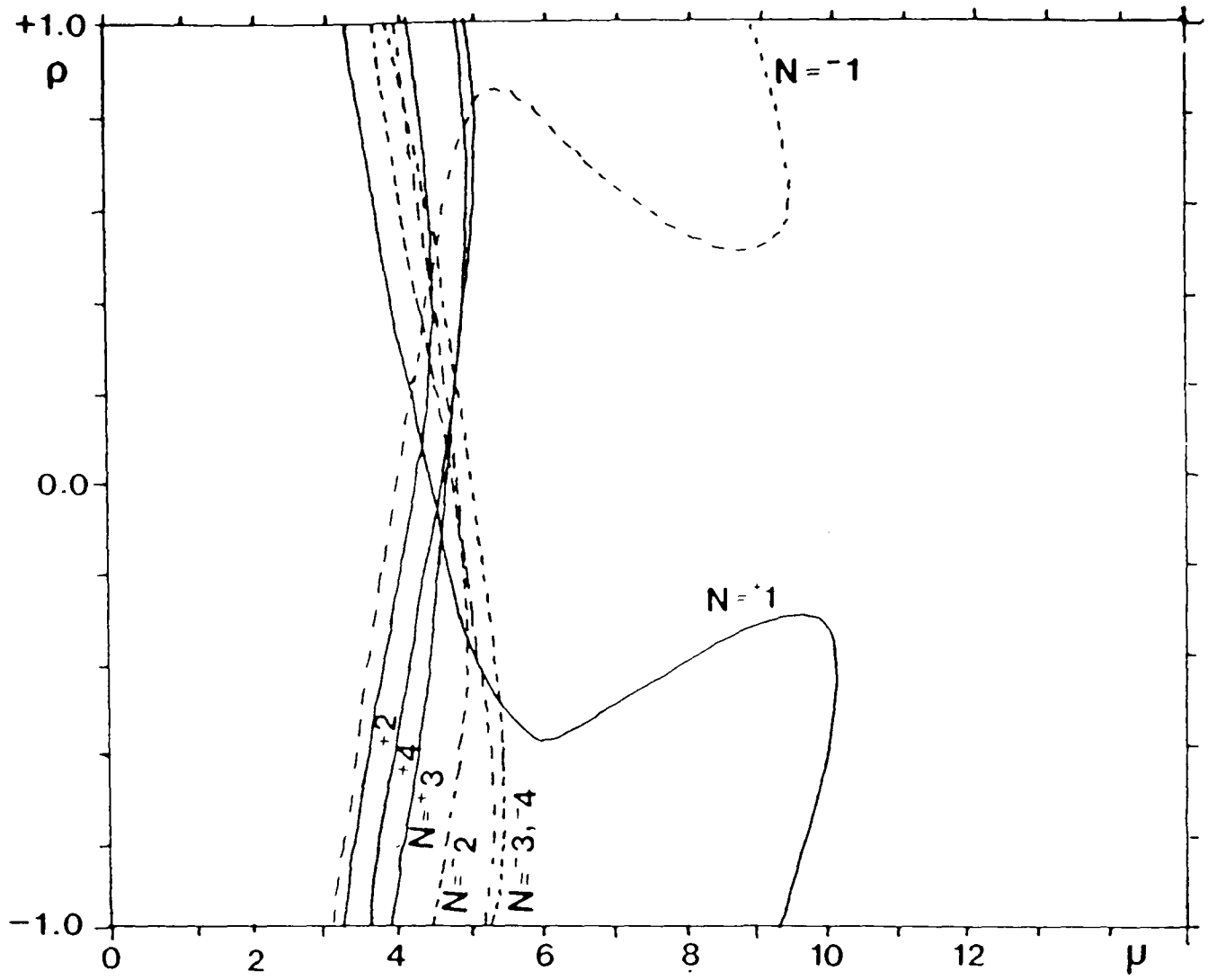


Figure 3.11

Contour plot for the theoretical example of two species with identical $\sigma_{iso}$ but different CSA's, using the method of Herzfeld and Berger [8]. There is no clear point of intersection of the contours.

case were calculated to be 0.087 and 0.103; the observed standard deviation is clearly well outide the outer limit.

The real example studied consisted of two zinc phosphates, $\alpha Zn_3(PO_4)_2$ and $Zn_{2.75}Mg_{0.25}(PO_4)_2$, both of which produce a single $^{31}P$ resonance with an isotropic shift of 3.5ppm. Slow MAS shows that the CSA of $\alpha Zn_3(PO_4)_3$ is considerably larger than that of $Zn_{2.75}Mg_{0.25}(PO_4)_3$ (Figure 3.12). Analysis of the spinning sideband intensities measured in the spectra of the two phosphates gave the tensor components shown in Table 3.4. The spectra were simulated using these values, and a comparison with the experimental spectra gave the standard deviations 0.3 and 0.15 respectively. A 1:1 mixture of the two phosphates was prepared by grinding them together with a pestle and mortar, and the slow MAS spectrum of the mixture was recorded. Moment analysis of the spinning sidebands in the resulting spectrum gave the tensor components 27.6, 7.6 and -24.7 ppm; graphical analysis showed no clear intersection of contours. The tensor values obtained were used to simulate the spectrum of the mixture and the result compared with the experimental spectrum: the standard deviation was found to be 0.27. This lies outside the control limits, which in this case were calculated to be 0.092 and 0.11. The standard deviation of the errors is thus outside the limits of a normal distribution.

In these two examples, the result of the test is that the errors in the fit of the observed and calculated MAS spectra are outside the control limits for a normal distribution of errors. If the test is accurate, this means that in both cases analysis of spinning sidebands has produced unrealistic tensor components. However, when this test is carried out on the simulated and experimental spectra obtained for $\alpha Zn_3(PO_4)_2$ (0.11), the standard deviation is only just within the outer control limit of 0.12. This suggests that, if in a

Figure 3.12

MAS spectra of the zinc phosphates.

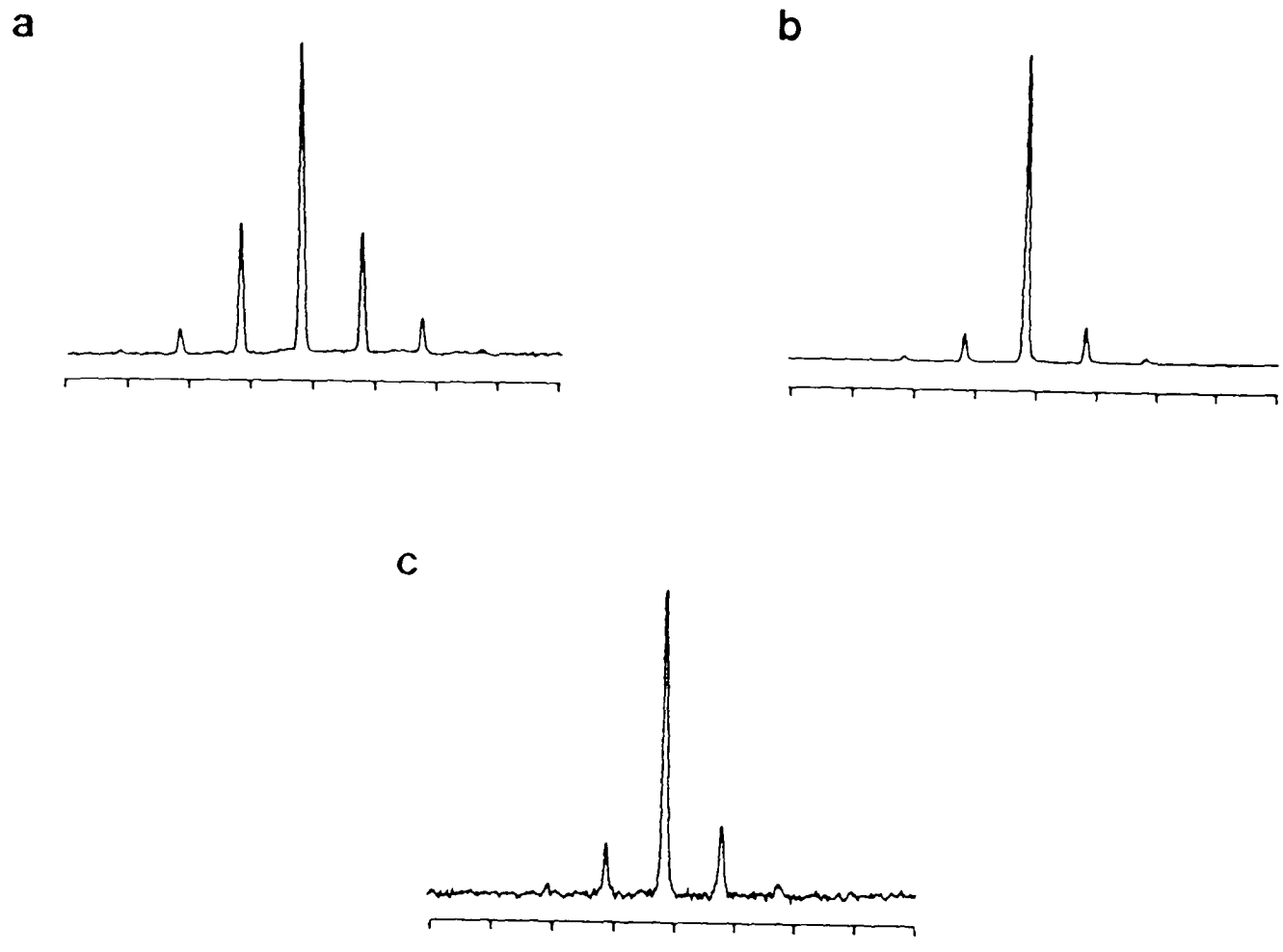


(a) Slow MAS spectrum of $Zn_3(PO_4)_2$ (15 scans).

(b) Slow MAS spectrum of $Zn_{2.75}Mg_{0.25}(PO_4)_2$ (10 scans).

(c) Slow MAS spectrum of a mixture of the two phosphates (20 scans).

(d) Spectrum simulated using the tensor components 28, 8, -25ppm obtained from a moment analysis of the spectrum of the mixture of phosphates.

TABLE 3.4

Results of sideband analysis for the zinc phosphates.

| Compound | $\sigma_{11}$ | $\sigma_{22}$ | $\sigma_{33}$ |
|---|---|---|---|
| $\alpha Zn_3(PO_4)_2$ | 40 | 8 | -37 |
| $Zn_{2.75}Mg_{0.25}(PO_4)_2$ | 24 | 5 | -19 |
| Mixture | 28 | 8 | -25 |

All tensor values are in ppm.

relatively well-defined case such as $\alpha Zn_3(PO_4)_2$ can be almost outside the calculated outer control limit, the control limit may be wrong, and the standard deviation for the normal distribution of errors may in fact be greater than the value of 0.063 used in the above calculations. If the standard deviation of $\alpha Zn_3(PO_4)_2$ is taken as the standard deviation of the distribution, however, both of the examples are still found to lie outside the 1% control limit.

It is clear that, without studying a number of well-defined systems, the validity of the standard deviation of the error used in the test cannot be established nor a more appropriate value obtained. The test used here does, however, provide some measure of the quality of the fit between observed and simulated MAS spectra: it points out cases which deviate by a considerable amount from the expected error distribution, suggesting that such tensor values be viewed with caution.

## 3.6 Conclusions.

The studies discussed in this chapter illustrate the advantages of the use of simulations of slow MAS spectra in the analysis of spinning sideband data to obtain the principal values of the chemical shielding tensor. The results suggest that the analysis of spinning sideband data should involve two stages: (i) calculation of approximate tensor components from the graphical method or moment analysis; (ii) simulation of the MAS spectrum. Stage (ii) enables the extent to which the derived tensor components provide an adequate description of the experimental spectrum to be established, and with the application of a statistical test a distinction between realistic and unrealistic tensors can be made. Simulations also allow the derived values of the tensor components to be refined.

3.7 References.

[1] M. Mehring, 'High resolution NMR in solids,' 2nd. ed., Springer-Verlag, Berlin (1983).

[2] W.S. Veeman, Prog. NMR Spectros. 16 (1984) 193.

[3] V. Galasso, J. Magn. Res. 58 (1984) 311.

[4] F.R. Prado, C. Geissner-Prettre, B. Pullman and J.P. Dudley, J. Amer. Chem. Soc. 101 (1979) 1737.

[5] N. Bloembergen and J.A. Rowland, Acta Metall. 1 (1953) 731.

[6] S.J. Opella and M.H. Frey, J. Amer. Chem. Soc. 101 (1979) 5854.

[7] M.M. Maricq and J.S. Waugh, J. Chem. Phys. 70 (1979) 3300.

[8] J. Herzfeld and A.E. Berger, J. Chem. Phys. 73 (1980) 6021.

[9] A. Bax, N.M. Szeverenyi and G.E. Maciel, J. Magn. Res. 52 (1983) 400.

[10] A. Bax, N.M. Szeverenyi and G.E. Maciel, J. Magn. Res. 54 (1983) 147.

[11] N.E. Burlinson, B.A. Durrell and J.A. Ripmeester, J. Magn. Res. 67 (1986) 217.

[12] H.J. Jakobsen, P.D. Ellis, R.R. Inners and C.F. Jensen, J. Amer. Chem. Soc. 104 (1982) 7442.

[13] P.S. Marchetti, P.D. Ellis and R.G. Bryant, J. Amer. Chem. Soc 107 (1985) 8191.

[14] J.B. Robert and L. Wiesenfeld, Mol. Phys. 44 (1981) 319.

[15] J.B. Robert and L. Wiesenfeld, J. Magn. Res. 38 (1980) 357.

[16] B.C. Ericker, 'Advanced general statistics', English Universities Press, London (1972).

# CHAPTER 4

## Studies of simple transition metal complexes and clusters.

### 4.1 Introduction.

Phosphines, and in particular triphenylphosphine, are widely used as co-ordinating ligands in transition metal complexes and clusters [1]. $^{31}P$ nmr in solution has developed into a powerful technique for the structural investigation of such compounds, with its large chemical shift range and scalar couplings to other nuclei making it a sensitive probe of molecular geometry and of the fluxionality which is frequently observed [2]. Meanwhile the recent advances in high resolution solid state nmr spectroscopy have led to its application in many fields previously well-studied by nmr in solution, providing a bridge between solution structures and those determined by X-ray diffraction [3]. A combination of these two approaches, i.e. the application of solid state $^{31}P$ nmr to the study of transition metal phosphines, should therefore provide much useful structural and dynamic information about these compounds.

Several groups have published the results of solid state $^{31}P$ nmr studies on phosphine-containing transition metal complexes, indicating the nature of the information which may be obtained [4-7]. These were discussed in detail in chapter 1. From this work it is clear that well-defined solid state $^{31}P$ nmr spectra can be obtained from such complexes in relatively short periods of time, and that structural information may be derived from the spectra.

Before extending the field of application of this technique to encompass more complex systems, it was decided to investigate a number of relatively simple transition metal complexes and clusters. In this context, 'simple' refers to compounds whose structures have

been well defined and whose solid state $^{31}P$ spectra were expected to be relatively straightforward. In addition to providing structural and possibly dynamic information on the compounds studied, these preliminary experiments should help to determine the optimal conditions for such studies and the factors influencing the solid state spectra, and should indicate the types of systems amenable to further investigation. Of the work discussed in this chapter, some forms the basis for the studies on surface-attached species discussed in chapter 7.

$^{13}C$ solid state nmr studies were also carried out on a number of the transition metal compounds. The use of high resolution $^{13}C$ solid state nmr spectroscopy to investigate the structure and dynamics of organometallic compounds has previously been reported [8-12]. It was hoped that $^{13}C$ studies of the carbon-containing ligands would provide further details about the compounds whose behaviour was not fully understood on the basis of solid state $^{31}P$ nmr spectroscopy. The application of $^{13}C$ nmr to the study of the transition metal carbonyl clusters was also explored. Several groups have published the results of $^{13}C$ nmr studies on solid metal carbonyls [9,12-14], but these have generally used high levels of $^{13}C$ sample enrichment and necessitated long recycle delays to allow for the long carbonyl carbon relaxation time. In one study, however, cross polarisation from organic ligands also present in the carbonyl cluster was used to improve the sensitivity and to reduce the recycle delay [9]. The spectra obtained show an excellent signal-to-noise ratio from 2000-5000 transients. This approach was investigated in the work discussed here, attempting cross polarisation from the protons of the phosphine ligands and from hydride ligands.

## 4.2 Materials and methods.

Many of the transition metal compounds studied by solid state nmr were kindly lent by other members of this department, who are acknowledged in the appropriate sections of this chapter. The molybdenum compounds were prepared by Dr. C. McAteer as part of a collaborative project with Dr. M.L.H. Green at Oxford. The rhodium, osmium and ruthenium carbonyl clusters were prepared by Dr. S.L. Cook, Dr. R.J. Crowte and V. Alexiev in a collaborative project with Dr. J. Evans from Southampton University. Other samples were lent by members of the research group of Dr. D.M.P. Mingos at Oxford.

Magic angle spinning and cross polarisation were used for most of the $^{31}P$ and $^{13}C$ experiments in this chapter. A number of non-spinning $^{31}P$ spectra were also aquired. For the phosphorus work, the optimum CP time, investigated for a variety of the metal phosphines, was found to be 1.0ms. The number of transients depended on the quantity of sample available. For the $^{13}C$ experiments on the organometallic compounds natural abundance $^{13}C$ was used; $^{13}C$ enrichment of the carbonyl groups of the rhodium and osmium clusters was typically 40%. A CP time of 2ms was used for these samples. Several thousand transients were accumulated for the carbonyl spectra to obtain good signal-to-noise; this took of the order of six hours.

## 4.3 Triosmium carbonyl clusters.

$Os_3(CO)_{11}PPh_3$, $H_2Os_3(CO)_{10}PPh_3$ and $H_2Os_3(CO)_9PPh_3$ (Figure 4.1) were prepared by S.L. Cook and V. Alexiev (Southampton) by methods similar to those described previously [15-17]. Typically several thousand transients were accumulated for each spectrum, using 10-15 mg of sample.

The solid state $^{31}P$ nmr spectra of both $Os_3(CO)_{11}PPh_3$ and

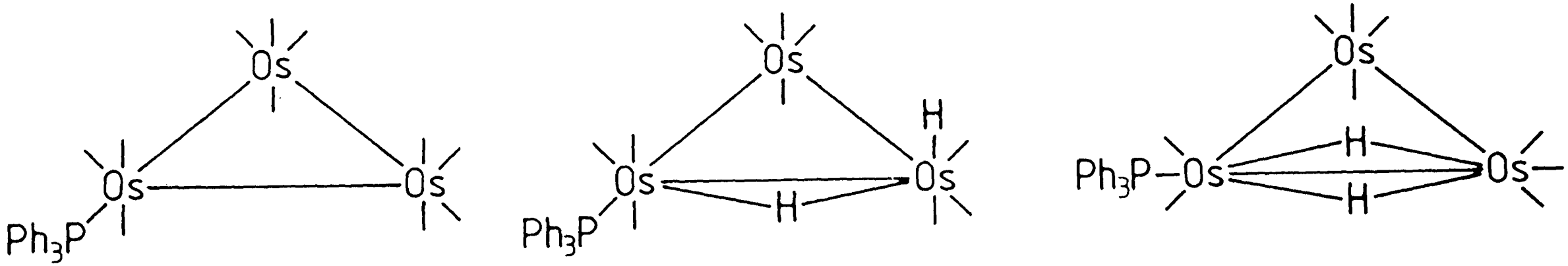


Figure 4.1

The structures of the triosmium clusters (a) $Os_3(CO)_{11}PPh_3$ (b) $H_2Os_3(CO)_{10}PPh_3$ (c) $H_2Os_3(CO)_9PPh_3$

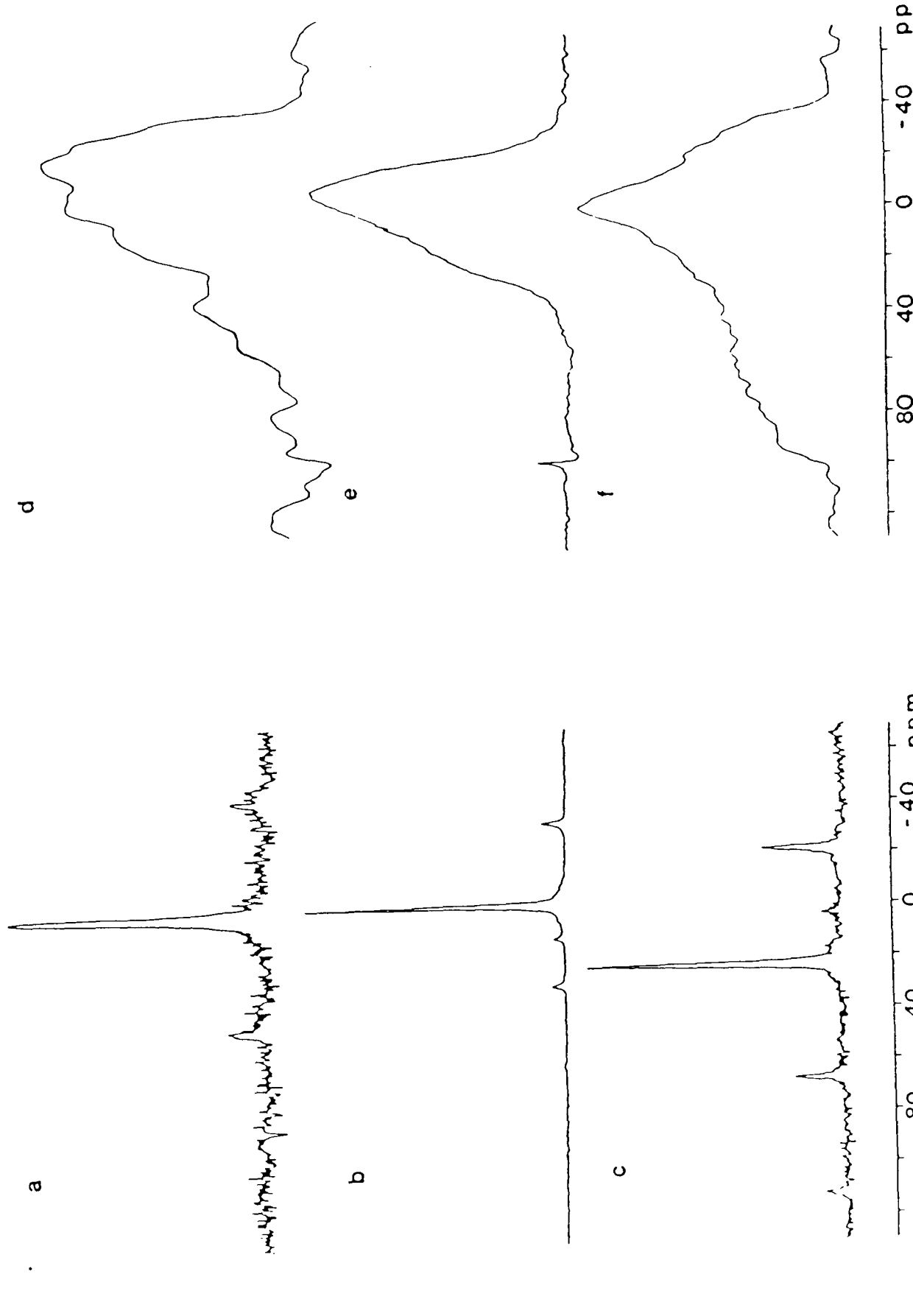


Figure 4.2 $^{31}P$ nmr spectra of the triosmium clusters. Spectra (a)-(c) were recorded using magic angle spinning and are of $Os_3(CO)_{11}PPh_3$, $H_2Os_3(CO)_{10}PPh_3$ and $H_2Os_3(CO)_9PPh_3$ respectively. Spectra (d)-(f) are the corresponding static spectra of these samples.

$H_2Os_3(CO)_{10}PPh_3$ show a single sharp line ($\Delta\nu_{1/2}$ of the order of 150Hz) (Figure 4.2). This is consistent with the previously reported crystal structures of these or related species [18-20], which show for each cluster the presence of only one crystallographic environment for the phosphine ligand. The solution nmr spectrum of each cluster also shows a single resonance. The initial solid state spectrum of $H_2Os_3(CO)_9PPh_3$, however, showed four lines of varying intensities, one having the same chemical shift as the single solution resonance. The sample was recrystallised and a new sample prepared in an attempt to discover if the additional lines were due to sample preparation or recrystallisation. The recrystallised sample gave a spectrum showing two lines of approximately equal intensity, with similar chemical shifts to two of the resonances in the previous spectrum. The spectrum of the new sample was almost identical to the spectrum of the first sample before recrystallisation. A further recrystallisation was carried out; this sample gave a single line spectrum, in accordance with the crystal structure of the cluster and the solution nmr spectrum.

The chemical shifts measured for all three clusters are close to those found in solution (see Table 4.1); in particular, those of $H_2Os_3(CO)_9PR_3$ derivatives are more than 20ppm downfield of the resonances of the other clusters.

The differences in phosphorus environment in the triosmium clusters are also apparent on studying the phosphorus chemical shift anisotropies. The nonacarbonyl has the largest anisotropy of the clusters, with $\Delta\sigma$ = 87ppm; the static (non-spinning) spectrum shows the powder pattern characteristic of non-axial symmetry at the phosphorus atom (Figure 4.2). For the decacarbonyl $\Delta\sigma$ = 30ppm, and the static spectrum is closer to axial.

TABLE 4.1

$^{31}P$ chemical shifts of the triosmium clusters.

| cluster | chemical shift (ppm) solution | solid |
|---|---|---|
| $Os_3(CO)_{11}PPh_3$ | 2.1 | 2.5 |
| $H_2Os_3(CO)_{10}PPh_3$ | -2.7 | -1.5 |
| $H_2Os_3(CO)_9PPh_3$ | 27.2 | 22.9 |
| $HOs_3(CO)_9PPh_3(O_2CMe)$ | 17.6 | 15.1 |
| $H(OH)Os_3(CO)_9PPh_3$ | 20.0 | 24.0 |

All chemical shifts are referenced to 85% $H_3PO_4$, with low field shifts taken as positive.

## 4.4 Compounds containing phosphines co-ordinated to rhodium.

### 4.4.1 Square planar complexes.

The complex $[Rh(CN\text{-}xylyl)_2(PPh_3)_2]PF_6$ was kindly lent by M. Watson (from Dr. D.M.P. Mingos' group) for solid state nmr studies. The $^{31}P$ spectrum shows a single resonance from phosphorus adjacent to rhodium at 30.6ppm, with a rhodium-phosphorus coupling constant of 122Hz ±10Hz (Figure 4.3). A multiplet resulting from the $PF_6^-$ group is centred at -144.2ppm ($J_{F-P}$ = 713Hz). The spectrum is well-resolved, with a width at half-height for the P-Rh doublet of ~50Hz. The magnitude of $J_{Rh-P}$ suggests that the two phosphine groups are trans to each other [21]. This is in agreement with the i.r. spectrum, in which a single sharp isocyanate peak is observed, showing the complex to adopt the trans geometry. In solution a similar spectrum is obtained, with a chemical shift for the rhodium phosphine of 28.75ppm ($J_{Rh-P}$ = 124Hz).

A $^{31}P$ solid state nmr spectrum of $RhCl(PPh_3)_3$, Wilkinson's catalyst, has already been published by Diesveld et al [4]. Studies on this compound were carried out for two reasons: firstly, to determine the reproducibility of the earlier spectrum, and secondly, to investigate the 'large' chemical shift anisotropy mentioned by the authors. The sample was kindly lent by M.A. Luke, from the group of Dr. D.M.P. Mingos.

The solid state spectrum obtained is shown in Figure 4.4, and reveals isotropic resonances closely similar to those in the published spectrum. The resolution obtained is very good, with an average linewidth of 92Hz. In order to obtain such resolution, care was taken to set the magic angle as accurately as possible (section 2.3.4). The chemical shifts and coupling constants measured from the solid state spectrum are shown in Table 4.2, where they are compared

Figure 4.3

$^{31}P$ nmr spectrum of $[Rh(CN\text{-}xylyl)_2(PPh_3)_2](PF_6)$ (500 scans, $\omega_r$ = 2.9kHz).

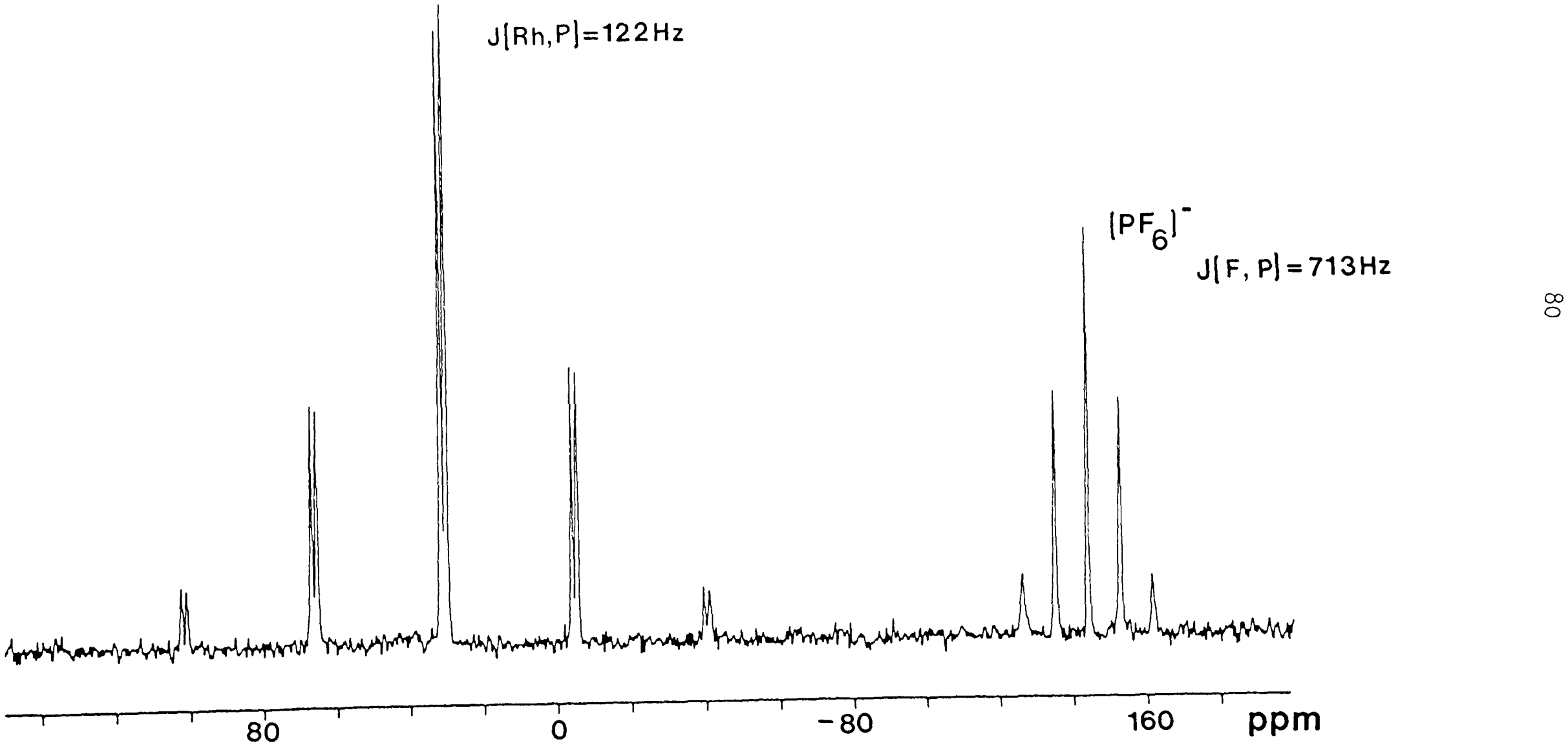

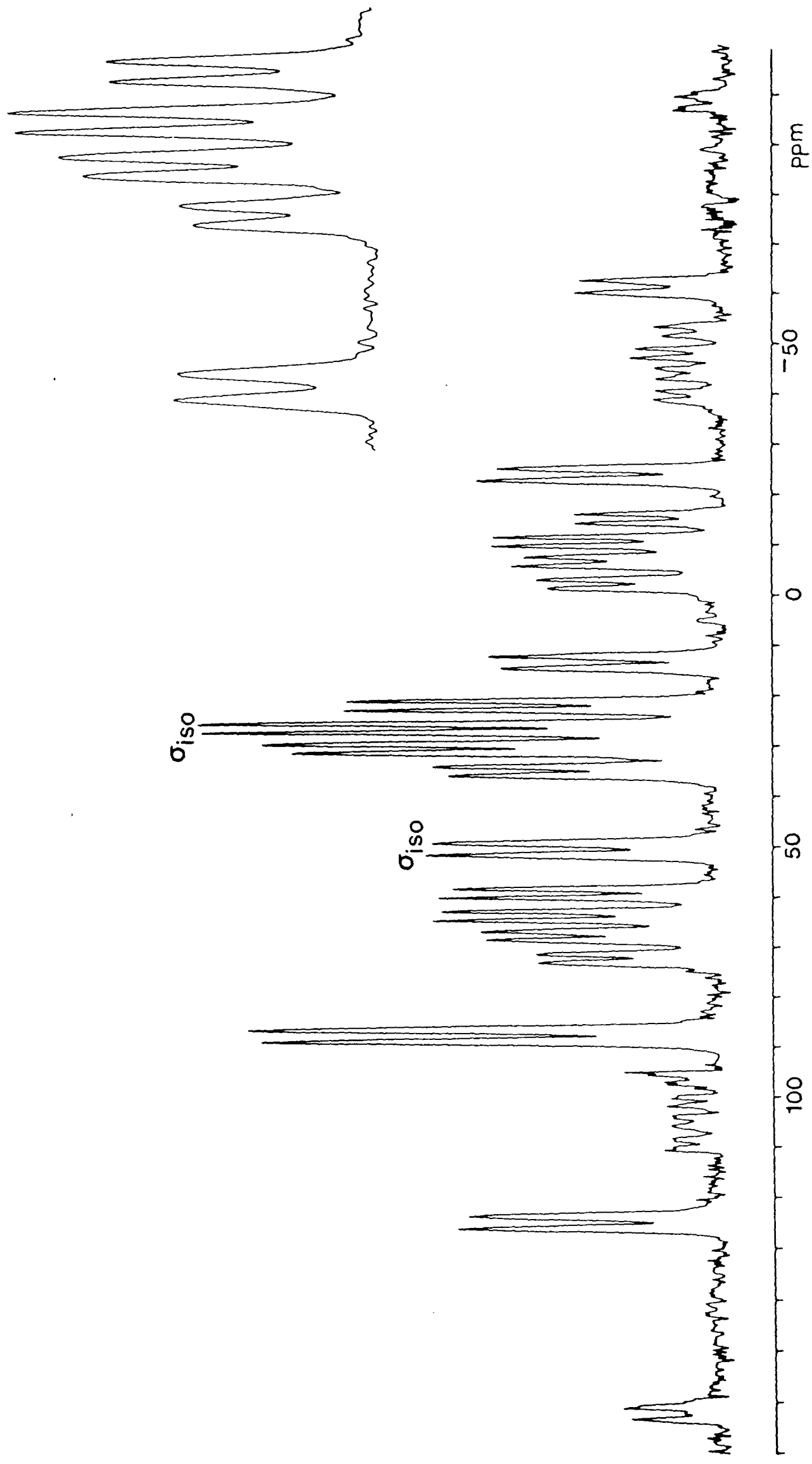


Figure 4.4

$^{31}P$ nmr spectrum of $[RhCl(PPh_3)_3]$ (700 scans, $\omega_r$ = 3.0kHz).

Inset: the isotropic resonances.

TABLE 4.2

A comparison of the $^{31}P$ chemical shifts and coupling constants measured for $RhCl(PPh_3)_3$ in the solid state with those observed in solution.

| | solid state | | | | solution | |
|---|---|---|---|---|---|---|
| phosphorus atom | this thesis | | Diesveld *et al* | | | |
| | $\sigma_{iso}$ (ppm) | J(Hz) | $\sigma_{iso}$ (ppm) | J(Hz) | $\sigma_{iso}$ (ppm) | J(Hz) |
| P trans to Cl | 50.2 | 188 | 50.2 | 185 | 48.0 | 189 |
| P trans to P | 32.6 | 142 | 32.0 | 139 | 31.5 | 142 |
| | 24.1 | | 24.6 | | | |
| | [$J_{p-p}$=366Hz] | | [$J_{p-p}$=365Hz] | | | |

All chemical shifts are referenced to 85% $H_3PO_4$.

with both solution $^{31}P$ nmr data and with that obtained by Diesveld et al [4]. The agreement between the two sets of solid state data is excellent.

The structure of $RhCl(PPh_3)_3$ is to a first approximation square planar, but with a distortion towards tetrahedral geometry [22]. There are four crystallographically equivalent molecules in the unit cell. The low field doublet in the solid state spectrum results from the phosphorus atom trans to chlorine, which is coupled to rhodium. At higher field the observed multiplet results from the two magnetically inequivalent, mutually trans phosphorus atoms, which are coupled both to each other and to rhodium. Any cis phosphorus coupling present is too small to be observed.

The chemical shift anisotropies of all three phosphorus atoms are indeed large, giving rise to a considerable number of spinning sidebands in the spectrum. Spectra were obtained at several spinning speeds in order to ascertain the positions of the isotropic resonances. The CSA's of the two types of phosphorus atoms (trans to $PPh_3$ and trans to Cl) are very different, as illustrated in the schematic diagram (Figure 4.5). That of the phosphorus atom trans to chlorine is the larger of the two, and is such that the isotropic resonance ceases to be the most intense line of the spinning sideband manifold.

An interesting comparison may be made between the two rhodium complexes. Despite obvious similarities between $RhCl(PPh_3)_3$ and $[Rh(CN\text{-}xylyl)_2(PPh_3)_2]PF_6$, their solid state spectra are very different, with the observation of inequivalence of the mutually trans phosphines in $RhCl(PPh_3)_3$ but equivalent trans phosphines in the other complex. However the chemical shifts and CSA's of these phosphines are closely similar in the two compounds. The resonance of the phosphorus

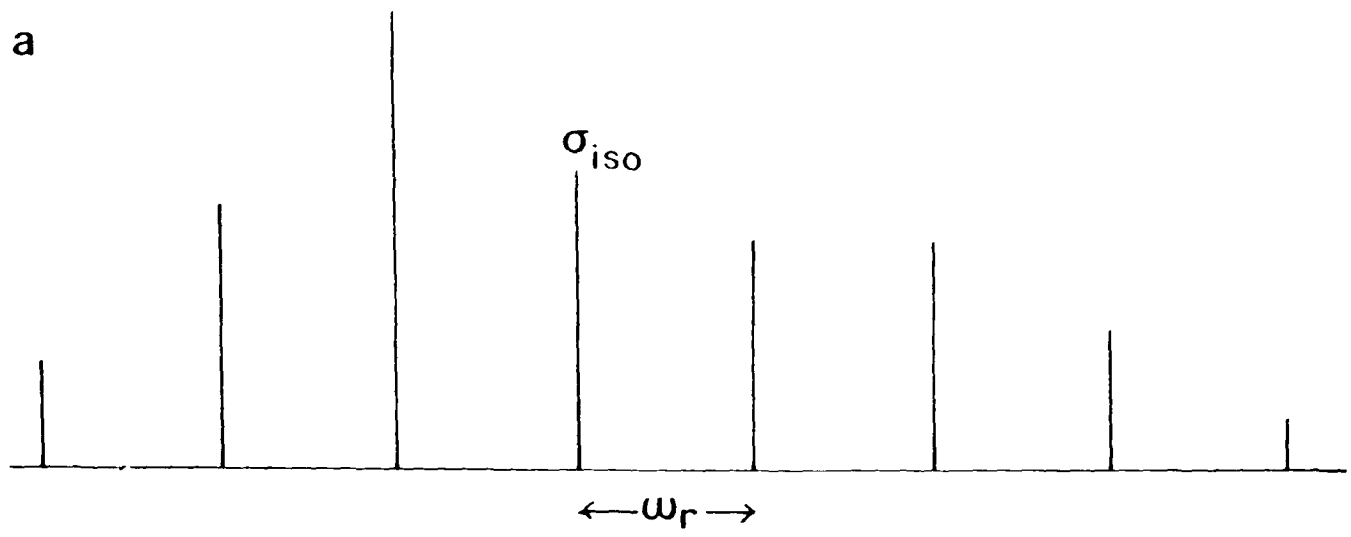


Figure 4.5

Schematic diagram comparing the magnitudes of the CSA's of the two types of phosphorus atom in $RhCl(PPh_3)_3$.
(a) phosphorus trans to Cl (b) phosphorus trans to $(PPh_3)$.

trans to chlorine, meanwhile, is shifted 20ppm downfield of these resonances and has a much greater anisotropy. This suggests that $\sigma_{iso}$, J and the CSA are characteristic of the geometry in square planar complexes, and may thus be used to determine the relative positions of phosphine ligands in other, similar complexes.

4.4.2 Rhodium carbonyl clusters.

The clusters $Rh_4(CO)_{11}PPh_2Et$ and $Rh_6(CO)_{15}PPh_2Et$ were prepared by R.J. Crowte (Southampton) by methods similar to those described previously [23,24]. Typically several hundred transients were accumulated for each spectrum.

The solid state $^{31}P$ spectrum of $Rh_4(CO)_{11}PPh_2Et$ is shown in Figure 4.6. It reveals a single resonance split to a doublet by scalar coupling to the rhodium nucleus. There are two possible isomers of this cluster; however only one is observed in solution [23]. It would appear that a single isomer is present in the solid state. Although the solution and solid state coupling constants are identical, at 122Hz, the chemical shift measured in the solid state is 9ppm to high field of that measured in solution. The chemical shift anisotropy of the cluster is small, spanning about 90ppm, and is almost symmetric about $\sigma_{22}$.

Two $^{31}P$ resonances are observed in the initial solid state spectrum of $Rh_6(CO)_{15}PPh_2Et$, with relative intensities of 2.5:1 (Figure 4.7a). Both show coupling to rhodium, with identical coupling constants of 122Hz. In solution a single resonance is observed, with a chemical shift similar to that of the less intense solid state resonance. The crystal structure of the cluster has not been determined. On the basis of the results obtained for $H_2Os_3(CO)_9PPh_3$ it was decided to recrystallise the sample. The spectrum of the

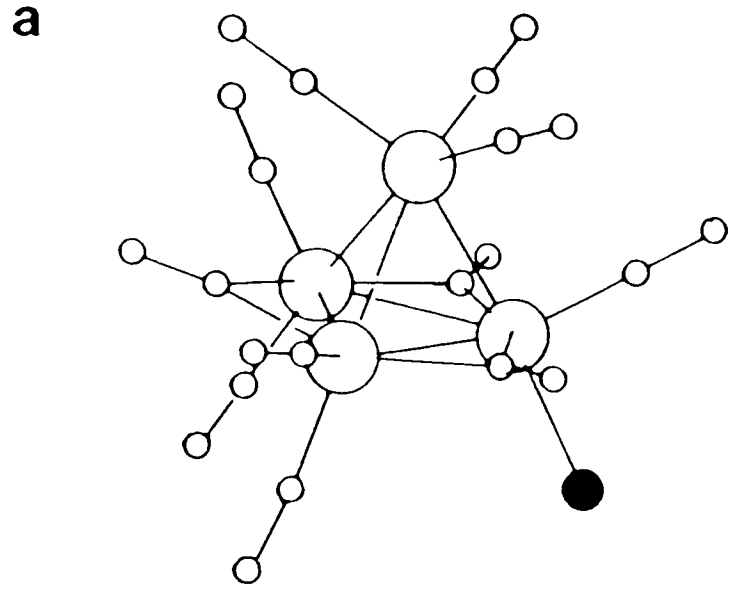





Figure 4.6

(a) Structure of $Rh_4(CO)_{11}PPh_2Et$.

(b) $^{31}P$ nmr spectrum of the cluster (1200 scans, $\omega_r$ = 3.8kHz).

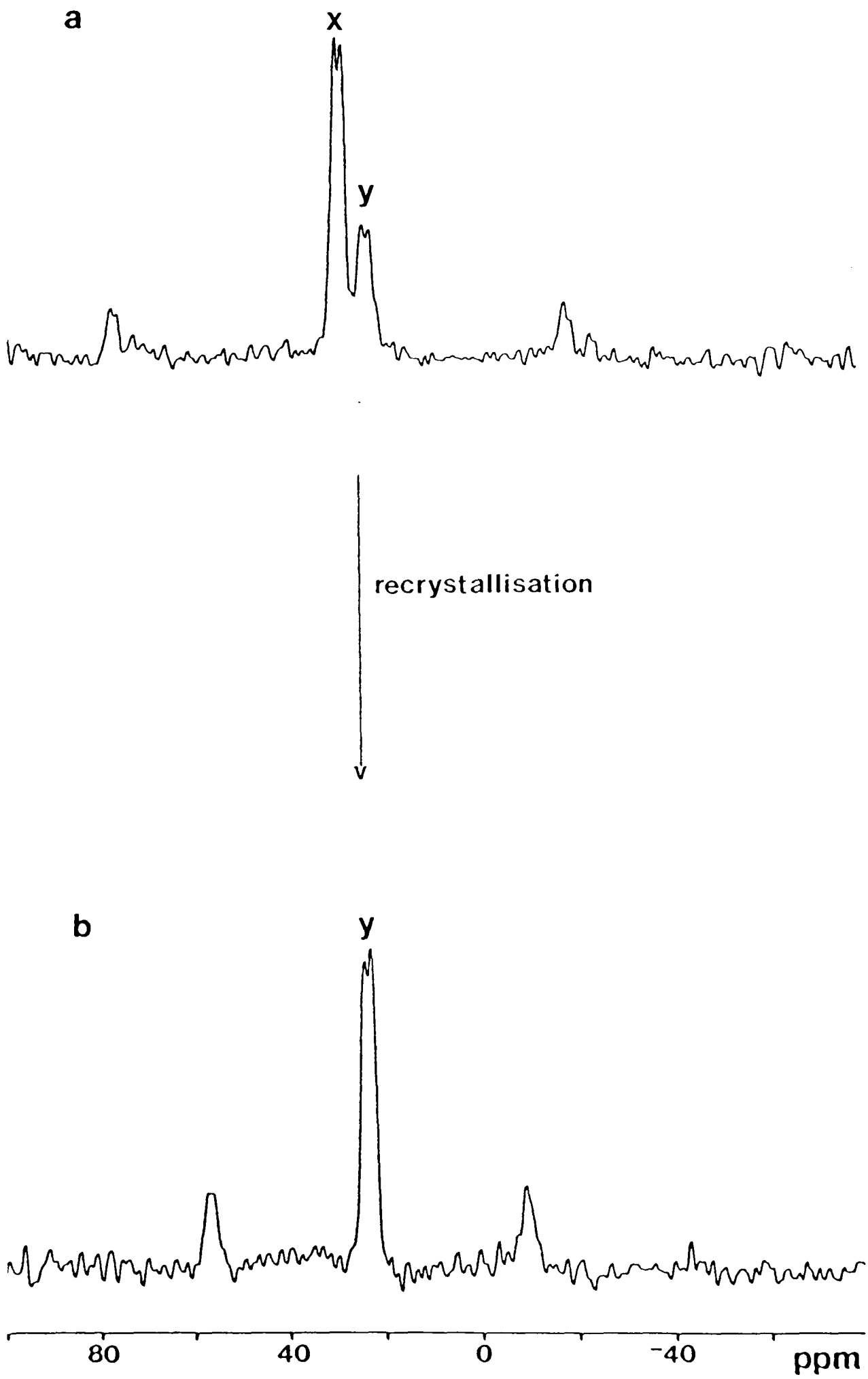


Figure 4.7

$^{31}P$ nmr spectra of $Rh_6(CO)_{15}PPh_2Et$, showing the effect of sample recrystallisation (approx. 1800 scans).

recrystallised cluster shows a single solid state resonance at the same chemical shift as the less intense resonance in the previous spectrum (Figure 4.7b). As no isomers of the cluster are possible with the exception of those produced by rotation about the Rh-P bond, a single resonance would be expected in the solid state, as is observed in solution. This implies that the two resonances in the initial spectrum arise from phosphorus nuclei in two different crystallographic environments.

The CSA of $Rh_6(CO)_{15}PPh_2Et$ is shown by the static spectrum to be symmetric about $\sigma_{22}$. A comparison of the shielding tensor components for this cluster with those of $Rh_4(CO)_{11}PPh_2Et$ shows a close similarity in the magnitude of $\sigma_{22}$ and $\sigma_{33}$ for the two clusters. The static spectra of both clusters may be reproduced using the above tensors in the powder pattern simulation programme described earlier (chapter 2).

TABLE 4.3

The shielding tensors for the two rhodium clusters (ppm).

| | $Rh_4(CO)_{11}PPh_2Et$ | $Rh_6(CO)_{15}PPh_2Et$ |
|---|---|---|
| $\sigma_{11}$ | 51 | 71 |
| $\sigma_{22}$ | 17 | 21 |
| $\sigma_{33}$ | -25 | -29 |

## 4.5 Tris(trimethylphosphine)tungsten hexahydride.

The compound $WH_6(PMe_3)_3$ was kindly lent by G. Parkin (from Dr. M.L.H. Green's group) for solid state nmr studies. In solution a single phosphorus resonance is observed for this compound even at low temperature, with a chemical shift of -24.2ppm [25]. The solid state

phosphorus spectrum of this compound shows two well-resolved lines of relative intensities 1:2, each with its manifold of spinning sidebands (Figure 4.8). Inspection suggests that the two phosphorus environments have different CSA's; this was confirmed by analysis of the spinning sidebands by the methods described in chapter 2 [26,27]. The calculated shielding tensors are shown below.

TABLE 4.4

The calculated shielding tensors for $WH_6(PMe_3)_3$ (ppm).

| | $\sigma_i$ = -2.3ppm [1P] | | $\sigma_i$ = -22.6ppm [2P] | |
|---|---|---|---|---|
| | MW | HB | MW | HB |
| $\sigma_{11}$ | 43 | 53 | 17 | 10 |
| $\sigma_{22}$ | 17 | 2 | -26 | -15 |
| $\sigma_{33}$ | -67 | -62 | -59 | -62 |

[MW-moment calculation; HB-graphical method.]

Although the crystal structure of $WH_6(PMe_3)_3$ has not been determined, that of the analogous compound $WH_6(PPhPr^i_2)_3$ is known [28]. This may be regarded as being derived from a tricapped trigonal prism, with one phosphorus atom in a capping position and two others occupying eclipsed positions on opposite axial prismatic faces. These two eclipsed phosphines are significantly further from the metal atom than the capping phosphine. Confirmation of this structure in solution was obtained from the low temperature (180K) $^{31}P$ nmr spectrum, which showed two phosphorus resonances at 69.3 and 47.8ppm with intensities of 1:2 [28]. At higher temperatures, however, a single resonance was observed at 55.5ppm.

The solid state nmr spectrum of $WH_6(PMe_3)_3$ is completely consistent with an analogous crystal structure, with the two

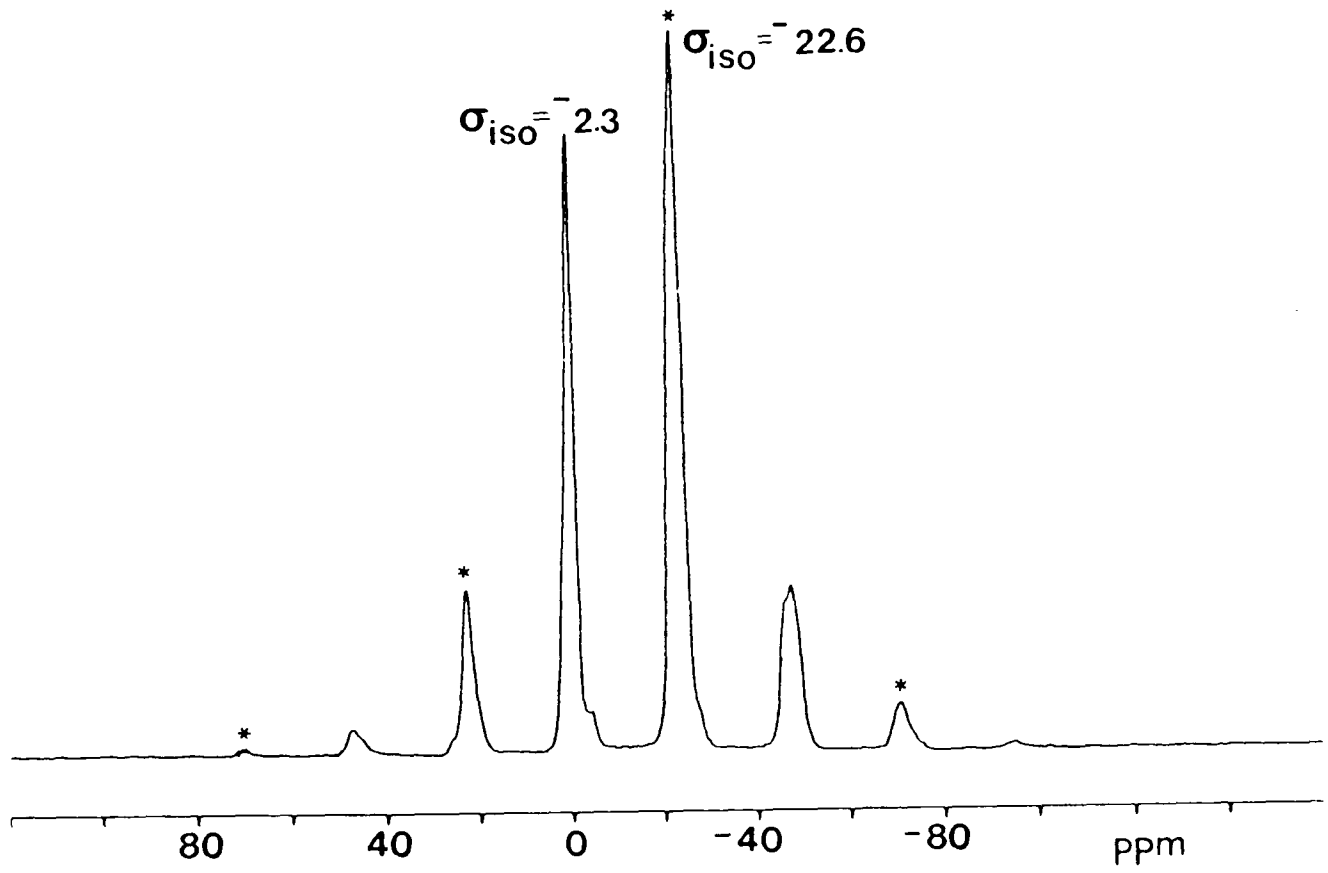


Figure 4.8

$^{31}P$ nmr spectrum of $WH_6(PMe_3)_3$ (200 scans, $\omega_r$ = 3.8kHz).

The two sets of sidebands are indicated.

phosphorus resonances resulting from two inequivalent phosphorus environments in the molecule. In solution $^{31}P$ nmr reveals the fluxionality well-known for nine-coordinate complexes, which cannot be frozen out even at low temperature but which is slowed by intermolecular interactions in the solid state. The solution chemical shift is close to the value which would be predicted from the solid state shifts on averaging of the phosphorus environments. The large difference in chemical shift between the two phosphorus resonances (similar in magnitude to the separation of the two resonances of $WH_6(PPhPr^i_2)_3$ [28]) may be contrasted with the small difference observed for the two sets of resonances of $Rh_6(CO)_{15}PPh_2Et$, which has been ascribed to crystallographic differences between phosphorus atoms.

4.6 Arenetris(tertiary phosphine)molybdenum compounds.

A series of arenetris(tertiary phosphine)molybdenum compounds were prepared by Dr. C. McAteer [29] and studied by $^{31}P$ and $^{13}C$ solid state nmr. The air-sensitive compounds were packed into rotors in a glovebox and the tops sealed with Teflon tape; the rotors were then kept under a nitrogen atmosphere until use. Typically several hundred transients were accumulated.

The $^{31}P$ spectra of $(C_6H_6)Mo(PR_3)_3$, where R = $PMe_3$, $P(OMe)_3$ or $PPhMe_2$, all show a single phosphorus resonance (Figure 4.9). For the first two compounds the lines are very sharp, with linewidths of 30Hz and <10Hz respectively. These are the narrowest lines obtained for phosphines in this work. The resonance of the $PPhMe_2$ compound is broader ($\Delta\nu_{1/2}$ = 315Hz). These results are in accord with the solution nmr spectra, which also show a single resonance for all three clusters. A sextet of peaks of equal intensity symmetric about the

TABLE 4.5

Solid state $^{31}P$ chemical shifts and linewidths measured for the series of molybdenum complexes.

| compound | chemical shift (ppm) | $\Delta\nu_{1/2}$ (Hz) |
|---|---|---|
| $(C_6H_6)Mo(PMe_3)_3$ | 4.5 | 30 |
| $(C_6H_6)Mo(P(OMe)_3)_3$ | 191.2 | >10 |
| $(C_6H_6)Mo(PPhMe_2)_3$ | 18.5 | 315 |
| $[(C_6H_6)Mo(PMe_3)_3H][PF_6]$ | 1.9 | 450 |
| $[(C_6H_6)Mo(PMe_3)_3H_2][PF_6]_2$ | -4.3 | 770 |

All chemical shifts are referenced to 85% $H_3PO_4$.

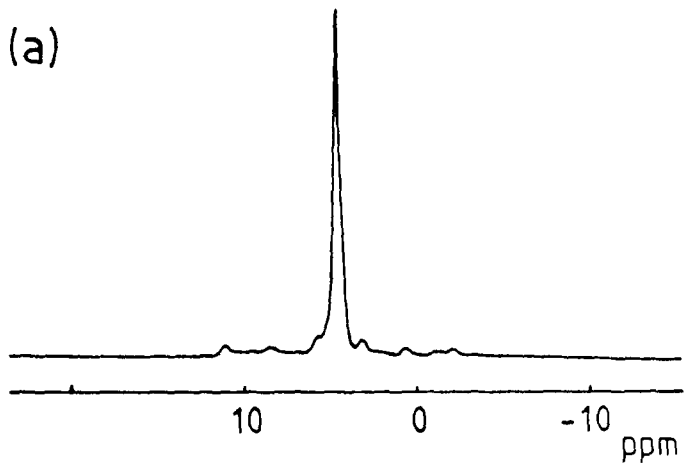


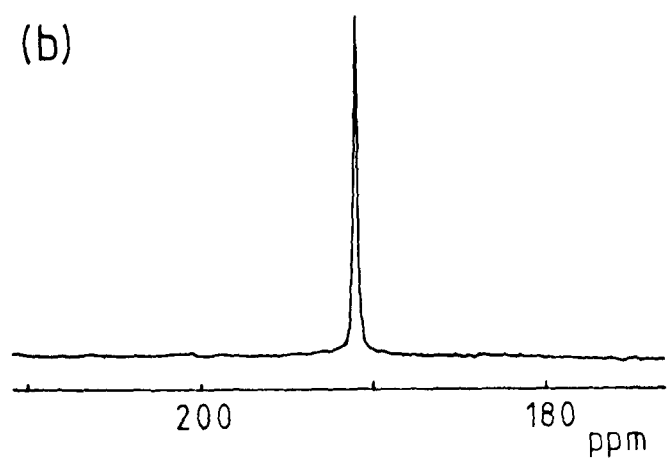


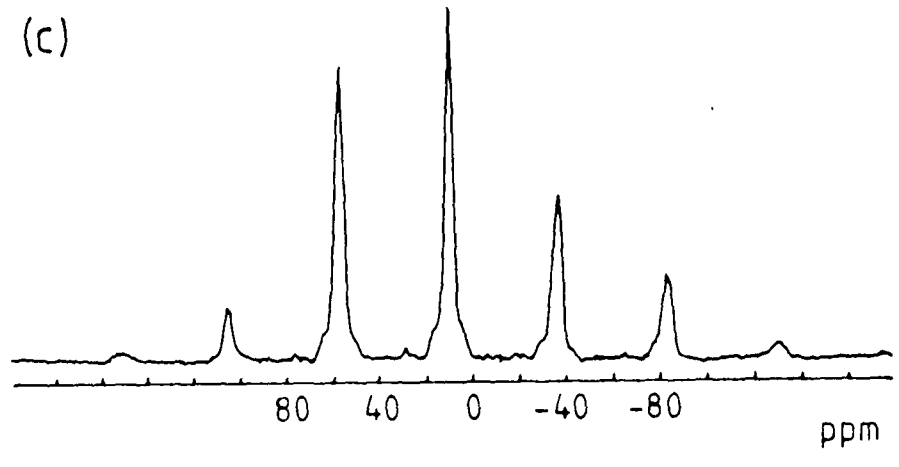


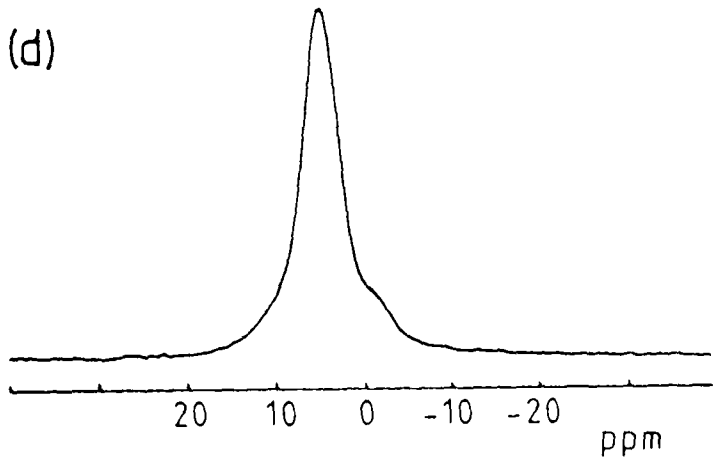


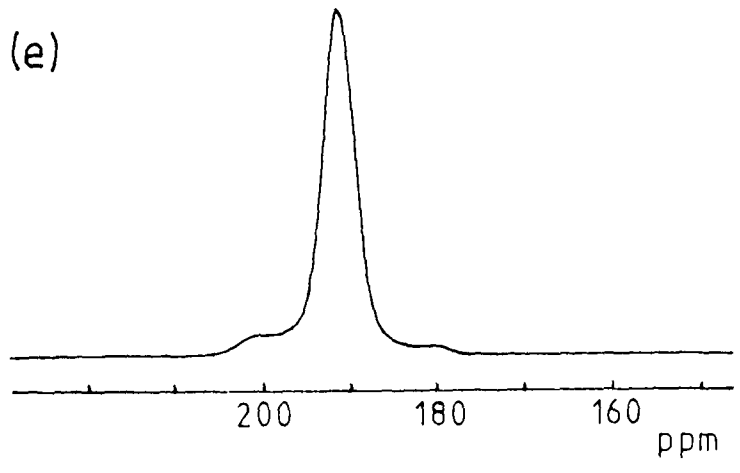


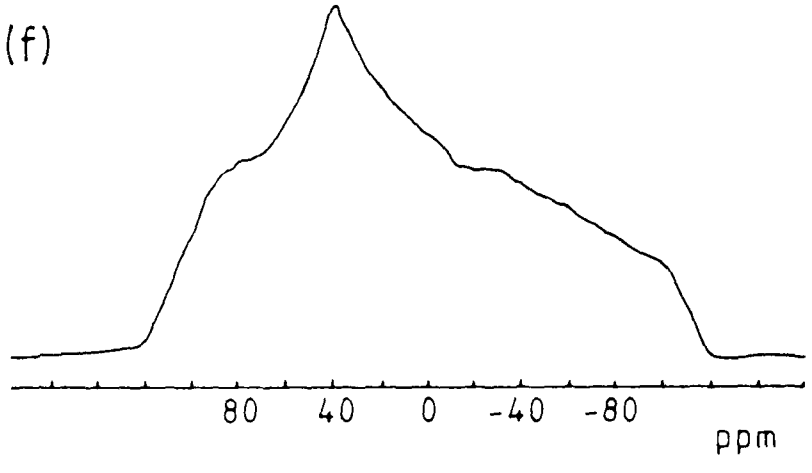


Figure 4.9

$^{31}P$ nmr spectra of the molybdenum complexes $(C_6H_6)MoL_3$. (a)-(c) were recorded using magic angle spinning for complexes with L = $PMe_3$, $P(OMe)_3$ and $PPhMe_2$ respectively; (d)-(f) are the corresponding static spectra.

base of the phosphorus resonance in $(C_6H_6)Mo(PMe_3)_3$ was identified as the result of scalar coupling between molybdenum and phosphorus. There are two magnetically active isotopes of molybdenum, $^{95}Mo$ (15.72% abundant) and $^{97}Mo$ (9.46% abundant), both with spin 5/2. The similarity of their magnetic moments suggests that it is unlikely that the two separate couplings will be resolved. This is in agreement with the solid state nmr spectrum, in which a single Mo-P scalar coupling was observed (Figure 4.10), with $J_{Mo-P}$ of 214Hz. Mo-P coupling is also observed in the solution spectrum of the compound; the coupling constant is identical to that measured in the solid state. Previous reports of scalar coupling to molybdenum have been limited to four nuclei, $^{19}F$ in $MoF_6$ [2], $^{17}O$ in molybdate ion [30] $^{13}C$ in $Mo(CO)_6$ [31] and $^{31}P$ in a series of ten $(OC)_5MoL$ complexes [32], where the Mo-P coupling constant was found to lie in the range 124-284Hz. This is the first example to our knowledge of such coupling in the solid state.

Further structural and motional information may be obtained from the shielding tensors of the three compounds. For both $(C_6H_6)Mo(PMe_3)_3$ and $(C_6H_6)Mo(P(OMe)_3)_3$ slow MAS does not produce any spinning sidebands, and the non-spinning spectra show isotropic lines of width 400Hz (Figure 4.9). In contrast, a considerable number of spinning sidebands are observed for $(C_6H_6)Mo(PPhMe_2)_3$, and the static spectrum spans ~250ppm (>20kHz), evidence of a much greater anisotropy. The powder pattern is that characteristic of a non-axial shielding tensor [33].

The differences between the $^{31}P$ spectra of the three compounds, both in the linewidth of the isotropic resonance and in CSA, suggest that a considerable degree of motion is present in the $(PMe_3)_3$ and $(P(OMe)_3)_3$ compounds. Motional averaging of the phosphorus environments produces a line of almost solution-like sharpness when

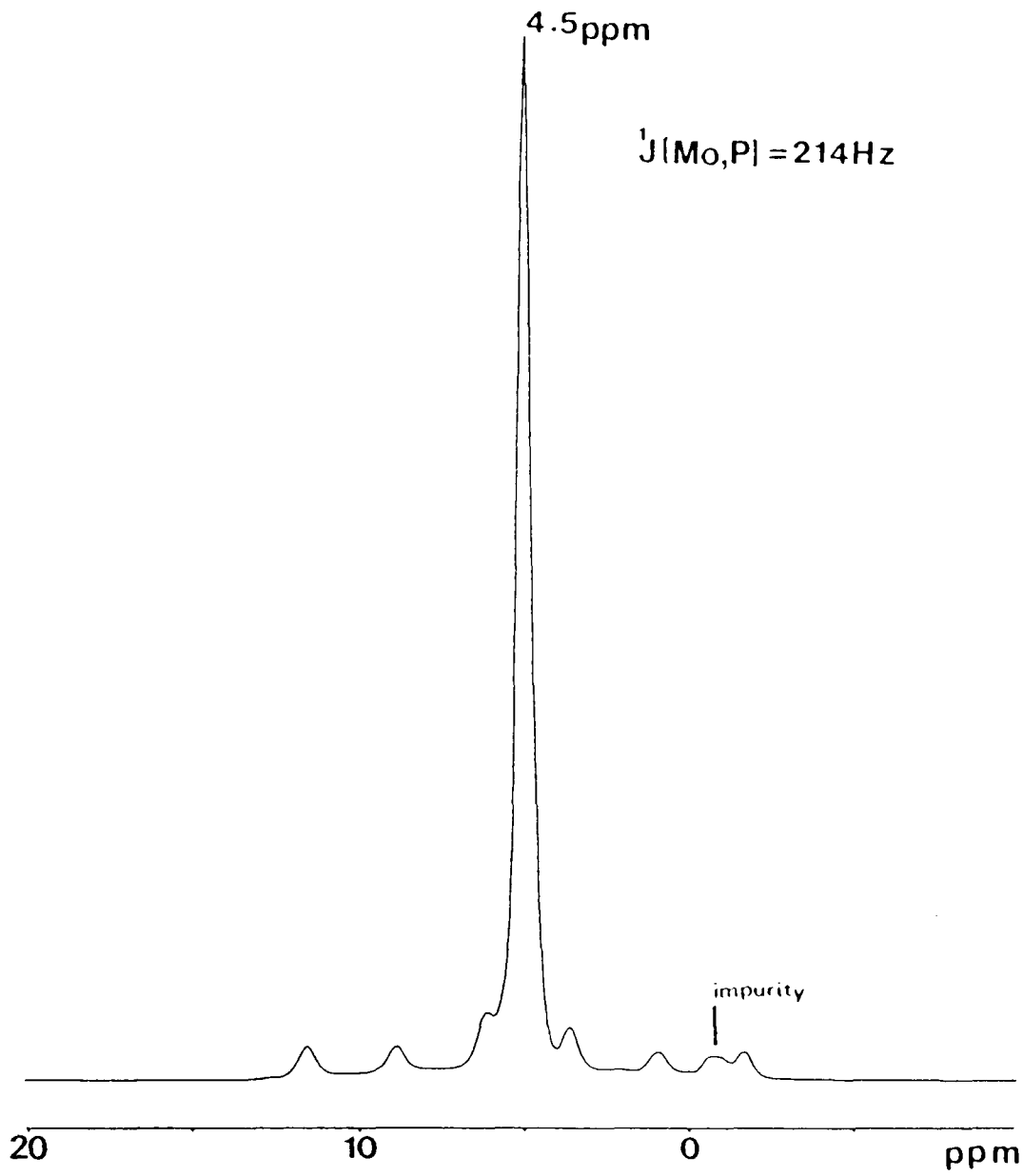


Figure 4.10

$^{31}P$ nmr spectrum of $(C_6H_6)Mo(PMe_3)_3$, showing the Mo-P scalar coupling (300 scans).

MAS is used, and this motion averages the phosphorus CSA to an isotropic tensor. Chemical shift anisotropy powder patterns are averaged by motions that occur more rapidly than $10^3$Hz [34]; this process requires large amplitude fluctuations. Such must be the rate of the dynamic process occurring in the two compounds.

In the hope of learning more about the nature of the dynamic process which was occurring, $^{13}C$ solid state nmr studies were carried out. As in the case of the $^{31}P$ spectra, narrow lines are observed for both $(C_6H_6)Mo(PMe_3)_3$ and $(C_6H_6)Mo(P(OMe)_3)_3$, with linewidths in the order of 30Hz. The spectra consist of two resonances, one from the $(C_6H_6)$ group and a second, to higher field, from the methyl groups. The $^{13}C$ spectrum of $(C_6H_6)Mo(PPhMe_2)_3$ shows the two methyl groups to be inequivalent; the resonances from the phosphine ligands are much broader than that of the $(C_6H_6)$ group (which is similar to that observed in the spectra of the other two clusters), and spinning sidebands are observed for these resonances.

The lack of spinning sidebands for the arene suggests that it is undergoing a dynamic process fast on the nmr timescale in the solid state; if it were static, or if the only motion was rotation of the arene group about its 6-fold axis, axial anisotropy would be expected [33].

The motions in analogous chromium compounds have been discussed extensively in the literature. Rotation of the $ML_3$ tripod was observed by McGlinchey _et al_ [10], and the solution nmr studies of Green and coworkers showed the three L groups to be equivalent down to low temperatures [29]. A general reorientation of the molecule around M was ruled out by Delise _et al_ [35], who found from variable temperature broad line $^1H$ nmr studies evidence for both a rotation of the arene about its six-fold axis and another motion whose nature was

not determined. Another group used neutron scattering to observe ring jumps [36]; they assumed the $ML_3$ unit to be fixed in the crystal. The solid state nmr results reported here, however, show that a simple rotation of the arene ring about its 6-fold axis cannot be the only motion present in the molybdenum compounds. In order to produce the extensive averaging of both $^{13}C$ and $^{31}P$ shielding tensors, the whole molecule must be rotating within the crystal. In contrast, for (arene)$Cr(CO)_3$ Maricq et al observed axial shielding for the arene carbon atoms [37].

Solid state $^{31}P$ studies have also been carried out on compounds derived from $(C_6H_6)Mo(PMe_3)_3$, to which first one and then two hydrogen atoms had been added [29]. The spectra show a shift of the trimethylphosphine resonance to higher field with increasing protonation, and an accompanying increase in linewidth, which reaches 770Hz for $[(C_6H_6)Mo(PMe_3)_3H_2][PF_6]_2$. The $PF_6^-$ group is observed as a septet at high field, centred at -144.2ppm. The CSA of the monoprotonated compound is small, and the static spectrum shows an isotropic line of width 1200Hz. However for the diprotonated species spinning sidebands are observed in the MAS spectrum, and the static spectrum is considerably broadened.

The structures of these two compounds have not been determined, but by analogy with the structures of similar compounds the dihydride is believed to contain two equivalent and one unique phosphine ligands [29]. In solution $^1H$ and $^{31}P$ nmr shows all three phosphines to be equivalent even at low temperature. The solid state spectrum suggests that a dynamic process renders the two phosphine environments equivalent in the solid on the nmr timescale. Such interconversion of stereochemistry has been observed in solution for many tertiary phosphine hydrides [28,29].

## 4.7 The ruthenium cluster $(\mu\text{-H})_2Ru_3(CO)_9(\mu_3\text{-PPh})$.

The cluster $(\mu\text{-H})_2Ru_3(CO)_9(\mu_3\text{-PPh})$ was studied by solid state $^{31}P$ nmr spectroscopy as a model prior to the study of a supported ruthenium system (chapter 7). The initial sample was prepared by S.L. Cook (Southampton) [38], and its solid state spectrum shows three approximately equidistant isotropic lines at a much lower field than the phosphorus resonances of the other phosphine-containing clusters studied (Figure 4.11). This shift is a result of the bridging mode of bonding adopted by the phosphine group. The sequence of three lines is repeated in the spinning sidebands. The solution phosphorus spectrum shows a single resonance at a similar chemical shift to those measured in the solid state.

In order to test the reproducibility of this result, a second sample of the ruthenium cluster was prepared by V. Alexiev. A small quantity (~7mg) of the cluster $(\mu\text{-H})Ru_3(CO)_{10}\text{-(PPhH)}$ was also synthesised; this may be formed as an impurity during the preparation of $(\mu\text{-H})_2Ru_3(CO)_9(\mu_3\text{-PPh})$. However the solid state spectrum of the new cluster shows a single resonance well upfield of the three resonances in the original spectrum, and it may therefore be eliminated as a possible contributor to this spectrum. The new sample of $(\mu\text{-H})_2Ru_3(CO)_9(\mu_3\text{-PPh})$ gives a three line spectrum closely similar to that obtained from the original sample.

An explanation of the unusual solid state spectrum was sought in the crystal structure of the ruthenium cluster [38]. This shows that there is one phosphorus site per molecule, and three crystallographically inequivalent molecules in the unit cell (Figure 4.11). Three phosphorus sites in the unit cell and three resonances in the solid state phosphorus spectrum suggests that the three phosphorus sites can be distinguished by solid state nmr.

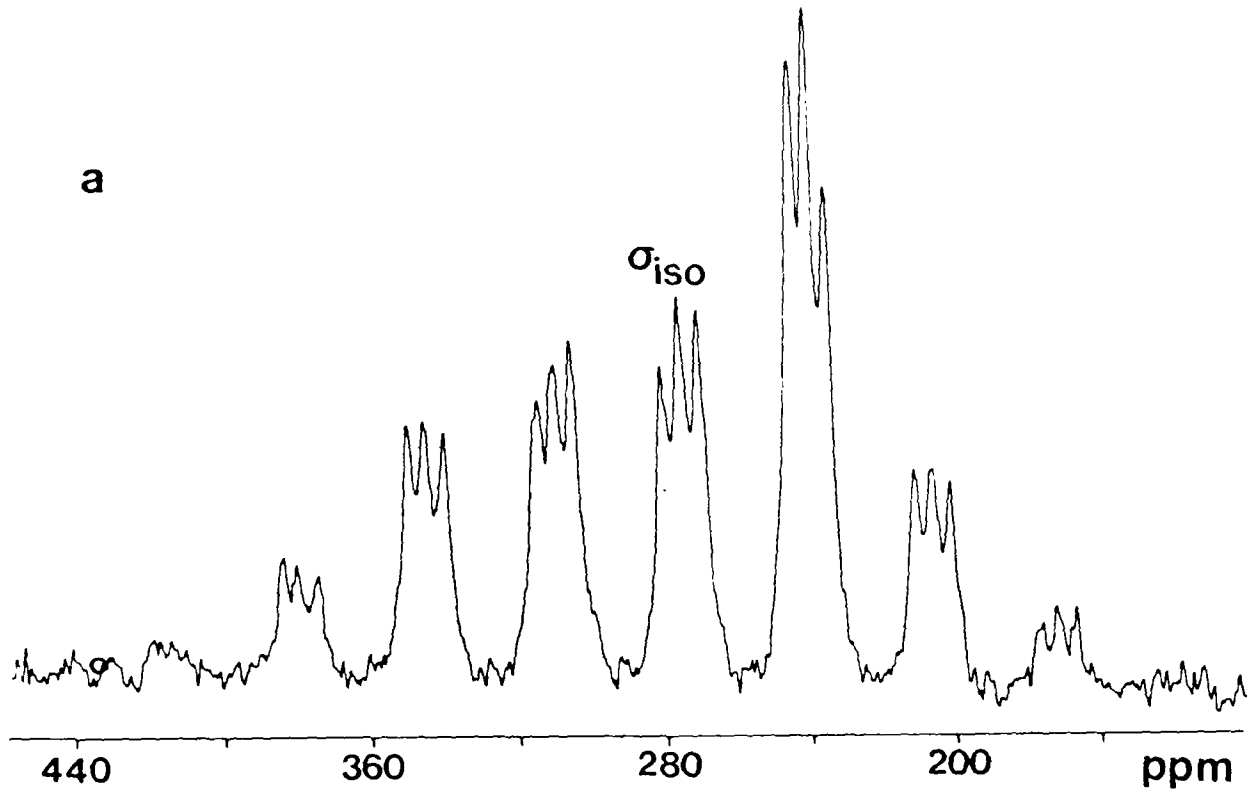


Figure 4.11

(a) $^{31}P$ nmr spectrum of $(\mu\text{-}H)_2Ru_3(CO)_9(\mu_3\text{-}PPh)$ (16000 scans, $\omega_r$ = 2.8kHz).

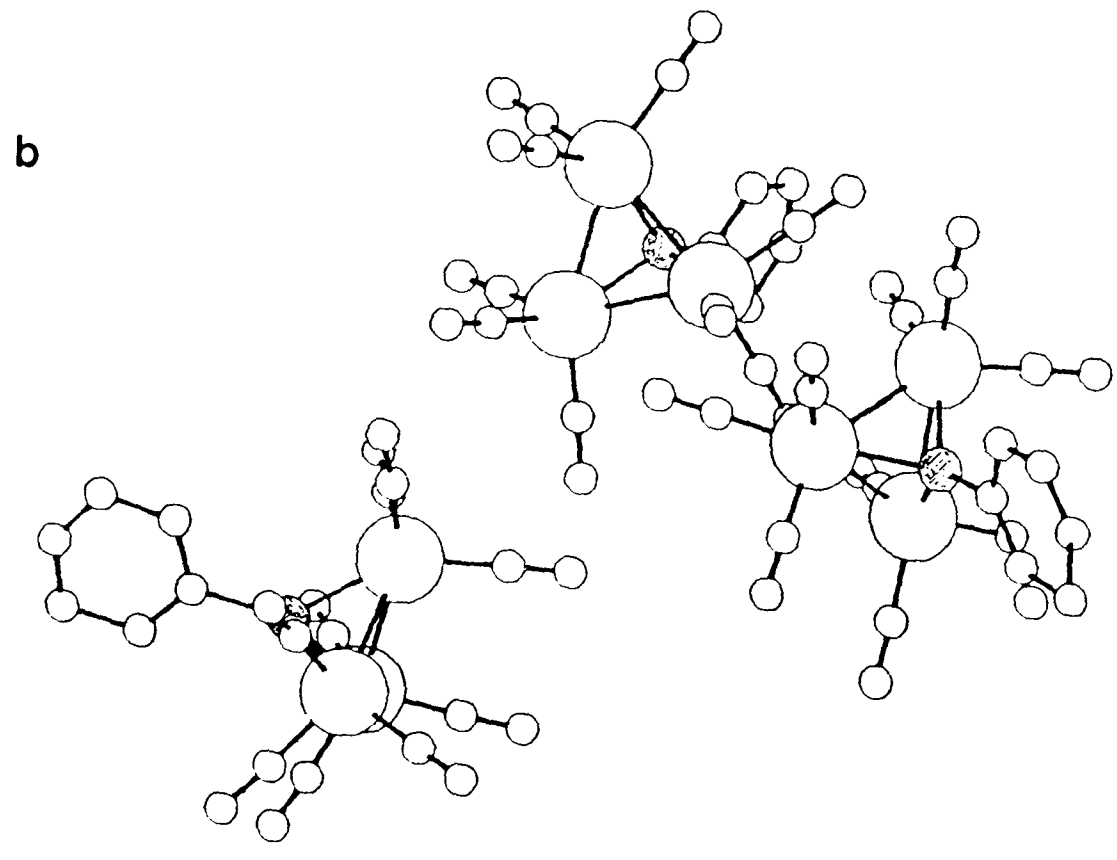


(b) The unit cell of the cluster, showing the relative positions of the three inequivalent molecules.

Further evidence towards this conclusion is provided by an examination of the CSA's associated with the three phosphorus resonances. Moment analysis [26] shows that all three phosphorus environments have closely similar, axial shielding tensors, with tensor values $\sigma_{\perp}$ = 190ppm and $\sigma_{\parallel}$ = 460ppm. Axial anisotropy would be consistent with the phosphorus environment in $(\mu\text{-H})_2Ru_3(CO)_9(\mu_3\text{-PPh})$ as shown by the crystal structure. The three resonances clearly arise from three phosphorus atoms closely similar in both chemical shift and CSA. On the basis of the crystal structure it would appear that they result from the three distinct phosphorus sites in the unit cell of the cluster.

## 4.8 $^{13}C$ spectra of transition metal carbonyls.

Two transition metal carbonyl clusters were studied by $^{13}C$ nmr: $H_2Os_3(CO)_9PPh_3$ and $H_2Os_3(CO)_{10}PPh_3$. These samples were prepared by the group at Southampton University. Preliminary studies rapidly ascertained that it was not possible to obtain $^{13}C$ spectra from the carbonyl groups of these clusters in a realistic period of time using natural abundance $^{13}C$. Samples enriched to 40% in $^{13}CO$ were therefore prepared by V. Alexiev from $^{13}C$-enriched $Os_3(CO)_{12}$; this was prepared using a method analogous to that described by Wilkinson and Todd [39]. In order to obtain the best possible signal from the small quantities of sample available (5-10mg), the deuterated plexiglass rotors were packed using KBr as described in section 2.3 4. This not only allowed the magic angle to be optimised on the sample under study, but enabled the entire carbonyl sample volume to be placed within the coil, so that maximum signal could be obtained. As discussed earlier in this chapter, cross polarisation was used to reduce the recycle delay and increase the sensitivity [9].

The results of these experiments show that satisfactory $^{13}C$ solid state spectra can be obtained from $^{13}C$ enriched metal carbonyl clusters, using cross polarisation, in an acceptable period of time (generally about 6 hours). The levels of enrichment were chosen to be sufficiently low such that $^{13}C$-$^{13}C$ dipolar coupling would be small; no broadening which could be attributed to such coupling was observed in the spectra.

The $^{13}C$ spectrum of $H_2Os_3(CO)_9PPh_3$ is shown in Figure 4.12. Eight carbonyl resonances are observed. The isotropic peaks show the intensity ratio 1:1:1:2:1:1:1:1, and this pattern is repeated in the spinning sidebands. It appears that in the solid state all except two of the carbonyl groups may be distinguished. The large anisotropy of the carbonyl groups (~400ppm) is revealed by the large number of spinning sidebands in the spectrum; the isotropic peaks are not the most intense of those originating from the carbonyls. The large CSA of terminal CO groups was discussed by Gleeson and Vaughan for a number of transition metal carbonyl cluster compounds, including $Os_3(CO)_{12}$ [40].

The CSA of the $^{13}CO$ resonances of the cluster $H_2Os_3(CO)_{10}PPh_3$ is also large, and again the isotropic resonances are less intense than some of their spinning sidebands. The resolution in the solid state spectrum is not as good as in that of the nonacarbonyl. However at least five resonances can be distinguished in the carbonyl region (Figure 4.13), and this pattern is repeated in the spinning sidebands. Variable temperature solution $^{13}C$ nmr spectra of this cluster have been obtained by Aime et al [41]. Six resonances were observed at -70°C, in intensity ratios 4:1:1:1:1:2, and as the temperature was increased a series of changes occurred in the spectrum until a different six line spectrum was seen at +30°C. The chemical

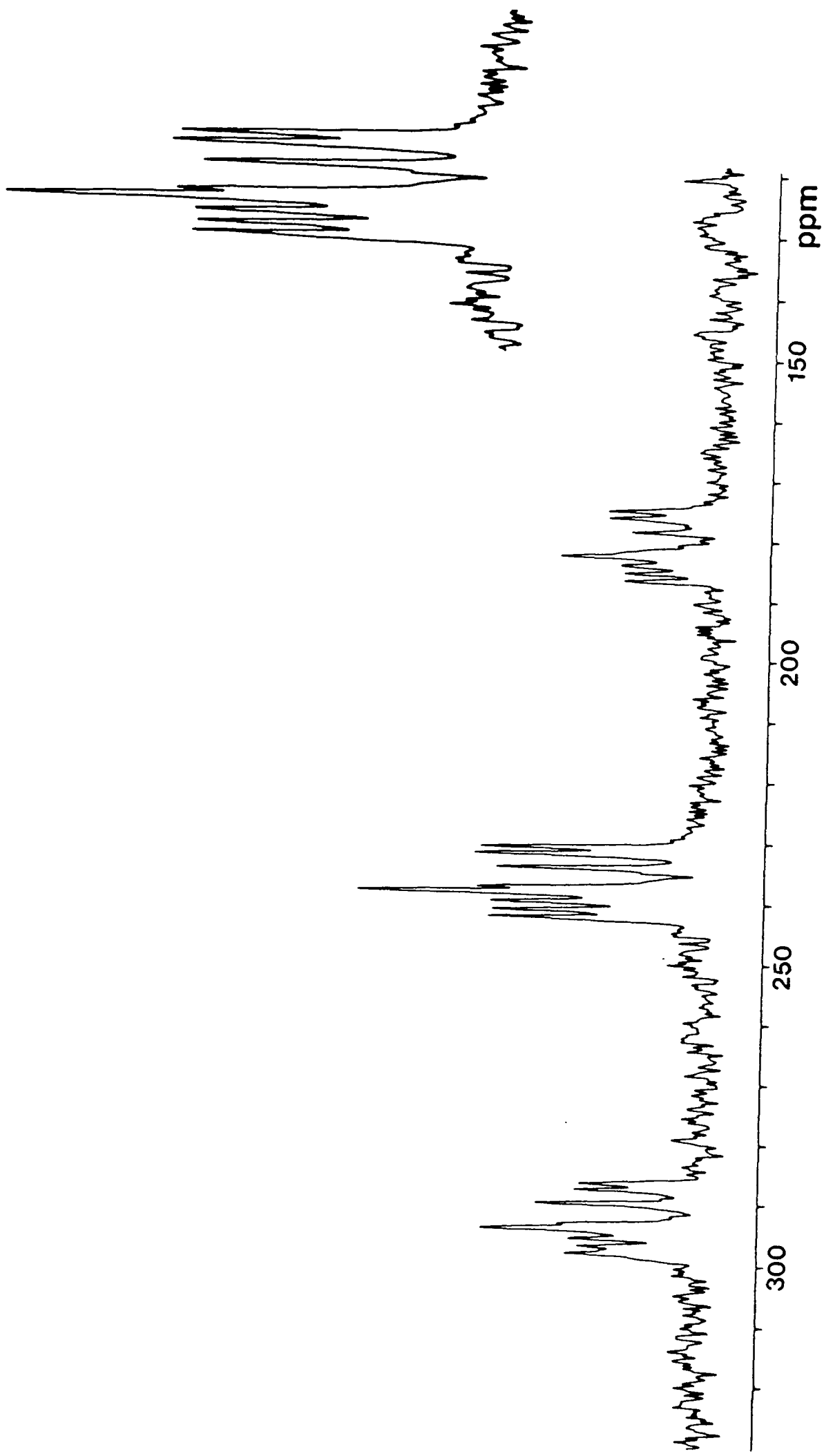


Figure 4.12

$^{13}C$ nmr spectrum of $H_2Os_3(CO)_9PPh_3$, 40% enriched in $^{13}CO$ (accumulated overnight). Inset: enlargement of the isotropic region.

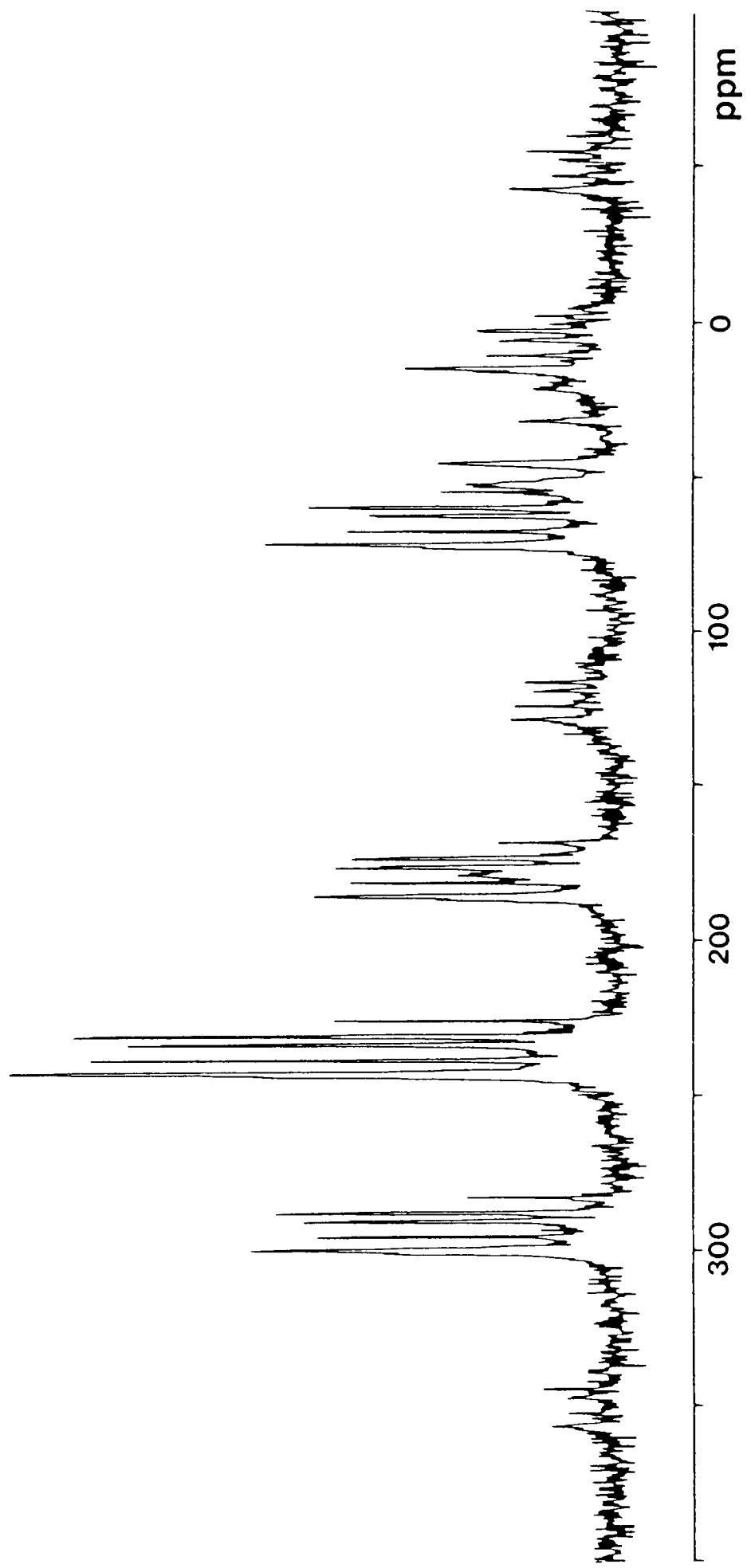


Figure 4.13

$^{13}C$ nmr spectrum of $H_2Os_3(CO)_{10}PPh_3$, 40% enriched in $^{13}CO$ (accumulated overnight).

shifts observed in the solid state are similar to those found in solution, with the solid state spectrum closely resembling the low temperature solution spectrum.

## 4.9 Discussion.

The work discussed in this chapter demonstrates the application of solid state $^{31}P$ and $^{13}C$ nmr spectroscopy to a variety of transition metal complexes and clusters. The spectra obtained were of excellent quality, and could be correlated with solution nmr data and the X-ray crystal structures of the compounds studied. This illustrates the position of solid state nmr as a bridge between the two techniques.

Many of the compounds discussed in this chapter were studied primarily because of the need to characterise simple compounds in preparation for solid state nmr investigations of the species they form on anchoring to oxide surfaces. However a number of interesting points have arisen from the results obtained from these 'simple' transition metal clusters which indicate the nature of the information available from solid state nmr spectroscopy and the power of the technique in disclosing small inequivalences in environment.

The sensitivity of solid state nmr to small variations in structure is such that, in the case of $Rh_6(CO)_{15}PPh_2Et$, two crystallographically distinct forms of the cluster may be distinguished. The presence of different environments for a molecule in the unit cell may also be revealed by solid state nmr; the three inequivalent molecules in the unit cell of $(\mu\text{-}H)_2Ru_3(CO)_9(\mu_3\text{-}PPh)$ produce three resonances in the solid state $^{31}P$ nmr spectrum. The differences in chemical shift between the resonances in these cases are small (of the order of 5ppm) but they can be clearly resolved.

Meanwhile, a larger separation between resonances in a solid state spectrum indicates a greater difference in magnetic environment. For the complex $WH_6(PMe_3)_3$ the two resonances in the $^{31}P$ nmr spectrum are separated by 20ppm. In this compound the presence of two inequivalent phosphorus sites in the molecule is revealed by solid state nmr, two sites which are rendered equivalent in solution by a fluxional process even at low temperature. Here the effect of intermolecular interactions in the solid enables solid state nmr to provide evidence for the existence of a structure previously postulated by analogy with a similar compound but for which neither solution nmr or X-ray diffraction evidence was available.

Structural information on the solid samples studied may be obtained not only from the isotropic shifts but from the CSA and from the scalar couplings which are clearly resolved in several of the solid state spectra. The difference in the principal values of the shielding tensor for the two phosphorus sites in $WH_6(PMe_3)_3$ further emphasises the difference between the two sites revealed by the large separation in their chemical shifts. The magnitude of both the phosphorus CSA and the Rh-P coupling constant is found to be characteristic of the phosphorus environment in the square planar complexes, enabling a distinction to be made between $PR_3$ trans to $PR_3$ and $PR_3$ trans to another ligand. The resolution in the solid state $^{31}P$ spectrum of $(C_6H_6)Mo(PMe_3)_3$ is such that coupling between phosphorus and the magnetically active isotopes of molybdenum, which are only 25% abundant, can be clearly observed.

Dynamic information may also be obtained from solid state nmr spectroscopy. In the tungsten complex studied the fluxional process operating in solution is frozen out in the solid state. However not all dynamic processes become slow on the nmr timescale in

solids as a result of the increased intermolecular interactions, and for the group of compounds $(C_6H_6)Mo(PR_3)_3$ a rapid fluxional process is operating in the solid at room temperature, revealed by the averaging of both $^{31}P$ and $^{13}C$ shielding tensors. The type of averaging indicates the nature of the motion: in this case, both of the averaged tensors are isotropic, which can only be accounted for by a process involving rotation of the entire molecule within the crystal.

The utility of the cross polarisation technique in the study of nuclei of low sensitivity is illustrated by the $^{13}C$ spectra obtained from the metal carbonyl clusters. The wider application of this method, particularly at higher field to obtain better separation of the carbonyl resonances, should provide much structural and dynamic information on carbonyl-containing compounds. Its use in the study of supported carbonyl clusters will be considered in chapter 7.

## 4.10 References.

[1] P.S. Pregosin and R.W. Kunz, NMR: Basic Princ. Prog. 16 (1979) 1.

[2] 'High resolution NMR spectroscopy' eds. J.W. Emsley, J. Feeney and L.H. Sutcliffe, Pergamon Press, N.Y. (1966) vol. 2 881.

[3] C.A. Fyfe, 'Solid state NMR for chemists", CFC Press, Guelph (1983).

[4] J.W. Diesveld, E.M. Menger, H.T. Edzes and W.S. Veeman, J. Amer. Chem. Soc. 102 (1980) 7935.

[5] L. Bemi, H.C. Clark, J.A. Davies, C.A. Fyfe and R.E. Wasylishen, J. Amer. Chem. Soc. 104 (1982) 438.

[6] L. Bemi, H.C. Clark, J.A. Davies, D. Drexler, C.A. Fyfe and R.E. Wasylishen, J. Organomet. Chem. 224 (1982) C5.

[7] G.E. Maciel, D.J. O'Donnell and R. Greaves, Adv. Chem. Ser. 196 (1982) 389.

[8] S.J. Heyes, Part II thesis, Oxford (1985).

[9] J.R. Lyerla, C.A. Fyfe and C.S. Yannoni, J. Amer. Chem. Soc. 101 (1978) 1351.

[10] M.J. McGlinchey, P. Bougeard, B.G. Sayer, R. Hofer and C.J.L. Lock, J. Chem. Soc., Chem. Commun. (1984) 789.

[11] N. Zumbulayadis and H.J. Gysling, J. Amer. Chem. Soc. 104 (1982) 3246.

[12] H.C. Dorn, B.E. Hanson and E. Motell, J. Organomet. Chem. 224 (1982) 181.

[13] H.C. Dorn, B.E. Hanson and E. Motell, Inorg. Chim. Acta 54 (1981) L71.

[14] B.E. Hanson, M.J. Sullivan and R.J. Davis, J. Amer. Chem. Soc. 106 (1984) 251.

[15] B.F.G. Johnson, J. Lewis and D.A. Pippard, J. Chem. Soc., Dalton Trans. (1981) 407.

[16] J.R. Shapley, J.B. Keister, M.R. Churchill and B.G. DeBoer, J. Amer. Chem. Soc. 97 (1975) 4145.

[17] A.J. Deeming and S.J. Hasso, J. Organomet. Chem. 114 (1976) 313.

[18] R.E. Benfield, B.F.G. Johnson, P.R. Raithby and G.M. Sheldrick, Acta Cryst. B34 (1978) 666.

[19] M.R. Churchill and B.G. DeBoer, Inorg. Chem. 16 (1977) 2397.

[20] R.E. Benfield, B.F.G. Johnson, J. Lewis, P.R. Raithby, C. Zuccaro and K. Henrick, Acta Cryst. B35 (1979) 2210.

[21] T.G. Appleton, H.C. Clark and L.E. Manzer, Coord. Chem. Rev. 10 (1973) 387.

[22] M.J. Bennett and P.B. Donaldson, Inorg. Chem. 16 (1977) 655.

[23] B.T. Heaton, L. Longhetti, D.M.P. Mingos, C.E. Briant, P.C. Minshall, B.R.C. Theobald, L. Garlaschelli and U. Sartorelli, J. Organomet. Chem. 213 (1981) 333.

[24] R.J. Crowte, Ph.D. thesis, Southampton (1986).

[25] G. Parkin, D.Phil thesis, Oxford (1985).

[26] M.M. Maricq and J.S. Waugh, J. Chem. Phys. 70 (1979) 3300.

[27] J. Herzfeld and A.E. Berger, J. Chem. Phys. 73 (1980) 6021.

[28] D. Gregson, J.A.K. Howard, J.N. Nicholls, J.L. Spencer and D.G. Turner, J. Chem. Soc., Chem. Commun. (1980) 572.

[29] M.L.H. Green, L.C. Mitchell and W.E. Silverthorn, J. Chem. Soc., Dalton Trans. (1974) 1361.

[30] R.R. Vold and R.L. Vold, J.Chem. Phys. 61 (1974) 4360.

[32] D.S. Milbrath, J.G. Verkade and R.J. Clark, Inorg. Nucl. Chem. Lett. 12 (1976) 921.

[33] E Fukushima and S.B.W. Roeder, 'Experimental pulse NMR: a nuts and bolts approach', Addison-Wesley, MA (1981).

[34] M.H. Frey, J.A. DiVerdi and S.J. Opella, J. Amer. Chem. Soc. 107 (1985) 7311.

[35] P. Delise, E.R. Mognaschi and A. Chierico, J. Chem. Soc., Faraday Trans. (1975) 207.

[36] G. Lucazeau, K. Chhor, C. Sourisseau and A.J. Dianoux, Chem. Phys. 76 (1983) 307.

[37] M.M. Maricq, J.S. Waugh, J.L. Fletcher and M.J. McGlinchey, J. Amer. Chem. Soc. 100 (1978) 6902.

[38] S.L. Cook, Ph.D. thesis, Southampton (1985).

[39] J.R. Wilkinson and L.J. Todd, J. Organomet. Chem. 118 (1976) 199.

[40] J.W. Gleeson and R.W. Vaughan, J. Chem. Phys. 78 (1983) 5384.

[41] S. Aime, D. Osella, L. Milane and E. Rosenberg, J. Organomet. Chem. 213 (1981) 207.

# CHAPTER 5

## Studies of gold phosphine cluster compounds.

### 5.1 Introduction

A variety of metal cluster compounds have now been prepared and characterised [1]. These clusters contain metal-metal bonds and have a sufficient number of atoms to define a three-dimensional polyhedral core. A considerable number of gold cluster compounds have been prepared since the first examples were reported almost twenty years ago [2]. Molecular clusters of gold are stabilised by tertiary phosphine ($PR_3$) and halide ligands (X) [3,4]. Low nuclearity clusters are defined by the formula $[Au_x(PR_3)_{x+y}]^{n+}$, where y = 0-2, whilst the higher nuclearity clusters have an additional central gold atom and can be described by $[Au_{x+1}(PR_3)_{x-y}X_y]^{n+}$.

$^{31}P$ nmr studies have shown that the majority of gold clusters are stereochemically non-rigid in solution, often giving averaged spectra even at low temperatures [5]. The fluxional behaviour is thought to result from facile skeletal rearrangement, and is common to all types of the clusters with the exception of the icosahedral compounds. Recently preliminary accounts of high resolution $^{31}P$ nmr spectra of gold clusters in the solid state have been reported [6,7]. The results indicated that there were differences between the solution and solid state spectra which could be related to fluxional behaviour. Differences in fluxional properties of molecules in the solid state and in solution have been observed for metal carbonyl cluster compounds [8,9]; further examples have been discussed in chapter 4.

In this chapter the results of a systematic solid state nmr study of a series of gold phosphine clusters are discussed. All of the clusters have known crystal structures. If fluxional process occurring

in solution are frozen out in the solid, the solid state $^{31}P$ nmr spectra will reveal more directly than the solution spectra the unique phosphine environments and hence the structure of the cluster. The studies already described on simple compounds provided a better understanding of the factors influencing solid state spectra on which to base the interpretation of the spectra of the gold clusters.

## 5.2 Materials and methods.

The gold clusters studied were kindly lent by Dr D.M.P. Mingos and Dr. K.P. Hall. The clusters were prepared as described previously: $[Au_6(P(o\text{-}C_6H_4Me)(C_6H_5)_2)_6](NO_3)_2$ [10]; $[Au_8(P(p\text{-}C_6H_4OMe)_3)_8(NO_3)_2$ [10]; $[Au_9(P(p\text{-}C_6H_4OMe)_3)_8]L_3$, $(L=NO_3^-, BF_4^-)$ [11,12]; $[Au_{13}Br_4(PMePh_2)_8]Br$ [10]; $[Au_{13}(PMe_2Ph)_{10}Cl_2](PF_6)_3$ [13]; $[Au_{11}(PMe_2Ph)_{10}](BPh_4)_3$ [14]. Crystal structures and solution nmr spectra have been reported previously.

The solid state nmr spectra were obtained using magic angle spinning and cross polarisation. As the use of cross polarisation can lead to deceptive relative intensities, the observed intensities were compared in nmr spectra obtained using a range of cross polarisation times (0.5-10ms) and by direct observation of the $^{31}P$ spectrum without enhancement. No significant differences in the relative intensities were observed upon altering the contact time. From these experiments, the optimum contact time was found to be 1.0ms. Typically several thousand transients were accumulated using a recycle delay of 2s with 50-100mg of sample at 20°C.

## 5.3 General features of the solid state spectra.

The $^{31}P$ spectrum of each of the gold cluster compounds in the solid state consists of a number of peaks with chemical shifts between 37 and 71ppm, each of which has a series of sidebands spaced at the spinning frequency. For the spinning speeds used in this work the sideband intensities are small, and represent less than 25% of the total signal intensity in each case. These could be neglected in the estimation of the relative intensities of the different peaks because the chemical shift anisotropies as revealed by the intensities of the sidebands were generally found to be similar for the different phosphines in a given molecule.

The linewidths of the resonances in the solid state nmr spectra were found to be typically 300Hz. At least part of the linewidth in the solid state can be attributed to dipolar broadening due to the $^{197}Au$ nuclei: this is not removed by MAS because the quadrupole interaction of the gold is comparable in magnitude to the nuclear Zeeman interaction ([15]; see section 2.5). Despite the broad lines, many of the peaks are well resolved, and the number of distinct resonances observed in the solid state is at least as great, and generally greater, than that observed in the corresponding room temperature solution spectra. In order to understand the solid state spectra, use was made of both the solution $^{31}P$ nmr spectra and the molecular structures as determined by X-ray diffraction studies. Table 5.1 summarises the chemical shift data.

TABLE 5.1

$^{31}P$ chemical shifts in the solid and solution states.[a]

| compound | solution (20°C) | solution (-90°C) | solid state (20°C) |
|---|---|---|---|
| $[Au_6(P(o\text{-}C_6H_4OMe)(C_6H_5)_2)_6](NO_3)_2$ | 46.5 | 52.6 [s,P] | 57.9[2P] |
| | | 42.6 [8,2P] | 48.6[4P] |
| $[Au_8(P(p\text{-}C_6H_4OMe)_3)_8](NO_3)_2$ | 44.3 | --- | 70.9[1P] |
| | | | 51.9<br>49.0 [7P] |
| $[Au_9(P(p\text{-}C_6H_4OMe)_3)_8](NO_3)_3$ | | | |
| brown isomer | 47.2 | 47.2[b] | 58.2[2P] |
| | | | 52.0[6P] |
| green isomer | 47.2 | 47.2[b] | 63.2[4P] |
| | | | 50.9[4P] |
| $[Au_9(P(p\text{-}C_6H_4OMe)_3)_8](BF_4)_3$ | 50.7 | 50.7[b] | 57.8[2P] |
| | | | 52.4[6P] |
| $[Au_{13}Br_4(PMePh_2)_8]Br$ | 44.0 [s,4P] | | 45.4[c] |
| | 34.5 [t,2P] | --- | 41.2 |
| | 32.0 [t,2P] | | 37.1 |
| $[Au_{13}(PMe_2Ph)_{10}Cl_2](PF_6)_3$ | 40.3 | 40.3 | 38.2 |

a all chemical shifts referenced to 85% $H_3PO_4$

b slight line broadening

c the relative intensities of the different peaks are not given because of overlap in spectra

## 5.4 Results of the $^{31}P$ nmr studies.

The nmr spectrum of $[Au_6(P(o\text{-}C_6H_4Me)(C_6H_5)_2)_6](NO_3)_2$ in the solid state at room temperature has two well-resolved peaks (Figure 5.1a). The chemical shifts and relative intensities (1:2) of these resonances are closely similar to those observed in solution at low temperature (180K) [10]. The spectrum can readily be interpreted in terms of the structure of the cluster determined by X-ray diffraction, which can be described in terms of two edge-sharing tetrahedra of gold atoms. There are two different phosphorus environments, with two edge-sharing Au-$PR_3$ and four external Au-$PR_3$ fragments. As the temperature is increased above 180K the solution spectrum changes as the two resonances broaden and collapse into a single average resonance. There is therefore a marked difference in the solution and solid state spectra at room temperature, and this can be attributed simply to a much faster intramolecular rearrangement process in solution compared with that in crystals.

A similar conclusion is reached by a study of the nmr spectra of the cluster $[Au_8(P(p\text{-}C_6H_4OMe)_3)_8(NO_3)_2$. The solid state nmr spectrum consists of one completely resolved peak at low field and a number, at least two, overlapping peaks at higher field (Figure 5.1b). The solution spectrum at room temperature shows only one resonance [10]. Low temperature solution spectra have not been obtained for this cluster, but they have been reported for the related cluster $[Au_8(PPh_3)_8]^{2+}$, which is isomorphous [7]. At low temperature, one resonance is found at low field at a chemical shift closely similar to that of the resolved resonance in the solid state spectrum, and three overlapping resonances were identified in the higher field peak. The crystallographically imposed symmetry is $C_{3v}$, and therefore four different phosphine sites exist. Of these, the unique phosphine at the

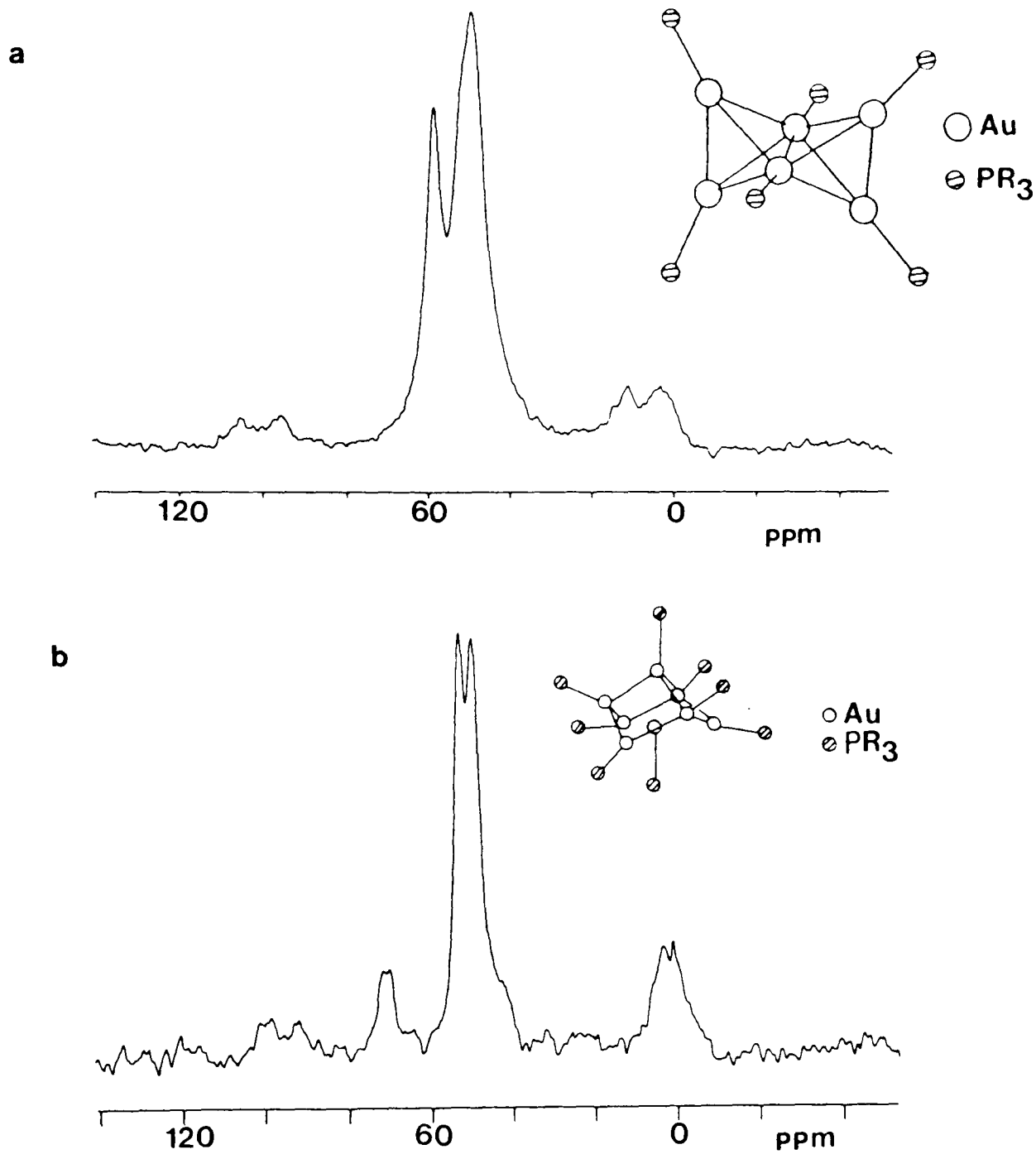


Figure 5.1

$^{31}P$ nmr spectra of (a) $[Au_6(P(o\text{-}C_6H_4OMe)(C_6H_5)_2)_6](NO_3)_2$

(b) $[Au_8(P(p\text{-}C_6H_4OMe)_3)_8](NO_3)_2$

centre of the cluster is markedly different from the remainder, having a longer Au-P distance (2.42Å) than that of the others (2.29-2.33Å), and the low field resonance is assigned to this. Again, the difference between the solid state and solution nmr spectra at room temperature can be attributed primarily to the difference in rate of intramolecular rearrangement. In solution two distinct processes, involving the equilibration of all the phosphorus atoms and the movement of Au-P units around the central Au atom, have been identified; both of these are 'frozen out' in the solid state.

$[Au_9(P(p\text{-}C_6H_4OMe)_3)_8](NO_3)_3$ also gives rise to a single resonance in solution at room temperature, and although slight line broadening takes place no further splitting of the resonance is observed even at low temperature [11]. Two crystal forms of this compound have been identified and characterised by X-ray diffraction studies. The solid state spectrum of one of these, the green isomer, shows two well-resolved peaks of approximately equal intensity (Figure 5.2a). The structure of this isomer is based on a centred icosahedron from which a rectangle of gold atoms has been removed, thus giving two types of phosphorus site, each containing four ligands. The structure is completely consistent with the solid state nmr spectrum. The golden-brown isomer gives a spectrum showing two peaks with an intensity ratio of 1:3 (Figure 5.2b). An identical spectrum is obtained for the $BF_4^-$ salt, which has the same structure as the brown isomer of the $NO_3^-$ salt. The idealised skeletal symmetry of the cluster is a centred crown of gold atoms possessing $D_{4d}$ symmetry, in which all of the phosphorus atoms are equivalent. The crystallographically imposed symmetry is however only $C_2$, permitting four different phosphorus environments. The solid state spectrum can therefore be explained by the overlap of the resonances of three

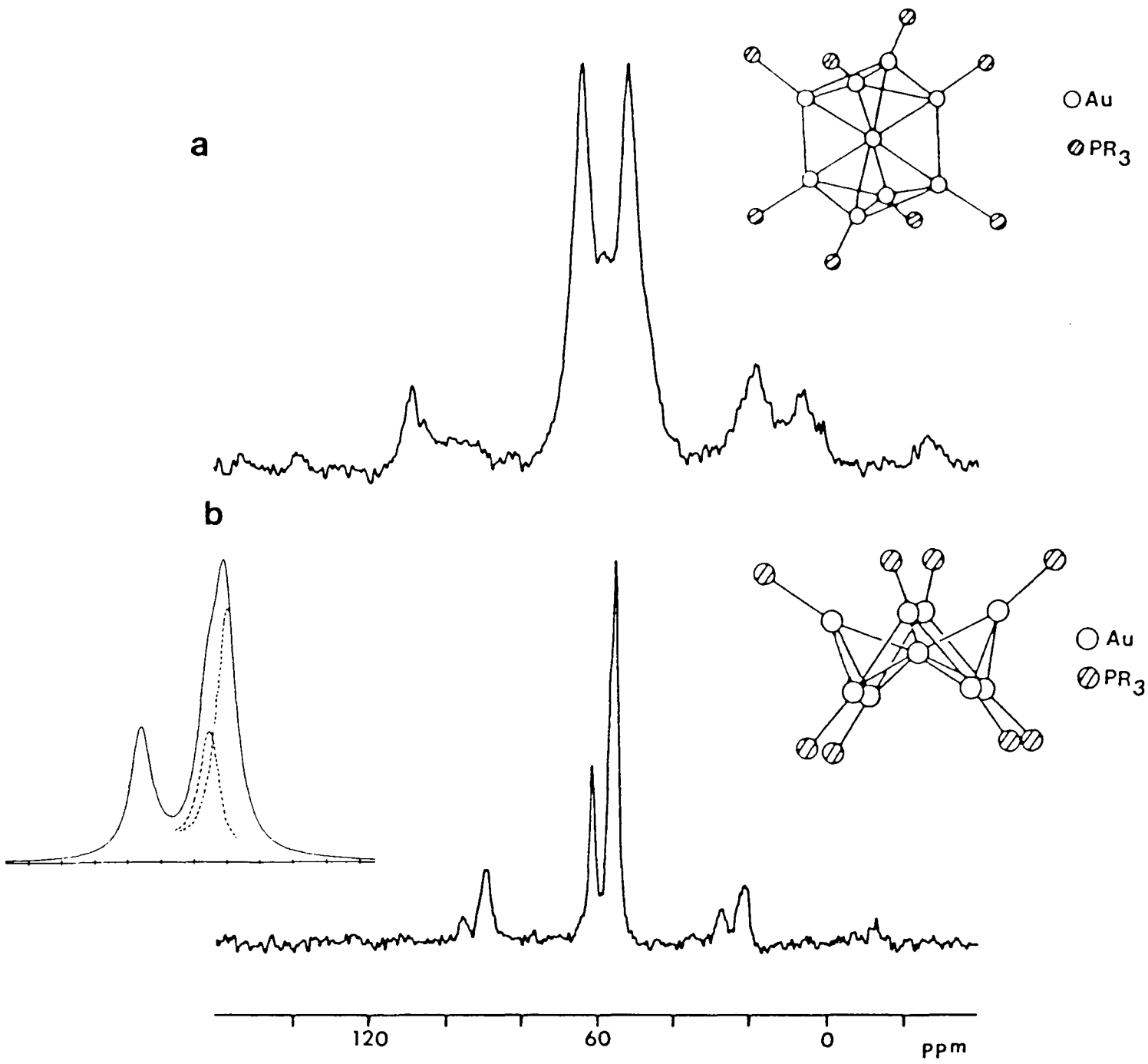


Figure 5.2

$^{31}P$ nmr spectra of $[Au_9(P(p\text{-}C_6H_4OMe)_3)_8](NO_3)_3$

(a) green isomer (b) golden brown isomer. Inset: simulation of the spectrum with the upfield peak taken to consist of 2 overlapping resonances with intensities of ratio 1:2.

nearly equivalent sites in the upfield resonance. The greater linewidth and asymmetry of this peak is consistent with this interpretation (see Figure 5.2b). The observed lineshape of the upfield resonance can be simulated exactly using three closely-spaced lines of intensities 1:1:1. In solution, not only are the molecules undergoing fluxional processes, but rapid interconversion of isomers on the nmr timescale is also taking place, giving rise to the single line spectrum.

$[Au_{13}Br_4(PMePh_2)_8]Br$ is an example of a cluster which is stereochemically rigid in solution at room temperature. The solution spectrum consists of three resonances, in accord with the centred icosahedral structure shown in Figure 5.3a [10]. The positions of the four bromine atoms give rise to three different phosphorus environments, with four, two and two phosphines in each. Despite some overlap of resonances in the solid state spectrum, three resonances at similar chemical shift values to those observed in solution can be detected. Resolution enhancement by Gaussian multiplication leads to a clear resolution of the three peaks.

The solid state spectrum of $[Au_{13}(PMe_2Ph)_{10}Cl_2](PF_6)_3$ consists of a single phosphorus resonance (Figure 5.3b). The solution spectrum also shows only one line, but in this case it is not necessary to invoke stereochemical non-rigidity. The crystal structure is that of a centred icosahedron with chlorine atoms at the <u>para</u>-positions [13]. All of the phosphorus atoms are equivalent in this idealised structure. There are, however, significant distortions to the icosahedron in the crystal, thus offering an explanation for the broad line (~800Hz) observed in the solid state spectrum.

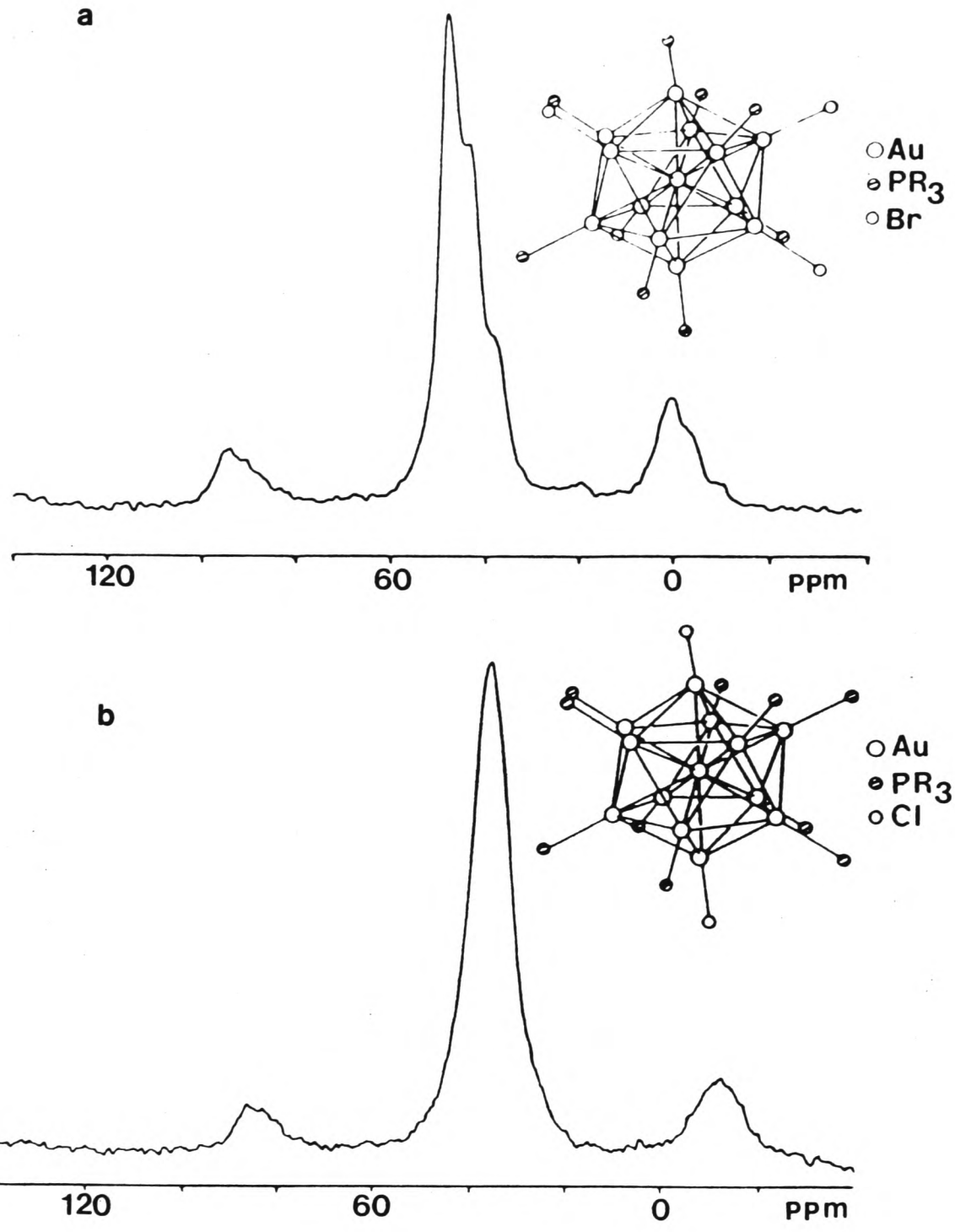


Figure 5.3

$^{31}P$ nmr spectra of (a)$[Au_{13}Br_4(PMePh_2)_8)]Br$, resolution enhanced by Gaussian multiplication. (b) $[Au_{13}(PMe_2Ph)_{10}Cl_2](PF_6)_3$

## 5.5 Discussion

In all of the clusters described above the solid state metal phosphine structures appear to be stereochemically rigid at room temperature. In solution all but one are non-rigid at room temperature, and several are not frozen out at temperatures of -90°C and below. This indicates the effect of intermolecular interactions in the crystal on intramolecular processes, and is in accord with observations discussed in the previous chapter. That this might not always be the case is indicated by studies of $[Au_{11}(PMe_2Ph)_{10}](BPh_4)_3$. The solid state nmr spectrum of this cluster consists of a single resonance, as does the room temperature solution nmr spectrum. The crystal structure has not been determined due to crystallographic disorder, but the related cluster $[Au_{11}I_3(P(p\text{-}C_6H_4F)_3)_7]$ has been structurally characterised and shown to have four chemically distinct phosphine environments [14]. This suggests that fluxionality is still present in the cluster in the solid state at room temperature. The next step in this case would be to determine whether the four phosphorus environments can be distinguished in the solid state at low temperature.

An important question for structure determination is whether intermolecular interactions affect the chemical shifts of the phosphines in addition to their dynamic properties. The shifts would be affected by through space interactions, for example ring current shifts or electrostatic perturbations or by distortion of the geometry either of the cluster or of the phosphine substituents. The evidence from these studies, and from the studies of simple compounds (chapter 4) is that such effects are observed, and that their existence cannot be ignored in structure determination. On average, the $^{31}P$ chemical shifts in the gold clusters are some 4.2ppm to higher field in the

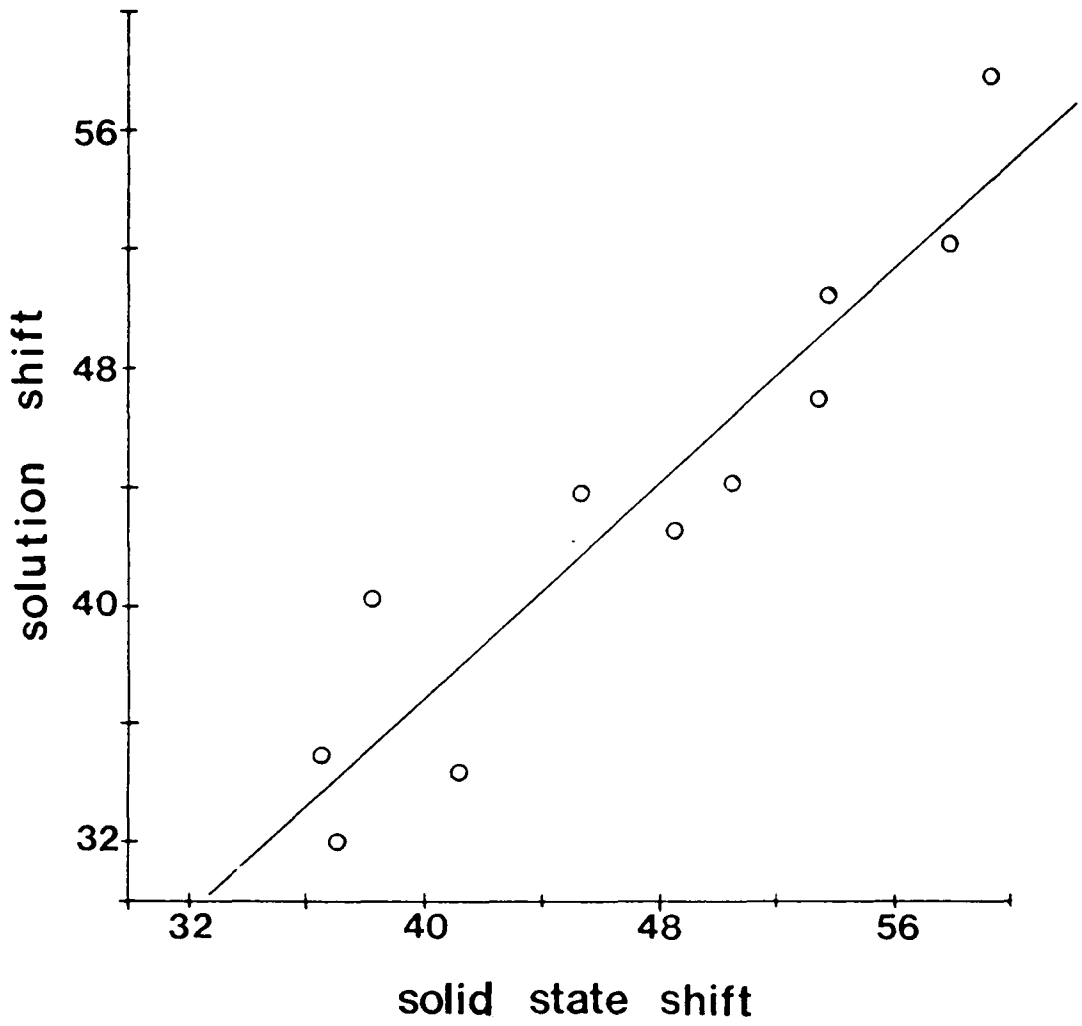


Figure 5.4

Plot of $^{31}P$ chemical shifts in the solid state against chemical shifts in solution. Low temperature solution data were used where available. In cases where more resonances were observed in the solid state than in solution, an average value of the solid state shifts weighted for the number of phosphines in each environment was plotted against the solution chemical shift. The solid line shows a least squares fit to the data.

solid state compared with those in solution (see Table 5.1). A plot of the chemical shifts in solution against those in the solid state (Figure 5.4) demonstrates this, but shows that the correlation between the two sets of shifts is otherwise good.

Stereochemical rigidity is valuable for structural studies in the solid state: this is shown by considering the isomers of the cluster $[Au_9(P(p\text{-}C_6H_4OMe)_3)_8](NO_3)_3$. Comparison of the spectrum of the $BF_4^-$ salt with those of the two isomers of the $NO_3^-$ salt enables the molecular structure to be assigned without the need for diffraction studies. Other related clusters could be similarly examined in the solid state. Whether or not separate resonances are observed for each distinct phosphorus environment in the molecule depends on the resolution of the spectrum. For the homonuclear gold phosphine clusters, the number of peaks represents a minimum value for the number of crystallographically distinct sites. The greater the difference in the environments, such as for example the Au-P bond lengths in $[Au_8(P(p\text{-}C_6H_4OMe)_3)_8(NO_3)_2$, the more likely the resolution of the separate resonances. The results described here suggest that in many cases all of the distinct sites of the cluster framework will be resolved, but that the differences in, for example, phosphine rotameric sites will not be.

Further information relating to the structures of the clusters is revealed by the chemical shift anisotropy, which can be obtained from the spinning sidebands observed in the MAS spectra (see chapter 2). Calculations using model systems have shown that, for quantitative conclusions to be drawn from such data, excellent resolution and spectral signal-to-noise are required ([17]; see chapter 3). This is not the case with the spectra of the gold phosphine clusters: however a simple comparison of the relative

intensities of the spinning sidebands enables some qualitative conclusions to be drawn. Considering the isomers of the cluster $[Au_9(P(p\text{-}C_6H_4OMe)_3)_8](NO_3)_3$, for example, the pattern of spinning sideband intensities is clearly different in the two cases. The two phosphine sites found in the green isomer have noticeably different chemical shift anisotropies; those of the two resolved resonances of the golden-brown isomer have closely similar anisotropies, indicative of similar geometry at the phosphorus sites. This again would help in identifying the structure of other, similar clusters. The calculated values of the shielding tensor are tabulated in Appendix B.

The results obtained for this series of cluster compounds further illustrate the advantages of using a combination of solid state and solution nmr spectroscopy in the study of fluxional compounds: the structural rigidity in the former and the high resolution of the latter can be used to investigate both structures and dynamics. The utility of the solid state technique is likely to be of unique importance in cases where crystal structures cannot be determined. This could occur if, for example, suitable crystals could not be obtained, as in the case of the cluster $[Au_{11}(PMe_2Ph)_{10}](BPh_4)_3$ discussed here. Another application would be if the molecule of interest were contained in a non-crystalline environment, such as attached to a surface. Simple clusters attached to surfaces will be discussed in chapter 7.

5.6 References.

[1] F.A Cotton, Inorg. Chem. 3 (1964) 1217.

[2] L. Malatesta, Gold Bull. 8 (1975) 46.

[3] K.P. Hall and D.M.P. Mingos, Prog. Inorg. Chem. 32 (1984) 311.

[4] D.M.P. Mingos, Gold Bull. 17 (1984) 5.

[5] F.A. Vollenbroek, P.C.P. Bouten, J.M. Trooster, J.P. van der Berg and J.J. Bour, Inorg. Chem. 17 (1978) 1345.

[6] J.W. Diesveld, E.M. Menger, H.T. Edzes and W.S. Veemen, J. Amer. Chem. Soc. 102 (1980) 7935.

[7] J.W.A. van der Velden, Ph.D. thesis, Nijmegen (1983).

[8] H. Dorn, B.E. Hanson and E. Motell, Inorg. Chim. Acta 54 (1981) 271.

[9] B.E. Hanson, M.J. Sullivan and R.J. Davis, J. Amer. Chem. Soc. 106 (1984) 251.

[10] K.P. Hall, D.Phil thesis, Oxford (1983).

[11] C.E. Briant, K.P. Hall and D.M.P. Mingos, J. Chem. Soc., Chem. Commun. (1984) 290.

[12] K.P. Hall, B.R.C. Theobald, D.I. Gilmour, D.M.P. Mingos and A.J. Welch, J. Chem. Soc., Chem. Commun. (1982) 528.

[13] C.E. Briant, B.R.C. Theobald, J.W. White, L.K. Bell, D.M.P. Mingos and A.J. Welch, J. Chem. Soc., Chem. Commun. (1981) 201.

[14] B.R.C. Theobald, D.Phil. thesis, Oxford (1981).

[15] J.G. Hexem, M.H. Frey and S.J. Opella, J. Amer. Chem. Soc. 103 (1981) 224.

[16] P. Bellon, M. Manassero and M. Sansoni, J. Chem. Soc., Dalton Trans. (1972) 1481.

[17] N.J. Clayden, C.M. Dobson, L-Y. Lian and D.J. Smith, J. Magn. Res. (in press).

# CHAPTER 6

Studies of heteronuclear metal cluster compounds.

## 6.1 Introduction

One class of metal cluster compound which has recently become well-established is that of heteronuclear metal clusters containing M-$PR_3$ moieties, where M is a group 1B metal and R an aryl or alkyl group [1-3]. In particular, species in which one, two or three Au-$PR_3$ fragments are incorporated into structures with ruthenium or osmium atoms ligated by carbonyl groups are becoming increasingly common [1,2]. Theoretical studies concerned with the bonding properties of the Au-$PR_3$ unit have shown it to be approximately isolobal with an $Mn(CO)_5$ fragment or a hydrido ligand [1,4]. This is in accord with almost all of the known structures of cluster compounds containing one such fragment, in which the Au-$PR_3$ unit adopts the position of a hydrido ligand in the analogous hydridometal cluster [1,3,5]. The situation becomes more complex in clusters containing two or more Au-$PR_3$ units, but generally the Au-$PR_3$ fragments adopt either a face-capping or an edge-bridging mode [1,3,5].

There have been fewer reports of analogous clusters in which Au is replaced by Cu or Ag [6], and until recently little experimental evidence concerning the bonding capabilities of Cu-$PR_3$ and Ag-$PR_3$ fragments was available. Theory suggests that the Cu-$PR_3$ fragment is isolobal with the $Mn(CO)_3$ unit [4,7], which does not function effectively as an edge-bridging group: if this theory is correct, it follows that the substitution of Cu for Au in a cluster may lead to a change in structure. However the theory has recently been questioned [8].

For many of the clusters in which two or more M-$PR_3$

fragments occupy structurally inequivalent positions in the ground state structure, fluxional behaviour involving coinage metal site-exchange has been observed in solution, revealed by $^{31}P$ nmr spectra in which the number of resonances observed is less than the number of inequivalent phosphorus environments in the molecule [1-3]. The results suggest that this site-exchange involves metal core rearrangement. For a series of clusters containing Ag-$PR_3$ units, the first application of $^{109}Ag\{^1H\}$ INEPT nmr to the study of metal clusters [9] has directly confirmed that for these species the fluxional process does involve intramolecular rearrangement of the metal core. Mingos has proposed [3] that for heteronuclear gold clusters the dynamic behaviour can be explained in terms of the bonding capabilities of the Au-$PR_3$ unit, with the possibility of facile interconversion between its two bonding modes providing a low energy pathway for the rapid skeletal rearrangements observed in these species. In view of the fact that a number of stable mixed-metal clusters containing edge-bridging Cu-$PR_3$ and Ag-$PR_3$ units have been characterised [10], despite suggestions that this mode of bonding is less favourable for these fragments than for Au-$PR_3$, it would seem reasonable to rationalize the observed core rearrangements of these clusters in the same way as for the clusters containing Au-$PR_3$ units.

Solid state $^{31}P$ nmr studies have been carried out on a series of heteronuclear metal carbonyl clusters containing group 1B metal fragments. The purpose of the studies was to further investigate the structures and dynamic behaviour of these compounds. It was hoped that solid state nmr would 'freeze out' the fluxionality at room temperature, as a result of intermolecular interactions, so that spectra due to the static structures could be observed. One aspect of the utility of the solid state nmr technique would then be in

providing structural information about the clusters whose X-ray structures had not been determined. For these clusters, the only source of structural information is the comparison of spectroscopic (infra-red and nmr) data with that of clusters whose structures are known: if solution nmr does not show spectra consistent with the ground state, there is the possibility that it will be revealed by solid state nmr, enabling a more accurate assessment of the structure of the cluster to be made. Clusters studied include a number utilising bidentate phosphine ligands and several containing two different coinage metals.

## 6.2 Materials and methods.

All of this work was carried out in collaboration with Dr I.D. Salter and S.S.D. Brown of Exeter University, who prepared the metal clusters studied. Details of the preparative methods have been published previously [10-16]. The clusters were initially recrystallised from $CH_2Cl_2$/light petroleum (b.p. 40-60°C), but for later samples a solvent system of diethyl ether/light petroleum was used. The crystal structures of a number of the clusters have been determined by X-ray diffraction, and will be discussed in conjunction with the solid state nmr results. Variable temperature solution nmr spectra have been obtained for these clusters by Dr. Salter and coworkers: the results have been discussed previously [9-16].

Solid state $^{31}P$ nmr spectra were obtained using high power $^{1}H$ decoupling, cross polarisation and magic angle spinning. Non-spinning spectra were also obtained in some cases. A CP time of 1.0ms was used. The number of transients varied from 200 to several thousand, depending on the quantity of sample available. This was typically 100 to 150mg. All spectra were recorded at room temperature.

## 6.3 General features of the solid state spectra.

### 6.3.1 Features common to all spectra.

The room temperature solid state $^{31}P$ nmr spectra were generally well-resolved, showing resonances over a wide range of chemical shift values. The number of resonances observed was not always that predicted on the basis of the room temperature solution nmr spectra. The linewidths measured in the solid state varied from 100Hz to >1000Hz, and were dependent on the identity of the metal bonded to the phosphorus atom. The sharpest lines were observed for silver species; the resonances of the gold clusters were generally broad, a result of the dipolar coupling discussed in chapter 5. A large variation was apparent in the linewidths recorded for the copper species. In some cases, the resonances were extremely broad, whereas in others linewidths were as small as 200Hz. The origins of the broad lines are quadrupolar, and will be discussed in section 6.3.3.

The chemical shift anisotropies as indicated by the intensities of the spinning sidebands were generally small, spanning on average 120ppm (1.0kHz) for monodentate phosphines. Differences in anisotropy between two phosphorus environments in the same molecule were observed in several cases. As the anisotropy should be characteristic of the phosphorus site, it was hoped that it could be used in the identification of the site in a cluster occupied by a particular metal phosphine group, of importance for clusters containing more than one coinage metal phosphine unit.

Additional interesting features of the solid state spectra were the presence of couplings to the metal atoms. The effect of these couplings on the solid state $^{31}P$ nmr spectra are shown schematically in Figure 6.1. The couplings fall into two categories, and will be discussed in turn.

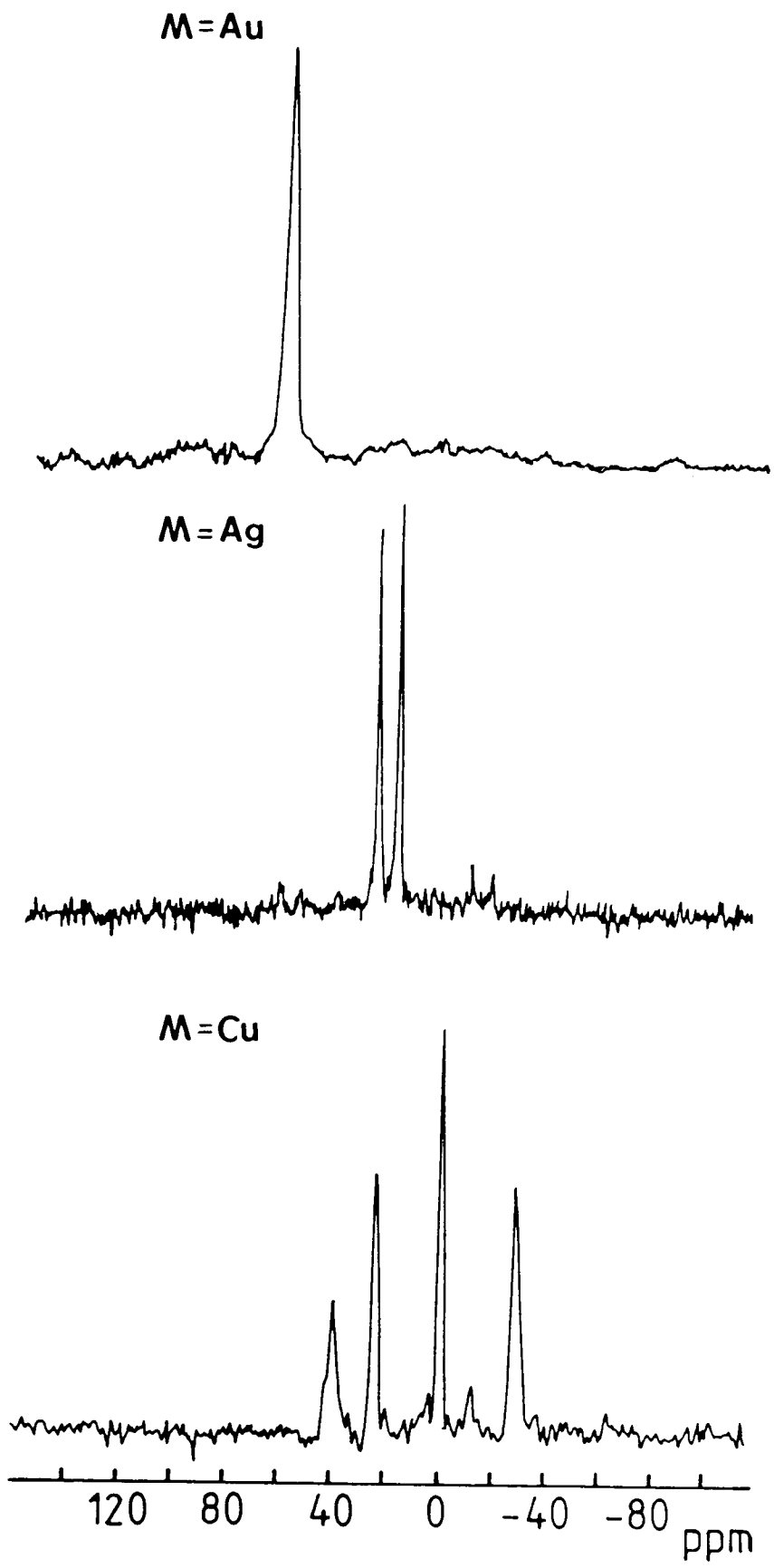


Figure 6.1

A comparison of the solid state $^{31}P$ nmr spectra from a cluster with a single $MPR_3$ group, showing scalar and quadrupolar couplings.

6.3.2 Silver phosphine-containing clusters: spin-spin coupling.

Spin-spin or scalar coupling is brought about by a magnetic interaction between neighbouring nuclei which are magnetically inequivalent [17]. Both of the naturally-occurring isotopes of silver ($^{107}Ag$, 51.8% abundant; $^{109}Ag$, 48.2% abundant) have spin-1/2, and spin-spin coupling between each of these and the directly-bonded phosphorus nuclei splits each $^{31}P$ nmr signal to a doublet. As a consequence of this, every solution $^{31}P$ nmr resonance appears as two overlapping doublets. However the scalar coupling constants for the two isotopes are similar due to the similar magnetogyric ratios of the two isotopes, and as the narrowest linewidth achieved in the solid state for these clusters is approximately 110Hz, it is unlikely that the two doublets will be resolved in the solid state spectra. A single doublet is in fact observed for each $^{31}P$ resonance of the silver phosphine-containing clusters in the solid state (Figure 6.1), with a coupling constant closely similar to the mean of the two coupling constants measured in solution.

Because spin-spin coupling is transmitted through chemical bonds, it is a sensitive indicator of the types of bonds involved and their spatial orientation in the molecule. The information obtained in this manner will be discussed in more detail below.

It should be noted when considering the $^{31}P$ nmr spectra of the silver phosphine-containing clusters that in solution all of the Ag-$PPh_3$ fragments undergo intermolecular $PPh_3$ exchange at room temperature [10].

6.3.3 Copper phosphine-containing clusters: quadrupolar coupling.

The high resolution $^{31}P$ spectra of several copper (I) phosphine complexes in the solid state have been reported in the

literature [18,19]. The spectra often show asymmetric 'quartets' when on the basis of the crystal structure a single resonance line would be expected. The line separations of the quartet are dependent on the applied magnetic field. Similarly, in the solid state $^{13}C$ spectra of compounds containing carbon atoms bonded to nitrogen, the resonances of these nuclei are broadened and often split to asymmetric doublets when all of the other carbon resonances are single lines [20]. This does not occur in the corresponding solution spectra, or when $^{15}N$ replaces $^{14}N$ in solids.

The two effects are analogous, and result from the presence of a quadrupolar nucleus bonded to the spin-1/2 nucleus under observation. Naturally-occurring copper consists of two isotopes, each with spin 3/2 and with abundances of 69% ($^{63}Cu$) and 31% ($^{65}Cu$). Both isotopes have medium value quadrupole moments ($eQ = 0.16 \times 10^{-28} cm^2$ and $0.15 \times 10^{-28} cm^2$ respectively) and couple to the phosphorus nuclei. The nuclear quadrupole coupling constant of 30MHz is of the same order of magnitude as the Zeeman interaction (50MHz on a 4.7T spectrometer). Under these conditions, the axis of quantization of the Cu nucleus (S) is tipped away from the magnetic field axis. Magic angle spinning will not now fully remove the dipolar coupling between S and the nuclear spin under observation (I) [19]. A similar problem occurs with the indirect nuclear spin-spin couplings. When both I and S spins are quantised along the magnetic field, the spectra obtained are relatively straightforward. However, if the S spin is subject to a quadrupolar interaction not small compared to its Zeeman interaction, S is no longer quantised along the field direction and the Hamiltonian governing the coupling becomes angle dependent. The effect of magic angle spinning is to make this Hamiltonian time-dependent, and 'distorted' multiplets occur.

The solid state resonance splittings which will arise from these interactions have been calculated [19], and the results averaged over all possible orientations within the sample in order to reproduce the spectrum of a powder. Initially the cases of dipolar and scalar coupling were considered separately, but this was found to be incompatible with the experimental results. A combination of the two gave the best fit with the experimental data. The splittings due to the two copper isotopes cannot generally be resolved as a result of their closely similar magnetogyric ratios. It should be noted that the 'lines' in the spectra are in fact powder patterns, with characteristic divergences and shoulders; the total width of each is, however, only a fraction of the relevant coupling constant for high magnetic fields. This means in practise that most experimental spectra will show single, slightly broadened lines. It is possible to use the asymmetric line splittings to obtain quantitative information about the compounds concerned. From the magnitude of the splittings, the coupling constants can be obtained and their signs determined; the approximate distance between the I and S atoms may also be calculated.

The solution $^{31}P$ nmr spectra of the clusters containing Cu-$PR_3$ groups discussed in this chapter show considerable broadening of the resonances at room temperature due to interaction with the quadrupolar Cu nucleus, although the lines are considerably sharper at -90°C. It is therefore not surprising that in the solid state $^{31}P$ nmr spectra of all of these clusters asymmetric splitting of the phosphine resonances is observed, accompanied in many cases by considerable line broadening. These spectra can be qualitatively accounted for on the basis of the studies discussed above.

In this chapter, the spectra of the copper clusters are first discussed in conjunction with those of the analogous silver and

gold clusters. A later section then considers further the additional information contained in the quadrupolar resonance splittings.

### 6.3.4 Interpretation of the solid state spectra.

The solid state $^{31}P$ spectra were interpreted in the light of variable temperature solution nmr data and, where available, the X-ray crystal structures of the clusters. The results obtained are collected together in Table 6.1. In the discussion which follows, particular aspects of the changes in structure and dynamic behaviour observed in the solid state upon varying the metal or the phosphine ligand(s) are first considered. Specific features of the spectra of the copper- and silver-containing clusters are then discussed.

## 6.4 The effect of varying the group 1B metal.

### 6.4.1 Clusters with a single group 1B metal site.

The solid state $^{31}P$ nmr spectra of the clusters $[MRu_4(\mu_3\text{-}H)_3(CO)_{12}PPh_3]$ (M = Ag, Cu) show a single resonance, split by the couplings discussed earlier to give a doublet and an asymmetric quartet respectively (Figure 6.2). Solution $^{31}P$ nmr spectra [10] also show a single resonance. Infra-red and solution $^{1}H$ spectroscopic evidence implies that the clusters have the same metal core structure as that of the analogous Cu cluster in which ($PPh_2Me$) replaces ($PPh_3$), and which has been characterised by X-ray diffraction [10]. The structure shows a single phosphorus environment, with the $M\text{-}PR_3$ unit capping a face of the ruthenium tetrahedron. This is completely consistent with the solid state nmr spectra.

The solid state spectrum of the gold cluster shows two resonances at a separation of 9ppm (Figure 6.2). The evidence from solution spectroscopic studies is that it adopts a different structure

TABLE 6.1

Solid state and solution $^{31}P$ nmr data for the Group 1B heteronuclear metal cluster compounds.

| cluster | solid, 20°C | solution, 20°C | solution, -90°C |
|---|---|---|---|
| $CuRu_4(\mu_3\text{-}H)_3(CO)_{12}PPh_3$ | 13.6 | | 10.9 |
| $CuRu_4(\mu_3\text{-}H)_3(CO)_{12}PMePh_2$ | -7 | -6.7 (vbr) | -5.5 |
| $AgRu_4(\mu_3\text{-}H)_3(CO)_{12}PPh_3$ | 18.5 (d) J=651Hz | | 22.0 (2xd) J=693,601Hz |
| $AuRu_4(\mu_3\text{-}H)_3(CO)_{12}PPh_3$ | 71.4, 62.4 | | 67.3 |
| $CuRu_3(CO)_9(C_2Bu^t)PPh_3$ | -1.0 | | -1.4 |
| $AgRu_3(CO)_9(C_2Bu^t)PPh_3$ | 13.9 (d) J=445Hz | | 12.2 (2xd) J=482,417Hz |
| $AuRu_3(CO)_9(C_2Bu^t)PPh_3$ | 62.7, 59.0, 55.4 | | 62.2 |
| | 64.3, 55.5 | | |
| $Cu_2Ru_4(\mu_3\text{-}H)_2(CO)_{12}(PPh_3)_2$ | 9, 2.5 | 4.3 (br) | 6.8, -0.4 |
| $Ag_2Ru_4(\mu_3\text{-}H)_2(CO)_{12}(PPh_3)_2$ | 15.1 (d) J=509Hz | 16.1 (2xd) J=552,444Hz | 18.4 (2xd) J=565,490Hz |
| | 12.9 (d) J=448Hz | | 13.4 (2xd) J=473,410Hz |
| $Au_2Ru_4(\mu\text{-}H)(\mu_3\text{-}H)(CO)_{12}(PPh_3)_2$ | 56.0, 49.0 | 58.7 | ~51 (vbr) |
| $Cu_2Ru_4(\mu_3\text{-}H)_2(CO)_{12}(Ph_2PCH_2PPh_2)$ | 0 | -3.8 (br) | 2.5 (d), -9.6 (d) |
| $Ag_2Ru_4(\mu_3\text{-}H)_2(CO)_{12}(Ph_2PCH_2PPh_2)$ | 3.2 | 6.7 (2xd) J=449, 432Hz | 6.7 (2xd) J=499,432Hz |
| $Ag_2Ru_4(\mu_3\text{-}H)_2(CO)_{12}(Ph_2P(CH_2)_2PPh_2)$ | 13.0 (vbr) | | 14.4 (2xd, br) J=585,507Hz |
| | | | 10.5 (2xd, br) J=457, 396Hz |
| $Ag_2Ru_4(\mu_3\text{-}H)_2(CO)_{12}(Ph_2P(CH_2)_3PPh_2)$ | 17.3 (d) J=549Hz | | 17.9 (2xd) J=589,510Hz |
| | 14.5 (d) J=448Hz | | 13.6 (2xd) J=471,408Hz |

| | | | |
|---|---|---|---|
| $Ag_2Ru_4(\mu_3\text{-}H)_2(CO)_{12}(Ph_2P(CH_2)_4PPh_2)$ | 19.2 (d) J=529Hz | | 17.9 (2xd) J=583,505Hz |
| | 14.2 (d) J=534Hz | | |
| | 0.4 (d) J=448Hz | | -1.8 (2xd) J=479,416Hz |
| | -4.4 (d) J=443Hz | | |
| $Au_2Ru_4(\mu\text{-}H)(\mu_3\text{-}H)(CO)_{12}(Ph_2PCH_2PPh_2)$ | 59.5, 56.5 | 52.3 | 50.5 |
| $Cu_2Ru_4(\mu_3\text{-}H)_2(CO)_{12}(\mu\text{-}Ph_2As(CH_2)_2PPh_2)$ | 2 | -2.6 (br) | 3.6 [0.37P], -5.1 [1.0P] |
| $AuCuRu_4(\mu_3\text{-}H)_2(CO)_{12}(PPh_3)_2$ | 67.2 | 66.9 | |
| | 10 | 4.8 | |
| $AgAuRu_4(\mu_3\text{-}H)_2(CO)_{12}(PPh_3)_2$ | 61.6 | 64.6 | |
| | 15.7 (d) J=529Hz | 17.4 (2xd) J=596,515Hz | |
| $AgCuRu_4(\mu_3\text{-}H)_2(CO)_{12}(PPh_3)_2$ | 14.3 (d) J=458Hz | 14.7 (2xd) J=481,417Hz | |
| | 8 | 6.4 | |
| $Au_2Ru_3(\mu_3\text{-}S)(CO)_9(PPh_3)_2$ | 66.7 | | 64.4 |
| $Au_2Ru_3(\mu_3\text{-}S)(CO)_9(Ph_2PCH_2PPh_2)$ | 48.5, 46.5 | 52.4 | 50.8 |
| $Cu_2Ru_3(\mu_3\text{-}S)(CO)_9(Ph_2PCH_2PPh_2)$ | -9, -16 | -7.3 | -7.5 |
| $Au_3Ru_4(\mu_3\text{-}H)(CO)_{12}(PPh_3)_3$ | 62.2 [2P] | 61.3 | 62.3 [2P] |
| | 55.3 [1P] | | 53.5 [1P] |
| $Au_3Ru_4(\mu_3\text{-}H)(CO)_{12}(Ph_2PCH_2PPh_2)PPh_3$ | 67.6 [1P] | 61.3 [1P] | 60.3 [1P] |
| | 44.2 [2P] | 42.0 [2P] | ~40 [2P] (vbr) |
| $CuRu_3(\mu\text{-}H)(\mu_3\text{-}S)(CO)_8(PPh_3)_2$ | 37.2 | 32.3 | 32.2 |
| | 3.7 | 4.0 | 4.1 |

All chemical shifts are in ppm and are referenced to 85% $H_3PO_4$.

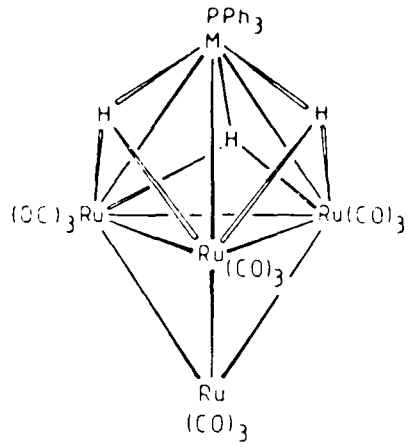





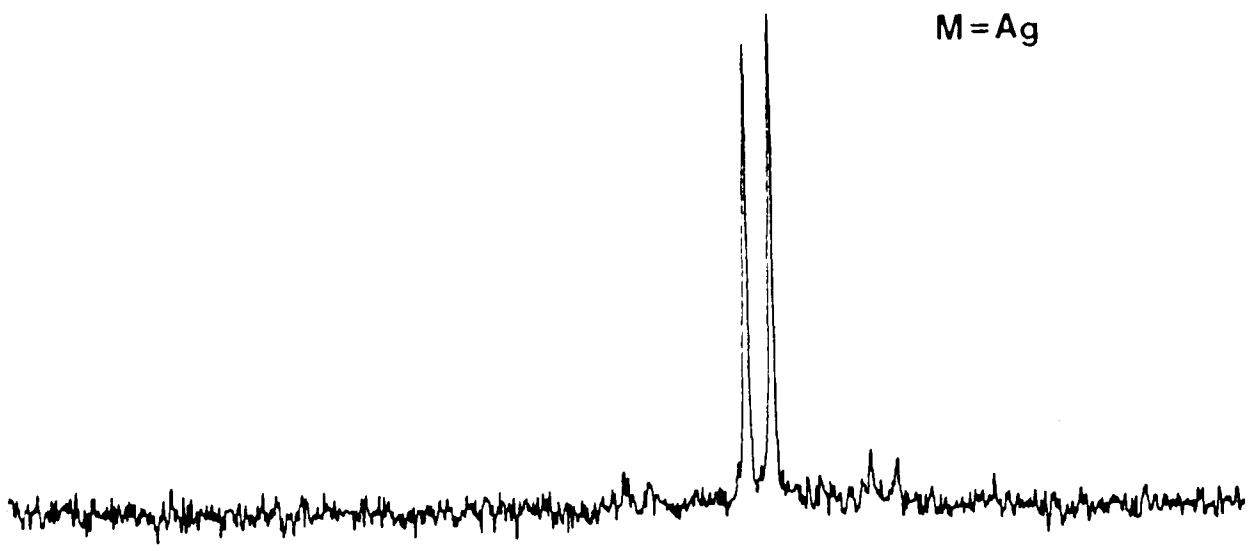


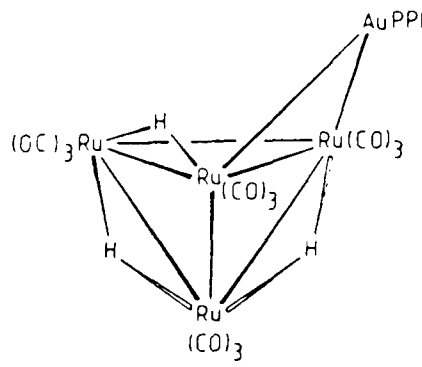





Figure 6.2

Solid state spectra of the clusters $[MRu_4(\mu_3\text{-}H)_3(CO)_{12}PPh_3]$.

Inset: structures.

from the Cu and Ag clusters, with the Au-$PR_3$ moiety bridging an edge of the $Ru_4$ tetrahedron. This structure has been found for the analogous cluster $[AuOs_4(\mu\text{-}H)_3(CO)_{12}PEt_3]$ [21]. A $^{197}Au$ Mössbauer study [22] reveals only one gold environment in the solid state. In an attempt to determine whether the two phosphorus environments arose from the crystallisation process, the sample was recrystallised from diethyl ether/light petroleum instead of $CH_2Cl_2$/light petroleum and the spectrum rerun. Two phosphorus resonances are again observed, and from the intensities of their respective sets of spinning sidebands each phosphorus appears to have a different chemical shift anisotropy (CSA). Calculation [23,24] shows one phosphorus atom to have an axial anisotropy, whereas that of the other phosphorus atom is non-axial. The solution chemical shift is intermediate between the two solid state shifts, which would be consistent with averaging of the two solid state phosphorus environments in solution. A further recrystallisation from light petroleum did not alter the solid state spectrum obtained.

For a second series of clusters $[MRu_3(CO)_9(C_2Bu^t)PPh_3]$, both the copper and gold clusters have been characterised by X-ray diffraction [10,25]. These are identical, with the M-$PR_3$ unit adopting an edge-bridging mode; spectroscopic evidence implies the same structure for the Ag analogue. Solid state nmr studies show a single phosphorus resonance in the spectra of both Cu and Ag clusters (Figure 6.3). The Au cluster initially gave rise to a spectrum showing three overlapping $^{31}P$ resonances in the solid state over a chemical shift range of 7ppm. Recrystallisation of the sample from diethyl ether/light petroleum did not alter the spectrum, but use of light petroleum alone resulted in a solid state spectrum showing two well-resolved resonances separated by 8.3ppm. This is in contrast to the

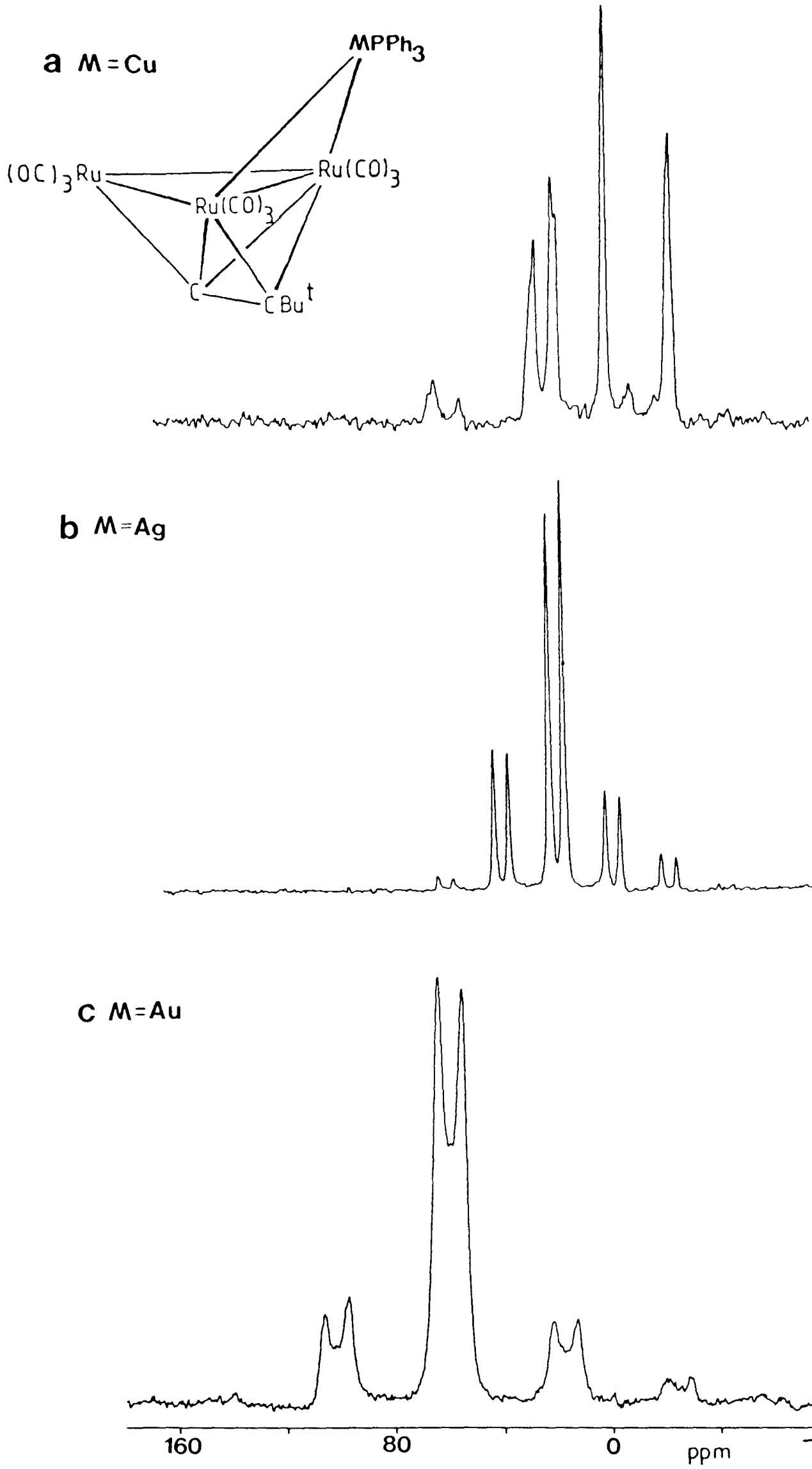


Figure 6.3

Solid state $^{31}P$ nmr spectra of the clusters $[MRu_3(CO)_9(C_2Bu^t)PPh_3]$. Inset: structure.

results of solution nmr studies, in which a single resonance is observed for all three clusters. X-ray powder diffraction studies were carried out on samples showing two and three solid state nmr resonances. The low angle reflections were considered: on reference to the unit cell parameters and space group it was apparent that more peaks than would be expected in this region were present for both samples. The resulting diffraction patterns were complex, but it appeared that the sample producing three nmr resonances gave rise to more diffraction peaks than the other sample.

6.4.2 Clusters with two group 1B metal sites: M = M'.

a) Triphenylphosphine ligands.

All three of the clusters $[MM'Ru_4H_2(CO)_{12}(PPh_3)_2]$ (M = M') have been studied by solid state nmr. The results are shown in Table 6.1 together with the solution nmr data obtained at room temperature and at -90°C.

The solid state spectrum of the copper cluster (1) shows multiple peaks (Figure 6.4a); these can be resolved into two phosphorus resonances, which are both split by coupling to the quadrupolar copper nuclei to give asymmetric quartets. This is completely consistent with the structure of the cluster as determined by X-ray diffraction [12], a tetrahedron of ruthenium atoms capped by $Cu\text{-}PPh_3$, with one of the $CuRu_2$ faces then capped by a second $Cu\text{-}PPh_3$ unit (Figure 6.5a). The overall structure is thus that of a capped trigonal bipyramid, with the two phosphines inequivalent. The solution spectrum at -90°C, like the solid state spectrum at room temperature, shows two resonances, but as the temperature is increased these broaden and collapse to a single peak. This can be attributed to a fast fluxional process in solution at room temperature. Solution

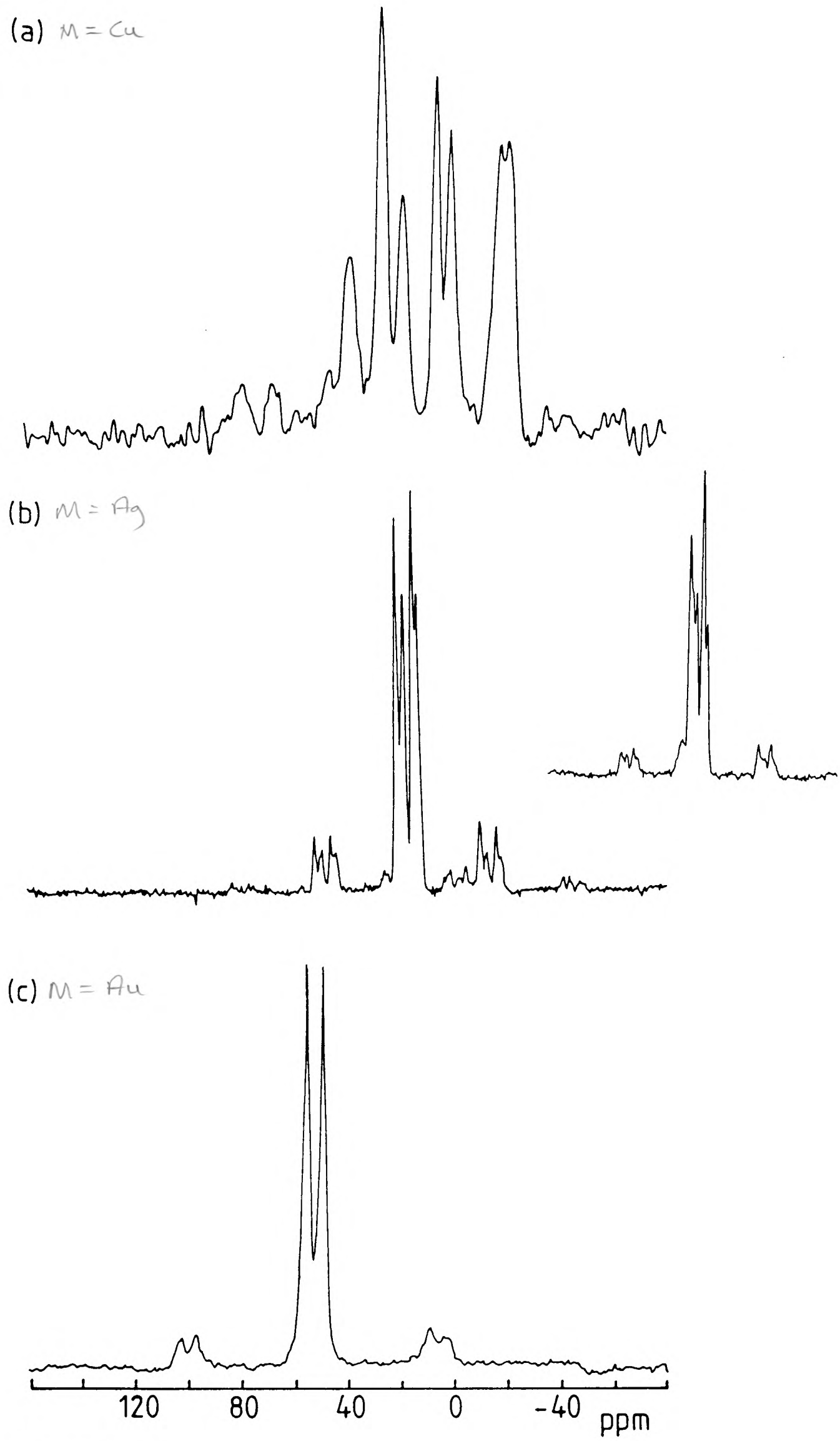


Figure 6.4

Solid state $^{31}P$ nmr spectra of the clusters $[M_2Ru_4H_2(CO)_{12}(PPh_3)_2]$, showing the effect of sample recrystallisation upon the disilver cluster.

coupling information and comparisons with exchange data obtained for similar clusters suggest that this process involves intramolecular metal core rearrangement.

The structure of the Ag cluster (2) has been determined by X-ray diffraction [12] to be identical to that of the Cu cluster. The initial solid state spectrum showed at least three resonances in the solid state (Figure 6.4b): the solution spectrum shows one resonance at room temperature which splits to give two at -90°C, in agreement with the solid state structure. One of the possible reasons for the presence of additional lines in solid state spectra is a difference between the structure of the unit cell determined for a single crystal and the same structure as found in the bulk material (section 2.6). The Ag cluster, like the analogous Cu cluster, is known to incorporate $CH_2Cl_2$ solvent molecules into the unit cell, which could create more than two inequivalent phosphorus environments. The problem would be made worse if some of the solvent molecules were then lost from the lattice. The sample was therefore recrystallised from diethyl ether/light petroleum and the solid state spectrum rerun. The new spectrum shows only two $^{31}P$ resonances, as would be expected from the crystal structure and the solid state spectrum of the Cu analogue if the Ag cluster was not fluxional in the solid state at room temperature. The chemical shifts and coupling constants are similar to those measured in solution.

The solid state nmr spectrum of the Au cluster (3) also consists of two resonances (Figure 6.4c), in agreement with the structure determined by X-ray diffraction [12]. The structure shows that the metal core of the cluster is identical to that of the analogous Cu and Ag compounds, but in the case of (3) one of the hydrido ligands bridges an Ru-Ru edge only (Figure 6.5b). The solid

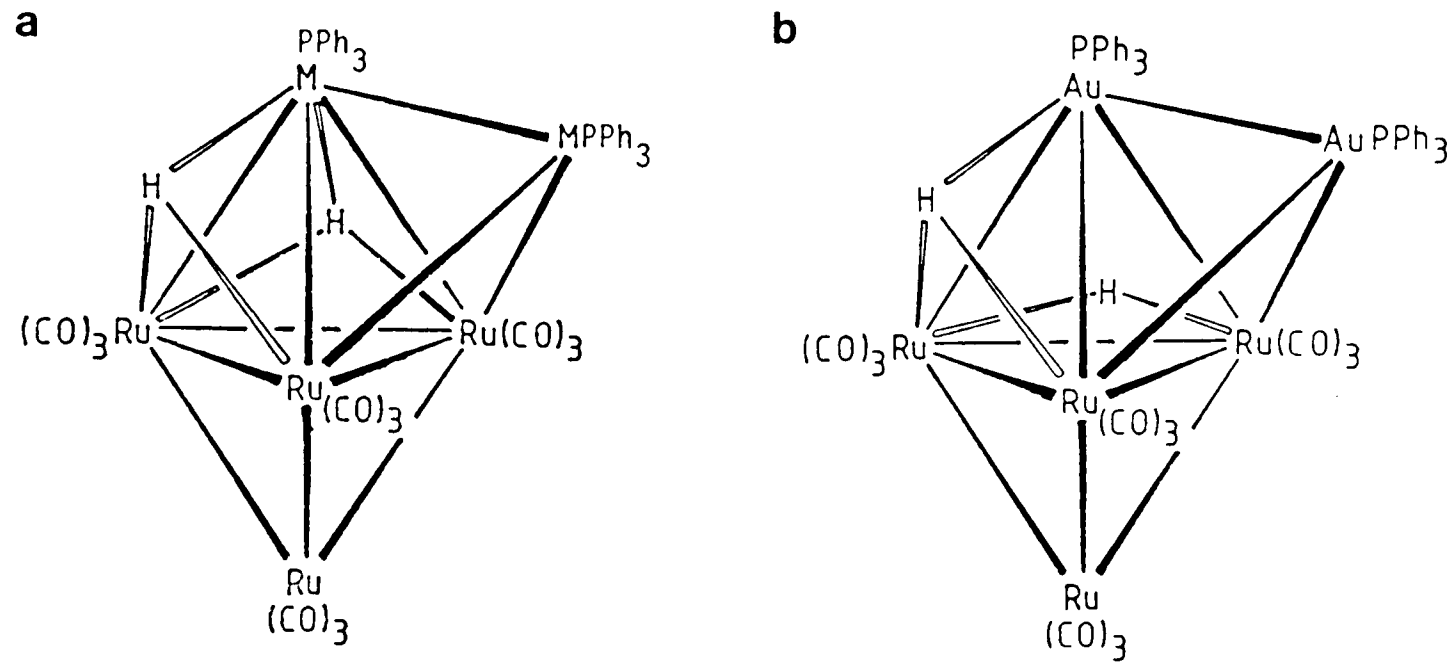


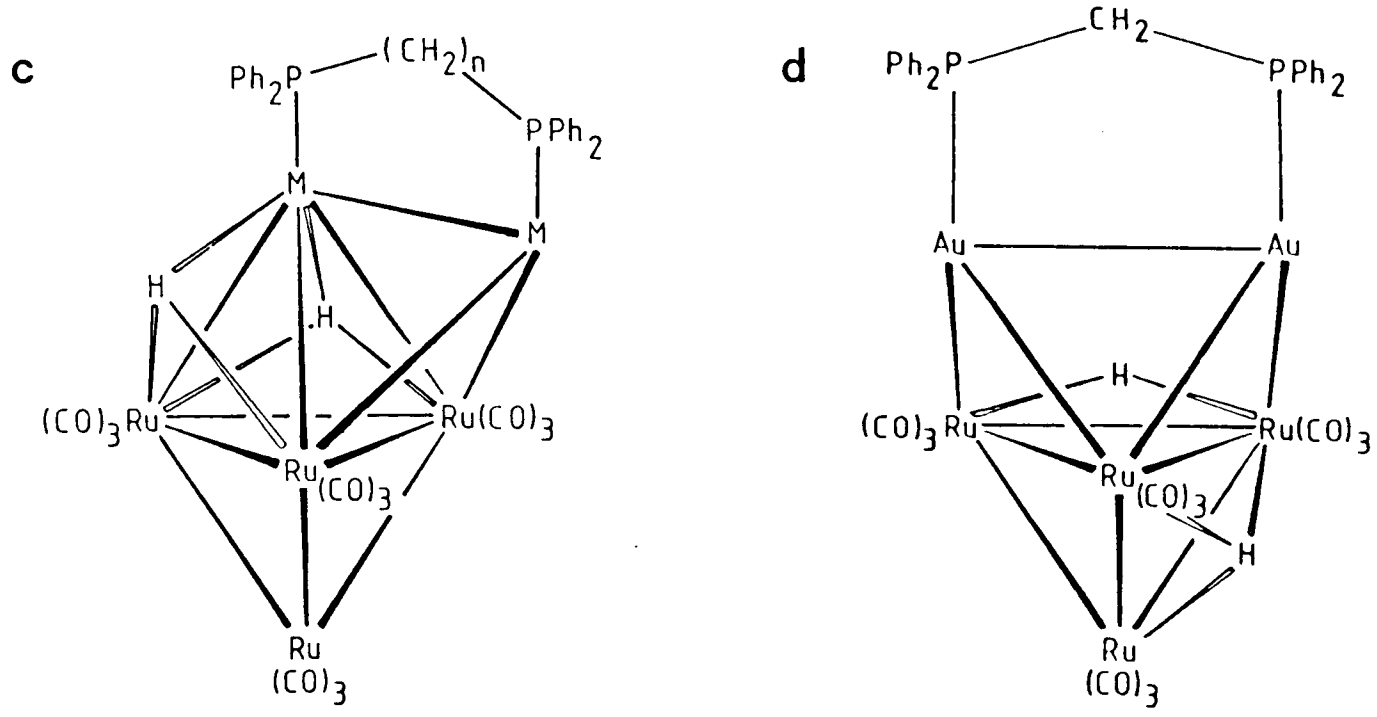


Figure 6.5

The metal core structures of the clusters $[M_2Ru_4H_2(CO)_{12}(PPh_3)_2]$.

(a) M = Cu or Ag, $L_2 = (PPh_3)_2$; (b) M = Au, $L_2 = (PPh_3)_2$;

(c) M = Cu or Ag, $L_2$ = (μ-dppm); (d) M = Au, $L_2$ = (μ-dppm).

state spectrum is in contrast to the solution spectrum, in which a single resonance is observed even at -90°C. Thus the fluxionality has been frozen out in the solid state. The free energies of activation for metal core rearrangement in solution have been calculated for the Cu and Ag clusters at 40.9±0.3 and 40±1.0 kJ/mol respectively [26,27]; that of the Au cluster has been estimated at ~35 kJ/mol.

b) A bidentate phosphine ligand.

The effect of the nature of the phosphine ligands on the structure and dynamics of some of the mixed metal clusters was examined by synthesising a series of clusters in which $(PPh_3)_2$ was replaced by $(Ph_2P(CH_2)_nPPh_2)$ (n = 1-6) [9,11,14]. A number of these clusters were found to be still fluxional in solution at -90°C, and it was hoped that this dynamic process would be frozen out in the solid, so that solid state nmr spectra would provide further information on the static structure of the clusters. The clusters $[MM'Ru_4(\mu_3\text{-}H)_2(CO)_{12}(\mu\text{-}Ph_2P(CH_2)PPh_2)]$ (M = M' = Cu, Ag, Au) were studied by solid state nmr.

The solid state nmr spectrum of the Cu cluster (4) is closely similar to that of the analogous cluster $[Cu_2Ru_4(\mu_3\text{-}H)_2(CO)_{12}(PPh_3)_2]$ (1), showing two phosphorus resonances split by coupling to the quadrupolar copper nucleus. The resulting spectrum shows 7 lines (Figure 6.6a); it appears that two lines of the expected 8 overlap in the peak at 28ppm. The structure of this cluster has not been determined, but spectroscopic data [14] suggests that it adopts a similar geometry to the $(PPh_3)_2$ cluster, with two inequivalent phosphorus sites. This would be in agreement with the solid state nmr spectrum. In solution a single resonance is observed at room temperature, which splits to an AB quartet at -90°C.

The spectrum of $[Ag_2Ru_4(\ _3\text{-}H)_2(CO)_{12}(\mu\text{-}Ph_2PCH_2PPh_2)]$ (5) in

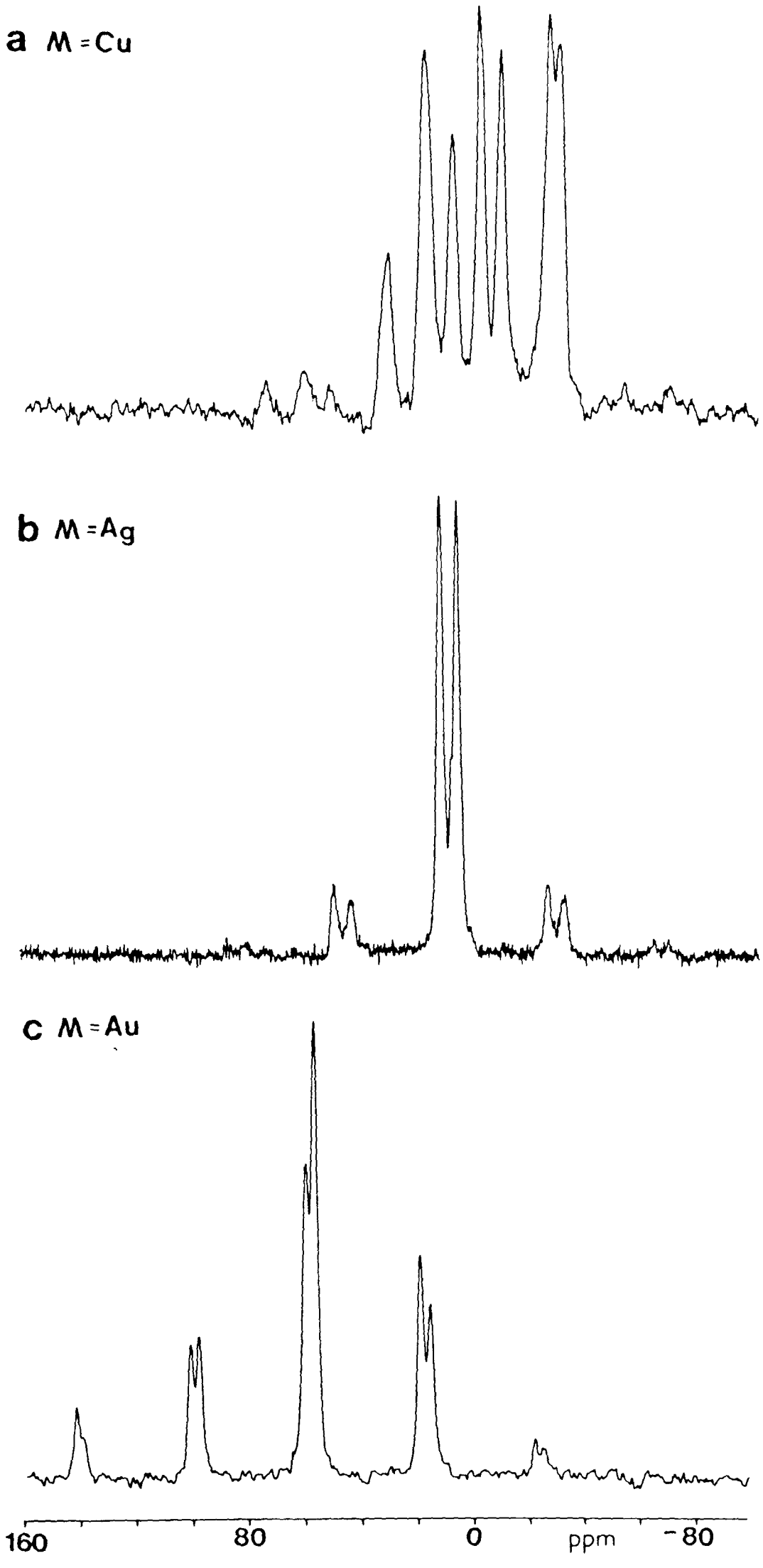


Figure 6.6

Solid state $^{31}P$ nmr spectra of the clusters $[M_2Ru_4H_2(CO)_{12}(\mu\text{-}Ph_2PCH_2PPh_2]$.

the solid state is a well-resolved doublet, with a linewidth of 112Hz (Figure 6.6b). In solution a single resonance showing Ag-P, Ag-Ag and P-P coupling is observed which becomes extremely broad but does not otherwise change at -90°C. The metal core structure of the cluster, as determined by X-ray diffraction [14], is the same as that exhibited by the three analogous clusters $[M_2Ru_4H_2(CO)_{12}(PPh_3)_2]$, a capped trigonal bipyramid in which the two phosphorus nuclei are inequivalent (Figure 6.5c). The stereochemical effect of the (μ-dppm) ligand is reflected in the decrease in Ag-Ag separation and the considerable distortion of the Ag-P vectors from their orientations in (2). The observation of a single resonance in the nmr spectra implies that the intramolecular fluxional process exchanging the 1B metal atoms between the two sites identified for (2) still operates for this cluster, and remains fast on the nmr timescale both in solution at -90°C and in the solid state at room temperature.

The Au cluster (6) gives a solid state nmr spectrum showing two $^{31}P$ resonances separated by 3.6ppm (Figure 6.6c). In solution a single resonance is observed which broadens but does not split at low temperature. This is the same behaviour as was observed for the analogous $(PPh_3)_2$ cluster (3). However differences in the infra-red and solution $^1H$ nmr spectra of the two clusters suggested that (6) adopted a different geometry. This was confirmed by X-ray diffraction [14], showing the core structure of (6) to consist of a capped square-based pyramid of metal atoms (Figure 6.5d). The $Au_2Ru_2$ base has a third Ru at the apex and the fourth Ru caps the $Ru_3$ face. Thus in the case of gold the steric strains found in the Ag cluster (5) are relieved by a change of metal geometry, resulting in approximately parallel Au-P vectors. Although the two phosphorus atoms in the molecule are inequivalent, the two environments are closely similar:

the only difference between them is their relationship to the hydrido ligands. If the hydrido ligands are ignored, there is a plane of symmetry through the structure. Thus there is no way of detecting whether a metal core rearrangement process occurs for this cluster. In solution, the hydrido ligands undergo site exchange, giving a single resonance in the room temperature $^{1}H$ nmr spectrum which broadens but does not split at -90°C, and so only a single phosphorus resonance would be expected in the solution $^{31}P$ spectrum whether the metal core is fluxional or not. It was therefore considered unlikely that the two phosphorus sites could be distinguished by nmr. However the solid state spectrum shows two phosphorus resonances. Two crystalline modifications of (6) are known, monoclinic and orthorhombic, with closely similar molecular geometries. From this structural information it can be seen that there are two possible sources of the two phosphine resonances observed in the solid state viz. the two inequivalent phosphines in one molecule or two different structural forms. It would seem unlikely, however, that crystals of both types would be present in equal amounts in the sample of (6) so to give two nmr resonances of equal intensity, even if both were formed under the recrystallisation conditions used to prepare the sample. A more reasonable explanation is that the motion of the metal core has been frozen out in the solid state, and that it is the two inequivalent phosphines in one molecule which give rise to the two phosphorus resonances.

The sample was recrystallised from diethyl ether/light petroleum and the solid state spectrum rerun, in the hope of determining whether the two lines resulted from a crystallographic effect rather than from two distinct phosphorus environments in the molecule. The new spectrum also showed two phosphorus resonances with

the same chemical shifts. It would appear that the two phosphorus sites in the molecule can be distinguished in the solid state.

Inspection of the spinning sideband manifolds associated with the two resonances shows them to be dissimilar, indicating a difference in the CSA's of the two phosphorus atoms. The methods of Maricq and Waugh [23] and of Herzfeld and Berger [24] were used to obtain the CSA from the spinning sidebands for the two phosphorus environments. It was found that the two had a similar overall anisotropy but different asymmetries, with $\eta$ = 1.6 and 0.8 respectively.

c) Increasing the size of the chelate ring.

Silver clusters analogous to (5) with additional methylene groups in the diphosphine backbone have also been studied by solid state $^{31}P$ nmr. When n, the number of methylene groups, is equal to 2, (cluster (7)), the solid state spectrum reveals a single resonance sufficiently broad ($\Delta\nu_{1/2} \sim 1000$Hz) that spin-spin coupling to silver cannot be resolved (Figure 6.7b). In solution at room temperature a single resonance is observed [9,14], but the low temperature (-90°C) spectrum shows two resonances, both rather broad but with couplings to silver clearly resolved. Two phosphorus resonances would be expected, given the structure of the cluster implied from solution spectroscopic data, if the core rearrangement process is frozen out. The difference between the low temperature solution and solid state nmr spectra suggest that although the fluxionality has been frozen out in solution, the core rearrangement process is still sufficiently rapid on the nmr timescale in the solid state for the two phosphorus environments to be indistinguishable at room temperature.

For both n = 3 and n = 4 clusters, the metal core

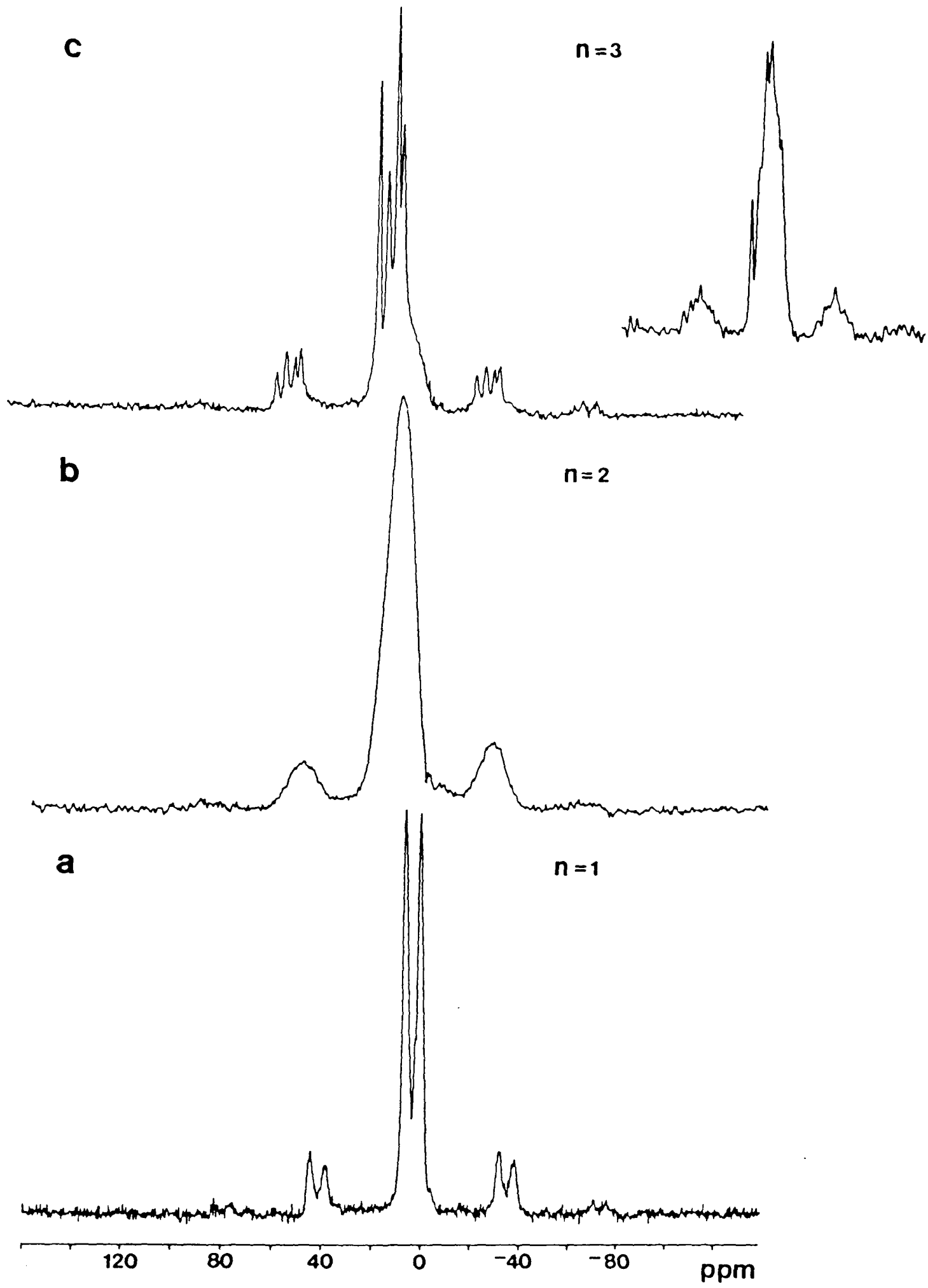


Figure 6.7

Solid state $^{31}P$ nmr spectra of the clusters $[Ag_2Ru_4H_2(CO)_{12}(\mu\text{-}Ph_2P(CH_2)_nPPh_2]$ (n=1-3). Inset: spectrum of the n=3 cluster before recrystallisation from diethyl ether/light petroleum.

rearrangement process is frozen out in solution at -90°C, giving rise to two $^{31}P$ resonances in the nmr spectrum [9,14]. The initial solid state nmr spectrum of the n = 3 cluster (8) showed a single resonance, which although broad had a linewidth less than that measured for the n = 2 cluster. Use of Gaussian multiplication to enhance the resolution showed the peak to be composed of a number of overlapping lines over a range of ~12ppm (Figure 6.7c), with the positions of some lines corresponding to those in the solution spectrum. Simulations of the solid state spectrum were carried out using the isotropic shifts and J values measured in solution and line broadenings from 200 to 300Hz. In all cases, three to four lines could be resolved in the simulated spectra spanning the same chemical shift range as found for the experimental spectrum. The partially resolved lines in the experimental spectrum were, however, much sharper than those in the simulations, bearing a closer resemblance to those seen in the spectra of clusters for which no rearrangement process was occurring. This suggested that what was being observed in the solid state was not two doublets broadened by residual motion, as would be expected on the basis of the nmr spectra and X-ray structures of related clusters, but rather the result of the overlap of a larger number of sharp lines.

The results already obtained from solid state nmr studies of similar compounds had shown that the process of recrystallisation could markedly alter the solid state spectrun of the sample, and so this sample was recrystallised from diethyl ether/light petroleum (previously $CH_2Cl_2$/light petroleum had been used). The spectrum of the recrystallised cluster showed two clearly resolved doublets, with isotropic shifts slightly closer together than found in solution but with identical coupling constants. This is completely consistent with the structure inferred from solution spectroscopic data. A broad

feature is apparent at the base of the peaks, which may result from the presence of a second species still fluxional in the solid state at room temperature. A further recrystallisation did not remove this broad feature.

A number of sharp lines, all with linewidths of about 130Hz, were observed in the initial solid state spectrum of the n = 4 cluster (9) (Figure 6.8a). These constitute at least five overlapping doublets of varying intensities, with chemical shifts and coupling constants closely similar to those measured in solution. A simulation of the experimental spectrum was carried out in an attempt to determine the number and relative intensities of the overlapping resonances. The spectrum was considered in terms of two groups of peaks corresponding to the two resonances observed in solution. A spectrum bearing a close resemblance to the experimental spectrum was simulated using the data shown in Table 6.2. The solution nmr data is given for comparison.

TABLE 6.2

A comparison of solution $^{31}P$ nmr data with that used to simulate the solid state $^{31}P$ spectrum of $[Ag_2Ru_4(\mu_3\text{-}H)_2(CO)_{12}(Ph_2P(CH_2)_4PPh_2)]$.

| | solution nmr | | simulation | | |
|---|---|---|---|---|---|
| | $\sigma_{iso}$/ppm | J/Hz | $\sigma_{iso}$/ppm | J/Hz | intensity |
| low field | 17.9 | 549 | 23.1 | | 2 |
| | | | 19.6 | 539 | 1 |
| | | | 13.3 | | 1 |
| high field | -1.8 | 448 | -1.9 | 437 | 2 |
| | | | -4.4 | 448 | 1 |

As with the other clusters which had shown more resonances than expected in their solid state spectra, the sample was

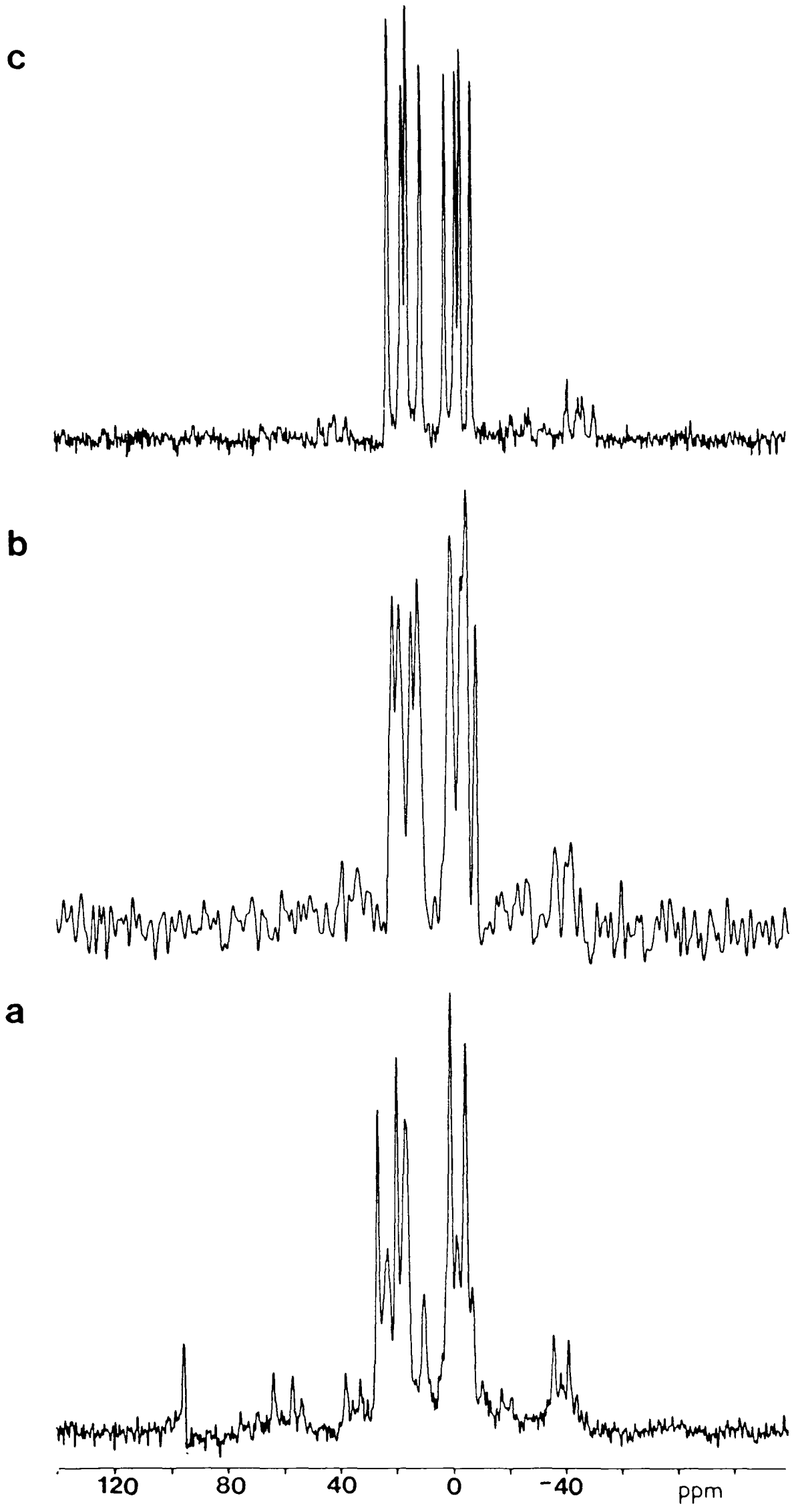


Figure 6.8

Solid state spectra of $[Ag_2Ru_4H_2(CO)_{12}(\mu\text{-}Ph_2P(CH_2)_4PPh_2]$.

(a) recrystallised from $CH_2Cl_2$/light petroleum.

(b) recrystallised from diethyl ether/light petroleum.

(c) recrystallised from toluene/light petroleum.

recrystallised from diethyl ether/light petroleum. The solid state spectrum of the new sample showed four well-resolved doublets, two corresponding to each of the solution resonances. These appeared to be of approximately equal intensities.

A further recrystallisation from toluene/light petroleum was then carried out. This sample also gave a solid state spectrum showing four well-resolved doublets of equal intensity. The chemical shift of one of the resonances was, however, 2.6ppm to higher field in this spectrum than in the previous spectrum.

Looking now at the structure determined for (5) [14], there are known to be two molecules in the unit cell, and so a possible four inequivalent phosphorus environments exist. The solid state nmr spectrum observed for (9) would be consistent with a similar crystal structure, with four inequivalent phosphorus environments. This suggests that for both upfield and lowfield resonances two phosphorus environments magnetically equivalent for the cluster with n = 3 become inequivalent in the n = 4 cluster. Possible reasons might be a small difference in crystal packing for (9), or accidental degeneracy of resonances in the nmr spectra of the other clusters in the series. The sensitivity to the solvent used for sample recrystallisation suggests a possible link with solvent incorporation into the unit cell.

d) An asymmetrical bidentate ligand.

The cluster $[Cu_2Ru_4(\mu_3\text{-}H)_2(CO)_{12}(\mu\text{-}Ph_2As(CH_2)_2PPh_2)]$ is one of the first examples of these heteronuclear metal clusters containing an asymmetrical bidentate ligand [16]. The cluster adopts the same metal core geometry as that established for (1), (2) and (5). Two distinct structural isomers of the cluster are possible (Figure 6.9a). In solution both isomers exist at -90°C in the ratio 1:0.37. These are

a

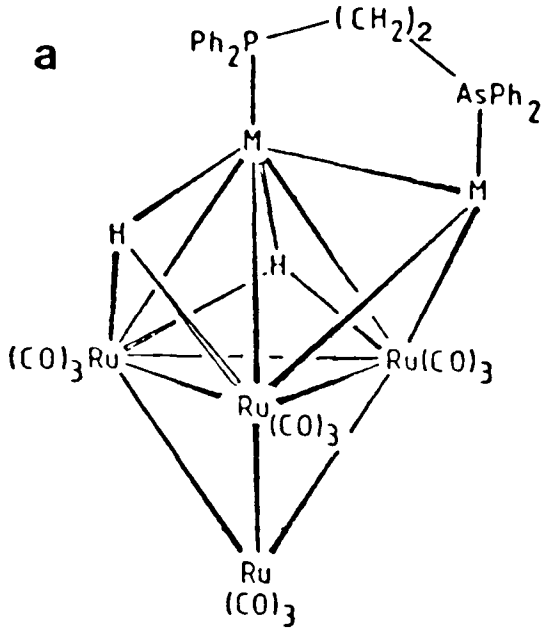


Isomer A

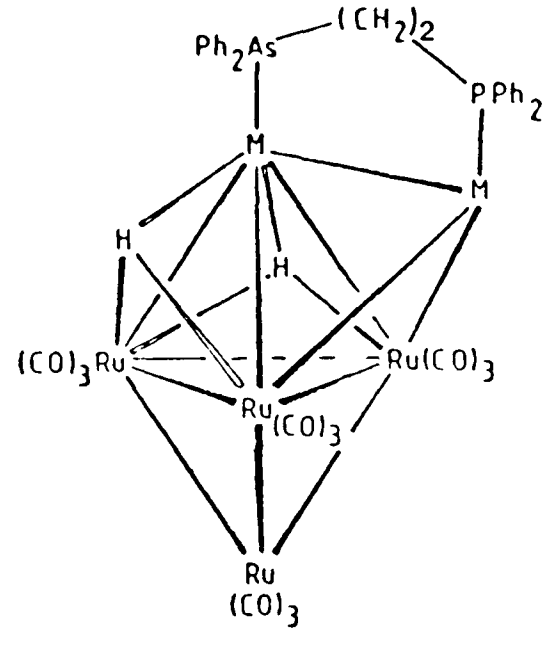


Isomer B

b

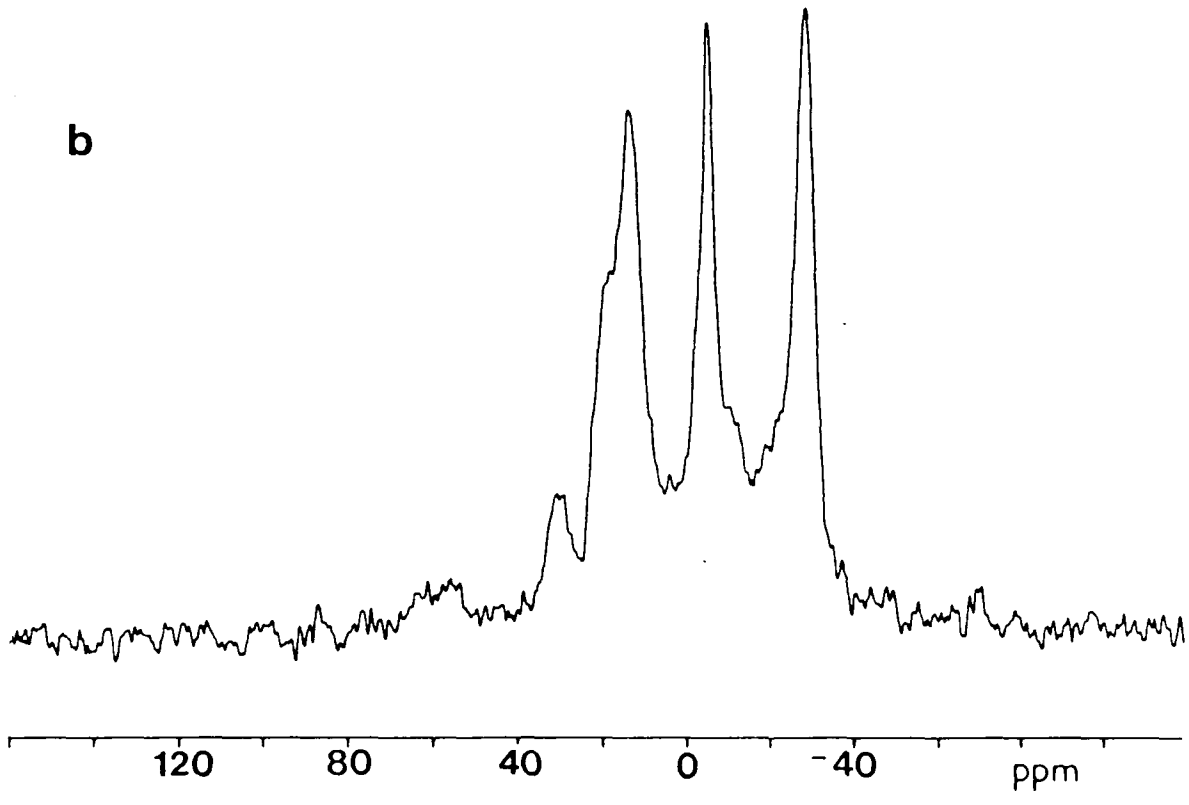


Figure 6.9

(a) The two isomers of $[Cu_2Ru_4H_2(CO)_{12}(\mu\text{-}Ph_2As(CH_2)_2PPh_2)]$.

(b) Solid state $^{31}P$ nmr spectrum of the cluster.

interconverted at ambient temperature by a fluxional process involving intramolecular metal core rearrangement.

In the solid state $^{31}P$ nmr spectrum four lines of differing linewidths are observed (Figure 6.9b). They result from one phosphorus resonance split by coupling to the adjacent copper nucleus. The breadth of the lines and the much lower intensity of the resonance which would be expected from the other isomer, if present, make it impossible to determine conclusively whether one or two isomers exist in this sample in the solid state.

### 6.4.3. Clusters with two group 1B metal sites: M ≠ M'.

Solid state nmr studies have also been carried out on the novel trimetal species $[MM'Ru_4(\mu_3\text{-}H)_2(CO)_{12}(PPh_3)_2]$ (M = Cu, M' = Ag (10) or Au (11); M = Ag, M' = Au (12)). Infra-red and solution nmr spectra indicate that the clusters have broadly similar structures [13,26], resembling those of the analogous bimetallic clusters (section 6.4.2). An X-ray diffraction study of the cluster $[CuAgRu_4(\mu_3\text{-}H)_2(CO)_{12}(PPh_3)_2]$ (10) confirmed the structure to be a capped trigonal bipyramid, with two distinct sites for the coinage metals [13]; one site, (M(2)), is in contact with four other metal atoms, the second, (M(1)), is in contact with three (Figure 6.10). In contrast to the bimetallic clusters, the trimetallic compounds show no evidence of core rearrangement in solution; there seems to be a thermodynamic preference for the structure in which the lighter group 1B metal occupies the M(2) site.

The solid state nmr spectra of these clusters were complicated by severe line broadening of the resonances and by the overlap of spinning sidebands and isotropic resonances. Spinning sideband suppression experiments using the TOSS pulse sequence [28]

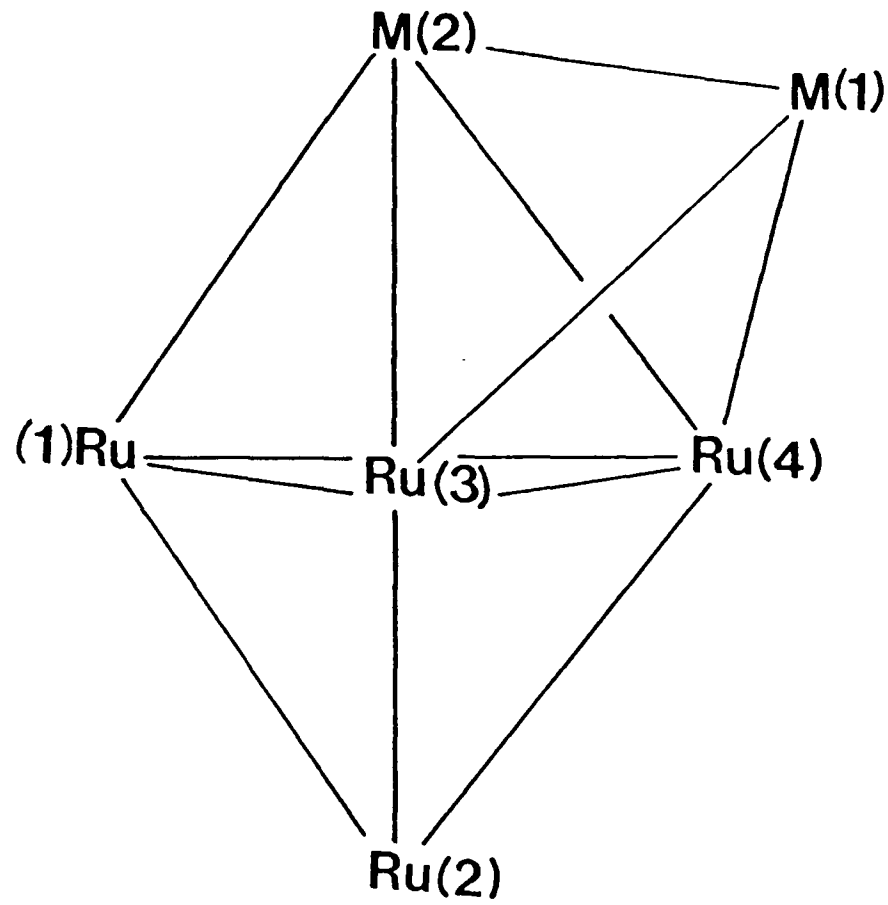


Figure 6.10

The two distinct group 1B metal sites (M(1) and M(2)) in the clusters $[M_2Ru_4H_2(CO)_{12}L_2]$.

assisted in clarification of the spectra. The results obtained are tabulated below with those of the corresponding bimetallic clusters, showing the phosphorus chemical shift in terms of the site occupied by the coinage metal. The solid state spectra of the clusters are shown in Figure 6.11.

TABLE 6.3

The correlation between the $^{31}P$ chemical shift of M-$PPh_3$ moieties (M = Cu, Ag or Au) in clusters (1)-(3), (10)-(12), and the site occupied by the group 1B metal in the cluster.

| | Cu | | Ag | | Au | |
|---|---|---|---|---|---|---|
| | M(1) | M(2) | M(1) | M(2) | M(1) | M(2) |
| $Cu_2$ | 2.5 | 9.0 | | | | |
| $Ag_2$ | | | 12.9 | 15.1 | | |
| $Au_2$ | | | | | [49.9,56.0]* | |
| CuAg | 8.0 | | 14.3 | | | |
| CuAu | 10.0 | | | | 67.2 | |
| AgAu | | | | 15.7 | 61.6 | |

All chemical shifts are in ppm, and are referenced to 85% $H_3PO_4$.

* site assignments not certain.

For all of the clusters two resonances were observed in the solid state nmr spectra. Both of the Cu-$PPh_3$ moieties gave rise to asymmetric 'quartets', but these were substantially broader than those observed for the other copper-containing clusters studied. The solution resonances of these clusters were also considerably broader than those of the other copper-containing clusters; the actual linewidths in solution were difficult to measure, as the lines merged

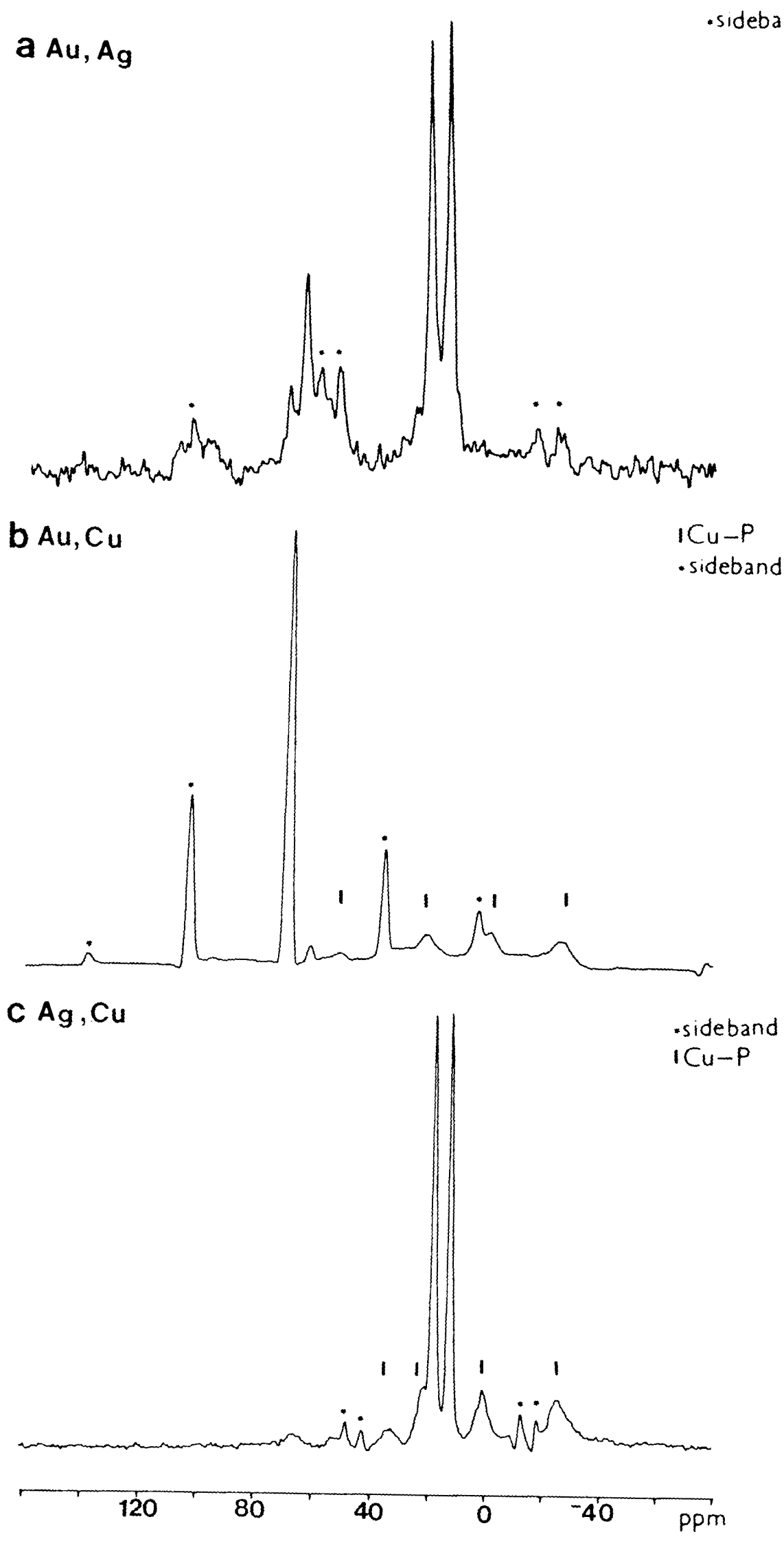


Figure 6.11

Solid state $^{31}P$ nmr spectra of the clusters $[MM'Ru_4H_2(CO)_{12}(PPh_3)_2]$.

into the baseline. The intensity of the Au-$PPh_3$ peak was much greater in the spectrum of the AuCu cluster than for the AuAg cluster.

The spectra indicate the difference in the chemical shift anisotropies associated with the two phosphine environments. This may be illustrated by comparing the CSA's of the Ag-$PPh_3$ units. When the Ag atom occupies the M(2) site, a number of spinning sidebands are observed even when spinning the sample at 3.0kHz, revealing a considerable CSA; however when the silver atom occupies the M(1) site, fewer sidebands are observed in the spectrum obtained at a comparable spinning speed. This may be useful in assigning the resonances of the clusters where M = M' to a metal phosphine group occupying a specific (M(1) or M(2)) site in the cluster. However difficulties arise when $[Au_2Ru_4(\mu_3\text{-}H)(\mu\text{-}H)(CO)_{12}(PPh_3)_2]$ (3) is considered. On the basis of the CSA's of the two phosphine groups, the peak at 56.5ppm should be assigned to the phosphine attached to the gold atom occupying the M(2) site. The two solid state $^{31}P$ resonances may also be assigned from a comparison of the spectrum with that of $[Au_3Ru_4(\mu_3\text{-}H)(CO)_{12}(PPh_3)_3]$ [29] (section 6.5.2). This cluster has a structure related to that of (3), with the ($\mu$-H) ligand replaced by an Au-$PPh_3$ unit: it may thus be considered to have two gold atoms occupying sites analogous to M(1) and one occupying a site analogous to M(2). The phosphorus chemical shifts are 62.2ppm [2P] and 55.3ppm [1P]. By analogy, the resonance of (3) with the low field chemical shift should be assigned to the phosphine attached to M(1). This is not the assignment suggested by the anisotropy data. Interestingly, the CSA's associated with the two different phosphine sites in $[Au_3Ru_4(\mu_3\text{-}H)(CO)_{12}(PPh_3)_3]$ are almost identical. This suggests that, whilst the information contained in the CSA may be used as a guideline in assigning the resonances in these clusters, no definite assignment can be made on this basis alone until

the factors influencing the anisotropy are better understood.

## 6.5 Further heteronuclear metal clusters containing bidentate phosphine ligands.

### 6.5.1 Clusters $[M_2Ru_3(\mu_3\text{-}S)(CO)_9L_2]$.

Three clusters of this type were studied by solid state nmr: M = Au, $L_2 = (PPh_3)_2$ or $(\mu\text{-}Ph_2PCH_2PPh_2)$; M = Cu, $L_2 = (\mu\text{-}Ph_2PCH_2PPh_2)$. The crystal structures of all of the clusters have been determined previously.

The $^{31}P$ nmr spectrum of $[Au_2Ru_3(\mu_3\text{-}S)(CO)_9(PPh_3)_2]$ in the solid state revealed a single phosphorus resonance with a linewidth of 1200Hz (Figure 6.12a). This was the broadest line observed for any of the heteronuclear clusters studied here. Solution nmr also showed a single line in the spectrum even at low temperature. The X-ray structure of the cluster [30] shows an $Au_2Ru_3$ trigonal bipyramid with gold atoms in one apical and one equatorial site and the sulphur atom capping the $Ru_3$ face. The two phosphorus environments are inequivalent. It would therefore be expected that two distinct phosphorus resonances would be observed in the nmr spectra. The nmr results obtained suggest that a fluxional process is operating not only in solution but also in the solid state which makes the two phosphorus environments equivalent on the nmr timescale.

The breadth of the line in the solid state nmr spectrum raised the possibility that it comprised several sharper, overlapping lines. The sample was therefore recrystallised from diethyl ether/light petroleum in the hope of obtaining a spectrum showing better resolution. However although the linewidth decreased slightly, to 1100Hz, a single spectral line was still observed.

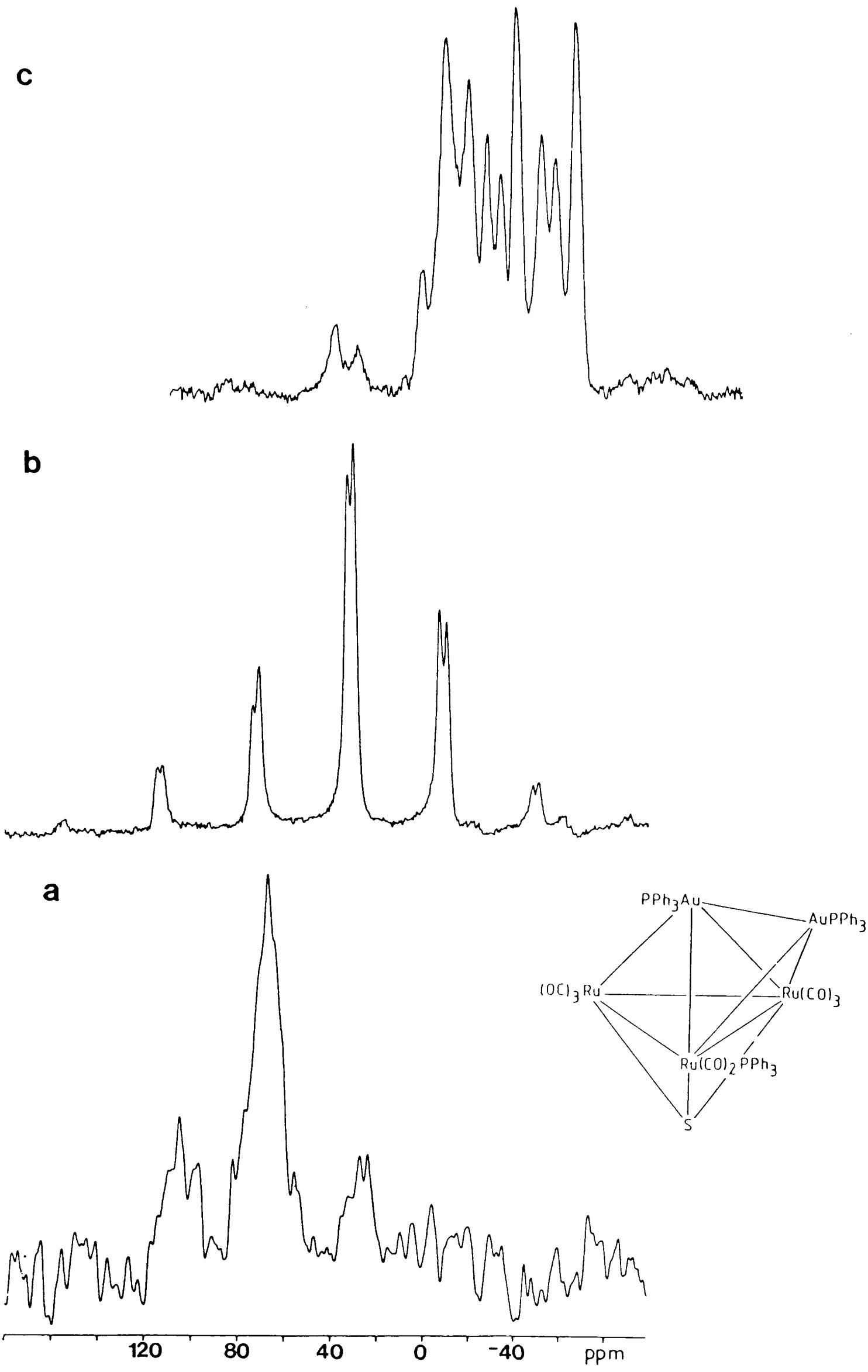


Figure 6.12

Solid state spectra of the clusters $[M_2Ru_3(\mu_3\text{-}S)(CO)_9L_2]$ ($L_2=(PPh_3)_2$, M=Au (a); $L_2=$ ($\mu$-$Ph_2PCH_2PPh_2$), M=Au (b) or Cu (c). Inset: structure.

The cluster $[Au_2Ru_3(\mu_3\text{-}S)(CO)_9(\mu\text{-}Ph_2PCH_2PPh_2)$ also gave rise to a single broad resonance in its solid state nmr spectrum. This was however narrower than the resonance line of the $(PPh_3)_2$ cluster, with $\Delta\nu_{1/2} \sim 750Hz$. An additional small resonance,shifted well upfield of the cluster resonance, was ascribed to an impurity. The solution nmr spectrum of this cluster showed a single line at low temperature. Recrystallisation of the sample was carried out both to remove the impurity and in an attempt to improve the resolution. The solid state nmr spectrum of the recrystallised sample differed considerably from the original spectrum. Two closely-spaced isotropic peaks could be distinguished (Figure 6.12b), with a separation of just 2.3ppm (186Hz). The splitting was repeated in the spinning sidebands present in the spectrum. The CSA's of the two phosphorus sites are different: calculation shows them to have the same anisotropy but different asymmetries. This result is entirely consistent with the X-ray crystal structure [15], which shows two inequivalent phosphorus environments. The metal core structure of this cluster, however, is different from that of the analogous $(PPh_3)_2$ cluster, being intermediate between a trigonal bipyramid and a square-based pyramid. It is apparent from the solid state nmr spectrum that the motion present in solution has been 'frozen out' in the solid cluster. This is surprising in view of the result obtained for the $(PPh_3)_2$ cluster. The structure of $[Au_2Ru_3(\mu_3\text{-}S)(CO)_9(\mu\text{-}Ph_2PCH_2PPh_2)$ is closer to that of the postulated intermediate in the dynamic process occurring in solution than is the trigonal bipyramidal structure [15], and so this cluster might be expected to have a lower free energy for the dynamic process than a cluster with the trigonal bipyramidal structure.

The solution spectrum of $[Cu_2Ru_3(\mu_3\text{-}S)(CO)_9\text{-}\ (\mu\text{-}Ph_2PCH_2PPh_2)$ shows a single resonance down to low temperature, which is broadened

in this case by the adjacent copper nuclei. In the solid state two phosphorus resonances are observed. This is in complete agreement with the X-ray crystal structure [15], which is analogous to that of $[Au_2Ru_3(\mu_3\text{-}S)(CO)_9(PPh_3)_2]$, with the phosphine group bridging the Cu-Cu edge. The fluxionality has again been frozen out in the solid state. A total of nine lines are observed in the solid state nmr spectrum (Figure 6.12c). Coupling to the quadrupolar copper nucleus not removed by MAS should split two resonances to give eight lines. The origin of the extra line is not clear, possibly resulting from resolution of the different couplings to the two spin-3/2 copper nuclei.

### 6.5.2 Clusters $[Au_3Ru_4H(CO)_{12}L_3]$.

Two clusters of this type have been studied by solid state nmr, with $L_3 = (PPh_3)_3$ and $L_3 = (\mu\text{-}Ph_2PCH_2PPh_2)_\wedge$ respectively. The solid state spectrum of $[Au_3Ru_4(\mu_3\text{-}H)(CO)_{12}(PPh_3)_3]$ shows two resonances in the intensity ratio 2:1 (Figure 6.13a). This is closely similar to the low temperature solution nmr spectrum, and is entirely consistent with the X-ray crystal structure [29]. The structure shows the metal core to consist of a trigonal bipyramid $AuRu_4$ unit, with two $AuRu_3$ faces capped by Au atoms. It is related to the structure of the cluster $[Au_2Ru_4(\mu_3\text{-}H)(\mu\text{-}H)(CO)_{12}(PPh_3)_2]$ (3), with formal replacement of the ($\mu$ -H) ligand by the isolobal Au-$PPh_3$ group. The room temperature solution spectrum shows a single resonance, and this equivalence of the phosphine groups is thought to result from a polytopal rearrangement of the metal core of the cluster at ambient temperature.

In an attempt to gain further insight into the dynamic

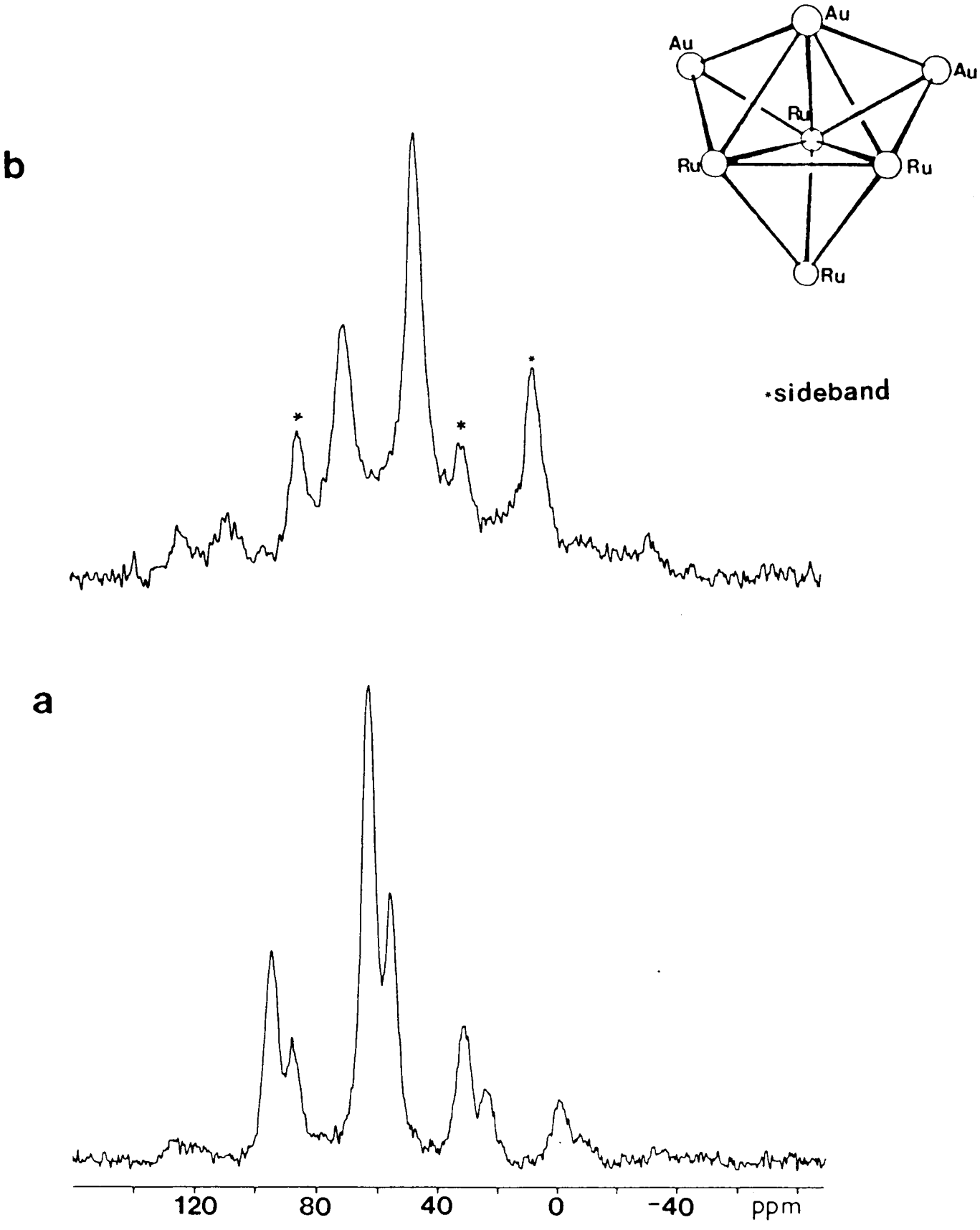


Figure 6.13

Solid state spectra of the clusters $[Au_3Ru_4(\mu_3\text{-}H)(CO)_{12}L_3]$ ($L_3$= $(PPh_3)_3$ (a) or $(\mu\text{-}Ph_2PCH_2PPh_2)PPh_3$ (b).

process the cluster $[Au_3Ru_4(\mu_3\text{-}H)(CO)_{12}(PPh_3)(\mu\text{-}Ph_2PCH_2PPh_2)]$ was studied. Spectroscopic evidence implies that this cluster has a similar metal core geometry to that of the $(PPh_3)_3$ cluster [29], with the (μ-dppm) ligand bridging adjacent gold sites. The room temperature solution $^{31}P$ nmr spectrum shows two resonances of intensity 1:2. The more intense peak broadens but does not otherwise change as the temperature is lowered to -90°C. The solid state spectrum at room temperature also shows two resonances of intensity 1:2 (Figure 6.13b). This indicates that either the two phosphorus atoms of the (μ-dppm) ligand are equivalent on the nmr timescale both in solution and in the solid state, or that the two resonances cannot be resolved in the solid state due to line broadening.

## 6.6 Copper-phosphorus quadrupolar coupling.

Ten heteronuclear metal clusters containing $Cu\text{-}PR_3$ moieties have been studied by solid state $^{31}P$ nmr. In all cases, the asymmetric resonance splittings discussed by Menger and Veeman [19] are observed in the phosphorus spectra. Analysis of the spectra should provide information regarding the structures of these clusters.

The positions of the spectral lines were calculated as functions of the parameter K, given by

$$K = \frac{3e^2qQ}{4S(2S-1)} \Big/ \gamma_S \hbar B$$

where $e^2qQ/h$ is the nuclear quadrupole coupling constant, and S is the spin not quantised along the magnetic field; for the clusters discussed here, S is the spin of the copper nuclei.

Figure 6.14 shows the theoretical form of the nmr spectra in the cases of pure dipolar and pure scalar coupling and for a combination of the two interactions. This combination was calculated

Figure 6.14

Calculated line positions of the I=1/2 multiplet relative to the unperturbed frequency resulting from (a) dipolar (b) scalar and (c) combined scalar and dipolar coupling to S=3/2 in units of K. One vertical unit corresponds to a/hHz. (From Menger and Veeman [19]).

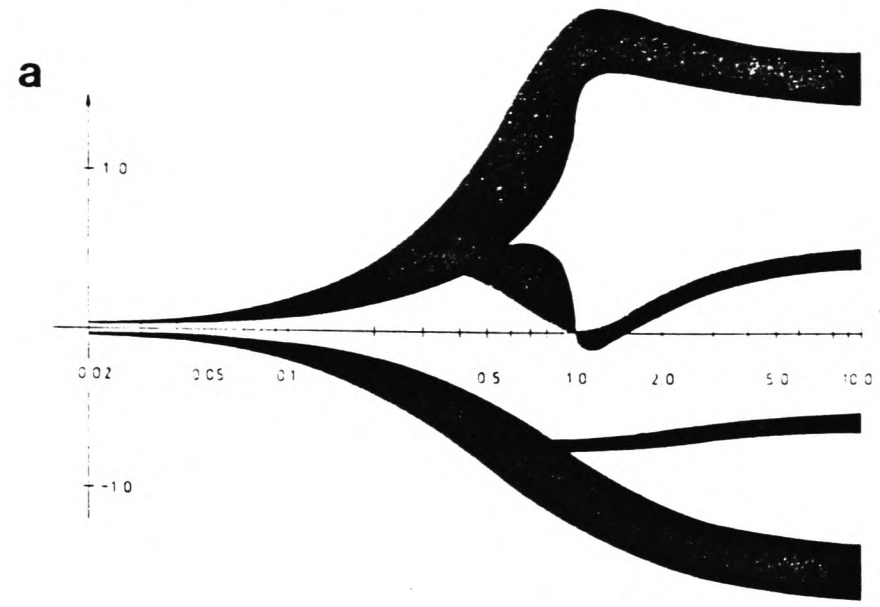


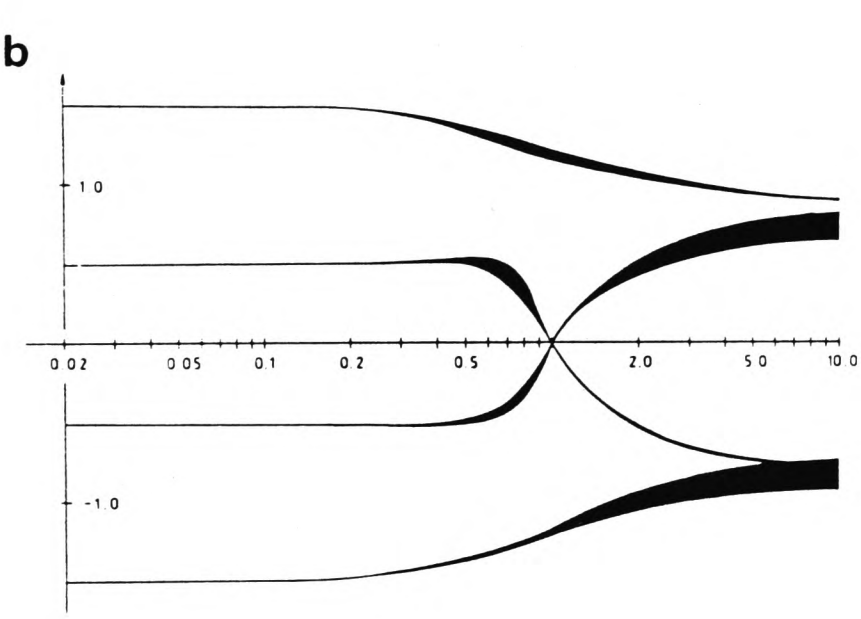


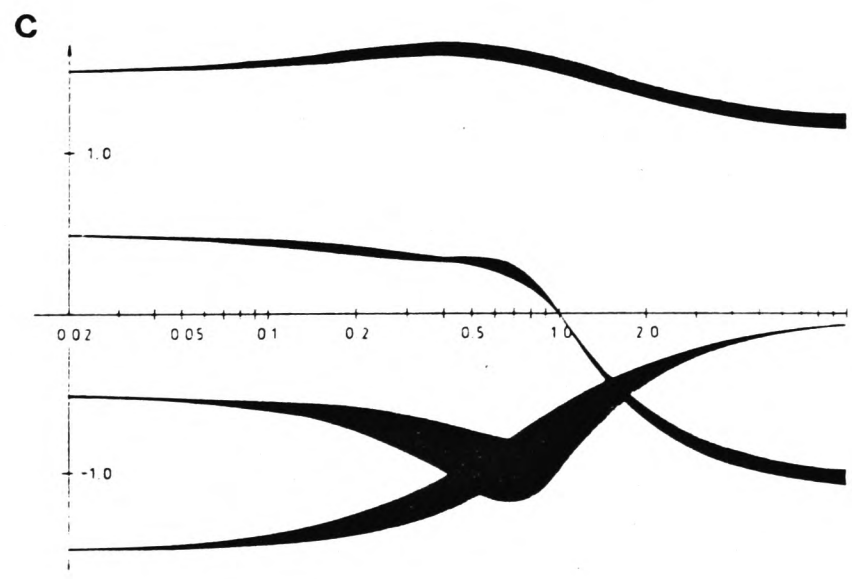

using the arbitrary ratio of the two coupling constants $\gamma_I\gamma_S\hbar^2/r^3$ = a/2. Vertical cross-sections of the figures correspond to the I = 1/2 spectra for particular values of K. A change in the sign of the coupling constant will invert the figures.

Copper nuclei in triphenylphosphine copper (I) complexes have pure quadrupole frequencies in the range 15-30MHz, the exact frequency depending on the coordination of the copper atom [19]. Using a frequency of 15MHz, a typical value for 4-coordinated copper, gives $e^2qQ/h \sim 30$MHz. The Zeeman frequency of copper at 4.7T, the field at which the experiments were conducted, is approximately 49MHz. This would make K approximately 0.15. Results corresponding to a K value in this area would be expected for the compounds studied here.

The solid state spectra obtained were initially compared with the theoretical spectra for the case of combined scalar and dipolar coupling. The experimental spectra were found to be qualitatively similar to those predicted for this case over a range of K values from 0.15 to 0.3. It should be noted that in the example in the literature [19] not only was an arbitrary ratio of the two coupling constants taken, but axial symmetry of the EFG tensor about the internuclear vector r was assumed. It is therefore not surprising that although the experimental spectra follow the trends shown in Figure 6.14 they do not match the predictions exactly.

By comparing the theoretically-calculated line splittings with those observed experimentally, a value for the isotropic shift was obtained for each of the clusters studied. These are shown in Table 6.4 together with the chemical shifts measured in solution. There is a close resemblance between the two sets of values.

An estimate of the internuclear separation r may also be made from the line splittings observed in the experimental spectra.

TABLE 6.4

A comparison of calculated solid state $^{31}P$ chemical shifts with those measured in solution for copper phosphine-containing clusters.

| cluster | solid, 20°C | solution, -90°C |
|---|---|---|
| $CuRu_4(\mu_3\text{-}H)_3(CO)_{12}PPh_3$ | 13.6 | 10.9 |
| $CuRu_4(\mu_3\text{-}H)_3(CO)_{12}PMePh_2$ | -7 | -5.5 |
| $CuRu_3(CO)_9(C_2Bu^t)PPh_3$ | -0.5 | -1.4 |
| $CuRu_3(\mu\text{-}H)(\mu_3\text{-}S)(CO)_8(PPh_3)_2$ | 3.7 | 4.1 |
| $Cu_2Ru_4(\mu_3\text{-}H)_2(CO)_{12}(PPh_3)_2$ | 9 | 6.8 |
| | 2.5 | -0.4 |
| $Cu_2Ru_4(\mu_3\text{-}H)_2(CO)_{12}(\mu\text{-dppm})$ | 0 | 2.5 |
| | -7 | -9.6 |
| $AuCuRu_4(\mu_3\text{-}H)_2(CO)_{12}(PPh_3)_2$ | 10 | 4.8 |
| $AgCuRu_4(\mu_3\text{-}H)_2(CO)_{12}(PPh_3)_2$ | 7.7 | 6.4 |
| $Cu_2Ru_4(\mu_3\text{-}H)_2(CO)_{12}(\mu\text{-}Ph_2As\text{-}(CH_2)_2PPh_2)$ | 2 | 3.6 [0.37P] |
| | | -5.1 [1.0P] |
| $Cu_2Ru_3(\mu_3\text{-}S)(CO)_9(\mu\text{-dppm})$ | -9 | -7.5 |
| | -16 | |

All chemical shifts are in ppm, and are referenced to 85% $H_3PO_4$.

Due to the broad lines observed in the solid state spectra of many of the copper-containing clusters, certain of the calculated chemical shifts are only accurate to the nearest ppm.

TABLE 6.5

A comparison of the Cu-P bond distances calculated from the solid state nmr spectra with those obtained from X-ray diffraction.

| cluster | r from solid state spectrum | r from X-ray diffraction |
|---|---|---|
| $CuRu_4(\mu_3\text{-}H)_3(CO)_{12}PPh_3$ | 2.2 | - |
| $CuRu_4(\mu_3\text{-}H)_3(CO)_{12}PMePh_2$ | 2.2 | 2.197 |
| $CuRu_3(CO)_9(C_2Bu^t)PPh_3$ | 2.3 | 2.22 |
| $CuRu_3(\mu\text{-}H)(\mu_3\text{-}S)(CO)_8(PPh_3)_2$ | 2.4 | - |
| $Cu_2Ru_4(\mu_3\text{-}H)_2(CO)_{12}(PPh_3)_2$ | 2.27 | 2.20 |
| | 2.38 | 2.27 |
| $AgCuRu_4(\mu_3\text{-}H)_2(CO)_{12}(PPh_3)_2$ | 2.3 | 2.203 |
| $Cu_2Ru_3(\mu_3\text{-}S)(CO)_9(\mu\text{-}dppm)$ | 2.8 | 2.23 |
| | 2.5 | 2.21 |

All bond lengths are in Angstroms.

Taking the ratio of coupling constants in the example gives

$$r^3 = \frac{\gamma_I \gamma_S \hbar}{\pi \times a/h} \times \frac{2\pi}{B_0}$$

For spectra measured at high field, the magnitude of a/h is in good approximation equal to the distance between the two centre lines of the spectra. This was used to obtain approximate values of r. The results were compared with the internuclear separations measured by X-ray diffraction, where available. The figures obtained are shown in Table 6.5. It is apparent from the Table that the estimated values are in reasonable agreement with those obtained by X-ray diffraction.

## 6.7 Silver-phosphorus scalar coupling.

All of the silver phosphine-containing clusters in this study except one show Ag-P spin-spin coupling in their solid state $^{31}P$ nmr spectra, and for the exception the spectral linewidth is such that coupling, if present, could not be resolved. This coupling is a source of information about the structures and dynamic properties of the silver-containing clusters [31]. For example, in the cluster $[Ag_2Ru_4(\mu_3\text{-}H)_2(CO)_{12}(\mu\text{-}Ph_2PCH_2PPh_2)]$ (5) spin-spin coupling is retained, despite the metal core rearrangement taking place in the solid state; this demonstrates that the dynamic process is intramolecular [9,14].

A comparison of the solid state coupling constants with those measured in solution shows a close agreement between the two. The error in measuring the coupling constants in the solid state was considered to be ±10Hz. All except three of the solid state values are within ±10Hz of their solution counterparts (see Table 6.6).

Metal-phosphorus scalar coupling in the solid state has been reported previously for both rhodium and platinum complexes [32-34].

TABLE 6.6

Solid state and solution Ag-P coupling constants.

| cluster | solid | solution | mean solution |
|---|---|---|---|
| $AgRu_4(\mu_3\text{-}H)_3(CO)_{12}PPh_3$ | 651 | 693, 601 | 647 |
| $AgRu_3(CO)_9(C_2Bu^t)PPh_3$ | 445 | 482, 417 | 449 |
| $Ag_2Ru_4(\mu_3\text{-}H)_2(CO)_{12}(PPh_3)_2$ | 509 | 565, 490 | 527 |
| | 448 | 473, 410 | 442 |
| $Ag_2Ru_4(\mu_3\text{-}H)_2(CO)_{12}(Ph_2PCH_2PPh_2)$ | 510 | 499, 432 | 477* |
| $Ag_2Ru_4(\mu_3\text{-}H)_2(CO)_{12}(Ph_2P(CH_2)_2PPh_2)$ | - | 585, 507 | 546 |
| | | 457, 396 | 426 |
| $Ag_2Ru_4(\mu_3\text{-}H)_2(CO)_{12}(Ph_2P(CH_2)_3PPh_2)$ | 549 | 589, 510 | 549 |
| | 448 | 471, 408 | 440 |
| $Ag_2Ru_4(\mu_3\text{-}H)_2(CO)_{12}(Ph_2P(CH_2)_4PPh_2)$ | 539 | 583, 505 | 544 |
| | 437 | 479, 416 | 447 |
| $AgAuRu_4(\mu_3\text{-}H)_2(CO)_{12}(PPh_3)_2$ | 529 | 596, 515 | 555 |
| $AgCuRu_4(\mu_3\text{-}H)_2(CO)_{12}(PPh_3)_2$ | 458 | 481, 417 | 449 |

* obtained using the average of both $^1J$ and $^2J$ Ag-P coupling constants.

All coupling constants are given in Hertz.

Maciel et al [32] compared the solution and solid state spectra of a series of rhodium (I) diphosphine catalysts, and found that solution and solid state coupling constants were generally within a few Hertz of each other. In two cases, there was greater disparity, for example J(solution) = 155, 156Hz, J(solid) = 162, 124Hz; this was ascribed to substantial differences in coordination geometry between the two states. Studies by Bemi and co-workers [33] on a series of platinum phosphine complexes, chosen in the hopes that the geometry of the complex in the solid state would be revealed by the Pt-P coupling, showed that it was possible to distinguish cis and trans geometries by the magnitude of the coupling constant. The J values measured were in reasonable agreement with those observed in solution.

Spin-spin coupling is transmitted via chemical bonds, and so is a sensitive indicator of the types of bonds involved and their spatial orientation in the molecule [31]. The close similarity between solution and solid state coupling constants implies very little change in the nature and orientation of the Ag-P bonds in these clusters upon the change of state.

A number of studies have been carried out in an attempt to find a correlation between the magnitude of a metal-phosphorus coupling constant and some measurable property of the M-P bond ([31] and references therein). The coupling between two covalently-bonded atoms A and B is believed to be dominated by the Fermi contact term [31,35], so that the size of the coupling constant is dependent upon the s character of the metal-phosphorus bond. This suggests that, for a given metal, a correlation should exist between $^{1}J(M-P)$ and the M-P bond length [31,35]: an increase in J would be expected to accompany the decrease in bond length indicating an increase in the s character of the bond. A rough correlation between $^{1}J(Pt-P)$ and Pt-P bond length

has been observed [35] for a series of Pt-phosphines of given coordination number. Further evidence is provided by the observation of similar trends for a number of triphosphine W, Rh and Pt complexes [35].

The X-ray crystal structures of most of the silver-containing clusters studied here have not been determined, and so a general trend cannot be sought. However it is interesting to consider the cluster $[Ag_2Ru_4(\mu_3\text{-}H)_2(CO)_{12}(PPh_3)_2]$ (2) in this light. The cluster contains two distinct group 1B metal sites, and two different Ag-P bond lengths have been measured. The two resonances observed may be assigned to specific $Ag\text{-}PPh_3$ groups, and hence a comparison of J and r made. For the unit with the shortest Ag-P bond length, the larger coupling constant of the two is observed (Table 6.7). This is consistent with the preceeding discussion.

TABLE 6.7

Correlation between Ag-P coupling constant, Ag-P bond length and the site occupied by the silver atoms in $[Ag_2Ru_4(\mu_3\text{-}H)_2(CO)_{12}(PPh_3)_2]$.

| J/Hz | r/Å | metal site |
|---|---|---|
| 509 | 2.382 | M(2) |
| 448 | 2.421 | M(1) |

The magnitude of the coupling constant is indicative of the group 1B metal site occupied by an $Ag\text{-}PR_3$ moiety in the clusters $[Ag_2Ru_4(\mu_3\text{-}H)_2(CO)_{12}L_2]$. The two sites differ in the number of other metal atoms with which the 1B metal atom is in close contact, three for the M(1) site and four for the M(2) site. When the silver atom occupies the M(1) site, $^1J(Ag\text{-}P)$ is in the range 437-458Hz. When the

silver atom occupies the M(2) position, the coupling constant increases to between 509 and 550Hz. This has implications for the determination of the type of site occupied by an Ag-P unit in a cluster of this type where M ≠ M'. A comparison of the above trends with the measured J value for the still fluxional cluster (5) suggests that, on the basis of its coupling constant, the average metal site observed on the nmr timescale might more closely resemble the M(2) site than the M(1) site.

## 6.8 Chemical shifts.

The isotropic chemical shift of a nucleus is determined by the frequency at which that nucleus resonates in a magnetic field [17]. It is highly characteristic of the environment of the resonant nucleus, and is therefore potentially a source of much information on the molecular structure of the compound studied. In order to extract this information, the contributions from the various parameters influencing the chemical shift must be considered. The chemical shift can be defined as the sum of various terms:

$$\sigma_{iso} = \sigma_d + \sigma_p + \sigma_{CSA} + \sigma_e + \sigma_x$$

where $\sigma_d$ represents the diamagnetic contribution

$\sigma_p$ " " paramagnetic "

$\sigma_{CSA}$ " " contribution from the CSA

$\sigma_e$ " electric field effects

$\sigma_x$ includes ring current shifts and solvent effects.

For nuclei other than protons, the paramagnetic term makes the most important contribution to the chemical shift [17,36]. For $^{31}P$ the size of this term leads to a range of shifts of approximately 500ppm, which should provide a useful means of characterising phosphorus-containing compounds [37].

Various attempts have been made to correlate $^{31}P$ chemical shifts with structural parameters such as bond angles, phosphorus oxidation state and the electronegativity of the phosphorus substituent. The quantum mechanical calculations of van Wazer and Letcher [38] demonstrate that three factors appear to dominate phosphorus chemical shifts: electronegativity differences along the P-X bond; changes in $\pi$-electron overlap; and changes in the $\sigma$ bond angle.

Solid state chemical shifts are generally found to be similar to those measured in solution [39]. In some cases differences arise from what have been termed 'solid state effects'. These include through space interactions such as ring current shifts, bulk susceptibility effects, solvent effects and distortions of the geometry of either the compound itself or of the phosphorus substituents. All of the studies on chemical shifts described above have been carried out using solution chemical shift data. It would seem reasonable that any relationship between the chemical shift and a structural parameter should hold at least as well, if not better, for solid state nmr data, and so could be meaningfully be applied to the interpretation of nmr spectra in the solid state.

The majority of work engaged in developing a correlation between structure and solid state chemical shifts has been carried out for $^{29}Si$ and $^{27}Al$ nmr data [40]. However, Cheetham et al [41] have recently examined the relationship between $^{31}P$ chemical shift and bond strength at phosphate oxygen for a series of crystalline inorganic phosphates, finding a good correlation between the two.

For the heteronuclear metal clusters in this study, the solid state chemical shifts were first compared with those measured in solution. The correlation between the two sets of shifts is very good,

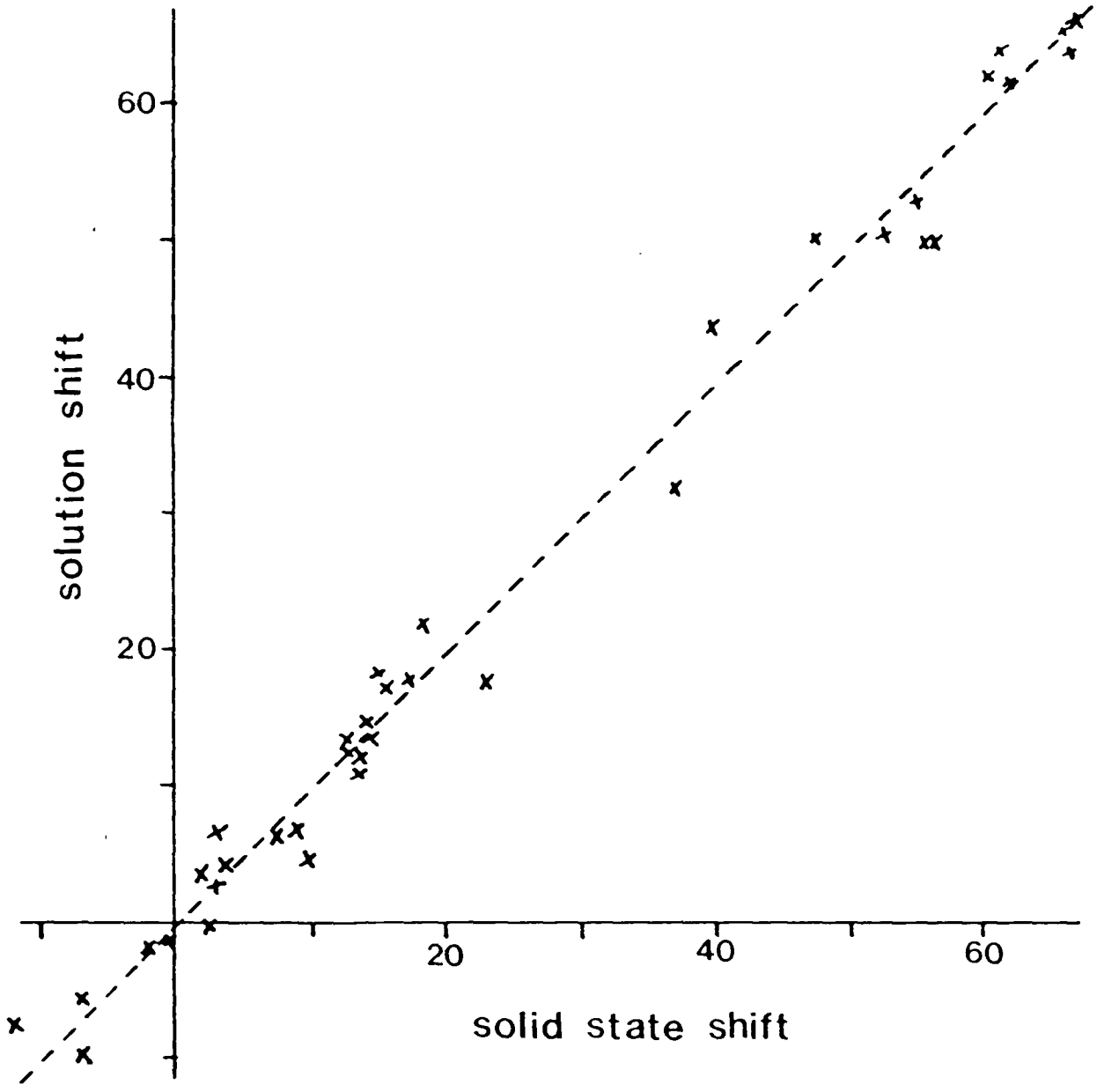


Figure 6.15

Plot of $^{31}P$ chemical shift in the solid state against solution shift for all of the heteronuclear metal clusters.

as shown by Figure 6.15. Considering the M-$PR_3$ units for each group 1B metal in turn, for the Au clusters there is an average decrease in chemical shift of 4.7ppm on going from solution to the solid state. A similar trend is observed for a series of homonuclear gold phosphine clusters [42]. For the Ag clusters there is a greater scatter in the chemical shift data. For the Cu clusters the solid state chemical shifts were estimated from the asymmetric 'quartets' observed using the calculations of Menger and Veeman ([19]; section 6.6), and were found to agree closely with the shifts measured in solution.

The significance of the differences between the chemical shifts measured in the two states is related to the range of chemical shift values obtained for the nucleus under observation. For example, most of the $^{13}C$ shifts of saturated carbon atoms lie in the range $\sigma_{iso}$ = 0-100 [43].It has been shown that, where a common structure exists in both solution and solid state, the differences in chemical shifts between the two states are typically 3ppm or less [44]. This is in contrast to the results obtained for heavier metal nuclei such as Sn and Pb, which have a much greater chemical shift range. A 15ppm change in chemical shift upon change of state for Sn is considered 'modest' [45], and is believed to indicate a lack of structural change on solidification. The phosphorus chemical shift range falls between these extremes, and in comparison the small variations in $\sigma_{iso}$ upon change of state appear to be of small structural significance.

The solid state data was next examined for a relationship between the solid state chemical shift and the M-P bond length, based on the generally-accepted dominance of the paramagnetic contribution to the chemical shift [17,36]. There was not sufficient structural data available for the silver and copper clusters, but the structures of seven of the gold clusters studied by solid state nmr had been

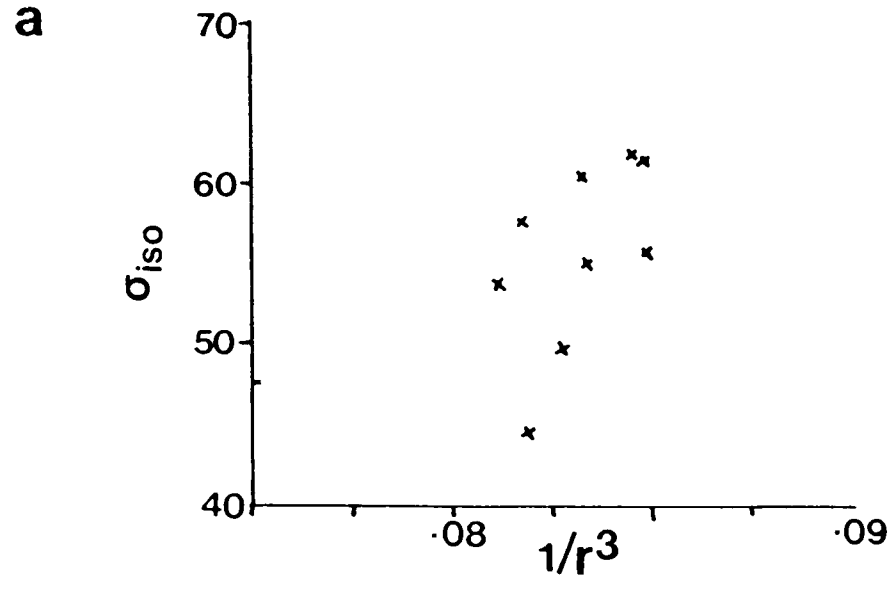


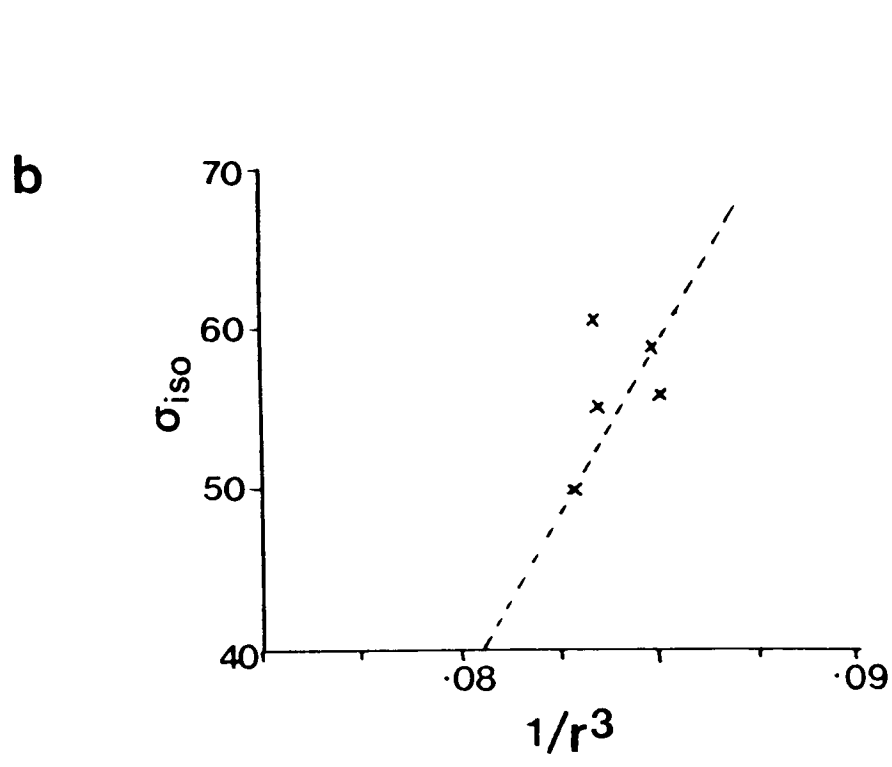


Figure 6.16

Plot of solid state $^{31}P$ chemical shift against $1/r^3$ for $AuPR_3$ units.

(a) All R groups.

(b) R=Ph.

determined. The correlation between $\sigma_{iso}$ and $1/r^3$ was not very good when considering all of the clusters; however when the data set was limited to clusters with Au-$PPh_3$ moieties an approximately linear relationship was observed (Figure 6.16).

## 6.9 Discussion.

The solid state nmr studies on heteronuclear metal cluster compounds discussed in this chapter have provided much information on the structures and dynamics of these clusters. A comparison of the solid state nmr spectra with those obtained in solution shows that two general classes of cluster may be distinguished. These are (i) clusters for which the room temperature solid state nmr spectrum corresponds to the low temperature solution nmr spectrum or the presumed low temperature solution nmr spectrum; and (ii) clusters for which there are marked differences between the results of solid state nmr and low temperature solution nmr. Examples of the two classes are illustrated below.

The results shown in Table 6.1 illustrate that for many of the heteronuclear metal clusters studied the structure of the solid cluster as revealed by solid state $^{31}P$ nmr is closely similar to that observed in solution at low temperature. In general terms, n resonances are observed from a cluster with n inequivalent phosphorus sites. For example, the cluster $[Cu_2Ru_4(\mu_3\text{-}H)_2(CO)_{12}(PPh_3)_2]$ (1) has been shown to undergo metal core rearrangement in solution at room temperature [12,26]; this proces is frozen out both in solution at -90°C and in the solid state at room temperature, so that in both spectra two phosphorus resonances are observed from the two inequivalent phosphine groups. Similar results are obtained for the isostructural cluster in which $(PPh_3)_2$ is replaced by ($\mu$-dppm) (4) and

for $[Au_3Ru_4(\mu_3\text{-}H)(CO)_{12}(PPh_3)_3]$. In some of the clusters, the dynamic processes occurring in solution cannot be frozen out at -90°C. However the solid state nmr spectra show that they are slow on the nmr timescale in the solid, and are consistent with the X-ray crystal structures of the clusters. This type of behaviour is exemplified by $[Au_2Ru_4(\mu_3\text{-}H)(\mu\text{-}H)(CO)_{12}(PPh_3)_2]$ (3), a cluster with two phosphorus environments, which gives rise to a single resonance in solution even at low temperature [12]; in the solid state two phosphorus resonances corresponding to the two phosphorus sites can be observed. The analogous silver cluster (2) also shows this behaviour, as do both of the clusters $[Au_2Ru_4(\mu_3\text{-}H)(\mu\text{-}H)(CO)_{12}\text{-}(\mu\text{-}Ph_2PCH_2PPh_2)$ and $[Au_2Ru_3(\mu_3\text{-}S)(CO)_9(\mu\text{-}Ph_2PCH_2PPh_2)$ containing bidentate phosphine ligands. The solid state stereochemical rigidity revealed by this class of clusters is analogous to that observed in the homonuclear gold phosphine clusters discussed in chapter 5, and indicates the effect of intermolecular interactions in the crystal on intramolecular processes.

However not all of the solid state spectra show the expected n resonances from clusters in which there are n phosphorus environments; many show less than n. For heteronuclear clusters such as $[Ag_2Ru_4(\mu_3\text{-}H)_2(CO)_{12}(\mu\text{-}Ph_2PCH_2PPh_2)]$ (5), the metal core rearrangement process occurring in solution at -90°C [9,14] also appears to be fast on the nmr timescale in the solid at room temperature, as a single resonance is observed in both solution and solid state spectra from a cluster known to contain two inequivalent phosphorus sites. Similarly in $[Au_2Ru_3(\mu_3\text{-}S)(CO)_9(PPh_3)_2]$ and in $[Au_3Ru_4(\mu_3\text{-}H)(CO)_{12}(\mu\text{-}Ph_2PCH_2PPh_2)$ the fluxional process present in solution at low temperature remains fast upon crystallisation. An example of metal core rearrangement in the solid state has been

discussed in the literature [50]. A more unusual case is that of the cluster $[Ag_2Ru_4(\mu_3\text{-}H)_2(CO)_{12}(PPh_2(CH_2)_2PPh_2)]$ (7), for which the metal core rearrangement process, although slow on the nmr timescale in solution at -90°C, is still fast in the solid state.

The solid state spectra of some of these metal clusters have also provided examples where the number of resonances is greater than the number of phosphorus sites. Recrystallisation has sometimes succeeded in removing these 'extra' peaks, for example with the clusters (2) and (8). For other samples, recrystallisation had little effect on the nmr spectra. The possibility remains that for these clusters, which include $[Ag_2Ru_4(\mu_3\text{-}H)_2(CO)_{12}(PPh_2(CH_2)_4PPh_2)]$, $[AuRu_4(\mu\text{-}H)_3(CO)_{12}PPh_3]$ and $[AuRu_3(CO)_9(C_2Bu^t)PPh_3]$, there is greater structural diversity in the solid state than in solution. For example, there may be more than one inequivalent molecule present in the unit cell; different conformations may exist in the solid which are averaged by molecular flexibility in solution; or the extra resonances may be due to polymorphism. It is important to consider such 'solid state effects' in the interpretation of solid state nmr data and in relating it to solution nmr studies (see section 2.6).

The results obtained for this series of clusters demonstrate that in many cases structural information may be obtained merely from the number of resonances in the nmr spectra. Further information is of course present in the measured values of the chemical shifts and coupling constants. For these clusters the similarity of the $\sigma_{iso}$ and J values obtained in the two states provides evidence for the similarity of solution and solid state structures, and the solid state spectra of the copper clusters give additional structural information. One particular aspect of this information is in determining for the clusters $[MM'Ru_4(\mu_3\text{-}H)_2(CO)_{12}(PPh_3)_2]$, when $M \neq M'$, which $M\text{-}PPh_3$ group

occupies which of the two distinct group 1B metal sites in the structure. Use of chemical shift, coupling constant and CSA data enables site assignment to be made in most cases.

A striking feature of the series of mixed-metal clusters $[M_2Ru_4H_2(CO)_{12}L_2]$ is the difference in dynamic behaviour between them. Solid state nmr spectroscopy provides further information on the mechanism of the dynamic process. The free energy of activation $\Delta G^{\neq}$ for the metal core rearrangement in solution has been calculated or estimated in each case [26,27], and the results are shown in Table 6.8.

TABLE 6.8

A comparison of the free energy of activation $\Delta G^{\neq}$ for metal core rearrangement in solution for the clusters $[MM'Ru_4H_2(CO)_{12}L_2]$

| | $\Delta G^{\neq}$ (kJ/mol) | |
|---|---|---|
| M | $L_2 = (PPh_3)_2$ | $L_2 = Ph_2PCH_2PPh_2$ |
| Cu | 40.9±0.3 | 40.8±0.2 |
| Ag | 40±1 | ca.33 |
| Au | 35 | (different structure) |

It can be seen that, whereas the change to a bidentate phosphine ligand barely alters the ease of rearrangement for Cu, in the case of Ag this process is facilitated. A mechanism has been postulated for the dynamic process based on a restricted Berry pseudo-rotation [14], in which the intermediate adopts the same geometry as (6). If this mechanism is correct, the results obtained may then be interpreted as follows. In the case of (6), the energy of the proposed intermediate has been lowered by the bidentate ligand to such an extent that the

thermodynamically preferred structure of the cluster has changed. The capped trigonal bipyramidal structure is destabilised sufficiently to make rearrangement slow or absent in the solid state. For silver, stereochemical demands do not change the relative energies of the two geometries enough to alter the ground state structure, but some stabilisation of the capped square-based pyramidal form occurs, decreasing $\Delta G^{\ddagger}$ for the rearrangement process. The small size of the copper atoms means that a change in phosphine ligand causes little steric strain, and therefore has little effect on the dynamic process.

The solid state nmr results reinforce this hypothesis. Fluxionality is 'frozen out' in both copper clusters in the solid state, as would be expected from their similar structures and similar solution free energies for the dynamic process. For silver, site exchange is aided by substitution of the bidentate ligand to such an extent that the process still occurs in the solid, whereas it is not observed for the monodentate cluster (2). With the gold clusters, in both cases the rearrangement appears to be frozen out in the solid state; the change in structure is suggested by the very small difference in isotropic shift of the two phosphine resonances observed for (6), showing the similarity of the two phosphorus environments to be greater for (6) than for the $(PPh_3)_2$ cluster with its capped trigonal bipyramidal geometry.

For the cluster (7), in which the number of methylene groups in the diphosphine backbone has increased to two, the free energy of the solution rearrangement process has been calculated at 36.0±0.2kJ/mol [27]. For this cluster, metal core rearrangement is slow on the nmr timescale in solution at -90°C but fast in the solid state. For $[Au_2Ru_4(\mu_3\text{-}H)(\mu\text{-}H)(CO)_{12}(PPh_3)_2]$ (3) $\Delta G^{\ddagger}$ for solution core rearrangement is lower: it has been estimated at ~35kJ/mol [26].

However the dynamic process in (3) is frozen out in the solid state, but not in solution at -90°C. This difference in behaviour upon a change of physical state highlights the effect of the nature of the phosphine ligands on the dynamic behaviour of the clusters. However it should be noted that both in solution and in the solid state an increase in the length of the diphosphine backbone causes an increase in the free energy of the rearrangement process.

The dynamic behaviour of the clusters $[M_2Ru_4H_2(CO)_{12}L_2]$ is in contrast to that of the clusters $[M_2Ru_3(\mu_3\text{-}S)(CO)_9L_2]$. For the latter compounds, the fluxional process which occurs in solution for all three of the clusters studied [15] only appears to be slow on the nmr timescale in the solid state for the two clusters containing a bidentate phosphine ligand; the two phosphorus sites cannot be distinguished for the $(PPh_3)_2$ cluster. The dynamic process is believed to occur via an intermediate with a square-based pyramidal structure. The cluster $[Au_2Ru_3(\mu_3\text{-}S)(CO)_9(\mu\text{-}Ph_2PCH_2PPh_2]$ has a structure intermediate between a trigonal bipyramid and a square-based pyramid, whereas the other two clusters studied have a trigonal bipyramidal geometry, and it would therefore be expected that, if this cluster is no longer fluxional in the solid state, that the core rearrangement in the others would also be frozen out. One possible explanation is that two phosphorus resonances are present in the solid state spectrum of the $(PPh_3)_2$ cluster, but they cannot be distinguished because of some other factor which has broadened the resonances (see section 2.5). No conclusions may be drawn until variable temperature solid state studies have been carried out.

There is not necessarily a simple correlation between solution and solid state chemical exchange processes, as different factors may control the exchange in the two states. Not all exchange

processes which occur in solution will occur in the solid state: reasons include the presence of bulky substituents which prevent the occurrence of motions necessary for exchange, and a modification of the structure of the molecule in the crystalline state. This behaviour has been observed for many of the heteronuclear metal clusters. When extrapolating from solution results to the solid state, the effects of the lattice must be taken into consideration, which frequently increase the free energy of fluxional processes in the solid state. In principle, lattice forces could also lower the energy barriers to dynamic processes, but no examples of this appear to have been presented in the literature. The silver cluster (7) seems however to show this behaviour. Considering the postulated mechanism for the core rearrangement, the nmr results suggest that in the solid the free energy of the intermediate is closer to that of the ground state than it is in solution, facilitating rearrangement in the solid cluster.This raises questions as to how intermolecular interactions in the solid state may in general alter dynamic processes from those in solution. The implication is that no general conclusion may be drawn as to solid state dynamic behaviour based on the free energy of such a process in solution. Thus it remains uncertain as to what degree it is possible to extrapolate from solution to solid state dynamic behaviour.

6.10 References.

[1] D.M.P. Mingos, Phil. Trans. R. Soc. A308 (1982) 75.

[2] P. Braunstein and J. Rose, Gold. Bull. 18 (1985) 17.

[3] K.P. Hall and D.M.P. Mingos, Prog. Inorg. Chem. 32 (1984) 237.

[4] D.G. Evans and D.M.P. Mingos, J. Organomet. Chem. 232 (1982) 171.

[5] For example L.W. Bateman, M. Green, K.A. Mead, R.M. Mills, I.D. Salter, F.G.A. Stone and P. Woodward, J. Chem. Soc., Dalton Trans. (1983) 2599.

[6] For example I.D. Salter and F.G.A. Stone, J. Organomet. Chem. 260 (1984) C71.

[7] D.M.P. Mingos, Polyhedron 3 (1984) 1289.

[8] P. Braunstein, J. Rose, A Dedieu, Y. Dusausoy, J.-P. Mangeot, A. Tiripicchio and M. T.-Camellini, J.Chem. Soc., Dalton Trans. (1986) 225.

[9] S.S.D. Brown, I.J. Colquhoun, W. McFarlane, M. Murray, I.D. Salter and V. Šik, J.Chem. Soc., Chem. Commun. (1986) 53.

[10] B.A. Brice, S.C. Pearse, I.D. Salter and K. Henrick, J.Chem. Soc., Dalton Trans. (in press).

[11] S.S.D. Brown, I.D. Salter and B.M. Smith, J.Chem. Soc., Chem. Commun. (1985) 1429.

[12] M.J. Freeman, A.G. Orpen and I.D. Salter, J.Chem. Soc., Dalton Trans. (in press).

[13] M.J. Freeman, A.G. Orpen and I.D. Salter, J.Chem. Soc., Dalton Trans. (in press).

[14] P.A. Bates, S.S.D. Brown, A.J. Dent, M.B. Hursthouse, E.F.M. Kitchen, A.G. Orpen, I.D. Salter and V. Šik, J.Chem. Soc., Chem. Commun. (1986) 600.

[15] S.S.D. Brown, S. Hudson, I.D. Salter and M. McPartlin, J.Chem. Soc., Dalton Trans. (submitted).

[16] S.S.D. Brown, P.J. McCarthy and I.D. Salter, J. Organomet. Chem. 306 (1986) C27.

[17] R.M. Lynden-Bell and R.K. Harris, 'Nuclear magnetic resonance spectroscopy', Nelson, London (1971).

[18] J.W. Diesveld, E.M. Menger, H.T. Edzes and W.S. Veeman, J. Amer. Chem. Soc. 102 (1980) 7935.

[19] E.M. Menger and W.S. Veeman, J. Magn. Res. 46 (1982) 257.

[20] J.G. Hexem, M.H. Frey and S.J. Opella, J. Amer. Chem. Soc. 103 (1981) 224.

[21] B.F.G. Johnson, D.A. Kaner, J. Lewis, P.R. Raithby and M.J. Taylor, J.Chem. Soc., Chem. Commun. (1982) 314.

[22] S.S.D. Brown, L.S. Moore, R.V. Parish and I.D. Salter, J.Chem. Soc., Chem. Commun. (in press).

[23] M.M. Maricq and J.S. Waugh, J. Chem. Phys. 70 (1979) 3300.

[24] J. Herzfeld and A.E. Berger, J. Chem. Phys. 73 (1980) 6021.

[25] P. Braunstein, G. Predieri, A. Tiripicchio and E. Sappa, Inorg. Chim. Acta 63 (1982) 113.

[26] M.J. Freeman, M. Green, A.G. Orpen, I.D. Salter and F.G.A. Stone, J.Chem. Soc., Chem. Commun. (1983) 1332.

[27] S.S.D. Brown, J.C. Frankland, I.D. Salter and V. Šik, unpublished results.

[28] W.T. Dixon, J. Chem. Phys. 77 (1982) 1800.

[29] J.A.K. Howard, I.D. Salter and F.G.A. Stone, Polyhedron 3 (1984) 567.

[30] M.I. Brice, D.B. Shawkataly and B.K. Nicholson, J. Organomet. Chem. 286 (1985) 427.

[31] P.S. Pregosin and R.W. Kunz, NMR: Basic Princ. Prog. 16 (1979) 1.

[32] G.E. Maciel, D.J. O'Donnell and R. Greaves, Adv. Chem. Ser. 196 (1982) 389.

[33] L. Bemi, H.C. Clark, J.A. Davies, C.A. Fyfe and R.E. Wasylishen, J. Amer. Chem. Soc. 104 (1982) 438.

[34] R.K. Harris, P.J. Reams and K.J. Packer, J. Chem. Soc., Dalton Trans. (1986) 1015.

[35] G.G. Mather, A. Pidcock and G.J.N. Rapsey, J. Chem. Soc., Dalton Trans. (1973) 2095.

[36] C.A. Tolman, L.W. Yarbrough and J.G. Verkade, Inorg. Chem. 16 (1977) 479.

[37] 'High resolution NMR spectroscopy' eds. J.W. Emsley, J. Feeney and L.H. Sutcliffe, Pergamon Press, N.Y. (1966) vol.2 881.

[38] J.H. Letcher and J.R. van Wazer, J. Chem. Phys. 44 (1966) 815.

[39] E.T. Lippmaa, M.A. Alla, T.J. Pehk and G. Engelhardt, J. Amer. Chem. Soc. 100 (1978) 1929.

[40] For example C.A. Fyfe, J.M. Thomas, J. Klinowski and G.C. Gobbi, Angew. Chem. Int. Ed. Engl. 22 (1983) 259 and references therein.

[41] R.J.B. Jakeman, A.K. Cheetham, N.J. Clayden and C.M. Dobson, J. Amer. Chem. Soc. 107 (1985) 6249.

[42] N.J. Clayden, C.M. Dobson, K.P. Hall, D.M.P. Mingos and D.J. Smith, J. Chem. Soc., Dalton Trans. (1985) 1811.

[43] 'NMR and the periodic table', eds. R.K. Harris and B.E. Mann, Academic Press, London (1978).

[44] M.H. Frey and S.J. Opella, J. Chem. Soc., Chem. Commun. (1980) 474.

[45] R.K. Harris, P. Reams and K.J. Packer, J. Mol. Struct. 141 (1986) 13.

# CHAPTER 7

## Studies of surface-attached transition metal clusters.

### 7.1 Introduction.

One important application of solid state nmr spectroscopy is the characterisation of the species formed when metal clusters are anchored to solid supports. As discussed in chapter 1, information on the nature and reactions of such species may be of considerable value in understanding a wide variety of catalytic processes [1]. Other techniques used in studies of supported metal clusters provide limited information. The usual method of characterising the chemical species present is infra-red spectroscopy, but interpretation of the spectra is frequently difficult [2,3]. Attempts have been made to use transmission electron microscopy for the identification of these species [4,5], but the clusters studied are at the limits of resolution. Solid state nmr studies of these systems may enable a more definite identification of the surface species to be made, and thus provide a more complete picture of what actually occurs when a metal cluster is anchored to a solid support.

Previous solid state nmr work in this area has centred on polymer-anchored phosphines and their metal complexes [6,7], with some studies extended to complexes on inorganic supports [8]. There have, with one or two notable exceptions, been few applications to oxide-supported clusters [8,9]. These are discussed in chapter 1. In this chapter solid state $^{31}P$ and $^{13}C$ nmr spectroscopy is used to study the species formed when transition metal carbonyl clusters are anchored via a pendant phosphine ligand to an oxide support. The ruthenium, rhodium and osmium clusters chosen were studied by solid state nmr prior to the studies on the species they form upon anchoring to

surfaces; the results are presented in chapter 4. Interestingly, some of the results obtained are not consistent with the simple attachment of the metal cluster to the surface.

## 7.2 Materials and methods.

All of the work described in this chapter was carried out in collaboration with Dr. J. Evans and his research group at Southampton University. Ruthenium, rhodium and osmium cluster compounds were prepared by Dr. S.L. Cook, Dr. R.J. Crowte and V.D. Alexiev by methods similar to those described previously [10-15]. $^{13}C$-enriched carbonyls were prepared by V.D. Alexiev ([16]; see section 4.8). Anchoring was achieved by stirring the silylated cluster with the inorganic support in dry $CH_2Cl_2$ under $N_2$ or CO (Figure 7.1). An alternative method of anchoring the osmium clusters, in which the surface of the support was phosphinated and then reacted with the cluster, was also utilized. Loadings were of the order of 5% wt/wt metal on $SiO_2$.

All spectra were accumulated using CP and HPPD. In addition to MAS spectra, static spectra were also recorded with the aim of obtaining further information about the surface species from its chemical shift anisotropy. Typically several thousand transients were accumulated for each spectrum using a full rotor (~400mg) of sample.

## 7.3 General features of the spectra.

One of the important features of the solid state $^{31}P$ nmr studies presented here is that phosphorus spectra were observed for all of the surface-attached samples. In contrast, in solution $^{31}P$ nmr studies on a series of solvent-swollen polymers, Grubbs et al [17] observed that the signal of an anchored phosphine group disappeared on coordination to rhodium, with no new peaks appearing. Similar results

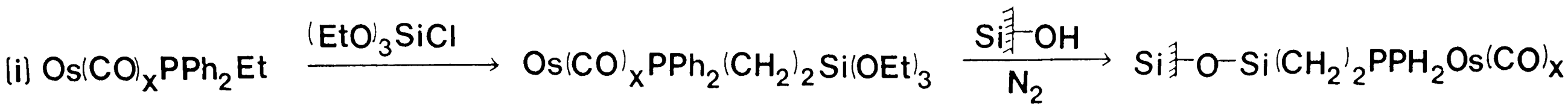


Figure 7.1

Reaction scheme showing the method used to anchor clusters to a surface, using an osmium cluster as an example. Method (ii) was found to lead to the formation of a significant amount of a phosphorus (V) species, and was therefore abandoned in favour of method (i).

were reported by Naaktgeboren et al [18]. This may be caused by an increase in phosphorus relaxation time on complexation to the metal centre, or may result from a severe restriction of motion of the phosphorus with coordination such that linebroadening prevents the detection of an nmr signal. In further solution studies by the Dutch group on linear phosphinated polymers to which rhodium complexes were coordinated, $^{31}P$ spectra were obtained on reaching high Rh:P ratios, but calibration revealed that only 5% of the phosphorus present was visible by nmr [18].

For the systems studied here, resolved $^{31}P$ spectra were obtained with an acceptable signal-to-noise ratio after a period of several hours. All of the spectra showed much broader lines than those observed for the precursor metal clusters. Broad resonances have been reported previously in other surface studies [8], and probably reflect some heterogeneity of environments on the surface. A comparison of the chemical shifts and CSA's measured for the anchored species with those of the corresponding unattached clusters was used in the interpretation of the spectra.

## 7.4 A ruthenium cluster anchored to alumina.

The solid state $^{31}P$ nmr spectrum of the species formed when $(\mu\text{-}H)_2Ru_3(CO)_9(\mu_3\text{-}P(CH_2)_2Si(OEt)_3)$ was anchored to alumina is shown in Figure 7.2. A single broad resonance ($\Delta\nu_{1/2}\sim$700ppm) is observed at a chemical shift similar to that of the precursor cluster. The resonance of the anchored species, whilst broader than that of the simple crystalline cluster (section 4.6), is not so broad that it would obscure three resonances similar to those observed in the solid state spectrum of the simple cluster if they were present.

The CSA revealed in the non-spinning spectrum is close to

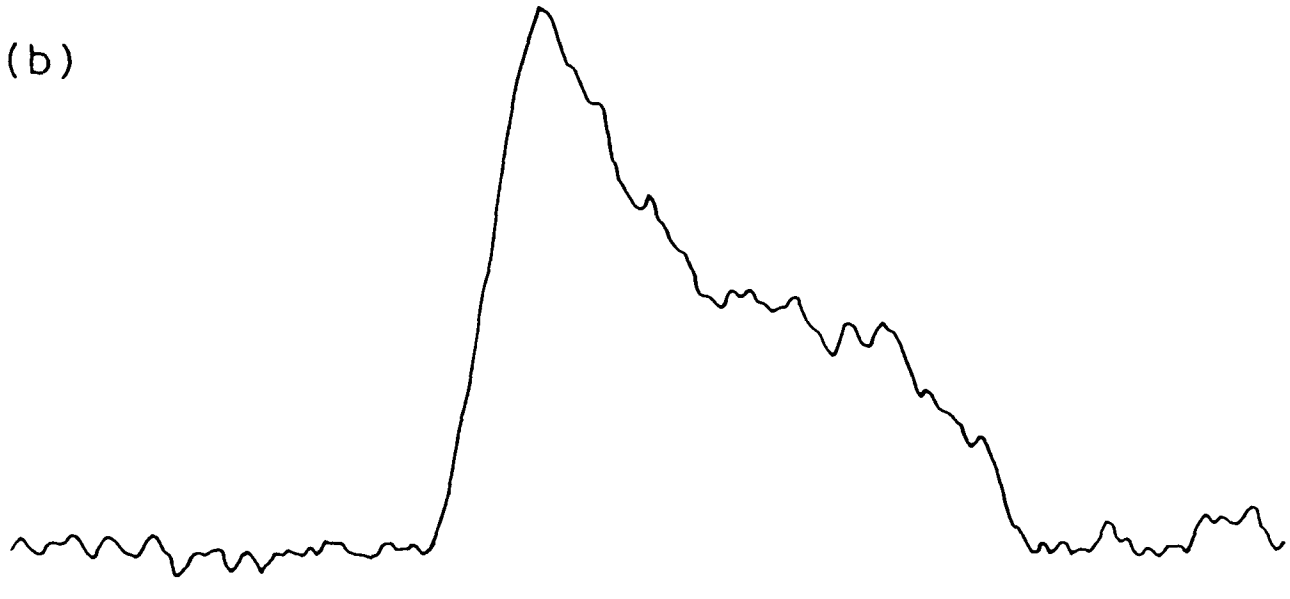


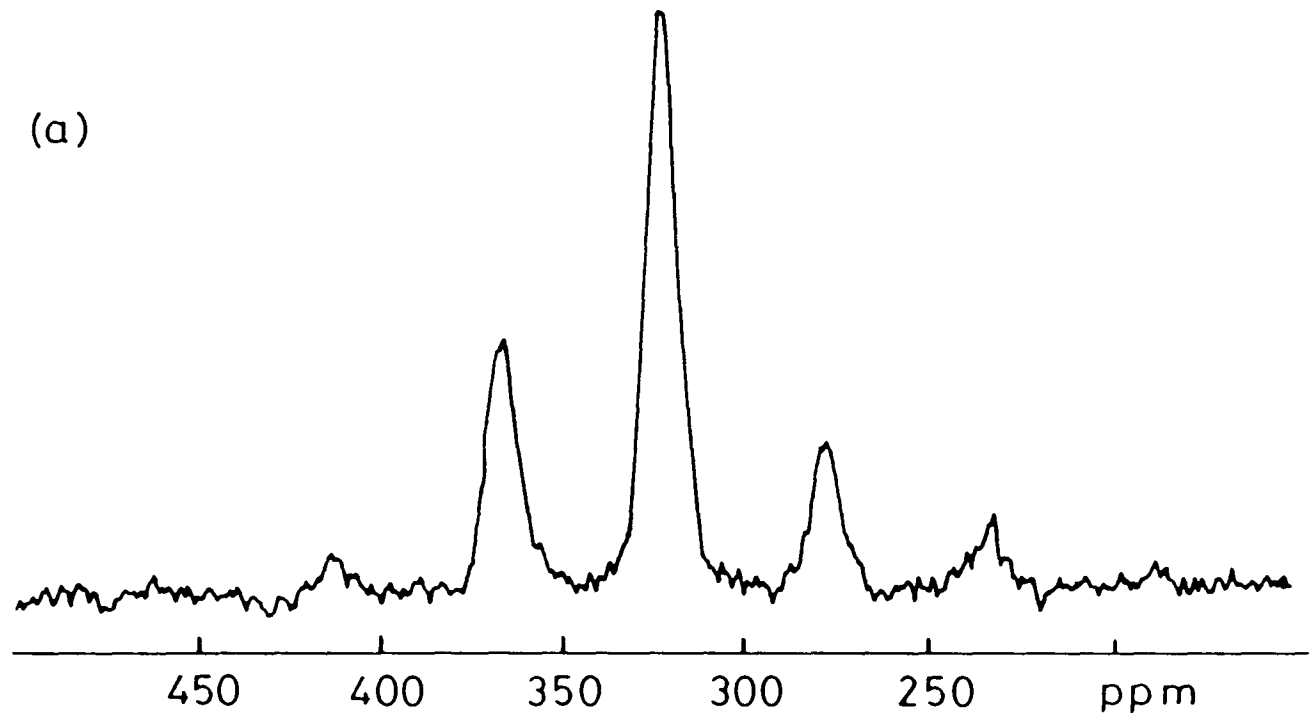


Figure 7.2

Solid state $^{31}P$ nmr spectra of the species formed on anchoring $(\mu\text{-}H)_2Ru_3(CO)_9(\mu\text{-}P(CH_2)_2Si(OEt)_3)$ to alumina. (a) Magic angle spinning and (b) static spectra.

axial, as is that of the crystalline cluster. The two CSA's differ however both in magnitude (that of the unattached cluster is larger by a factor of 2) and in direction. Using the convention that $\sigma_{11}$ is the most shielded element gives for the anchored species $\sigma_{11} = \sigma_{22}$ and for the unattached cluster $\sigma_{22} = \sigma_{33}$. The decrease in anisotropy on anchoring suggests the possibility of some averaging of the shielding tensor caused by motion, probably around the -P-$(CH_2)_2$-OAl bond, which would reduce the CSA whilst retaining its axial character. A study of the variation of the CSA with temperature will be necessary in order to test this hypothesis.

## 7.5 Supported rhodium clusters.

The rhodium carbonyl clusters $[Rh_4(CO)_{11}L']$ and $[Rh_6(CO)_{15}L']$, where L' = $Ph_2P(CH_2)_2Si(OEt)_3$, were anchored to silica and titania as described previously. The initial $^{31}P$ spectra obtained from the anchored clusters are shown in Figure 7.3. All show one resonance at ~41ppm, with spinning sidebands apparent even using fast MAS, and all except that of the sample of $[Rh_4(CO)_{11}L']$ anchored to titania show a second peak at ~26ppm with no spinning sidebands. The chemical shift data are shown in Table 7.1. The relative intensities of the two peaks are different for each sample. Infra-red spectra recorded immediately after the anchoring reaction are consistent with the presence of intact rhodium cluster species. The samples were kept at -14°C and the nmr experiments repeated several days later. The appearance of the spectrum of $[Rh_4(CO)_{11}L']$ anchored to titania, which previously showed a single resonance, was unchanged. For the sample of $[Rh_4(CO)_{11}L']$ on silica, a decrease in the intensity of the peak at 26ppm was observed with a concommitant increase in the intensity of the 41ppm resonance. This process of change continued over a period of

TABLE 7.1

$^{31}P$ chemical shifts of the rhodium carbonyl clusters.

| | chemical shift (ppm) | |
|---|---|---|
| cluster | solution | solid |
| L = $PPh_2Et$ | | |
| $Rh_4(CO)_{11}L$ | 24.7 | 16.1 |
| $Rh_6(CO)_{15}L$ | 23.3 | 23.3 |
| | | |
| L' = $Ph_2P(CH_2)_2Si(OEt)_3$ | | |
| $Rh_4(CO)_{11}L'$ on silica | | 40.7, 25.5 |
| $Rh_4(CO)_{11}L'$ on titania | | 41.2 |
| $Rh_6(CO)_{15}L'$ on silica | 27.3 | 41.9, 25.7 |
| $Rh_6(CO)_{15}L'$ on titania | 27.3 | 42.0, 28.5 |

All chemical shifts are referenced to 85% $H_3PO_4$.

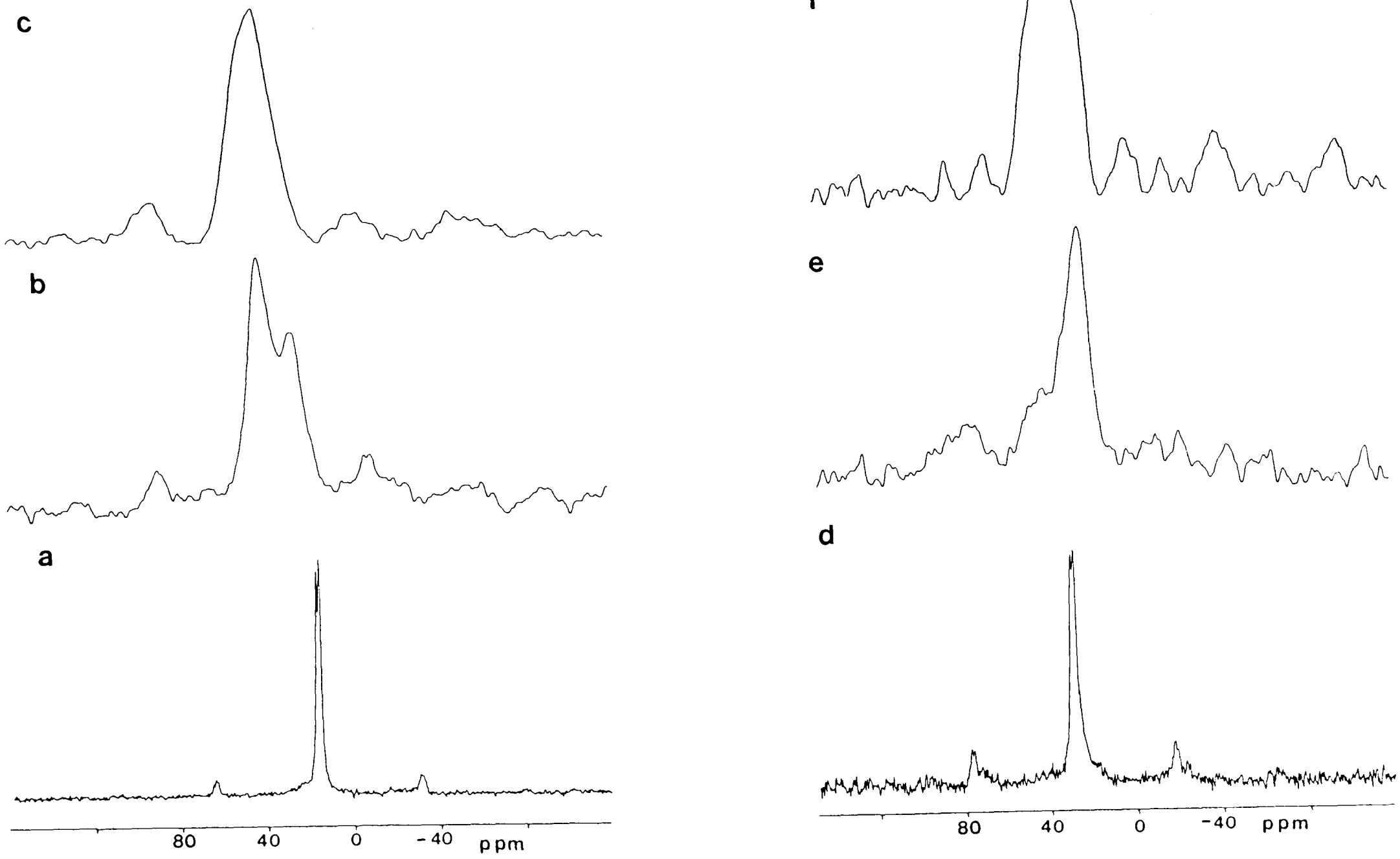


Figure 7.3 Solid state $^{31}P$ nmr spectra of (a) $Rh_4(CO)_{11}L$; (b)-(c) $Rh_4(CO)_{11}L'$ on silica and titania respectively; (d) $Rh_6(CO)_{15}L$; (e)-(f) $Rh_6(CO)_{15}L'$ on silica and titania respectively (L = $PPh_2Et$, L' = $Ph_2P(CH_2)_2Si(OEt)_3$).

two weeks until only the 41ppm resonance remained in the nmr spectrum. Similarly in the spectra of the anchored $[Rh_6(CO)_{15}L']$ species, the 26ppm peak disappeared as the resonance at 41ppm decreased in intensity until only the 41ppm peak remained. Changes in the nature of the surface species with time are also apparent from the i.r. spectra. A further change was then recorded for both of the titania samples: a new sharp line apppeared at high field in addition to the 41ppm resonance. However this peak was not observed in subsequent spectra.

To assist in the interpretation of these spectra, samples of phosphinated silica and phosphinated titania were prepared and studied by solid state nmr spectroscopy. Two species are observed in the $^{31}P$ spectra of phosphinated silica (Figure 7.4). One may be identified as anchored $Ph_2P(CH_2)_2Si(OEt)_3$ from the similarity of the chemical shift (-9ppm) to that of $Ph_2P(CH_2)_2Si(OEt)_3$ in solution (-10.3ppm). The other, on the basis of its low field chemical shift and its CSA, corresponds to a phosphorus (V) species formed by air oxidation of the initial phosphine. The sample of phosphinated titania shows two resonances corresponding to the same two species. In studies of phosphinated silica and glass beads carried out by two groups [8,19], the formation of closely similar species has been observed.

The spectra of the anchored rhodium clusters may be understood in the light of the results for the phosphinated surfaces. The species observed for three of the samples, with a chemical shift (~26ppm) closely similar to that of the silylated rhodium clusters, would appear to correspond to an intact rhodium cluster anchored via the phosphine ligand. The second resonance has a similar chemical shift to the phosphorus (V) species formed upon phosphination of both silica and titania; however its CSA, whilst large, does not appear to resemble that of the P(V) species very closely. The other possibility

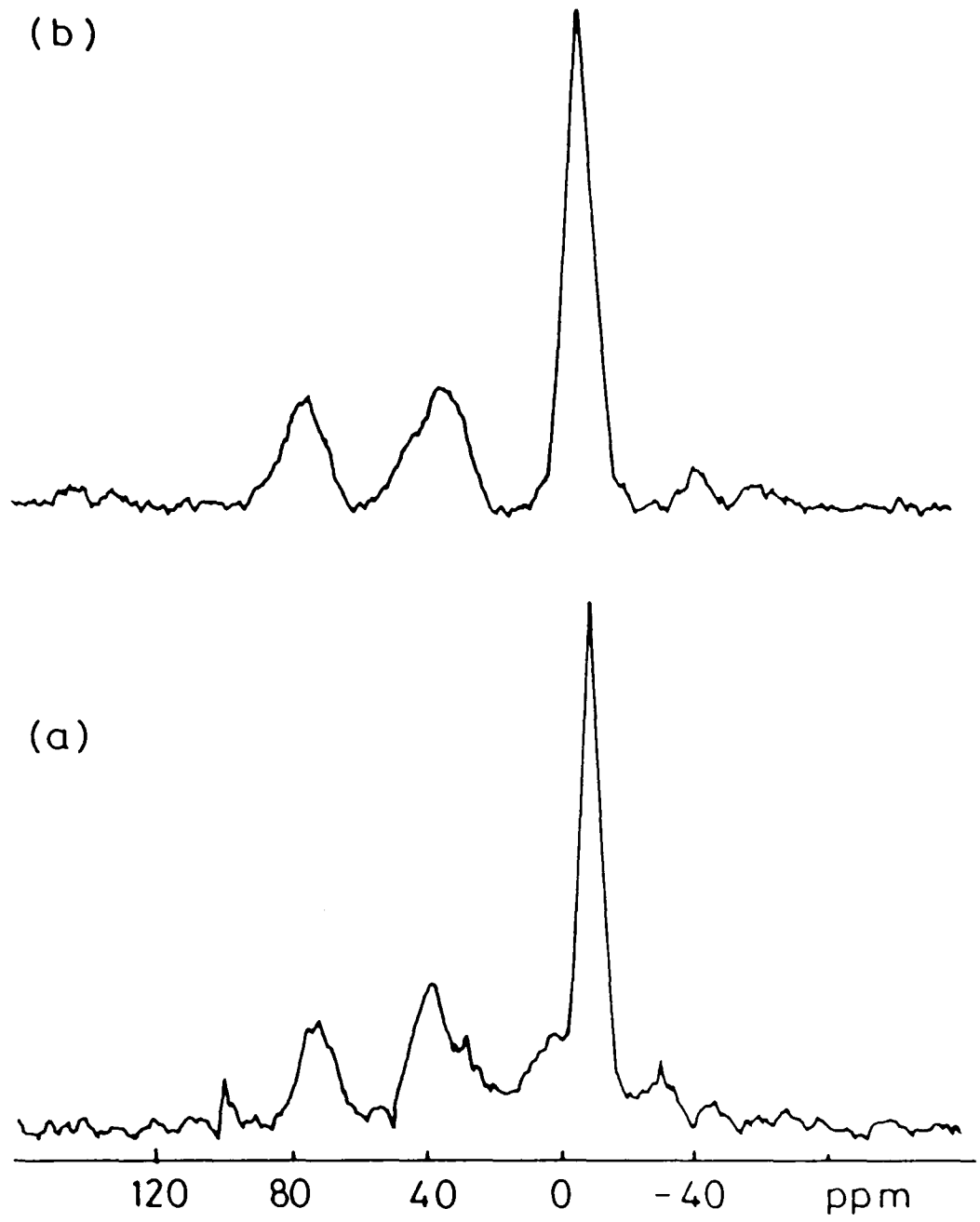


Figure 7.4

Solid state $^{31}P$ nmr spectra of (a) phosphinated silica and (b) phosphinated titania.

is that a rhodium (I) species is formed on the surface. A large phosphorus CSA was observed for the square planar rhodium (I) complexes discussed in chapter 2. However in a solution $^{31}P$ nmr study in which a rhodium (I) complex was reacted with a phosphinated silica surface [20], a supported rhodium (I) phosphine species was observed with a resonance at 30ppm : the shift of the surface species is more similar to that of the phosphorus (V) species observed on phosphinated silica and titania. This suggests that in the anchoring reaction an intact cluster species is attached to the surface via the pendant phosphine ligand; this is subsequently oxidised to form a second species whose identity cannot definitely be established, but which is postulated to be a phosphorus (V) species. The rate of the oxidation reaction on the surface depends upon the identity of both cluster and support, with the $[Rh_6(CO)_{15}L']$ species being more stable when anchored than the $[Rh_4(CO)_{11}L']$ clusters, and decomposition occurring more readily on titania than on silica. Previous studies of adsorbed rhodium carbonyl clusters, principally $Rh_4(CO)_{12}$ and $Rh_6(CO)_{16}$, on oxide supports have used mainly infra-red spectroscopy: these have shown the clusters to undergo air oxidation and to fragment to form a species believed to be $Rh(CO)_2$ [21-23]. This is entirely consistent with the solid state nmr results. Furthermore, sensitivity of the adsorption reactions of rhodium carbonyl clusters to the nature of the surface has previously been observed by Smith et al [24].

In order to test the reproducibility of these results, a second series of samples was prepared. Other questions which it was hoped would be answered by these experiments were whether or not the formation of the oxidised species accompanied the anchoring of the cluster in each case, and if an anchored $[Rh_4(CO)_{11}L']$ species could be observed on titania. The silylated clusters were reacted with the

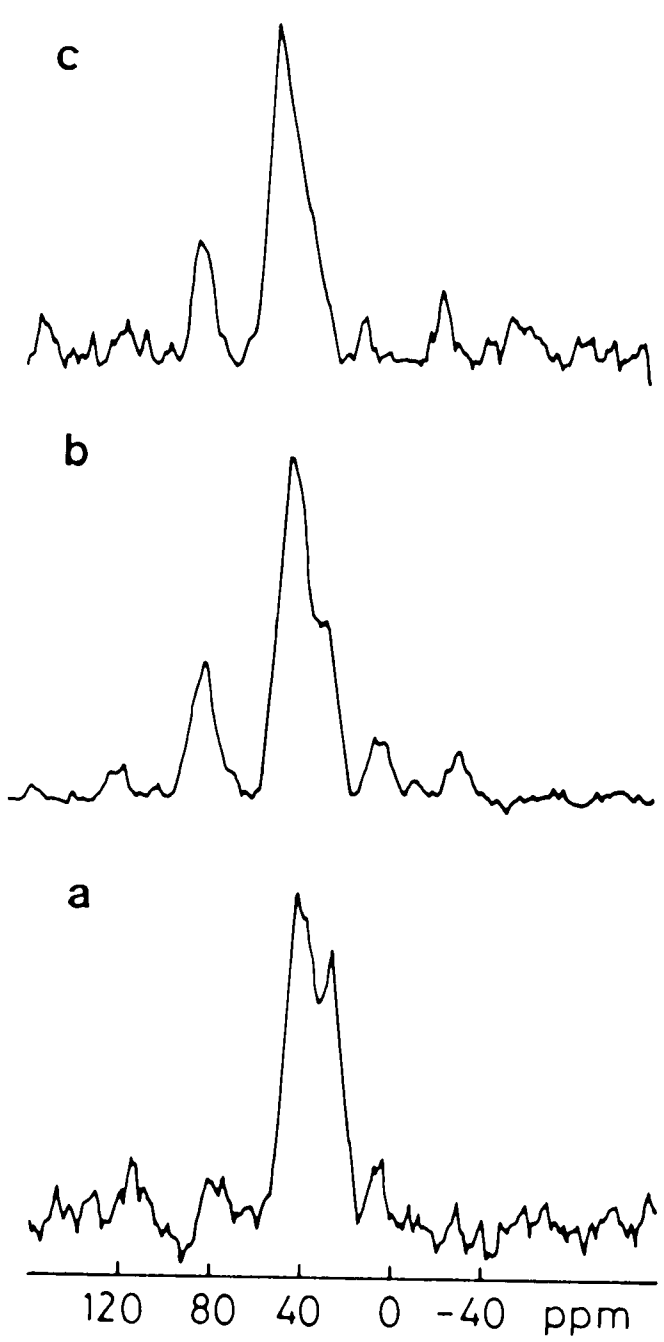


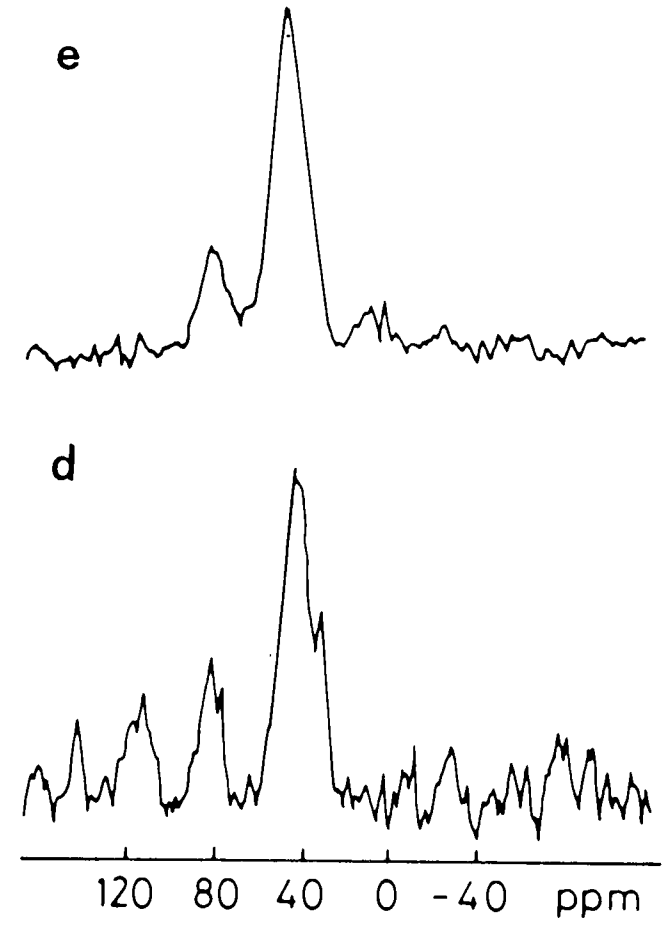


Figure 7.5

Solid state $^{31}P$ nmr spectra of the species formed from $Rh_4(CO)_{11}L'$ on (a)-(c) silica and (d)-(e) titania, showing the changes with time.

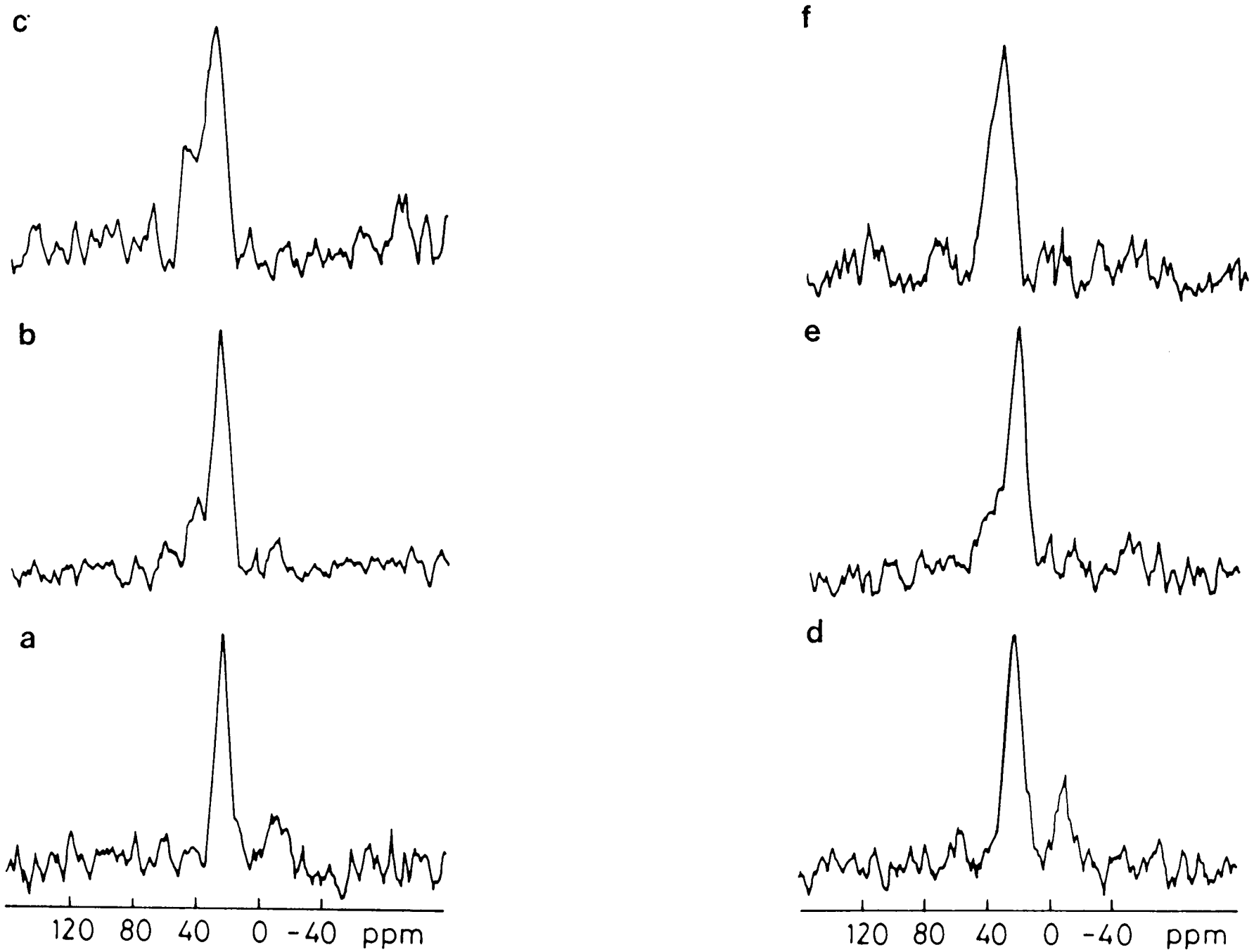


Figure 7.6

Solid state $^{31}P$ nmr spectra of the species formed from $Rh_6(CO)_{15}L'$ on (a)-(c) silica and (d)-(f) titania, showing the changes with time.

support immediately prior to the nmr studies: the resulting spectra are shown in Figures 7.5 and 7.6.

For both of the samples of anchored $[Rh_4(CO)_{11}L']$ two peaks, at 42 and 28ppm, were observed in the spectra (Figure 7.5), showing the presence of an anchored cluster species on both titania and silica. The most intense resonance was that at 41ppm. This peak was considerably broader than the resonance at 26ppm, and was the only peak to possess spinning sidebands. Over a period of two weeks, during which time the samples were stored at -14°C, further spectra showed the gradual disappearance of the 26ppm resonance.

The spectra of the species formed when $[Rh_6(CO)_{15}L']$ was anchored show in both cases a single resonance with no spinning sidebands at 24ppm (Figure 7.6). They show that $[Rh_6(CO)_{15}L']$ can be anchored to both surfaces without any observeable oxidation. Over 2-3 weeks, during which period the samples were stored at -14°C, a second peak appeared at 42ppm with a considerable CSA, with synchronous decrease in the intensity of the original resonance, until only a single phosphorus-containing species could be observed on the surface.

For neither of the titania samples was the very high field resonance observed in the second series of nmr experiments, suggesting that if it does result from a species formed on the surface it is one with a very transient existence.

In another series of experiments, $^{13}CO$-enriched rhodium clusters were anchored to the surface with the aim of determining whether CO groups were present in the surface species. Cross polarisation from protons was used in an attempt to improve the sensitivity. However the results obtained were inconclusive, with the only clear $^{13}C$ resonances in the spectra those of the $-CH_2-$ units in the anchoring ligand. This may be due to the low surface loading, and

hence the small quantity of enriched cluster present on the surface.

## 7.6 Triosmium clusters anchored to silica.

The three clusters $[Os_3(CO)_{11}L']$, $[H_2Os_3(CO)_{10}L']$ and $[H_2Os_3(CO)_9L']$, where L' = $PPh_2(CH_2)_2Si(OEt)_3$, were anchored to silica as described previously. Figure 7.7 shows the nmr spectra obtained for the anchored clusters; the chemical shift values are presented in Table 7.2. The species formed on anchoring $[Os_3(CO)_{11}L']$ and $[H_2Os_3(CO)_{10}L']$ have similar chemical shifts to those of their precursors. The same result was obtained for the decacarbonyl whether anchored under CO or under $N_2$. Infra-red spectra of the anchored species are consistent with the maintenance of the cluster structure on the surface. EXAFS studies on the species formed on silica from $[H_2Os_3(CO)_{10}L']$ suggest that all three Os-Os bonds are retained [10]. The new spectra show broader lines (of the order of 1000Hz) for the anchored clusters than for their crystalline precursors, a broadening observed in the nmr spectra of all the surface species studied. Interestingly, the overall chemical shift anisotropies revealed in the non-spinning spectra are little changed from those of the crystalline osmium clusters. As molecular motion causes averaging of the shift tensor, it follows that the attached species are rather firmly immobilised on the surface of the silica.

Reaction of $[H_2Os_3(CO)_9L']$ with silica under CO resulted in a peak in the $^{31}P$ nmr spectrum at -1.0ppm. This chemical shift is markedly different from that of the precursor (23ppm), and from that of another nonacarbonyl cluster, $[HOs_3(CO)_9PPh_3(O_2CMe)]$, which has a chemical shift of 15.1ppm. The static $^{31}P$ spectrum of the supported species is also quite different from the characteristic powder pattern observed for the crystalline nonacarbonyl cluster (Figure 4.2). When

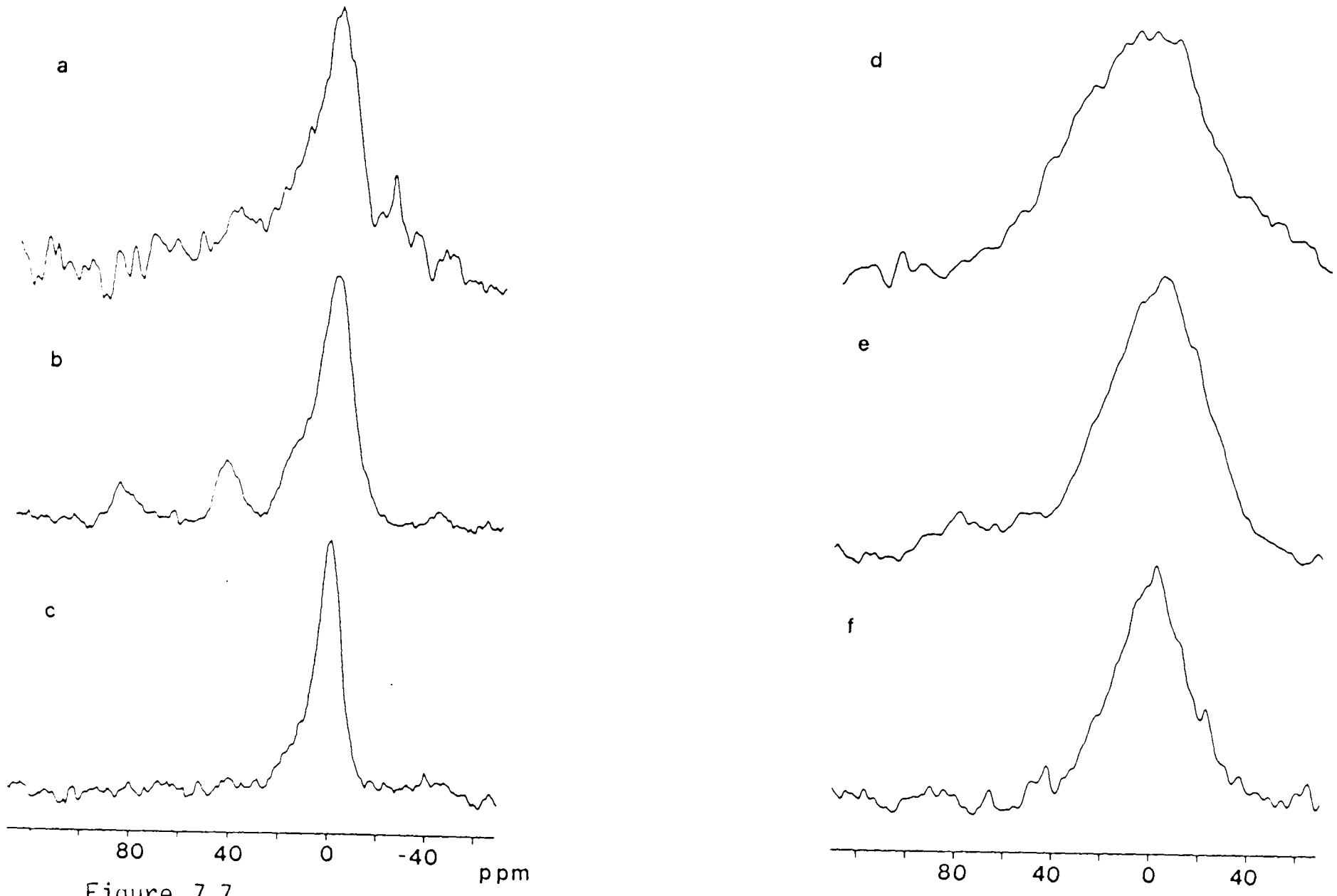


Figure 7.7

Solid state $^{31}P$ spectra of the anchored species. MAS spectra (a)-(c) show the species formed from $Os_3(CO)_{11}L'$, $H_2Os_3(CO)_{10}L'$ and $H_2Os_3(CO)_9L'$ respectively ($L' = Ph_2P(CH_2)_2Si(OEt)_3$); (d)-(f) are the corresponding static spectra.

TABLE 7.2

$^{31}P$ chemical shifts of the triosmium clusters.

| | chemical shift (ppm) | |
|---|---|---|
| L = $PPh_3$ | solution | solid |
| $Os_3(CO)_{11}L$ | 2.1 | 2.5 |
| $H_2Os_3(CO)_{10}L$ | -2.7 | -1.5 |
| $H_2Os_3(CO)_9L$ | 27.2 | 22.9 |
| $H(OH)Os_3(CO)_9L$ | 20.2 | 24.0 |
| $[HOs_3(CO)_9PPh_3(O_2CMe)]$ | 17.6 | 15.1 |
| L' = $Ph_2P(CH_2)_2Si(OEt)_3$ | solution | anchored to silica |
| $Os_3(CO)_{11}L'$ | -2.1 | -0.1 |
| $H_2Os_3(CO)_{10}L'$ | -1.5 | -1.0 |
| $H_2Os_3(CO)_9L'$ | 22.9 | -1.0 |

All chemical shifts are referenced to 85% $H_3PO_4$.

the anchoring reaction was carried out under nitrogen, in order to reduce the possibility that addition of CO to form a decacarbonyl species had occurred, a similar result was obtained. In addition, infra-red spectra recorded immediately after the anchoring reaction (under CO and under $N_2$) were similar to that of their precursor, and quite different from the spectra of the decacarbonyl species. No significant changes in the i.r. spectra took place over the period of time (ca. 45 min) needed to record the nmr spectra. Thermal decarbonylation of anchored $[H_2Os_3(CO)_{10}L']$, reported as an alternative route to anchored $[H_2Os_3(CO)_9L']$, again produced a species whose nmr spectrum showed the major resonance to be close to 0ppm.

The solid state nmr data, in contrast to the i.r. data, show clearly that the species present on the surface under these conditions is not that which would be formed by simple reaction of coordinated $PPh_2(CH_2)_2Si(OEt)_3$ with the silica. One species that might be formed by reaction of the nonacarbonyl cluster with the silica surface is $[(\mu\text{-H})(\mu\text{-OSIL})Os_3(CO)_9(PPh_2(CH_2)_2SIL)]$. The model cluster $[H(OH)Os_3(CO)_9PPh_3]$ was therefore prepared by a method derived from that of Deeming et al [25]. However this was also found to have a relatively lowfield $^{31}P$ chemical shift (24ppm), and so the presence of a species such as this does not adequately account for the nmr spectra of the surface-attached species reported here. There is evidence, however, that reactions with surface -OH groups or water molecules do take place. EXAFS data on attached clusters prepared by previously-reported means [26-28], which exhibit an i.r. spectrum similar to that of $[H_2Os_3(CO)_9L']$, indicates the formation of Os-O bonds as well as the maintenance of Os-Os and Os-P bonds [10]. This suggests that the coordinative unsaturation in $[H_2Os_3(CO)_9L']$ is alleviated by an oxygen donor on the oxide surface. The similarity of the nmr spectra of the

three surface species, however, raises the question as to whether similar reactions between surface groups and the metal centres have taken place for $[H_2Os_3(CO)_{10}L']$ and $[Os_3(CO)_{11}L']$. In these latter two samples all the evidence is consistent with a simple attachment at the ligand silyl group (colour, nmr and i.r. data). The i.r. evidence in the carbonyl region is much stronger for these two samples, with the spectra having better resolution and matching the frequencies and relative intensities of the precursor compounds much more closely [26].

Further evidence for the simple attachment of these two clusters comes from $^{13}C$ nmr. A sample of $^{13}CO$-enriched $[H_2Os_3(CO)_{10}L']$ was anchored to silica, and the resulting $^{13}C$ spectrum shows a broad resonance in the carbonyl region with a chemical shift similar to the chemical shifts measured for the carbonyl resonances of the unattached cluster. The linebroadening is such that the individual carbonyl resonances of the anchored species cannot be resolved. The CSA of the anchored carbonyl groups (of the order of 300ppm) is also little changed from that of the carbonyls of the precursor. This suggests that in the case of $[H_2Os_3(CO)_{10}L']$, and from its very similar nmr and i.r. behaviour $[Os_3(CO)_{11}L']$, the surface species formed closely resembles that which would be formed on simple anchoring of the osmium cluster via the pendant phosphine ligand.

## 7.7 Discussion.

The results presented in this chapter illustrate the use of solid state $^{13}C$ and in particular $^{31}P$ nmr spectroscopy in monitoring the reactions of metal cluster compounds with an oxide support. In all of the examples considered, it was possible to observe the $^{31}P$ nmr spectrum of the phosphine ligand used to anchor the cluster to the

surface. The chemical shift of the phosphine was found to be a sensitive indicator of the nature of the phosphorus-containing species present. Hence, subsequent changes in this surface species could be monitored. The identity of the anchored species could not, however, be fully established in all cases (see discussion below), showing that despite its success the solid state nmr technique has its limitations.

The chemical shift anisotropy measured for the surface species may be used to provide further information about the anchored species by means of a comparison with the CSA of the unanchored compound. It may also provide information about the mobility of the supported species, but should be interpreted with caution unless the variation of the CSA with temperature is known.

For all of the cluster compounds studied here, it had been postulated that the anchoring reaction would result in simple anchoring of the metal cluster to the support via the pendant phosphine ligand. However previous studies have noted considerable variations in behaviour between ruthenium, rhodium and osmium carbonyls on oxide supports [29], and it was therefore not entirely surprising that the anchoring reaction did not proceed in an identical fashion in each case.

When the cluster $(\mu\text{-}H)_2Ru_3(CO)_9(\mu_3\text{-}P(CH_2)_2Si(OEt)_3)$ was reacted with alumina, a comparison of the chemical shift of the surface species with that of the simple cluster suggested that straightforward attachment via the phosphine ligand had occurred. The CSA of the surface species shows a decrease in magnitude from the CSA of the crystalline cluster, which may result from mobility of the surface species; this cannot be determined without variable temperature studies.

In the case of the rhodium clusters, although initially

simple attachment of the cluster occurs there is subsequently rapid formation of an oxidised species by a reaction which continues until intact cluster molecules are no longer present. The chemical shift anisotropy of the cluster species on the surface is less than that of the unattached clusters. This suggests the possibility of some degree of mobility of the surface species, producing averaging of the shielding tensor; again, variable temperature studies are necessary to determine if this in fact the case. The second phosphorus-containing species appears to be a phosphorus (V) species, with a CSA considerably larger than that of the attached cluster species. As the $^{13}C$ studies on these species were inconclusive, it has not been possible to fully identify the second species formed on the surface.

The results obtained for the triosmium clusters show that, whereas two of the clusters appear to react by simple attachment at the ligand silyl group, the third behaves in a very different manner. The species formed by reaction of $[H_2Os_3(CO)_9L']$ with silica which has been previously described as $[H_2Os_3(CO)_9PPh_2(CH_2)_2SIL]$ [[26-28,30] is at most short-lived. The major species present in this case appears to result from further reaction of surface groups with the pendant cluster. This is of particular interest because the significant catalytic activity of surfaces produced in this way in alkene isomerisation and hydrogenation has been ascribed to the presence of the species $[H_2Os_3(CO)_9PPh_2(CH_2)_2SIL]$.

Solid state nmr, then, has shown itself to be a valuable technique in the characterisation of supported metal cluster compounds. It does not, however, enable a complete identification of the surface species to be made. Considering the supported osmium clusters as an example, the solid state nmr spectra obtained for $[H_2Os_3(CO)_{10}L']$ and $[Os_3(CO)_{11}L']$ show little change in phosphorus

chemical shift or CSA upon anchoring, which is consistent with but not total proof of the maintenance of the intact cluster structure on the surface. This does not completely identify the surface moiety, which although based on the cluster structure may, for example, have lost some CO ligands; it may have formed other bonds with the surface in addition to that via the silylated phosphine ligand; or may in some other way be different from the species formed by simple attachment of the osmium cluster.

The situation is even less clear for supported $[H_2Os_3(CO)_9L']$. That the surface species is not the intact cluster simply attached via the phosphine ligand is immediately clear from the solid state nmr spectra, but a positive identification of the species formed on silica is not possible from these results. The solid state nmr technique works in this instance by comparing the spectrum of the unknown species with that of a suitable model compound, and establishing similarity, or the lack of it, between the two. Until a more appropriate model for the species formed when $[H_2Os_3(CO)_9L']$ is anchored to silica is postulated, synthesised and found to produce a solid state $^{31}P$ nmr spectrum similar to that of the surface species, no further identification can be made. In the meantime, $^{13}C$ nmr studies may provide more information if the problem of low sensitivity can be overcome.

However, despite these limitations, further solid state nmr studies should be of considerable importance in the study of similar systems and their catalytic applications, providing at least a negative result (this species is <u>not</u> present) if not a more positive identification of the species formed when transition metal clusters are anchored to solid supports.

7.8 References.

[1] D.C. Bailey and S.H. Langer, Chem. Rev. 81 (1981) 109.

[2] J. Evans and G.S. McNulty, J. Chem. Soc., Dalton Trans. (1984) 1123.

[3] J.E. Crawford, G.A. Melson and L.E. Makovsky, J. Catal. 83 (1983) 454.

[4] G. Collier, D.J. Hunt, S.D. Jackson, R.B. Moyes, I.A. Pickering and P.B. Wells, J. Catal. 80 (1983) 154.

[5] J. Schwank, L.F. Allard, M. Deeba and C.J. Gates, J. Catal. 84 (1983) 27.

[6] G.E. Maciel, D.J. O'Donnell and R. Greaves, Adv. Chem. Ser. 196 (1982) 389.

[7] C.A. Fyfe, H.C. Clark, J.A. Davies, P.J. Hayes and R.E. Wasylishen, J. Amer. Chem. Soc. 105 (1983) 6577.

[8] L. Bemi, H.C. Clark, J.A. Davies, C.A. Fyfe and R.E. Wasylishen, J. Amer. Chem. Soc. 104 (1982) 438.

[9] D.K. Liu, M.S. Wrighton, D.R. McKay and G.E. Maciel, Inorg. Chem. 23 (1984) 212.

[10] S.L. Cook, Ph.D. thesis, Southampton (1985).

[11] B.T. Heaton, L. Longhetti, D.M.P. Mingos, C.E. Briant, P.C. Minshall, B.R.C. Theobald, L. Garlaschelli and U. Sartorelli, J. Organomet. Chem. 213 (1981) 333.

[12] R.J. Crowte, Ph.D. thesis, Southampton (1986).

[13] B.F.G. Johnson, J. Lewis and D.A. Pippard, J. Chem. Soc., Dalton Trans. (1981) 407.

[14] J.R. Shapley, J.B. Keister, M. R. Churchill and B.G. DeBoer, J. Amer. Chem. Soc. 97 (1975) 4145.

[15] A.J. Deeming and S. Hasso, J. Organomet. Chem. 114 (1976) 313.

[16] J.R. Wilkinson and L.J. Todd, J. Organomet. Chem. 118 (1976) 199.

[17] R.H. Grubs and S.C.-H. Su, Prepr., Div. Pet. Chem., Am. Chem. Soc. 22 (1977) 1193.

[18] A.J. Naaktgeboren, R.J.M. Nolte and W. Drenth, J. Amer. Chem. Soc. 102 (1980) 3350.

[19] S. Shinoda, K. Nakamura and Y. Saito, Chem. Lett. (1983) 1449.

[20] S. Shinoda, K. Nakamura and Y. Saito, J. Mol. Catal. 17 (1982) 775.

[21] J. Evans and G.S. McNulty, J. Chem. Soc., Dalton Trans. (1984) 587.

[22] M. Bartholin, C.H. Graillat, A. Guyot, G. Coudurier, J. Bandiera and C. Naccache, J. Mol. Catal. 3 (1977-8) 17.

[23] J.L. Bilhou, V. B.-Bougnol, W.F. Graydon, J.M. Basset, A.K. Smith, G.M. Zanderighi and R. Ugo, J. Organomet. Chem. 153 (1978) 73.

[24] G.C. Smith, T.P. Chojnacki, S.R. Dasgupta, K. Iwatate and K.L. Watters, Inorg. Chem. 14 (1975) 1419.

[25] A.J. Deeming, J. Manning, I.P. Rothwell, M.B. Hursthouse and W.P.C. Walker, J. Chem. Soc., Dalton Trans. (1984) 2039.

[26] S.C. Brown and J. Evans, J. Chem. Soc., Chem. Commun. (1978) 1063.

[27] R. Pierantozzi, K.J. McQuade, B.C. Gates, M. Wolf, H. Knozinger and W. Ruhman, J. Amer. Chem. Soc. 101 (1979) 5436.

[28] M.B. Freeman, M.A. Patrick and B.C. Gates, J. Catal. 73 (1982) 82.

[29] S.L. Cook, J. Evans, G.S. McNulty and G.N. Greaves, J. Chem. Soc., Dalton Trans. (1986) 7.

[30] S.C. Brown and J. Evans, J. Mol. Catal. 11 (1981) 143.

# APPENDIX A

Variation in the standard deviation of samples.

If a parent population is normally distributed, control limits can be set up to test whether samples fit the specifications of that population. For the normal hypothesis, considering a population with mean $\mu$ and standard deviation $\sigma$, 1 in 40 or 2.5% will exceed $\mu + 1.96\sigma$; and 2.5% will be less than $\mu - 1.96\sigma$; 1 in 1000 or 0.1% will exceed $\mu + 3.09\sigma$; and 0.1% will be less than $\mu - 3.09\sigma$.

Looking at variation in the standard deviation s of samples, the mean variation of the standard deviation ($\mu_s$) for samples of size n is given by

$$\mu_s = c_n\sigma$$

$c_n$ depends on the magnitude of the sample taken: it has been calculated for various values of n, and the results can be found in standard statistical tables. If the parent population is approximately normal, s for the distribution of standard deviations is $\sigma/\sqrt{2n}$. With this, and knowledge of the mean of s ($\mu_s$), the inner and outer control limits become

$$\text{inner limit: } c_n\sigma \pm \frac{1.96\sigma}{\sqrt{(2n)}}$$

$$\text{outer limit: } c_n\sigma \pm \frac{3.09\sigma}{\sqrt{(2n)}}$$

Reference.

B.C. Erriker, 'Advanced general statistics', English Universities Press, London (1972).

# APPENDIX B

Chemical shift anisotropies of some tertiary phosphines.

The table below shows the chemical shielding tensor values obtained for a number of the phosphine-containing complexes and clusters studied in this thesis. The values were obtained from (i) the static spectrum of the compound; (ii) analysis of the spinning sidebands in the MAS spectrum; (iii) simulating the MAS spectrum using the tensor components derived from sideband analysis and refining the components until the best fit between the simulated and experimental MAS spectra was obtained (chapter 3). The method used in each case is indicated in the table. Unless stated to the contrary, the error in components from both static spectra and sideband analysis was estimated to be ±5ppm.

| (a) 'simple' compounds | $\sigma_{11}$ | $\sigma_{22}$ | $\sigma_{33}$ | |
|---|---|---|---|---|
| $Os_3(CO)_{11}PPh_3$ | 99 | 84 | -6 | (i) |
| $H_2Os_3(CO)_{10}PPh_3$ | 26 | -9 | -30 | (iii) |
| $H_2Os_3(CO)_9PPh_3$ | 100 | 3 | -36 | (iii) a |
| $[Rh(CN\text{-}xylyl)_2(PPh_3)_2]PF_6$ | 96 | 29 | -35 | (ii) |
| $RhCl(PPh_3)_3$ | | | | (ii) b |
| P trans to P | 100 | 36 | -45 | |
| P trans to Cl | 154 | 84 | -99 | |
| $Rh_4(CO)_{11}PPh_2Et$ | 51 | 17 | -25 | (i) |
| $Rh_6(CO)_{15}PPh_2Et$ | 71 | 21 | -29 | (i) |
| $WH_6(PMe_3)_3$ [1P] | 13 | 20 | -61 | (ii) |
| [2P] | 48 | 10 | -65 | |
| $(C_6H_6)Mo(PPhMe_2)_3$ | 112 | 48 | -108 | (ii) |
| $(\mu\text{-}H)_2Ru_3(CO)_9(\mu_3\text{-}PPh)$ | 460 | 190 | 190 | (ii) c |

a ±2ppm (refined)

b ±10ppm

c ±8ppm

| | | | | |
|---|---|---|---|---|
| (b) homonuclear gold clusters | | | | (ii) |
| $[Au_9(P(p\text{-}C_6H_4OMe)_3)_8][NO_3]_3$ | | | | |
| green isomer | 115 | 75 | 0 | |
| | 92 | 52 | 10 | |
| golden-brown isomer | 99 | 65 | 13 | |
| | 90 | 65 | 4 | |
| $[Au_9(P(p\text{-}C_6H_4OMe)_3)_8][BF_4]_3$ | 101 | 58 | 14 | |
| | 93 | 62 | 2 | |
| (c) heteronuclear clusters | | | | |
| $AuRu_4H_3(CO)_{12}PPh_3$ | 107 | 107 | -1 | (ii) |
| | 130 | 82 | 1 | |
| $AgRu_3(CO)_9(C_2Bu^t)PPh_3$ | 47 | 22 | -26 | (iii) d |
| $Au_2Ru_4H_2(CO)_{12}(PPh_3)_2$ | 112 | 60 | -7 | (iii) d |
| | 94 | 66 | -10 | |
| $Au_2Ru_4H_2(CO)_{12}$(dppm) | 164 | 36 | -21 | (iii) e |
| | 125 | 64 | -19 | |
| $Au_2Ru_3(\mu_3\text{-}S)(CO)_9$(dppm) | 141 | 25 | -20 | (ii) |
| | 132 | 36 | -28 | |
| $Au_3Ru_4H(CO)_{12}(PPh_3)_3$ | 109 | 78 | 1 | (ii) |
| | 104 | 68 | -6 | |

d ±2ppm (refined)

e the powder pattern simulated using the tensor values obtained from sideband analysis did not resemble the experimental powder pattern